Winter 2018

THE IMPACT OF DAMS ON FLOODS AND NITROGEN FLUX IN THE LAMPREY RIVER WATERSHED, NH

David Simon
University of New Hampshire, Durham

THE IMPACT OF DAMS ON FLOODS AND NITROGEN FLUX IN THE LAMPREY RIVER WATERSHED, NH

BY

David Simon

B.S. Biology, Salem State University, 2014

THESIS

Submitted to the University of New Hampshire

in Partial Fulfillment of

the Requirements for the Degree of

Master of Science

In

Hydrology

December, 2018

This thesis has been examined and approved in partial fulfillment of the requirements for the degree of Master of Science in Hydrology by:

Thesis Director, Anne Lightbody, Associate Professor of Hydrology

Matt Davis, Associate Professor of Hydrogeology

Wilfred Wollheim, Associate Professor of Environmental Sciences

Arthur Gold, Professor of Natural Resources Science, University of Rhode Island

Sean Smith, Associate Professor of Earth and Climate Sciences, University of Maine

On September 25, 2018

Original approval signatures are on file with the University of New Hampshire Graduate School.

Table of Contents

Acknowledgements vi

List of Tables vii

List of Figures xiii

Abstract xx

Chapter 1: Introduction 1

1.1 Background Information
1.1.1 Dam Removal Tradeoffs 1
1.1.2 Tools Used to Quantify Dam Removal Tradeoffs 1
1.1.3 Effects of Dams on Flood Peak Attenuation 2
1.1.4 Modeling Hydrologic Alteration by Dams 3
1.1.5 River Network Nitrogen Retention 3
1.1.6 Effects of Dams on River Network N Retention 5
1.1.7 Modeling N Retention 6
1.1.8 Effect of Climate Change on Flooding and N Fluxes 7
1.1.9 Effect of Land Use Change on Flooding and N Fluxes 8
1.2 Lamprey River Watershed Site Description
1.2.1 Watershed Overview 8
1.2.2. Impact on Great Bay 9
1.2.3 Watershed Management Plan and Instream Flow Policy 11
1.2.4 Dams 14
1.2.5 Historic Land Cover and Population 16
1.2.6 Historic Climate and Flooding 18
1.2.7 Historic Nitrogen Flux 19
1.2.8 Historic Fish Runs 21
1.3 Research Objectives 22

Chapter 2: Field Methods 24

2.1 Pawtuckaway Lake Site Description
2.1.1 Watershed and Reservoir Overview 24
2.1.2 Dam Management 29
2.2 Field Methods Overview 30
2.3 Tributary N Inputs and Dam Outlet N Outputs
2.3.1 Sampling Locations 31
2.3.2 Continuous Stage Measurements 32
2.3.3 Field Discharge Measurements and Uncertainty 36
2.3.4 Stage-Discharge Rating Curves and Uncertainty 39
2.3.5 Continuous Discharge Records and Uncertainty 39
2.3.6 Discharge Record Gap Filling and Uncertainty 41
2.3.7 Grab Sample Measurements of N Concentration and Uncertainty 47
2.3.8 Estimates of N Flux at Monitoring Stations 48
2.3.9 Tributary Discharge and N Inputs at Unmonitored Tributaries 49

2.4 Nearshore Hydrology and N Inputs from SWAT Modeling
2.4.1 SWAT Model Overview 50
2.4.2 SWAT Input Data 50
2.4.3 SWAT Model Calibration 52
2.5 Atmospheric N Inputs and Uncertainty 58
2.6 N Mass Balance, Retention, and Uncertainty 59

Chapter 3: Field Results and Discussion 61

3.1 Pawtuckaway Lake Water Balance 61
3.2 Monitored Tributary and Dam Outlet N Solute Concentrations 70
3.3 Tributary and Dam Outlet N Flux 81
3.4 N Loading from Atmospheric Deposition and the Near Shore Loading from SWAT 91
3.5 Reservoir N Retention Results and Discussion 93
3.6 N Flux from the Pawtuckaway Lake Watershed 95

Chapter 4: FrAMES Modeling Methods 98

4.1 FrAMES Model Background 98
4.2 Model Application Overview 99
4.3 Model Input Data
4.3.1 River Network 99
4.3.2 Dam Management 100
4.3.3 Contemporary Climate and Land Use 104
4.3.4 Future Climate and Land Use 106
4.4 Model Calibration
4.4.1 Hydrologic Calibration Methods 114
4.4.2 Hydrologic Calibration Results 119
4.4.3 DIN Loading Calibration 121
4.4.4 Modeled DIN Reservoir and River Retention 124
4.4.5 DIN Concentration Variation with Discharge 125
4.4.6 Modeled DIN Flux 128
4.4.7 Estimation of Hydrologic Parameter Uncertainty 128
4.5 Model Scenarios 129
4.6 Comparison Metrics 131

Chapter 5: FrAMES Modeling Results 133

5.1 Flood Magnitudes
5.1.1 Dam Scenarios Under Contemporary Climate & Land Use 133
5.1.2 Dam Scenarios Under Late-Century Climate and/or Land Use 135
5.2 Winter DIN Load, Flux, and Retention
5.2.1 Dam Scenarios Under Contemporary Climate & Land Use 137
5.2.2 Dam Scenarios Under Late-Century Climate and/or Land Use 140
5.3 Summer DIN Load, Flux, and Retention
5.3.1 Dam Scenarios Under Contemporary Climate & Land Use 143
5.3.2 Dam Scenarios Under Late-Century Climate and/or Land Use 146

Chapter 6: Conclusion 149

6.1 Summary 149
6.2 Comparing Results to other Watershed Models 149
6.3 Suggestions for Future Field Work 150
6.4 Sources of Model Error and Suggestions for Future Modeling 151
6.5 Implications for Decision Making 157

References 159

Appendix A: Field Measurement Data 168

Appendix B: FrAMES Modeling Structure 191

Acknowledgements

I would like to thank my advisor Anne Lightbody for taking a chance on me and showing me what it takes to be a professional hydrologist. I would also like to extend my thanks to my committee members for their support and guidance throughout my research. I'm very thankful towards members of the UNH Water Systems Analysis Group for sharing modeling tools and data used in this project, specifically Shan Zuidema for showing me the ropes of hydrologic modeling and to Danielle Grogan and Alex Prusevich for their help with troubleshooting. I would like to acknowledge members of the UNH Water Resources Research Center for generously providing data for model calibration and Wayne Ives of the New Hampshire Department of Environmental Services for his help with field work at Pawtuckaway Lake. I would also like to thank undergraduate research assistants Brady Malave and Matt Healy for their assistance with field work and modeling and my colleagues Christian Olsen and Harrison Simbliaris for their support. Lastly, this work would not have completed if not for the unrelenting support of my friends and family, especially my fiancée, Ally Hughes.

Funding for this project was provided by the National Science Foundation's Research Infrastructure Improvement NSF #IIA-1539071. Any opinions, findings, and conclusions or recommendations expressed in this material are those of the author(s) and do not necessarily reflect the views of the National Science Foundation.

List of Tables

Table 1.1. Database of dams and reservoir attributes within the Lamprey River watershed. ... 13

Table 1.2 Historic human population in the Lamprey River watershed. 16

Table 1.3 Historic land cover of the Lamprey River watershed. 17

Table 2.1 Pawtuckaway Lake subbasins and land cover. 28

Table 2.2 Values used to calculate relative uncertainties associated with a single discharge measurement using the velocity-area method (cf. Herschy 1985), ... 38

Table 2.3 Prepared and measured nitrate standards that were used to estimate error of N solute concentration measurements analyzed at the Water Quality Analysis Laboratory at UNH. 48

Table 2.4 Table relating monitored tributaries and the tributaries to which discharge and N flux measurements were extrapolated. 49

Table 2.5 Source land cover reclassified to SWAT land cover classification. 55

Table 2.6 Manually adjusted urban land cover parameters. 55

Table 2.7 Pond and wetland characteristics obtained from USGS NHDPLUSv2 and NHDES bathymetry data used in SWAT to represent ponds and wetlands. 56

Table 2.8 Septic density values for various subbasin and land cover types. 56

Table 2.9 Hydrologic and N transport parameters and final calibration values for SWAT. 57

Table 2.10 Historic measurements of wet dissolved inorganic nitrogen (DIN), wet dissolved organic nitrogen (DON), and wet and dry total dissolved nitrogen (TDN) deposition 59

Table 2.11 Estimates of total annual wet and dry nitrate (NO_3^-) and ammonium (NH_4^+) from ClimCalc model for Pawtuckaway Lake area. 59

Table 3.1 Monthly totals of rainfall from 2017-05-19 to 2018-05-18 measured at NOAA weather station USC00272800 in Epping, NH. 63

Table 3.2 Stop log gate management at the Drowns Dam outlet by NHDES 65

Table 3.3 Stop log management at the Dolloff Dam outlet by NHDES 66

Table 3.4 Monthly totals of water inputs to Pawtuckaway Lake from 5/19/17 to 5/18/18. 67

Table 3.5 Monthly totals of water outputs from Pawtuckaway Lake from 5/19/17 to 5/18/18. ... 68

Table 3.6 Seasonality of total dissolved nitrogen (TDN) and nitrate (NO_3^-) concentration 73

Table 3.7 Seasonality of ammonium (NH_4^+) and dissolved organic nitrogen (DON) concentration at each sampling station. 73

Table 3.8 Seasonality of nitrate (NO_3^-) concentration at each sampling station for the study period (5/19/17 - 5/18/18) and measurements taken by New Hampshire Department of Environmental Services (NHDES) from 12/1/1991 to 11/30/1992. 74

Table 3.9 Best fit regression equations to the relationship between total dissolved nitrogen (TDN), nitrate (NO_3^-), ammonium (NH_4^+), and dissolved organic nitrogen (DON) concentration (y) and discharge (x) at Fernald's Brook A from 5/19/17 – 5/18/18. 75

Table 3.10 Best fit regression equations to the relationship between total dissolved nitrogen (TDN), nitrate (NO_3^-), ammonium (NH_4^+), and dissolved organic nitrogen (DON) concentration (y) and discharge (x) at Mountain Cove Brook from 5/19/17 – 5/18/18. 76

Table 3.11 Best fit regression equations to the relationship between total dissolved nitrogen (TDN), nitrate (NO_3^-), ammonium (NH_4^+), and dissolved organic nitrogen (DON) concentration (y) and discharge (x) at Back Creek B from 5/19/17 – 5/18/18. 77

Table 3.12 Best fit regression equations to the relationship between total dissolved nitrogen (TDN), nitrate (NO_3^-), ammonium (NH_4^+), and dissolved organic nitrogen (DON) concentration (y) and discharge (x) at Round Pond Brook from 5/19/17 – 5/18/18. 78

Table 3.13 Best fit regression equations to the relationship between total dissolved nitrogen (TDN), nitrate (NO_3^-), ammonium (NH_4^+), and dissolved organic nitrogen (DON) concentration (y) and discharge (x) at Mile Brook from 5/19/17 – 5/18/18. 79

Table 3.14 Best fit regression equations to the relationship between total dissolved nitrogen (TDN), nitrate (NO_3^-), ammonium (NH_4^+), and dissolved organic nitrogen (DON) concentration (y) and discharge (x) at Pawtuckaway River from 5/19/17 – 5/18/18. 80

Table 3.15 Monthly total dissolved nitrogen (TDN) flux to and from Pawtuckaway Lake from tributaries and the two dam outlets respectively. 85

Table 3.16 Monthly nitrate (NO_3^-) flux to and from Pawtuckaway Lake from tributaries and the two dam outlets respectively. 86

Table 3.17 Monthly total and mean and annual total ammonium (NH_4^+) flux to and from Pawtuckaway Lake from tributaries and the two dam outlets respectively. 87

Table 3.18 Monthly total and mean and annual total dissolved organic nitrogen (DON) flux to and from Pawtuckaway Lake from tributaries and the two dam outlets respectively. 88

Table 3.19 Annual total and areal flux of total dissolved nitrogen (TDN), dissolved inorganic nitrogen (DIN), nitrate (NO_3^-), ammonium (NH_4^+), and dissolved organic nitrogen (DON) to Pawtuckaway Lake from the four monitored tributaries from 5/19/17 to 5/18/18. 89

Table 3.20 Annual total dissolved nitrogen (TDN), dissolved inorganic nitrogen (DIN), nitrate (NO_3^-), ammonium (NH_4^+), and dissolved organic nitrogen (DON) flux to Pawtuckaway Lake from the extrapolated tributaries from 5/19/17 to 5/18/18. 90

Table 3.21 Total annual nitrate (NO_3^-) flux measurements at tributaries and dam outlets from 5/19/17 to 5/18/18 compared to total annual flux measurements obtained by NHDES 90

Table 3.22 Nearshore flux, total flux, and percent of nearshore flux that makes up total flux of total dissolved nitrogen (TDN), dissolved organic nitrogen (DON), and nitrate (NO_3^-) to Pawtuckaway Lake from the Soil and Water Assessment Tool (SWAT) 92

Table 3.23 Annual total dissolved nitrogen (TDN), dissolved inorganic nitrogen (DIN), nitrate (NO_3^-), ammonium (NH_4^+), and dissolved organic nitrogen (DON) retention for Pawtuckaway Lake from 5/19/2017 to 5/18/2018. 95

Table 3.24 A synoptic comparison of total dissolved nitrogen (TDN), dissolved inorganic nitrogen (DIN), and dissolved organic nitrogen (DON) loading from the Pawtuckaway watershed and the upper (at USGS gauge 01073319) and lower Lamprey River watershed 97

Table 4.1 Parameter values used to model different reservoir management types. 104

Table 4.2 Name, institution, and references of the five statistically downscaled global climate models whose projections of precipitation and air temperature 108

Table 4.3 Projected land cover for the Lamprey River watershed. 112

Table 4.4 Optimized hydrologic parameter default, bounds (min and max), delta (Δ), and tolerance (tol) values that were used during hydrologic calibration. 117

Table 4.5 Values of 26 evaluations points used during the hydrologic calibration 118

Table 4.6 Hydrologic parameter ranges and best values after calibration. Best values are from the hydrologic parameter set with the lowest objective function. 120

Table 4.7 Locations and human land use (sum of agriculture and development) of first-order tributaries used to calibrate DIN loading. 122

Table 4.8 Parameters optimized during DIN loading calibration and final values calibrated for the Ipswich (cf. Wollheim et al. 2008) and Lamprey River watersheds. 123

Table 4.9 Best-fit power laws of observed and modeled dissolved inorganic nitrogen concentration to discharge. 127

Table 5.1 Results of the Mann-Whitney U test for statistical significance between modeled 2-yr flood discharge at the Lamprey River watershed outlet for two different scenarios using contemporary climate and land use. 134

Table 5.2 Results of the Mann-Whitney U test for statistical significance between modeled 2-yr flood discharge at the Lamprey River watershed outlet for two different scenarios using projections of future climate and/or land use. 136

Table 5.3 Results of the Mann-Whitney U test for statistical significance between modeled wintertime DIN flux at the Lamprey River watershed outlet compared with the contemporary climate and land use scenario with all dams under current management. 139

Table 5.4 Results of the Mann-Whitney U test for statistical significance between modeled wintertime DIN flux at the Lamprey River watershed outlet for two different scenarios using projections of future climate and/or land use. 142

Table 5.5 Results of the Mann-Whitney U test for statistical significance between modeled summertime DIN flux at the Lamprey River watershed outlet compared with the contemporary climate and land use scenario with all dams under current management. 145

Table 5.6 Results of the Mann-Whitney U test for statistical significance between modeled summertime DIN flux at the Lamprey River watershed outlet for two different scenarios using projections of future climate and/or land use. 148

Table A.1. Dates and times when barometric transducer data was trimmed and filled with linear interpolation due to data retrieval. 169

Table A.2. Number of measurements kept and measurements trimmed and filled through linear interpolation for the Barometric transducer from 2017-05-19 to 2018-05-18. 170

Table A.3. Dates and times when pressure transducer data was trimmed and filled with linear interpolation at Round Pond Brook. 171

Table A.4. Dates and times when pressure transducer data was corrected for intentional and unintentional transducer relocations at Round Pond Brook. 171

Table A.5. Discharge measurements obtained at Round Pond Brook using the velocity-area method and corrected stage used in the construction of the stage-discharge rating curve 172

Table A.6. Nitrogen solute concentration measurements obtained at Round Pond Brook. 173

Table A.7. Dates and times when pressure transducer data was trimmed and filled with linear interpolation at Back Creek B. 175

Table A.8. Dates and times when pressure transducer data was corrected for intentional and unintentional transducer relocations at Back Creek B. 175

Table A.9. Discharge measurements obtained at Back Creek B using the velocity-area method and corrected stage used in the construction of the stage-discharge rating curve 175

Table A.10. Nitrogen solute concentration measurements obtained at Back Creek B. 177

Table A.11. Dates and times when pressure transducer data was trimmed and filled with linear interpolation at Mountain Cove Brook. 178

Table A.12. Dates and times when pressure transducer data was corrected for intentional and unintentional transducer relocations at Mountain Cove Brook. 178

Table A.13. Discharge measurements obtained at Mountain Brook Cove using the velocity-area method and corrected stage used in the construction of the stage-discharge rating curve 178

Table A.14. Discharge measured at the two parallel road culverts at Mountain Cove Brook using bucket technique on 10/13/17 at 15:50. 178

Table A.15. Nitrogen solute concentration measurements obtained at Mountain Cove Brook 180

Table A.16. Dates and times when pressure transducer data was trimmed and filled with linear interpolation at Fernald's Brook A. 181

Table A.17. Dates and times when pressure transducer data was corrected for intentional and unintentional transducer relocations at Fernald's Brook A. 181

Table A.18. Discharge measurements obtained at Fernald's Brook A using the velocity-area method and corrected stage used in the construction of the stage-discharge rating curve 181

Table A.19. Discharge measured at the Fernald's Brook A using bucket technique 181

Table A.20. Discharge measured at the Fernald's Brook A using bucket technique 181

Table A.21. Discharge measured at the Fernald's Brook A using bucket technique 182

Table A.22. Nitrogen solute concentration measurements obtained at Fernald's Brook A. 183

Table A.23. Dates and times when pressure transducer data was trimmed and filled with linear interpolation at Mile Brook. 184

Table A.24. Dates and times when pressure transducer data was corrected for intentional and unintentional transducer relocations at Mile Brook. 185

Table A.25. Discharge measurements obtained at Mile Brook using the velocity-area method and corrected stage used in the construction of the stage-discharge rating curve 185

Table A.26. Nitrogen solute concentration measurements obtained at Mile Brook. 186

Table A.27. Dates and times when pressure transducer data was trimmed and filled with linear interpolation at Pawtuckaway River. 188

Table A.28. Dates and times when pressure transducer data was corrected for intentional and unintentional transducer relocations at Pawtuckaway River. 188

Table A.29. Discharge measurements obtained at Pawtuckaway River using the velocity-area method and corrected stage used in the construction of the stage-discharge rating curve 188

Table A.30. Nitrogen solute concentration measurements obtained at Pawtuckaway River .. 190

Table A.31. Nitrogen solute concentration measurements obtained in the reservoir. 190

Table A.32. Nitrogen solute concentration measurements obtained at USGS gauge 190

Table A.33. Nitrogen solute concentration measurements obtained at USGS gauge 190

List of Figures

Figure 1.1 A representation of a reservoir and all pathways of N 5

Figure 1.2 Map of the Lamprey River watershed 10

Figure 1.3 Digital elevation model (at 30-meter resolution) of the Lamprey River watershed. Source: NH GRANIT Database. 10

Figure 1.4 Map of the Lamprey River watershed showing run-of-river dams, actively managed recreation dams, major reservoirs, the NOAA weather gauge, two USGS discharge gauges, and the waste water treatment plant in Epping. 15

Figure 1.5 Example of dam management at Pawtuckaway Lake, showing changes in water level recorded at the NHDES station above Dolloff Dam 16

Figure 1.6 Land cover of the Lamprey River watershed for year 2015 17

Figure 1.7 Median daily discharge of the Lamprey River 19

Figure 1.8 Median dissolved inorganic nitrogen (DIN) and dissolved organic nitrogen (DON) concentration on the Lamprey River 21

Figure 1.9 Median dissolved inorganic nitrogen (DIN) and dissolved organic nitrogen (DON) flux (calculated by multiplying discharge and concentration for each day) on the Lamprey River ... 21

Figure 2.1 Bathymetry profile of Pawtuckaway Lake surveyed by NHDES showing northern and southern basins (contour label units are meters and range from 2 to 17 m). 25

Figure 2.2 Area of the Pawtuckaway Lake watershed and sub-watersheds that drain to the lake. Numbered sub-watershed names, area, and land cover correspond to Table 2.1. 27

Figure 2.3 Dam outlet structures at (A) Dolloff Dam on 4/8/18 and (B) Drowns Dam 30

Figure 2.4 Pawtuckaway Lake watershed (left) and Lamprey River watershed (right) showing the locations where water samples were collected (red triangles) and the NOAA weather gauge USC00272800 in Epping, NH. 32

Figure 2.5. Pictures of instream Solinst Levelogger PVC housings attached to (A) a rebar stake at Round Pond Brook and (B) a cement block at Mile Brook. 33

Figure 2.6. Pictures at Back Creek B on 8/3/17 of the (A) Sokkia C410 Automatic Leveland (B) surveying rod used to measure the relative elevations of the top of the instream Levelogger PVC housing and the nearest downstream control structure. 35

Figure 2.7. Schematic stream cross section showing elevations of the top of the PVC housing ($h_{top\_of\_housing}$) and the downstream control ($h_{downstream\_control}$) relative to a local vertical datum and the distance of the transducer below the top of the PVC housing ($h_{below\_top\_housing}$). 36

Figure 2.8 Measuring discharge using the velocity area method at Mountain Cove Brook 37

Figure 2.9 Best fit linear regression line of Mountain Cove Brook runoff (discharge normalized by drainage area) to Back Creek B runoff 44

Figure 2.10 Best fit linear regression line of Fernald's Brook A runoff (discharge normalized by drainage area) to Round Pond Brook runoff 45

Figure 2.11 Best fit linear regression line of Pawtuckaway River runoff (discharge normalized by drainage area) to Mile Brook runoff 46

Figure 2.12 Pawtuckaway Lake watershed SWAT 2012 subbasins and hydrologic response unites (HRUs) created in ArcSWAT. 54

Figure 3.1 Daily runoff for the four monitored tributaries and daily rainfall from 2017-05-19 to 2018-05-18. 64

Figure 3.2 Daily runoff for Mile Brook, daily rainfall, and reservoir pool level for Pawtuckaway Lake (in meters above sea level) from 5/19/17 to 5/18/18. 64

Figure 3.3 Daily runoff for the Pawtuckaway River, daily rainfall, and reservoir pool level for Pawtuckaway Lake (in meters above sea level) from 5/19/17 to 5/18/18. 65

Figure 3.4 Monthly totals of tributary inflow (Back Creek B, Mountain Cove Brook, Round Pond Brook, Fernald's Brook A, and nine unmonitored tributaries) and overland runoff and groundwater seepage (Nearshore), and direct precipitation into the reservoir (Precip) to outflow from Mile Brook, Pawtuckaway River, and evaporation from the reservoir's surface (Evap) from Pawtuckaway Lake. 69

Figure 3.5 Hourly reservoir release (Q) normalized by mean annual hourly reservoir release (Q_{AVG}) compared to relative active reservoir storage (S) normalized by the maximum relative reservoir storage (S_{MAX}) for Pawtuckaway Lake from 5/19/17 to 5/18/18. 70

Figure 3.6 Relationship between total dissolved nitrogen (TDN; A.), nitrate (NO_3^-; B.), ammonium (NH_4^+; C.), and dissolved organic nitrogen (DON; D.) concentration and discharge (Q) at Fernald's Brook A. 75

Figure 3.7 Relationship between total dissolved nitrogen (TDN; A.), nitrate (NO_3^-; B.), ammonium (NH_4^+; C.), and dissolved organic nitrogen (DON; D.) concentration and discharge (Q) at Mountain Cove Brook. 76

Figure 3.8 Relationship between total dissolved nitrogen (TDN; A.), nitrate (NO_3^-; B.), ammonium (NH_4^+; C.), and dissolved organic nitrogen (DON; D.) concentration and discharge (Q) at Back Creek B. 77

Figure 3.9 Relationship between total dissolved nitrogen (TDN; A.), nitrate (NO_3^-; B.), ammonium (NH_4^+; C.), and dissolved organic nitrogen (DON; D.) concentration and discharge (Q) at Round Pond Brook. 78

Figure 3.10 Relationship between total dissolved nitrogen (TDN; A.), nitrate (NO_3^-; B.), ammonium (NH_4^+; C.), and dissolved organic nitrogen (DON; D.) concentration and discharge (Q) at Mile Brook. 79

Figure 3.11 Relationship between total dissolved nitrogen (TDN; A.), nitrate (NO_3^-; B.), ammonium (NH_4^+; C.), and dissolved organic nitrogen (DON; D.) concentration and discharge (Q) at Pawtuckaway River. 80

Figure 3.12 Measurements of total dissolved nitrogen (TDN), nitrate (NO_3^-), ammonium (NH_4^+), and dissolved organic nitrogen (DON) concentration obtained in the reservoir above the Dolloff Dam outlet. 81

Figure 3.13 Monthly totals of total dissolved nitrogen (TDN) flux loaded to (Back Creek B, Mountain Cove Brook, Round Pond Brook, and Fernald's Brook A) and leaving (Mile Brook and Pawtuckaway River) from Pawtuckaway Lake. 83

Figure 3.14 Monthly totals of nitrate (NO_3^-) flux loaded to (Back Creek B, Mountain Cove Brook, Round Pond Brook, and Fernald's Brook A) and leaving (Mile Brook and Pawtuckaway River) from Pawtuckaway Lake. 83

Figure 3.15 Monthly totals of ammonium (NH_4^+) flux loaded to (Back Creek B, Mountain Cove Brook, Round Pond Brook, and Fernald's Brook A) and leaving (Mile Brook and Pawtuckaway River) from Pawtuckaway Lake. 84

Figure 3.16 Monthly totals of dissolved organic nitrogen (DON) flux loaded to (Back Creek B, Mountain Cove Brook, Round Pond Brook, and Fernald's Brook A) and leaving (Mile Brook and Pawtuckaway River) from Pawtuckaway Lake. 84

Figure 3.17 Total annual dissolved organic nitrogen (DON), nitrate (NO_3^-), ammonium (NH_4^+), and total dissolved nitrogen (the summation of DON, NO_3^-, and NH_4^+) of fluxes into (tributaries, nearshore loading, and atmospheric deposition) and leaving (dam outlets) Pawtuckaway Lake from 5/19/2017 to 5/18/2018. 94

Figure 3.18 Estimates of the percentage of N removed in waterbodies versus the ratio of water depth to residence time (modified from Seitzinger et al. 2002). Blue and black square and error bars show dissolved inorganic nitrogen (DIN) and total dissolved nitrogen (TDN) retention within Pawtuckaway Lake from 5/19/2017 to 5/18/2018. 95

Figure 4.1 Figure of the simulated topological network (STN) for the Lamprey River watershed used in FrAMES. 100

Figure 4.2 Reservoir outflow/storage curves for managed dams with operating types of flood control and water supply. 103

Figure 4.3 Reservoir outflow/storage curves for unmanaged dams with different reservoir flooding area rates (fld). 103

Figure 4.4 Historic total annual rainfall and maximum 1-day rainfall from METDATA and measured at the NOAA weather gauge USC00272800 105

Figure 4.5 Historic annual mean air temperature from METDATA (averaged over the watershed) and measured at the NOAA weather gauge USC00272800 in Epping 106

Figure 4.6 Historic annual mean air temperature from METDATA (water years 1996 - 2015) and mean late century projections (water years 2007 - 2099) of air temperature from five LOCA downscaled global climate models (GCM) in the Lamprey River watershed. 108

Figure 4.7 Boxplots of historic total annual rainfall from METDATA (water years 2007 - 2015) and projected total annual rainfall from LOCA downscaled global climate models ACCESS1-0 (A.), CESM1-CAM5 (B.), GFDL-ESM2G (C.), HadGEM2-ES (D.), and MIROC-ESM (E.). 109

Figure 4.8 Boxplots of historic maximum 1-day rainfall from METDATA (water years 2007 - 2015) and projected maximum 1-day rainfall from LOCA downscaled global climate models ACCESS1-0 (A.), CESM1-CAM5 (B.), GFDL-ESM2G (C.), HadGEM2-ES (D.), and MIROC-ESM (E.) 110

Figure 4.9 Boxplots of historic maximum 7-day rainfall from METDATA (water years 2007 - 2015) and projected maximum 7-day rainfall from LOCA downscaled global climate models ACCESS1-0 (A.), CESM1-CAM5 (B.), GFDL-ESM2G (C.), HadGEM2-ES (D.), and MIROC-ESM (E.) 111

Figure 4.10 Projected land cover of the Lamprey River watershed for year 2090. 113

Figure 4.11 Flow chart of the Python 2.x script used to calibrate the five hydrologic parameters (parameter set). 115

Figure 4.12 The 26 evaluation points used during hydrologic calibration across the flow duration curve of historic observations of mean daily discharge (Q) at USGS gauge # 01073500 118

Figure 4.13 Observed and modeled flow duration curves of mean daily discharge (Q) at USGS gauge 01073500 for (A) water years 2000 to 2009 and (B) water years 2010 to 2015. 120

Figure 4.14 Observed and modeled median daily discharge (Q) for day of year at USGS gauge 01073500 for water years 2000 to 2015. 120

Figure 4.15 Calibration of dissolved inorganic nitrogen (DIN) concentration in runoff at five headwater sites in the Lamprey River watershed. 123

Figure 4.16 Observed and modeled median mean daily dissolved inorganic nitrogen (DIN) concentration for day of year at USGS gauge 01073500 for water years 2000 to 2015. 125

Figure 4.17 Observed and modeled dissolved inorganic nitrogen (DIN) concentration to discharge (Q) for (A) winter, (B) spring, (C) summer, and (D) fall seasons. 127

Figure 4.18 Observed and modeled median mean daily dissolved inorganic nitrogen (DIN) flux for day of year at USGS gauge 01073500 for water years 2000 to 2015. 128

Figure 4.19 Kernel density estimation plots of calibrated hydrologic parameters (A) α, (B) $\mathrm{RhRt2}$, (C) β, (D) RRPMax, and (E) $infiltr$ obtained during hydrologic calibration and used to estimate model uncertainty associated with parameter selection. 129

Figure 4.20 Figure of all scenarios modeled in FrAMES showing each combination of climate, land use, and dam management. 131

Figure 5.1 Median discharge (Q) of the 2-year flood at the Lamprey River watershed outlet for water years 1996 to 2015 for dam scenarios under contemporary climate and land use conditions. 134

Figure 5.2 Median discharge (Q) of the 2-year flood at the Lamprey River watershed outlet for dam scenarios under contemporary, baseline global climate model (GCM) projections, late-century GCM-projected climate, and contemporary and late-century projected land use conditions. 136

Figure 5.3 Wintertime (1/1 – 3/21) daily (A) DIN load and flux and (B) retention for the Lamprey River watershed averaged over water years 1996 to 2015 under contemporary climate and land use conditions. 138

Figure 5.4 Wintertime (1/1 – 3/21) daily (A) DIN load and flux and (B) retention for the Lamprey River watershed for dam scenarios under contemporary, baseline global climate model (GCM) projected, late-century GCM projected climate and contemporary and late-century projected land use conditions. 141

Figure 5.5 Summertime (6/10 – 10/1) daily (A) DIN load and flux and (B) retention for the Lamprey River watershed for water years 1996 to 2015 for dam scenarios under contemporary climate and land use conditions. 144

Figure 5.6 Summertime (6/10 – 10/1) daily (A) DIN load and flux and (B) retention for the Lamprey River watershed for dam scenarios under contemporary, baseline global climate model (GCM) projected, late-century GCM projected climate and contemporary and late-century projected land use conditions. 147

Figure 6.1 Hourly reservoir release (Q) normalized by mean annual hourly reservoir release (Q_{AVG}) compared to relative active reservoir storage (S) normalized by the maximum relative reservoir storage (S_{MAX}) for Pawtuckaway Lake from 5/19/17 to 5/18/18. 154

Figure 6.2 Summer DIN flux leaving the Lamprey River watershed versus total watershed water storage (river network plus reservoirs) averaged over the summer for water years 1996 to 2015 for dam management scenarios under contemporary climate and land use conditions. 155

Figure 6.3 Summer DIN retention provided by the dam network within the Lamprey River watershed versus the distribution of reservoirs within the river network (reservoir storage skewness) for water years 1996 to 2015 for four dam management scenarios under contemporary climate and land use conditions. 156

Figure 6.4. Contour plot of summer DIN retention provided by a dam network within a watershed as a function of reservoir storage skewness to human land use skewness for two scenarios of similar reservoir storage volumes for water years 1996 to 2015 under contemporary climate and land use conditions. 157

Figure A.1. Location of barometric transducer, sampling stations, and NOAA Local Climatological Data (LDC) station id WBAN:54791 at Skyhaven Airport in Rochester, NH. ... 168

Figure A.2. Barometric transducer pressure head (recorded at 5-minute intervals) compared to daily mean pressure head measured at the NOAA Local Climatological Data (LDC) 169

Figure A.3. Barometric transducer air temperature (recorded at 5-minute intervals) compared to daily mean air temperature measured at the NOAA Local Climatological Data (LDC) 169

Figure A.4. Corrected stage (recorded at 5-minute intervals) at Round Pond Brook 170

Figure A.5. Water temperature (recorded at 5-minute intervals) at Round Pond Brook 170

Figure A.6. Stage-discharge rating curve for Round Pond Brook. 172

Figure A.7. Time series of discharge (Q) at 5-minute intervals for Round Pond Brook 173

Figure A.8. Corrected stage (recorded at 5-minute intervals) at Back Creek B 174

Figure A.9. Water temperature (recorded at 5-minute intervals) at Back Creek B 174

Figure A.10. Stage-discharge rating curve for Back Creek B. 176

Figure A.11. Time series of discharge (Q) at 5-minute intervals for Back Creek B 176

Figure A.12. Corrected stage (recorded at 5-minute intervals) at Mountain Cove Brook 177

Figure A.13. Water temperature (recorded at 5-minute intervals) at Mountain Cove Brook ... 177

Figure A.14. Stage-discharge rating curve for Mountain Cove Brook. 179

Figure A.15. Time series of discharge (Q) at 5-minute intervals at Mountain Cove Brook 179

Figure A.16. Corrected stage (recorded at 5-minute intervals) at Fernald's Brook A 180

Figure A.17. Water temperature (recorded at 5-minute intervals) at Fernald's Brook A 180

Figure A.18. Stage-discharge rating curve for Fernald's Brook A. 182

Figure A.19. Time series of discharge (Q) at 5-minute intervals at Fernald's Brook A 183

Figure A.20. Corrected stage (recorded at 5-minute intervals) at Mile Brook 183

Figure A.21. Water temperature (recorded at 5-minute intervals) at Mile Brook 184

Figure A.22. Stage-discharge rating curve for Mile Brook. 186

Figure A.23. Time series of discharge (Q) at 5-minute intervals at Mile Brook 186

Figure A.24. Corrected stage (recorded at 5-minute intervals) at Pawtuckaway River 187

Figure A.25. Water temperature (recorded at 5-minute intervals) at Pawtuckaway River 187

Figure A.26. Stage-discharge rating curves for Pawtuckaway River. 189

Figure A.27. Time series of discharge (Q) at 5-minute intervals at Pawtuckaway River 189

Figure B.1 Visualization of water and DIN flow paths within a single model grid cell. 191

Figure B.2 Reservoir outflow/storage curves for managed dams 197

Figure B.3 Reservoir outflow/storage curves for unmanaged dams 198

Abstract

The impact of dams on floods and nitrogen flux in the Lamprey River watershed, NH

By

David Simon

University of New Hampshire, December, 2018

Decisions about dam management require weighing many tradeoffs. Among many other factors, dams and their reservoirs can reduce peak flows and retain nutrients that could otherwise cause downstream eutrophication. This study quantifies how dams and their management alter flows and nutrient retention within a coastal New Hampshire watershed. An annual nitrogen budget was estimated at Pawtuckaway Lake, a dammed reservoir within the Lamprey River watershed, through field work. Results showed that annual total dissolved nitrogen (TDN) and dissolved inorganic nitrogen (DIN) retention within Pawtuckaway Lake were close to estimates predicted by an empirical model developed by Seitzinger et al. 2002. A coupled hydrologic and biogeochemical model, the Framework for Aquatic Modeling of the Earth System, was used to estimate flood flows and DIN flux at the watershed outlet. Model results show that dams within the Lamprey River watershed decrease the magnitude of peak flows and reduce seasonal DIN export from the watershed to the coast. Modeling alternative conditions within the watershed shows how climate, land use, and dam management alter flood flow magnitudes as well as seasonal DIN export, suggesting the potential for dams to help mitigate projected climate and land use change within the region.

Chapter 1: Introduction

1.1 Background Information

1.1.1 Dam Removal Tradeoffs

Dams are found in most river networks across the United States and throughout much of the world. In New England alone, there is estimated to be more than 14,000 dams, most of which are small (8 meters high or less), built over a century ago, and are no longer used for their original purpose (Gold et al. 2016). Many dams are now being considered for removal, forcing decision makers to weigh many tradeoffs (Johnson et al. 2002). For example, dams and their reservoirs have the potential to attenuate floods, reduce the severity of droughts, increase water supply, and augment the capacity of river networks to retain or remove nutrients (FiztHugh and Vogel 2011, Richter et al. 2007, Gold et al. 2016), but their presence can prevent fish migration, alter sediment delivery patterns and surface water temperatures, and disrupt natural flow regimes (Larinier et al. 2000, Vörösmarty et al. 2003, Todd et al. 2005, Poff et al. 1997). In addition, dams can also hold historic significance and/or provide economic benefits through hydropower production to local communities (Lejon et al. 2009, Doyle et al. 2003). To choose the most beneficial option regarding a dam, decision makers must be provided with usable information on the array of tradeoffs (Johnson et al. 2002). Although these tradeoffs have been measured for individual dams, the cumulative effect and interplay of these tradeoffs for a hierarchical network of dams within a watershed is less well known but could be particularly useful for watershed and coastal management planning and river restoration strategies (Zimmerman et al. 2010, Craig et al. 2008).

1.1.2 Tools Used to Quantify Dam Removal Tradeoffs

Models are a simplified representation of a naturally occurring process (Sharma 2008), and hydrologic models aim to simulate hydrologic processes. Simple empirical hydrologic

models have been used to aid decision-making about water resources (Boyer et al. 2006, Guswa et al. 2014, Caldwell et al. 2015) and how dams impact flood magnitudes (FiztHugh and Vogel 2011) and frequencies (Ayalew et al. 2013). Models can differ in terms of their structure, parameters, calibration, and ideal spatial and temporal applications (Caldwell et al. 2015). The watershed scale is appropriate for the assessment of a network of dams, and in fact the watershed/dam network scale has been successfully used to aid dam decision making in the past (Opperman et al. 2011). Hydrologic models have been used as tools to inform and complement ecosystem service evaluations, such as those provided by dams, through scenario analysis (Guswa et al. 2014). Models have also been used with projections of future climate from global climate models to forecast how the hydrology and nutrient retention within a catchment might respond to climate and land use change (Campbell et al. 2011). However, different model structure and different calibration methods can lead to different interpretations of climate change impacts; therefore, sensitivity and uncertainty analyses are warranted (Mendoza et al. 2016). Gaps in spatial data and process simulation capacity, such as stationarity of underlying model processes, underscore the need for complementary field measurements to improve confidence and quantify uncertainty with model estimates through site-specific analysis (Boyer et al. 2006, Dietrich et al. 2003).

1.1.3 Effects of Dams on Flood Peak Attenuation

High magnitude river flow events (flooding events) have important anthropological ramifications as they are the most frequent and costly natural disaster in the U.S. (Lightbody 2017) and result in an average of 85 fatalities annually (NOAA 2014). The economic benefits of flood attenuation by dams have been estimated by the US Army Corps of Engineers at $706 billion nationwide since 1935 (USACE-IWR 2000).

Dams have been shown to alter flow regime characteristics of rivers, including flooding events, by decreasing flood peak magnitudes downstream of an impoundment as compared to

a free-flowing river channel (Poff et al. 1997, Magilligan & Nislow 2005). Many dam characteristics determine the magnitude of incoming flood peak attenuation including reservoir capacity at the time of the surface flow inputs, the release capacity of the dam's outlet structure, and the management of the dam (Ayalew et al. 2013). Dam management can also lead to flooding downstream; for example, flooding as a result of a large volume of water released at the Ripongenus Dam on the Penobscot River in Maine in the spring of 2017 (Waterline 2017).

1.1.4 Modeling Hydrologic Alteration by Dams

Hydrologic alteration by dams has been previously quantified by pre-dam post-dam statistical analysis (FiztHugh and Vogel 2011). However, a lack of pre-dam stream flow data limits this approach in many locations, especially in New England where many dams pre-date the start of discharge records. Hydrologic modeling provides a tool to explore hydrologic alterations by dams while avoiding constraints such as data limitations. In addition, although the hydrologic impact of a single large dam has been studied (Magilligan & Nislow 2001), the cumulative effect of a network of dams of varying sizes is less well known (Melis et al. 2011, Ayalew et al. 2017). Hydrologic modeling of a network of small dams has been shown to reduce daily peak flows within a watershed (Lui et al. 2014, Ayalew et al. 2017). Dams can be managed for many different purposes, such as flood control or water supply. Some models incorporate specific management decisions about how much flow to release (Hirsch 1981, Lui et al. 2015). Other models represent dam management using operating rules, in which reservoir release is a function of reservoir water storage (Grogan et al. 2017). Previous modeling has confirmed that varied dam operations can affect flood frequencies downstream (Ayalew et al. 2013) and how a dam's location within a watershed impacts flood peak attenuation (Ayalew et al. 2015).

1.1.5 River Network Nitrogen Retention

Anthropogenic land use, such as fertilizer application, forest clearing, and increased impervious surfaces, has greatly contributed to an increase in nutrient loading to freshwater

systems worldwide and will likely continue to increase in future years (Vitousek et al. 1997). Nutrients, such as nitrogen (N) and phosphorus (P), limit primary productivity in aquatic ecosystems; therefore, excessive loading, also known as eutrophication, can lead to harmful algae blooms and hypoxia and as a result poses a threat to water quality and aquatic organisms within a river network and in the coastal areas downstream (Anderson et al 2002). Unlike lakes, where primary production is typically phosphorus (P) limited, primary production in coastal marine ecosystems is frequently limited by N, in part due to differences in N fixing microbes and N:P ratios (Howarth and Marino 2006). Therefore, it is important to estimate and if possible reduce riverine delivery of N to coastal waters (Filoso and Palmer 2011, Craig et al. 2008).

However, through physical and biological processes, a sizable portion of these nutrient inputs are removed or retained within a watershed through both terrestrial and aquatic retention (in some cases over 90% of terrestrial N inputs were retained as estimated by Daley et al. 2010), which provides an important ecosystem service to mitigate eutrophication at receiving waterbodies downstream (Boyer et al. 2002). Aquatic N retention ($\mathrm{N_R}$) is defined as a fractional difference between mass fluxes of N loaded to ($\mathrm{N_{inputs}}$) and leaving ($\mathrm{N_{outputs}}$) a water body and can be scaled from a single reservoir or stream reach to an entire river network.

$$\mathrm{N_R} = \frac{(\mathrm{N_{inputs}} - \mathrm{N_{outputs}})}{\mathrm{N_{inputs}}} \qquad \text{Equation 1.1}$$

Aquatic N retention within a waterbody has been quantified through N mass balance methods that estimate all N inputs and N outputs (Burns 1998, David et al. 2006). N inputs include N loading from inflowing upstream tributaries, overland runoff, direct atmospheric deposition to the water surface, groundwater inflow, and N released from benthic sediment. Total atmospheric N deposition includes both wet N deposition, the amount of dissolved N contained in rain and snow that are deposited during precipitation events, and dry N deposition, the amount of N

deposited via aerosols and dust during no precipitation. N outputs include N flux leaving as outflow downstream or groundwater outflow.

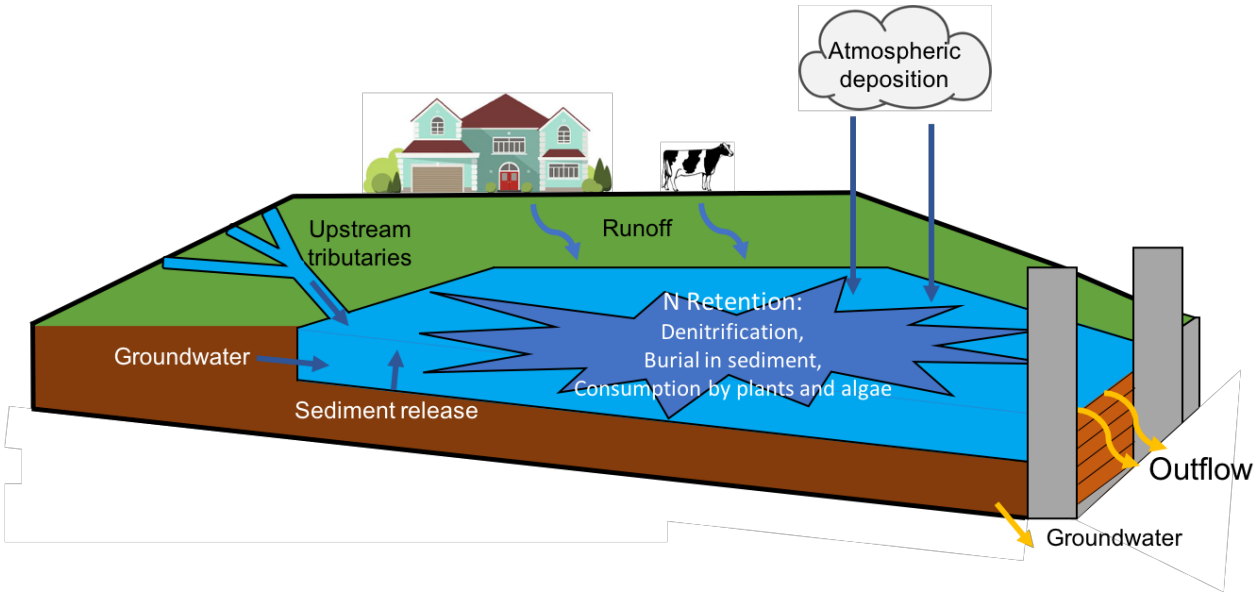

Figure 1.1 A representation of a reservoir and all pathways of N inputs (blue arrows), N outputs (orange arrows), and N retention (the difference between N inputs and N outputs).

N retention includes both temporary sinks such as assimilation into plant tissues by algae and macrophytes and burial in sediment, and permanent ones such as denitrification (Figure 1.1). Denitrification, the process by which anaerobic bacteria reduce nitrate (NO_3^-) or nitrite (NO_2^-) to nitrogenous gas (N_2 or N_2O), has been shown to be the largest contributor to total N retention in aquatic systems (Seitzinger et al. 1998, Saunders and Kalff 2001). Biotic uptake only accounts for a small portion of total N (Hill 1979); however, the presence of plants indirectly increases N retention by promoting denitrification through the production of organic carbon and by slowing stream velocities creating localized areas of increased residence times and sedimentation rates (Howard-Williams 1983, Hill 1986).

1.1.6 Effects of Dams on River Network N Retention

Lentic systems, such as wetlands, lakes, reservoirs, and beaver ponds are especially important sinks for N (Powers et al 2014, Cheng et al 2017, Lazar et al. 2015), as anoxic

benthic conditions, abundant organic material storage, and increased residence times allow for more N retention compared to a free-flowing river channel (Seitzinger et al. 2002). Even though reservoirs only make up a small fraction of the surface area of these systems, they have been estimated to contribute as much as one third of all total N retention from lentic systems (Harrison et al 2009). Increased residence times of reservoirs allow for more opportunity for dissolved N to interact with benthic substrates, where most denitrification occurs, and allows organic matter to settle (McClain et al. 2003). The buildup of organic matter also provides energy, i.e. carbon, for microbes to immobilize inorganic N as well as denitrify N (Bernhardt and Likens 2002). In addition, temperate reservoirs are usually dimictic, which further promotes denitrification in suboxic and anoxic zones during stratification (Seitzinger et al 2006).

1.1.7 Modeling N Retention

To model denitrification, simple empirical models using hydrologic parameters and first order N retention rates have been shown to be appropriate at both a reservoir and watershed scale over annual time periods (Alexander et al. 2000, Seitzinger et al 2002, Cheng et al. 2017). One such model, RivR-N (Seitzinger et al 2002), relates the fraction of N retained ($\mathrm{N_R}$) within rivers, lakes, and reservoirs to the ratio of mean depth (d) and hydraulic residence time (τ).

$$\mathrm{N_R} = 88.453 \cdot \left(\frac{d}{\tau}\right)^{-0.3677} \qquad \text{Equation 1.2}$$

Kellogg et al. (2010) modified this relationship to only include data from lakes and reservoirs and Gold et al. (2016) used this relationship along with geospatial data to estimate N retention within over 2,000 New England reservoirs.

Another empirical water-quality model SPARROW (spatially referenced regression on watershed attributes; Smith et al. 1997, Alexander et al. 2000), relates mean annual total N (TN) loading to watershed characteristics and uses a flow-dependent reaction rate to estimate long term TN loss, loading, and flux within watersheds under mean annual flow conditions and has

been applied to the northeastern United States (Moore et al. 2004). SPARROW represents the fraction of TN removed within reservoirs (S_R) as a first-order reaction rate,

$$S_R = \frac{1}{1+\theta_R \cdot (q_R)^{-1}} \quad \text{Equation 1.3}$$

where θ_R is the settling velocity coefficient [L T^{-1}] and q_R is the areal hydraulic load [T L^{-1}].

Reactive N tracer studies also have shown that N retention rates saturate at higher N concentrations (Mulholland et al. 2008). The FrAMES model (the Framework for Aquatic Modeling in the Earth System; Wollheim et al 2008) is a deterministic river network N removal model, using non-linear reaction rates, and has been used to show that river networks become less efficient at removing N at higher flows.

1.1.8 Effect of Climate Change on Flooding and N Fluxes

Climate change brought about by anthropogenic activities is projected to increase annual average precipitation, as well as the frequency of extreme precipitation events that cause flooding and extreme droughts, in the New England region over the next century (Hayhoe et al. 2007, Collins et al. 2009). This increase in very wet and dry periods is expected to change both short- and long-term N storage and flux cycles within watersheds, as changes in both discharge and in-stream N concentration will alter N fluxes (Howarth et al. 2006). In addition, rising winter temperatures will result in a decrease in the amount of winter snowpack and thus change the timing and magnitude of high spring flows resulting from snow melt and groundwater recharge (Hodgkins et al. 2003, Campbell et al. 2011). Wetter conditions and rising temperatures are also expected to increase evapotranspiration and decrease overall stream flow (Huntington et al. 2003). Warmer winters will also result in more precipitation falling as rain and will increase the amount of rain on snow events, which has been shown to be a significant source of annual N loading to streams (Crossman et al. 2016). The extent to which a network of

dams within a watershed could mitigate flooding and N fluxes associated with projected climate change is unclear.

1.1.9 Effect of Land Use Change on Flooding and N Fluxes

Populations are projected to increase in the northeast and will result in a subsequent increase in urban and agricultural land use (Thorn et al. 2017). Since urban, suburban, and agricultural areas load more N to streams than forests (through septic leaching, pet waste, and fertilizer application; Meyer et al. 2005, Jordan et al. 1997) this will inevitably increase N loads to aquatic systems. This will result in more N being retained, but less efficiently (Mullholland et al. 2008). Also, increases in impervious surfaces produce more overland runoff and shorter runoff routing times to the drainage network (pipes, swales, streams) where conveyance is most efficient in the landscape streams, thus altering streamflow response, which can result in more flooding (Lane et al. 2003). Modeling the watershed under future land use projections with and without dams provides a framework to understand how dams and their reservoirs could alleviate some of these adverse changes such as increases in N loading and changes in hydrology as a result of projected changes in land use.

1.2 Lamprey River Watershed Site Description

1.2.1 Watershed Overview

The Lamprey River watershed is located in Rockingham and Strafford counties in southeastern New Hampshire. Like other smaller coastal New England watersheds, it contains multiple active dams, with reservoirs of varying size and management, along the lower river mainstem and within its headwaters. At 549 km^2 (NHDES 2013), it is the largest sub-watershed in the larger Piscataqua Region watershed, which drains to Great Bay and Portsmouth harbor. The Lamprey River originates near Saddleback Mountain in the town of Northwood, then flows 75.6 km through the towns of Deerfield, Raymond, Epping, Lee, and Durham to the head of tide dam, the Macallen Dam, in Newmarket. Major tributaries include the North Branch River,

Pawtuckaway River, North River, Little River, and Piscassic River (Figure 1.2). Maximum elevation within the watershed is 348 meters at Saddleback Mountain and minimum elevation is sea level at the watershed outlet (Figure 1.3). Underlying subsurface geology within the watershed is composed mostly of glacial till, sand, and gravel, which is typical for coastal New England.

1.2.2 Impact on Great Bay

The Great Bay Estuary's tidal waters span an area of 53.4 km^2, and it is one of 28 estuaries established under the Environmental Protection Agency's (EPA) National Estuary Program as being "estuaries of national significance" (EPA 1989). The Piscataqua Region Estuaries Partnership (PREP) has estimated that the Lamprey River watershed is the largest average annual contributor of non-point source total N (TN; 172.17 metric tons yr^{-1}) and dissolved inorganic nitrogen (DIN; 54.21 metric tons yr^{-1}) loading to Great Bay (PREP 2012). Due in part to river N loading from both point and nonpoint sources, levels of DIN have increased in Great Bay over the past thirty years, and Great Bay has recently been declared impaired for nitrate (PREP 2018). As a result, native eel grass habitat has decreased and invasive macroalgae growth has increased, leading to decreases in dissolved oxygen and loss of biodiversity (PREP 2018). Recent measurements have shown a 26% decrease in average annual TN loading to Great Bay from 2012 to 2016 as compared to 2009 through 2011, primarily as a result from improvements to wastewater treatment plants within the upstream watershed and consecutive years of low annual rainfall, which results in less non-point source loading from runoff (PREP 2018). Reducing river N loading to Great Bay is an ongoing regional challenge. Due to the ecological and societal values provided by estuaries like Great Bay, it is important to study watersheds on the scale of the Lamprey River watershed (Anthony et al. 2009).

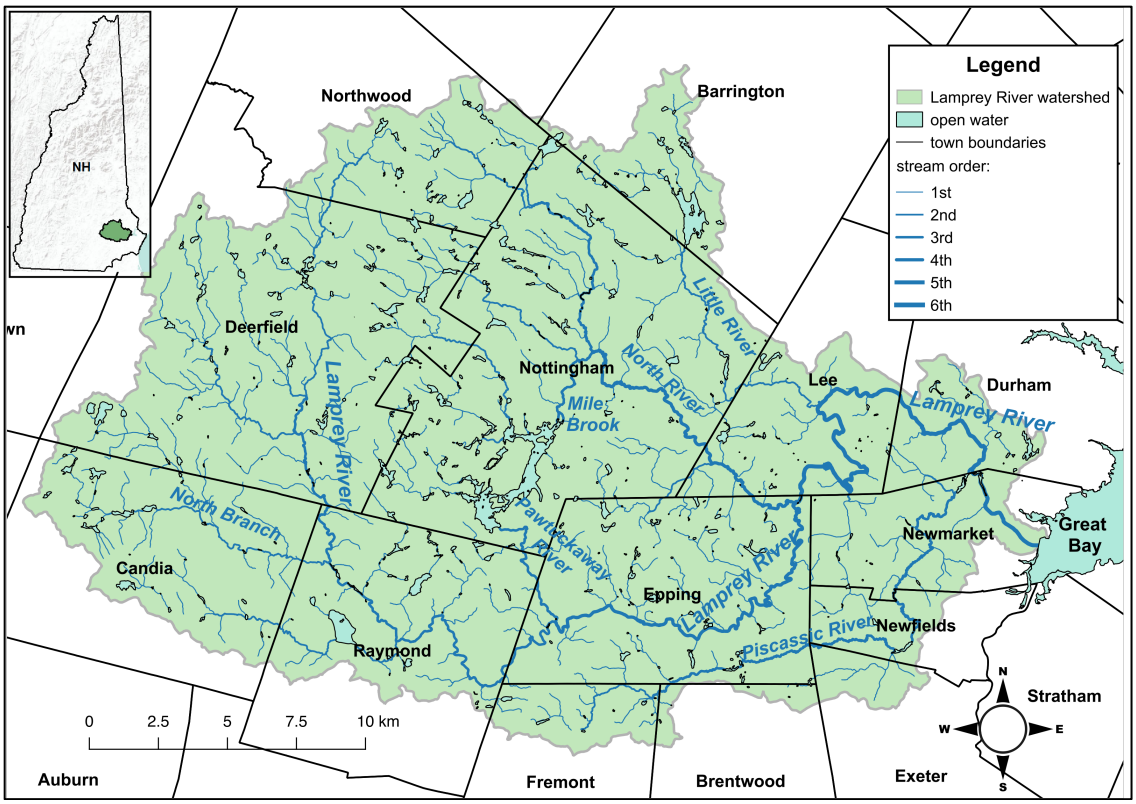

Figure 1.2 Map of the Lamprey River watershed showing major tributaries and town boundaries.

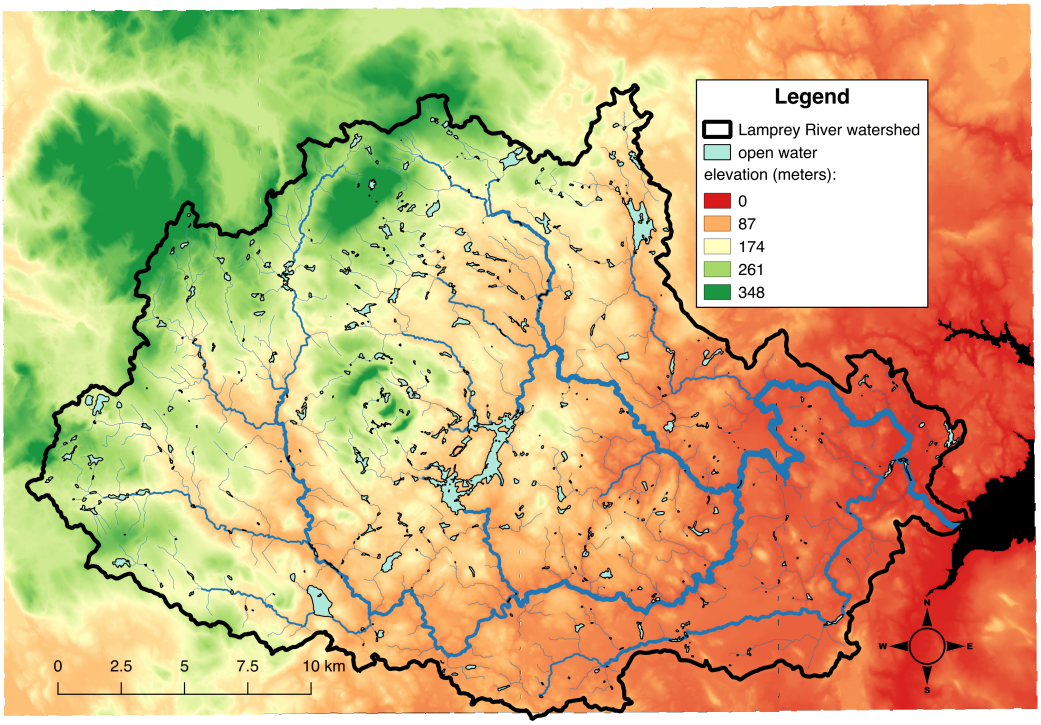

Figure 1.3 Digital elevation model (at 30-meter resolution) of the Lamprey River watershed. Source: NH GRANIT Database.

1.2.3 Watershed Management Plan and Instream Flow Policy

In 1990, the state of New Hampshire designated 19.4 km of the Lamprey River's lower mainstem (starting near the confluence of the North River in Lee and ending upstream of the Macallen Dam in Newmarket) under the Rivers Management and Protection Program. This state designation was expanded in 2011 to include the entire Lamprey River mainstem and five major tributaries (NHDES 2013). In 2013, a new watershed management plan for the Lamprey River went into effect and established an instream flow policy. This policy was designed to maintain natural river flows, defined by the Lamprey River Instream Flow Report (NHDES 2009), along the designated river reach to protect ecological and human uses. The policy affects both water users that withdraw directly from the river and dam owners upstream.

Affected dam owners are defined as owners of a dam upstream of the designated reach whose reservoir has a surface area greater than ten acres (0.04 km^2), which currently includes 19 dams within the watershed (Table 1.1). However, the New Hampshire Department of Environmental Services (NHDES) has decided only to regulate outflow from the two largest reservoirs, Pawtuckaway Lake or Mendum's Pond. Therefore, during prolonged periods where instream flows are insufficient along the designated reach, a relief pulse is released at either Dolloff Dam or Drowns Dam on Pawtuckaway Lake or Mendum's Pond Dam over a 48-hour period to simulate a typical small storm event within the watershed (NHDES 2013).

Affected water users are municipalities or businesses that withdraw or return water within 500 feet of the designated reach and include the Durham–UNH water system, which withdraws water upstream of Wiswall Dam in Durham; Epping Water Works; Raymond Water Department; and Scenic Nursery Inc. in Raymond. Active water users are required to curtail withdrawal from the river and use alternative sources when streamflow falls below critical thresholds during summer and fall months. In addition to the state's protection, 37.7 km of the

lower Lamprey River is also protected under the federal government's Wild and Scenic designation that promotes river management and prohibits the construction of new dams.

Table 1.1. Database of dams and reservoir attributes within the Lamprey River watershed.

Dam Name	Source	Dam Type	Outlet Structure Type	Longitude	Latitude	Maximum Storage [10^6 m^3]	Drainage Area [km^2]	Surface Area [km^2]	2-yr Storm Runoff Volume to Reservoir Storage	Notes
DOLLOFF DAM	NID	Recreation	Spillway & stop logs	-71.154	43.0708	10.1	16.2	1.10	0.041	
DROWNS DAM	NID	Recreation	Spillway & stop logs	-71.1252	43.1072	4.32	37.8	2.54	0.226	
MENDUMS POND DAM	NID	Recreation	Spillway & stop logs	-71.0686	43.1627	4.10	17.95	1.07	0.113	
NORTH RIVER POND DAM	NID	Recreation	Spillway & stop logs	-71.1316	43.1925	0.441	3.40	0.323	0.199	
ONWAY LAKE DAM	NID	Recreation	Spillway & stop logs	-71.2158	43.0344	1.08	21.76	0.776	0.520	
BUNKER POND DAM	NHDES	Run-of-river	Spillway	-71.1297	43.0405	0.148	197.83	0.117	34.461	Removed (2011)
MACALLEN DAM	NID	Run-of-river	Spillway & sluice gates	-70.9347	43.0811	2.14	543.54	0.485	6.548	
DEER POND DAM	NHDES	Run of river	Spillway	-71.2002	43.0863	0.214	1.57	0.153	0.189	
WISWALL DAM	NID	Run-of-river	Spillway	-70.9625	43.104	0.616	471.41	0.121	19.730	
FREESES POND DAM	NID	Run of river	Spillway & stop logs	-71.2344	43.1502	0.532	22.10	0.223	1.071	
MEADOW LAKE DAM	NHDES	Run-of-river	Spillway	-71.208	43.2022	0.129	1.21	0.068	0.242	
NOTTINGHAM LAKE DAM	NHDES	Run of river	Spillway	-71.0508	43.1197	0.328	37.56	0.165	2.952	
DOLE MARSH DAM	NHDES	Run-of-river	Spillway	-71.1891	43.1741	0.128	1.33	0.101	0.268	
SOCHA DAM	NHDES	Run of river	Spillway	-71.3144	43.0777	0.111	11.32	0.121	2.630	
SAULS POND	NHDES	Run-of-river	Spillway	-71.1776	43.1809	0.157	0.43	0.032	0.071	
BEAVER POND DAM	NHDES	Run of river	Spillway	-71.3286	43.1066	0.082	2.30	0.202	0.723	
LUCAS POND DAM	NHDES	Run-of-river	Spillway	-71.1629	43.1821	0.113	2.60	0.161	0.593	
PISCASSIC ICE POND DAM	NHDES	Run of river	Spillway	-70.9679	43.0342	0.134	35.95	0.055	6.917	
PISCASSIC RIVER DAM	NHDES	Run-of-river	Spillway	-70.9478	43.08262	0.298	61.42	0.143	5.314	
THURSTON POND DAM	NHDES	Run of river	Spillway	-71.2959	43.1379	0.053	3.16	0.054	1.537	
WOODMAN MARSH DAM	NHDES	Run-of-river	Spillway	-71.1799	43.17116	0.151	2.71	0.027	0.463	
HOAR POND DAM	NHDES	Run of river	Spillway	-71.0863	43.04805	0.080	1.35	0.105	0.435	
WADLEIGH FALLS DAM	NHDES	Run-of-river	-	-71.0066	43.0913	-	395.66	0.117	-	Breached

1.2.4 Dams

According to the National Inventory of Dams (NID) and NHDES, the 22 active dams (Table 1.1, Figure 1.4) located within the Lamprey River watershed range in height from 1 to 10 m and are mostly privately owned (NID 2013, NHDES 2013). There are two run-of-river dams, Wiswall Dam and Macallen Dam, located along the river's lower mainstem and one breached dam, Wadleigh Falls Dam, in Lee. The Bunker Pond Dam, which was located along the mainstem in west Epping, was removed in 2011. The Macallen Dam has been recently considered for removal by the town of Newmarket. It received a letter of deficiency by NHDES in 2010 because it was identified as lacking the required spillway capacity to safely pass the 100-year flood, which is expected to increase in frequency due to increasing urbanization and climate change (Wake et al. 2010). The Macallen Dam was also labeled as a high-risk dam because if the dam were to fail, there is the possibility for loss of human life downstream (NHDES 2014). From Fall 2015 to Spring 2017, Mendum's Pond in Nottingham was emptied, and the Mendum's Pond Dam was completely overhauled to prevent seepage and potential failure.

There are currently seventeen passively managed run-of-river dams that account for up to 5.4 x 10^6 m^3 of storage capacity and five dams that are actively managed for recreational activities, which include an annual fall drawdown, and account for up to 20.1 x 10^6 m^3 of storage capacity (Table 1.1, Figure 1.4). Four dams are actively managed by NHDES Water Resources Division: Mendum's Pond Dam and North River Pond Dam in Barrington and the two dams impounding Pawtuckaway Lake in Nottingham. The fifth actively managed dam, Onway Lake Dam in Raymond, is privately owned and operated by the town. Active management of these five dams includes the placement and removal of stop logs or the opening and closing of gates in the dam outlet structure to control reservoir water level. During the recreation season (late spring to early fall), water level is kept high to promote fishing, boating, and swimming. Water

level is then lowered during a fall drawdown and kept at a lowered state to prevent the buildup of ice on docks during the winter, to control macroalgae, and to allow for increased reservoir storage to mitigate flooding resulting from winter storms and spring thaw (Figure 1.5). Many recreation lakes across New England are managed similarly making these sites representative of other reservoirs in other watersheds.

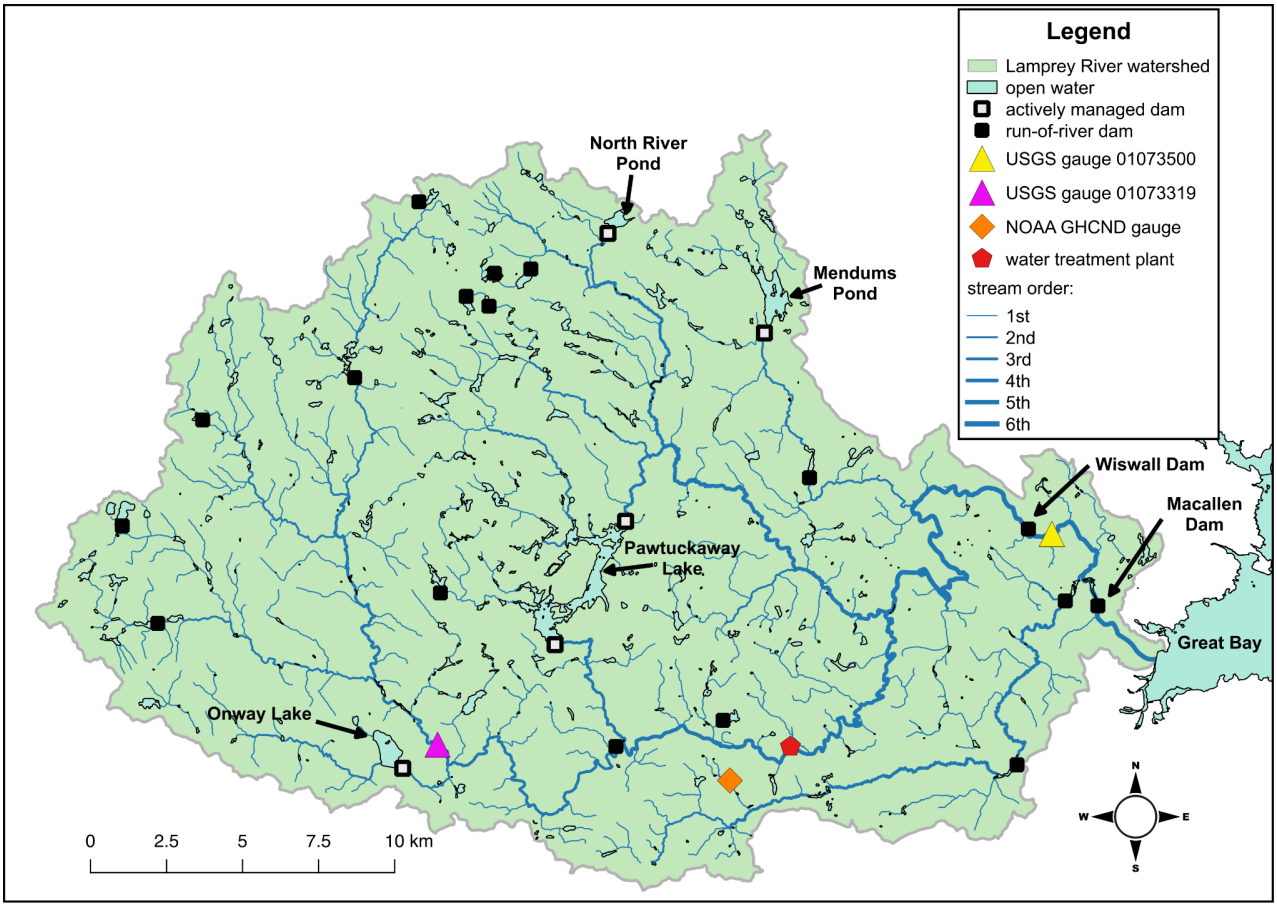

Figure 1.4 Map of the Lamprey River watershed showing run-of-river dams, actively managed recreation dams, major reservoirs, the NOAA weather gauge, two USGS discharge gauges, and the waste water treatment plant in Epping.

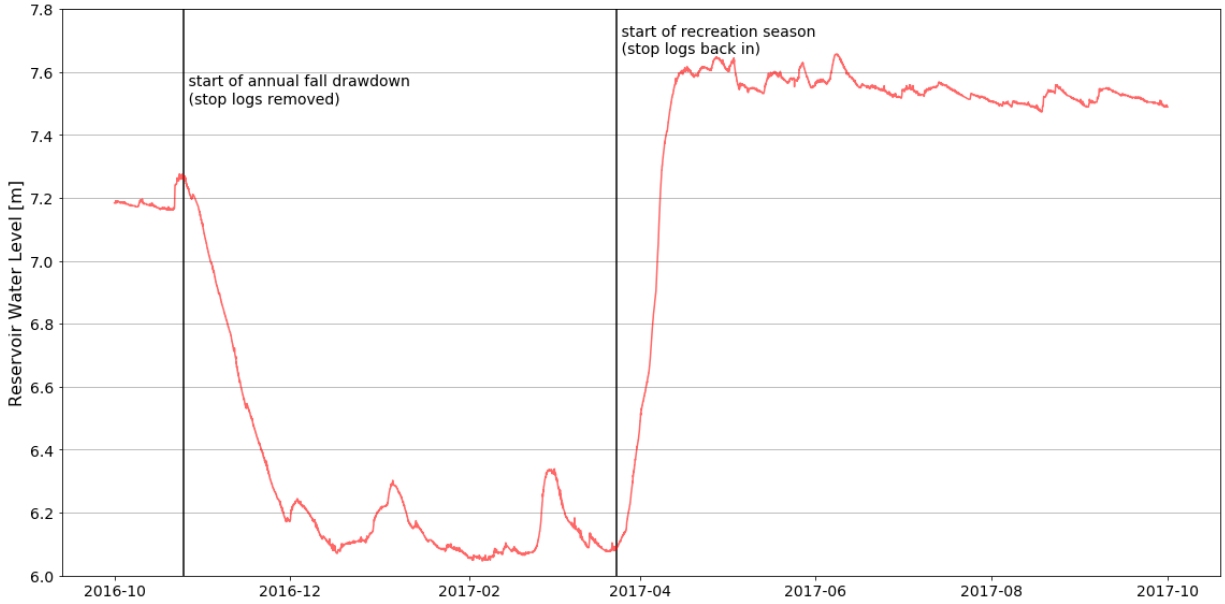

Figure 1.5 Example of dam management at Pawtuckaway Lake, showing changes in water level recorded at the NHDES station above Dolloff Dam (station name PAWNH) for water year 2017.

1.2.5 Historic Land Cover and Population

Human population has nearly doubled within the Lamprey River watershed over the past 50 years (Table 1.2); as a result, human development and impervious surfaces have increased by 9.9% and 3.2% respectively (Table 1.3). The upper watershed is characterized by low population density, rural development, and abundant forests, while the lower watershed has more development along the lower main stem of the river in the towns of Raymond, Epping, and Newmarket (Figure 1.6). Agricultural land cover, which consists mostly of cattle pastures, has remained relatively constant at approximately 7% over the past thirty years (Table 1.3). Human land use distribution (developed + agricultural) has a skewness index of 0.91 (Mineau et al. 2015), where a value of less than 1 indicates human land use is skewed toward the watershed outlet. This indicates that N loaded into the river network from human land use is on average closer the watershed outlet and therefore more likely to enter to Great Bay.

Table 1.2 Historic human population in the Lamprey River watershed. Source: EPSCoR NHLC 2015.

Year	1960	1970	1980	2003	2015
Population	21,257	28,022	36,905	38,163	39,386

Table 1.3 Historic land cover of the Lamprey River watershed. Source: EPSCoR NHLC 2015.

	Land Cover					
Year	Agriculture (%)	Development (%)	Impervious (%)	Forest (%)	Water (%)	Wetland (%)
1960	6.3	2.5	0.2	75.5	1.8	13.9
1970	4.4	3.7	0.4	76.1	1.8	13.9
1987	6.7	9.1	2.0	68.5	1.8	13.9
2000	6.9	10.7	2.9	66.6	1.8	13.9
2006	7.0	11.1	3.0	66.2	1.8	13.9
2015	7.0	12.4	3.4	64.9	1.8	13.9

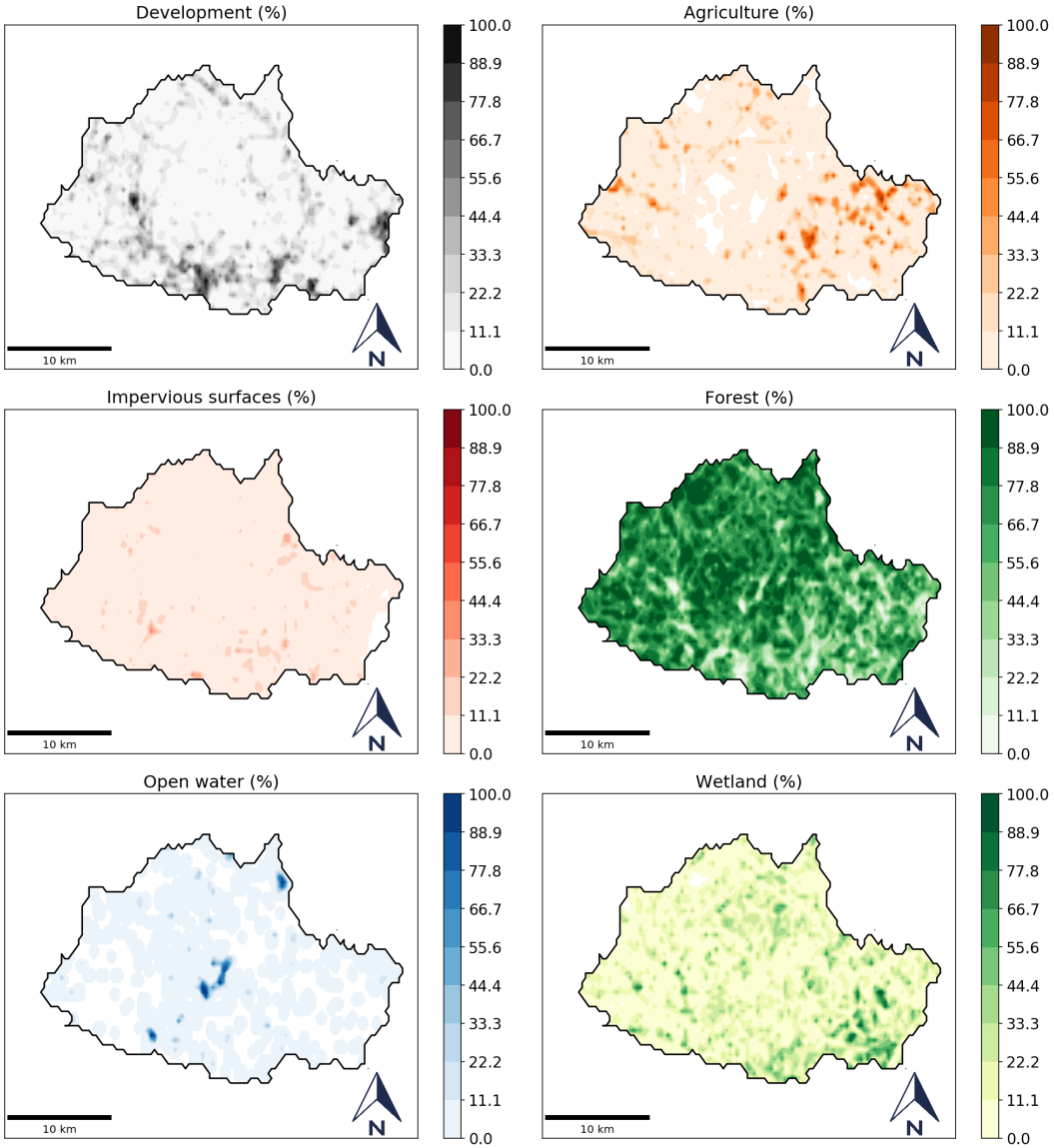

Figure 1.6 Land cover of the Lamprey River watershed for year 2015. Source: EPSCoR NHLC 2015.

1.2.6 Historic Climate and Flooding

Historic measurements of precipitation and temperature have been recorded since 1963 at the National Oceanic and Atmospheric Administration's (NOAA) meteorological station in Epping (Global Historic Climatology Network (GHCN) station USC00272800 in Epping; Figure 1.4). Over the past 50 years, annual temperature and precipitation have averaged 8.5 °C and 1130 mm respectively and have both shown an increasing trend over the past century (Hayhoe et al. 2007). Rainfall intensity has also increased within this time period as the magnitude of the 100-year rainfall event increased from 6.3 inches to 8.5 inches (NRCC and NRCS 2012).

Historic measurements of discharge have been recorded at the two United States Geologic Survey's (USGS) gauges located within the watershed: USGS gauge 01073319 at Langford Rd. in Raymond, which has been active since 7/4/2018 and drains 144 km^2 of the upper watershed, and USGS gauge 0173500 at Packer's Falls near Newmarket, which has been active since 7/24/1934 and drains 474 km^2. Since 1935, annual mean runoff at Packer's Falls has been 508 mm, most of which comes in the months of March, April, and May (Figure 1.7). Large flood events are becoming more frequent: three of the four highest flows measured at the Packer's Fall gauge have occurred within the past 12 years, two of which were 100-yr flood magnitudes (May 2006 and April 2007) and the other a 50-yr flood magnitude in March 2010 (Wake et al. 2013).

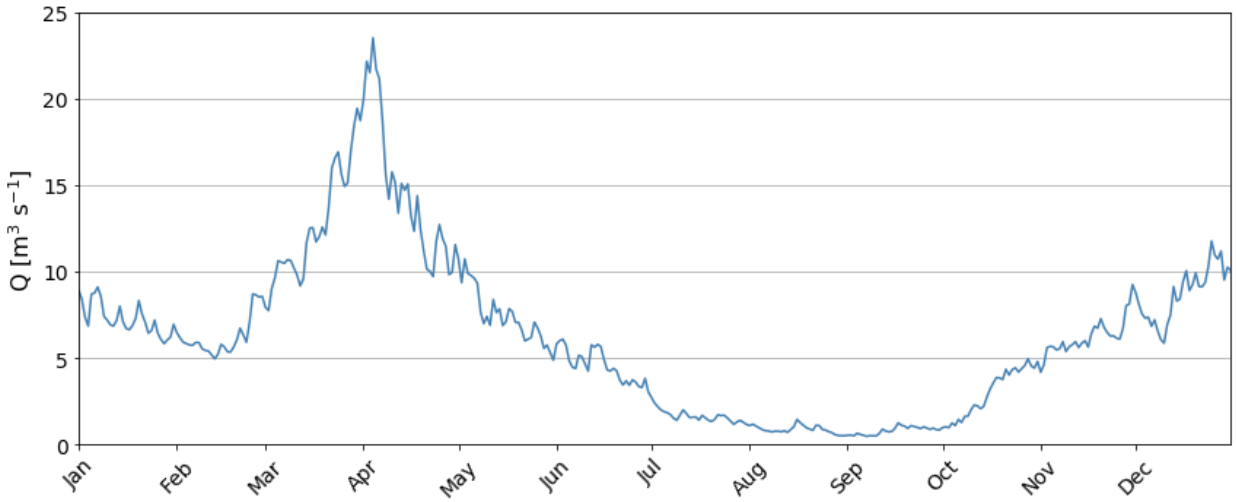

Figure 1.7 Median daily discharge of the Lamprey River recorded at USGS gauge 01073500 for day of the year over water years 2000 to 2015.

1.2.7 Historic Nitrogen Flux

Water quality has been measured extensively throughout the Lamprey River watershed by organizations such as the Water Resources Research Center at UNH (WRRC) and the Lamprey River Watershed Association. Continuous water monitoring by the WRRC includes grab samples taken at weekly to monthly intervals both in the headwaters and along the mainstem and has provided insight into nitrogen transport within the Lamprey River. Measurements taken at USGS gauge 01073500 from water years 2010 to 2016 show that total dissolved nitrogen (TDN) is the largest fraction of total nitrogen (TN) within the Lamprey River (approximately 87%), suggesting that particulate nitrogen plays a limited role (WRRC). TDN can be categorized further as either being dissolved organic nitrogen (DON) or dissolved inorganic nitrogen (DIN); within the Lamprey River, approximately half of TDN is DIN (WRRC). DIN-N is made up of ammonium (NH_4^+), nitrite (NO_2^-), and nitrate (NO_3^-), 98% of DIN-N in the Lamprey is NO_3^-N (WRRC). The annual median concentration of NO_3^- varies from 0.07 to 0.16 mg/L, while the annual median concentration of DIN varies from 0.09 to 0.19 mg/L on the mainstem (WRRC). Daily DIN and DON concentration vary throughout the year with the highest prolonged DIN concentrations occurring in winter and highest prolonged DON concentrations occurring in

summer and early fall (Figure 1.8). Daily DIN flux was calculated through the product discharge (expressed as a daily volumetric rate) and DIN concentration. Similar to DIN concentration, DIN flux is greatest during the late winter/early spring season while DON flux is greatest in late spring and late fall (Figure 1.9).

A recent study using high-frequency in-situ nitrate sensors deployed at four headwater locations of varying land use within the Lamprey River watershed found that the concentration and flow response of nitrate at headwater sites are highly dependent on the amount of developed and agricultural land that exist upstream (Koenig et al. 2017). Following storm events, instream nitrate concentration increased with increased flow at a heavily forested headwater site, while concentration diluted for headwater sites with more human land development and along the Lamprey River mainstem. This concentration-discharge dilution response was found to be greatest during the growing season for headwaters and not found to vary seasonally for the Lamprey mainstem. Developed headwater sites in the neighboring Oyster River watershed also exhibited a similar nitrate response to storm events (Wollheim et al. 2017).

There is also a wastewater treatment plant (WWTP) within the watershed in Epping (Figure 1.3) that discharges 1860 kg of DIN into the Lamprey River per day on average (EPA 2012).

Figure 1.8 Median dissolved inorganic nitrogen (DIN) and dissolved organic nitrogen (DON) concentration on the Lamprey River at USGS gauge 01073500 for day of the year over water years 2000 to 2015. Measurements were collected through weekly grab samples obtained by the WRRC at UNH and linearly interpolated to daily estimates.

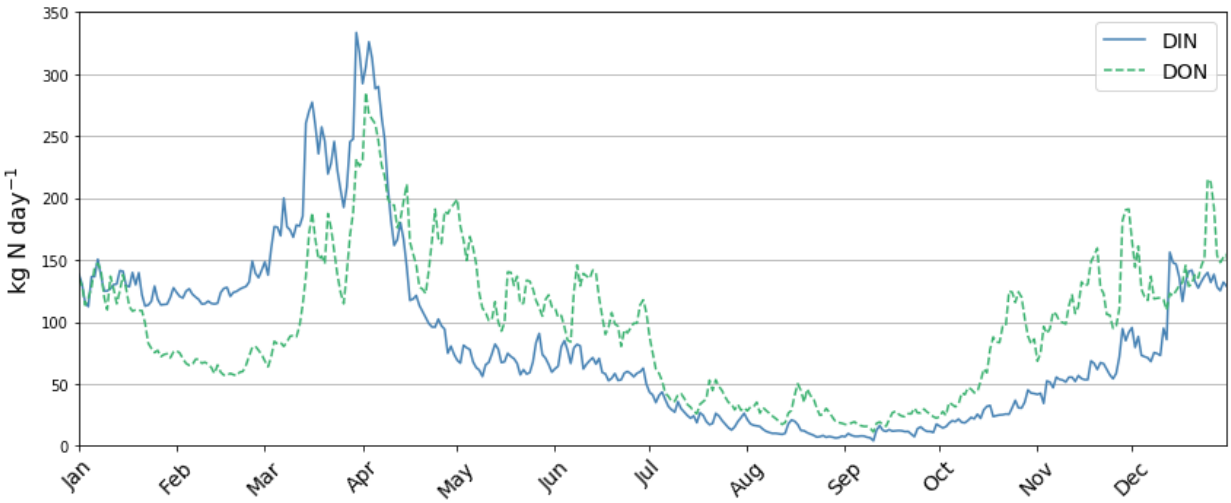

Figure 1.9 Median dissolved inorganic nitrogen (DIN) and dissolved organic nitrogen (DON) flux (calculated by multiplying discharge and concentration for each day) on the Lamprey River at USGS gauge 01073500 for day of the year over water years 2000 to 2015.

1.2.8 Historic Fish Runs

The Lamprey River provides spawning habitat to many diadromous fish species and currently boasts the largest alewife run in New Hampshire (NH Fish and Game 2015). Sea lamprey, Atlantic salmon, blueback herring, and American shad have also been documented entering and leaving the watershed (NH Fish and Game 2015). Both Macallen Dam and Wiswall

Dam have fish ladders that allow for fish passage upstream of the dams, however the natural falls at the breached dam at Wadleigh Falls prevents fish migration further up the Lamprey mainstem. Of the 60,000 to 90,000 Alewife in the annual fish run, 8,000 to 9,000 are collected by NH Fish & Game and are transferred to the Merrimack River as a donor population and an additional 500 to 1,000 are stocked at Pawtuckaway Lake annually (NH Fish and Game 2015). This migration of fish to and from the Lamprey River watershed adds another potential source of N flux to and from reservoirs.

1.3 Research Objectives

This study quantified two important tradeoffs that dams and their reservoirs provide: attenuation of floods and increased N retention within the Lamprey River watershed. This study focused on the following questions:

(1) can N retention within a New England reservoir be predicted accurately using simple empirical models?
(2) how does a dam network influence the frequency and magnitude of high-flow events downstream?
(3) how does a dam network influence in-stream nutrient retention at a watershed scale?
(4) can a network of dams mitigate changes in hydrology and increases in N loading as a result of future climate and land use change?

Using a mass balance approach, N retention was measured at a dammed reservoir (Pawtuckaway Lake; Figure 1.3) within the Lamprey River watershed over an annual time period (5/19/17 – 5/18/18). Field estimates of N retention were compared to empirical model estimates utilized in watershed scale modeling (Seitzinger et al. 2002). The FrAMES model (Wollheim et al. 2008) was used to simulate changes in flood peak magnitudes and frequencies and seasonal N flux associated with different climate, land use, and dam management

scenarios over twenty-year periods in the Lamprey River watershed. Results of this research will potentially be used to improve future dam tradeoff assessments.

Chapter 2: Field Methods

2.1 Pawtuckaway Lake Site Description

2.1.1 Watershed and Reservoir Overview

Pawtuckaway Lake is a dammed reservoir located in the town of Nottingham, New Hampshire. With a surface area of 3.6 km^2 and a full pond capacity of approximately 14 million cubic meters, it is the largest water body in the Lamprey River watershed. Pawtuckaway State Park, located along the lake's western shoreline, is one of the most popular parks in New Hampshire and Pawtuckaway Lake is frequented by boaters, swimmers, and fishermen.

NHDES has identified Pawtuckaway Lake as a dimictic lake that experiences thermal stratification during the summer and mixes completely during a spring and fall overturn (NHDES 1995). The reservoir's bathymetric profile shows that lake depth varies spatially with a mean depth of 3.3 meters and maximum depth of 17 meters, and contains two distinct basins with the deepest area located in the center of the lake (Figure 2.1). Like most lakes in the region, it is phosphorus limited and has been classified as borderline oligotrophic/mesotrophic and impaired for phosphorus from limnological surveys (NHDES in 1979, 1989, and 1998) using the New Hampshire Trophic Classification scheme (NHDES 1995). More recently, Pawtuckaway Lake has also been declared impaired for bacteria (NHDES 2010).

The reservoir contains two concrete outlet structures, Dolloff Dam and Drowns Dam, located in the southeastern and northern ends of the lake respectively (Figure 2.2). Discharge leaving from Dolloff Dam flows southward forming Pawtuckaway River, while discharge leaving from Drowns Dam flows northward forming Mile Brook and eventually joins the North River; both the Pawtuckaway and North Rivers are tributaries of the Lamprey River. The dams were originally constructed for hydropower in 1836 and created two separate waterbodies (NHDES 1995). An earth and gravel embankment, named Gove Dam, was also constructed on the eastern side of the lake at this time to alleviate flooding. It was not until 1955, when the Electric

Company signed over their water rights to the state of New Hampshire, that water levels were raised to present day levels, resulting in the formation of a single waterbody (NHDES 1995).

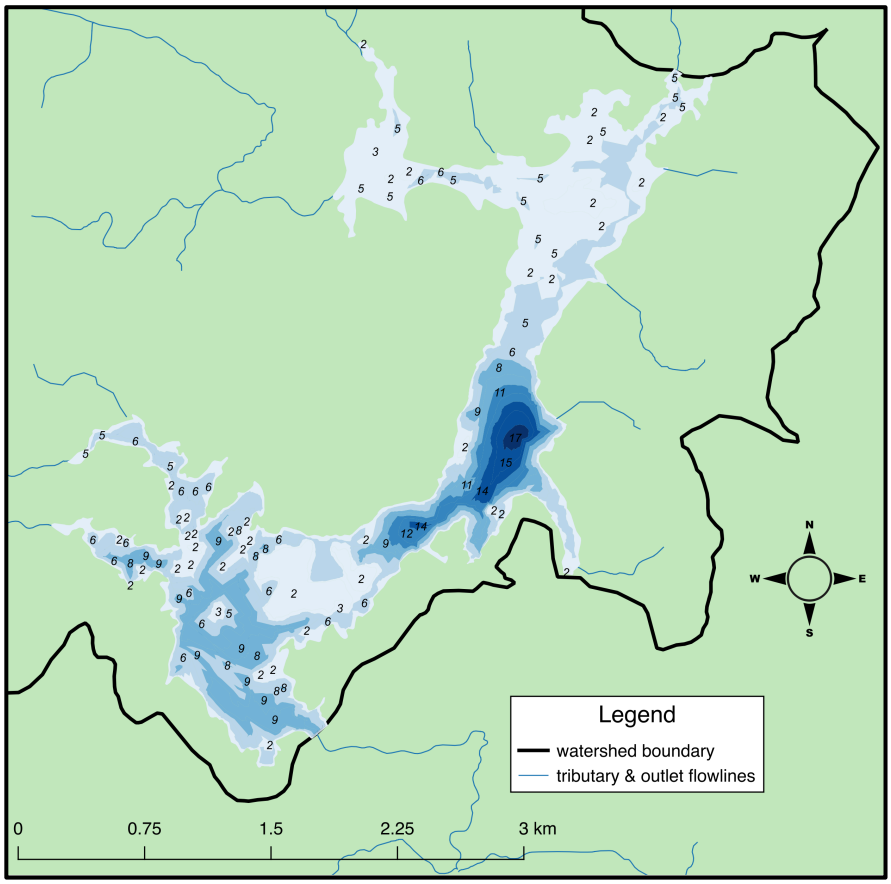

Figure 2.1 Bathymetry profile of Pawtuckaway Lake surveyed by NHDES showing northern and southern basins (contour label units are meters and range from 2 to 17 m).

The New Hampshire Department of Fish & Game (NH F&G) manages fish populations in Pawtuckaway Lake to promote recreational fishing. The lake is home to many predatory fish species such as bass, pickerel, perch, and bullhead, however fish surveys in the 1970s and 1980s indicated that populations were in decline in part due to the lack of prey such as golden shiners (NHDES 1995). In 1994, NH F&G began stocking alewife in Pawtuckaway Lake to help reduce pressure on the golden shiner population by providing an additional food source to predatory fish (NHDES 1995). The alewife, being an anadromous fish, leave the lake in the fall to return to the ocean, historically via the Dolloff Dam outlet (NH Fish & Game 2015).

The Pawtuckaway Lake watershed, an area of approximately 54 km^2, in the towns of Nottingham and Deerfield, contains many ponds, wetlands, and tributaries that drain to the lake. Thirteen tributaries discharge into Pawtuckaway Lake (Figure 2.2; Table 2.1). Of these, Back Creek B, Mountain Cove Brook, and Round Pond Brook drain 68.5% of the upper watershed area. The watershed is predominantly forested, especially the areas lying within the state park. Development within the watershed comprises both seasonal and year-round single-family residential homes, most of which are located along the lake's southeastern and southwestern shoreline. Agriculture within the watershed includes Fernald's dairy farm located along the watershed's eastern border and various small horse pastures located in the northwestern headwaters.

Pawtuckaway Lake has a large water volume capacity relative to drainage area and the amount of storm runoff produced upstream. For example, the predicted volume of water runoff produced from the historic 2-yr 24-hour precipitation event upstream only accounts for approximately 10% of reservoir storage (Table 1.1), showing Pawtuckaway Lake's high potential for attenuating floods downstream.

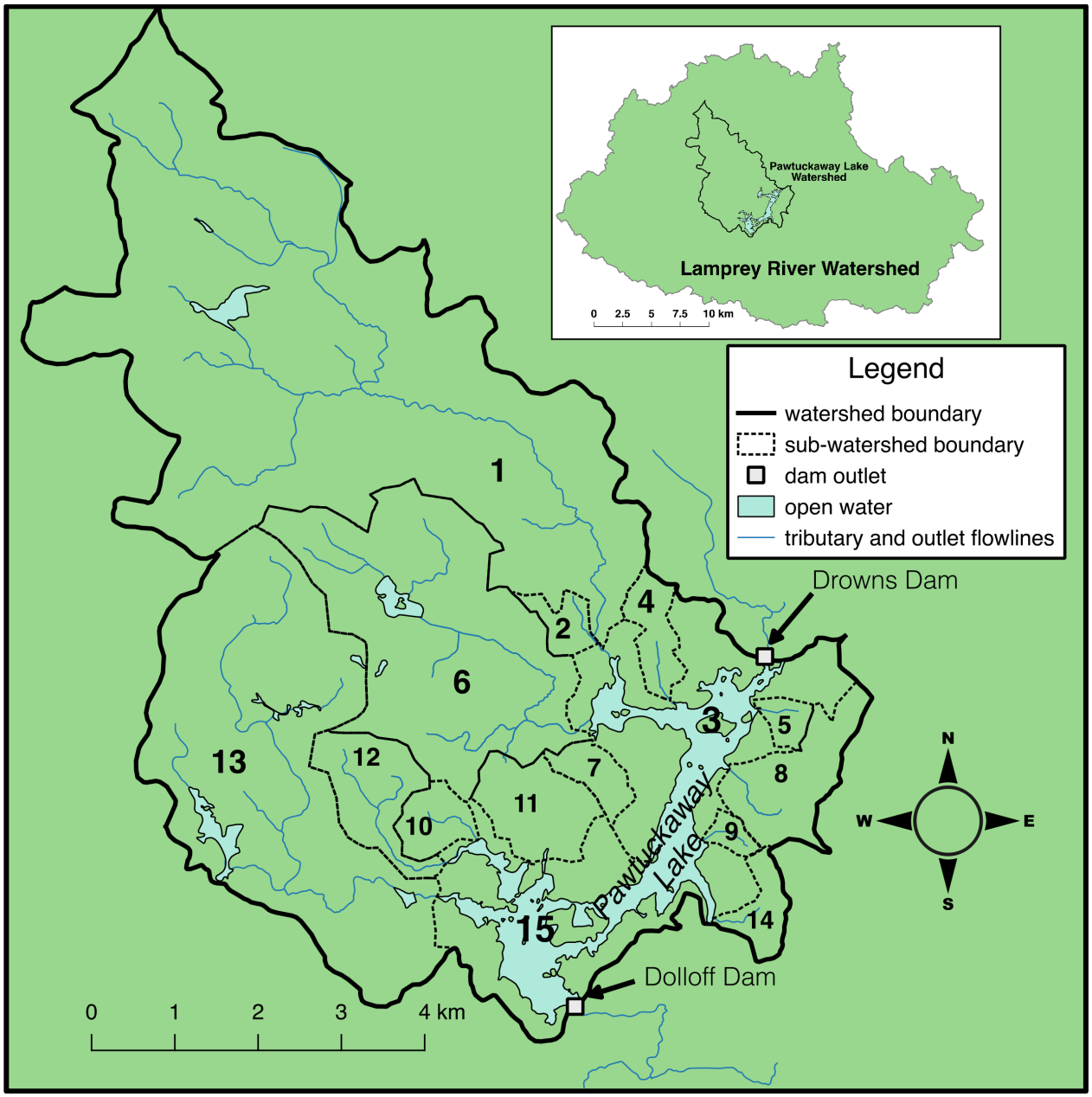

Figure 2.2 Area of the Pawtuckaway Lake watershed and sub-watersheds that drain to the lake. Numbered sub-watershed names, area, and land cover correspond to Table 2.1.

Table 2.1 Pawtuckaway Lake subbasins and land cover. Subbasin boundaries were delineated using ArcGIS. Land cover data from 1998 and 2015 were downloaded from NH Granit. Locations of each sub-watershed are shown in Figure 2.2.

		Land Cover									
Subbasin # & Name	Area [km^2]	Industrial (%)	Low density residential (%)	Medium-low density residential (%)	Transportation (%)	Pasture (%)	Forest (%)	Water (%)	Wetland (%)	Barren (%)	Range grass (%)
1. Back Creek B	20.65	0.2	0	4.1	0.4	1.3	81.6	3.6	5.5	3.0	0.2
2. Back Creek A	0.36	0	0	0	0	0	90.4	3.1	6.6	0	0
3. North Lake	3.85	0	0	2.5	0.1	0	59.2	35.8	2.0	0.4	0
4. Fundy Brook	0.60	0	0	0	0	0	81.5	0.2	15.3	3.0	0
5. Fernald's Brook B	0.25	0	0	0	0	0	98.0	0.5	1.4	0	0
6. Round Pond Brook	6.70	0	0	0.2	0.2	0.4	85.4	5.3	7.5	0.9	0
7. Burnham's Marsh North	0.45	0	0	0	0	0	74.3	16.3	9.5	0	0
8. Fernald's Brook A	1.43	0	0	2.6	1.0	3.1	77.7	0.9	9.9	2.4	2.3
9. White's Grove Brook	0.18	0	0	13.1	3.6	0	77.9	0	5.9	0	0
10. Loon Cove Brook B	0.56	0	0	0	0%	0	94.0	4.8	1.1	0	0
11. Burnham's Marsh South	1.22	0	0	0.2	0.8	0	71.4	1.3	24.0	0.4	0
12. Loon Cove Brook A	1.27	0	0	0.1	0.1	0	90.8	2.3	6.6	0	0
13. Mountain Cove Brook	9.38	0	0	0.6	0.3	0	84.8	5.6	5.8	2.7	0.1
14. Gove Dam Brook	0.51	0	0	4.7	0	0	80.8	6.7	6.1	1.8	0
15. South Lake	2.57	0	5.5	16.2	1.8	0	35.6	39.4	0.9	0.4	0.2

2.1.2 Dam Management

Outflow from the lake is controlled by wooden boards (stop logs) at both the Dolloff Dam and Drowns Dam outlets, which are maintained and operated by the NHDES Water Resources Division. At Dolloff Dam, individual stop logs are placed and removed in the three-bay outlet where water spills from the lake's surface over the top (Figure 2.3.A), while at Drowns Dam stop logs are lifted or lowered in unison as a gate where water is released from the bottom of the lake (Figure 2.3.B). In addition, both dams contain spillways that allow for water to flow freely over the dam when the lake water level is higher than full pool Pawtuckaway Lake is managed under the Instream Flow Policy established as part of the Lamprey River Management Plan (NHDES 2013), which allows for the release of water from Pawtuckaway Lake or from Mendum's Pond to simulate a 48-hour rain event during periods of prolonged low flow along the lower Lamprey.

Since 1955, stop logs have been removed annually during mid-October to allow lake levels to drop and remain low until April of the following year when the logs are put back into place or gates are closed. This drawdown serves multiple purposes including preventing ice buildup on residential docks during winter, exposing and killing off nuisance aquatic plants along the shoreline, and increasing reservoir capacity to absorb excess runoff from events such as winter rain on frozen ground and spring snow melt.

Historically, Pawtuckaway Lake's water level was drawn down in the fall by 7 ft (NHDES 1995) until the implementation of the Lamprey River Water Management Plan in 2013, after which time the drawdown was incrementally reduced annually until reaching a final drawdown of 4.8 feet in 2017 (NHDES 2013). This new drawdown level is meant to aid in the reservoir's fishery as well as provide additional winter reservoir storage in the event that a wintertime relief pulse is needed. Until 2013, the fall drawdown was created by releasing water from Dolloff Dam. Starting in 2014, NHDES began releasing more water from Drowns Dam to aid in phosphorus

export from the lake, as most phosphorus is loaded to the lake and resides closer to the Drowns outlet (NHDES 2015). This change in dam management has reduced reservoir total phosphorus concentration, which has led to decreased algae growth and increased water clarity (NHDES 2015). In 2017 NHDES targeted 70% release from Drowns Dam and 30% release from Dolloff Dam during the fall drawdown, which is directly proportional to the drainage areas of the sub-watersheds draining to the northern and southern areas of the lake. This change in management is designed to increase phosphorus export from Drowns Dam while still enabling alewife out-migration from the lake at Dolloff Dam (NHDES 2016).

Figure 2.3 Dam outlet structures at (A) Dolloff Dam on 4/8/18 and (B) Drowns Dam on 10/13/17.

2.2 Field Methods Overview

Pawtuckaway Lake N mass tributary inputs and outputs were quantified at six monitoring stations between 5/19/17 to 5/18/18 through the construction of a continuous record of discharge by continuously gauging the stage height and converting that to discharge using stage-discharge rating curves constructed from multiple discharge measurements over a range of flow stages. Bimonthly measurements of N concentration sampled at each monitoring station

were interpolated throughout the rest of the year and used to obtain a continuous record of N flux. Monitored tributary N inputs were used to estimate N inputs from unmonitored tributaries based on drainage area. The Soil and Water Assessment Tool (SWAT) was used to estimate N inputs to the reservoir from nearshore N sources during the study period. Atmospheric N inputs to the reservoirs water surface during the study period were estimated using precipitation weighted mean historical observations of atmospheric N deposition at Thompson Farm in nearby Durham, NH.

2.3 Tributary N Inputs and Dam Outlet N Outputs

2.3.1 Sampling Locations

The six monitoring stations consisted of four tributaries and two outlet streams (Figure 2.4) each of which had characteristics consistent with USGS ideal gauging site criteria (USGS 1982). The four tributaries were Back Creek B, Mountain Cove Brook, Round Pond Brook, and Fernald's Brook A. The tributaries Back Creek B, Mountain Cove Brook, and Round Pond Brook were chosen as sampling sites since they drain the three largest subwatersheds, representing 41.3%, 18.7%, and 13.4% of the total drainage area to the reservoir, respectively. Fernald's Brook A, 2.8% of the total drainage area, was chosen due to its historically high concentrations of NO_3^-, presumably resulting from cow manure runoff from Fernald's Farm (NHDES 1995). The two outlet streams were the Pawtuckaway River downstream of Dolloff Dam before the Route 156 crossing and on Mile Brook downstream of Drowns Dam at the foot bridge adjacent to Beach Road. An additional sampling station was located in the reservoir above Dolloff Dam.

In addition, N solute concentration measurements were obtained at the two United States Geological Survey (USGS) gauges located within the Lamprey River watershed: USGS gauge 01073319 (Lamprey River at Langford Rd. in Raymond, NH) and USGS gauge 01073500 (Lamprey River at Packer's Falls in Durham, NH, near Newmarket, NH).

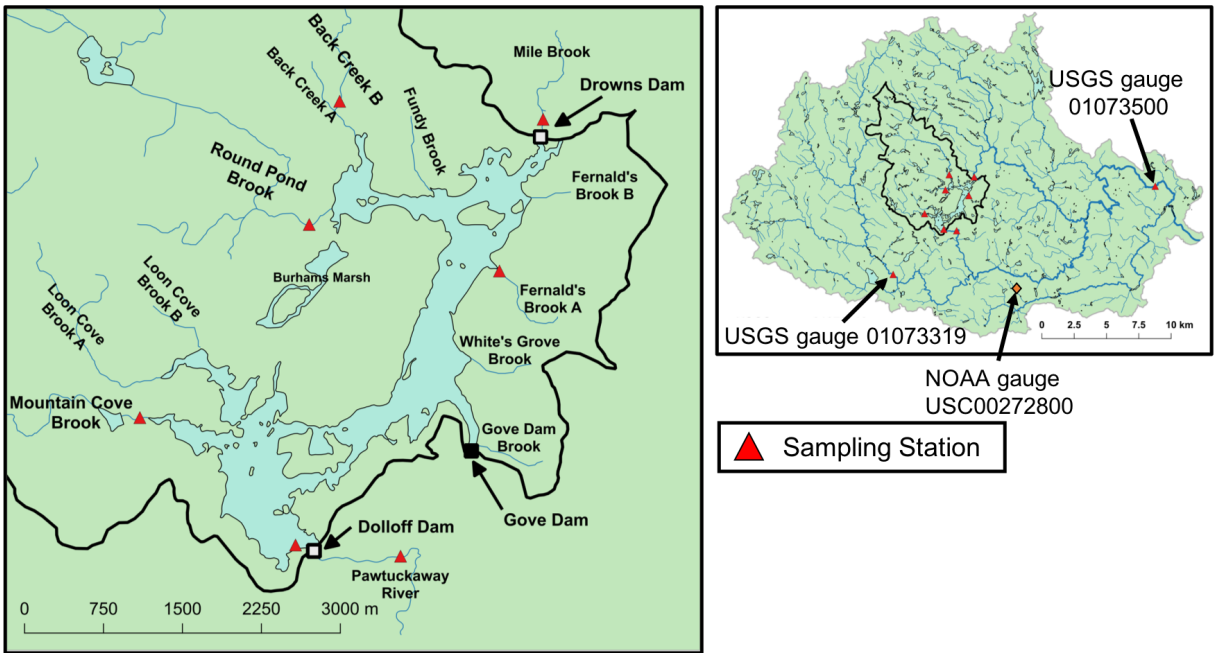

Figure 2.4 Pawtuckaway Lake watershed (left) and Lamprey River watershed (right) showing the locations where water samples were collected (red triangles) and the NOAA weather gauge USC00272800 in Epping, NH.

2.3.2 Continuous Stage Measurements

Each monitoring station was gauged for stage height through the deployment of a Solinst Levelogger Junior Edge pressure transducer, which recorded both stage [m] and temperature [°C] at five-minute intervals. Uncertainty on raw pressure transducer stage measurements (h_o) was estimated to be 0.005 m (Solinst 2018). Leveloggers were deployed in a perforated PVC housing either attached with hose clamps to rebar driven into the stream bed, or zip tied to a cement block (Figure 2.5). Stage records were corrected for atmospheric pressure (h_{atm}), transducer removals and relocations both within ($h_{relocation\_1}$) and of the housings ($h_{relocation\_2}$), and for stage at zero discharge ($h_{Q=0}$), which were calculated as follows.

Figure 2.5. Pictures of instream Solinst Levelogger PVC housings attached to (A) a rebar stake at Round Pond Brook and (B) a cement block at Mile Brook. Pictures were taken on 7/6/17 and 8/1/17 respectively.

Because the Leveloggers measured absolute pressure (water pressure plus atmospheric pressure), a Solinst Barologger was also deployed to allow correction for atmospheric pressure (h_{atm}). The barometric pressure transducer was deployed upstream of Mountain Cove Brook in a PVC pipe driven below ground to prevent additional error from diurnal temperature swings (McLaughlin and Cohen 2011). Atmospheric pressure and air temperature measured from the barometric pressure transducer were similar to atmospheric pressure and air temperature measured at Rochester Skyhaven Airport, located 26 km away.

Throughout the study, transducers were repeatedly removed from their housings to download data. Short gaps in the stage record that occurred during these removals were filled through linear interpolation. Prior to 6/1/2017, transducers were secured to the perforated PVC housing via zip ties that needed to be cut and retied during each removal. To keep each transducer's vertical position within the housing more consistent following removal and replacement, transducers were either tied to a washer that was zip tied to the top of the housing or tied to a screw eye drilled into a PVC cap that was secured on top of the housing beginning

on 6/1/17. To correct for this transducer relocation within the housing, all stage measurements prior to 6/1/17 were reduced by the difference in stage of the former location and the permanent location ($h_{relocation\_1}$).

Flow gradually declined during the summer months of 2017, exposing some housings above the water surface. In order to ensure transducers stayed inundated, several transducers and housings were relocated to deeper areas within the same pool in the stream. To correct for this transducer housing relocation, all stage measurements prior to the housing relocation were reduced by the difference in stage of the two locations ($h_{relocation\_2}$).

Finally, each stage measurement was offset relative to the expected stage at zero discharge. Each stage measurement location was surveyed on 8/3/17 relative to a local vertical datum using a Sokkia C410 Automatic Level and a surveying rod (Figure 2.6), which were used to determine the relative elevations of the top of the PVC housing ($h_{top\_of\_housing}$) and the nearest downstream control structure ($h_{downstream\_control}$; Figure 2.7). The elevation of the transducer below the top of the PVC housing ($h_{below\_top\_housing}$) was calculated by comparing recorded transducer stage measurements with the stage above the top of the PVC housing measured with a meter stick at the same time as transducer surveys and transducer data retrieval. Stage height at zero discharge ($h_{Q=0}$) was then calculated as,

$$h_{Q=0} = h_{top\_of\_housing} + h_{below\_top\_housing} - h_{downstream\_control} \quad \text{Equation 2.1}$$

Surveying also included the location of multiple benchmarks (usually large rocks) near each in-stream transducer. The horizontal and vertical distances between benchmarks and the sensor were measured to ensure that the housing could be deployed in the same location in the event that it was unintentionally moved or lost. Fortunately, these benchmarks proved unnecessary, since all transducers were recovered.

The raw measurements of water pressure (h_o) were combined with the estimated offset to obtain a final corrected stage record (h).

$$h = h_o - h_{atm} - h_{relocation\_1} - h_{relocation\_2} - h_{Q=0}$$ Equation 2.2

Figure 2.6. Pictures at Back Creek B on 8/3/17 of the (A) Sokkia C410 Automatic Leveland (B) surveying rod used to measure the relative elevations of the top of the instream Levelogger PVC housing and the nearest downstream control structure.

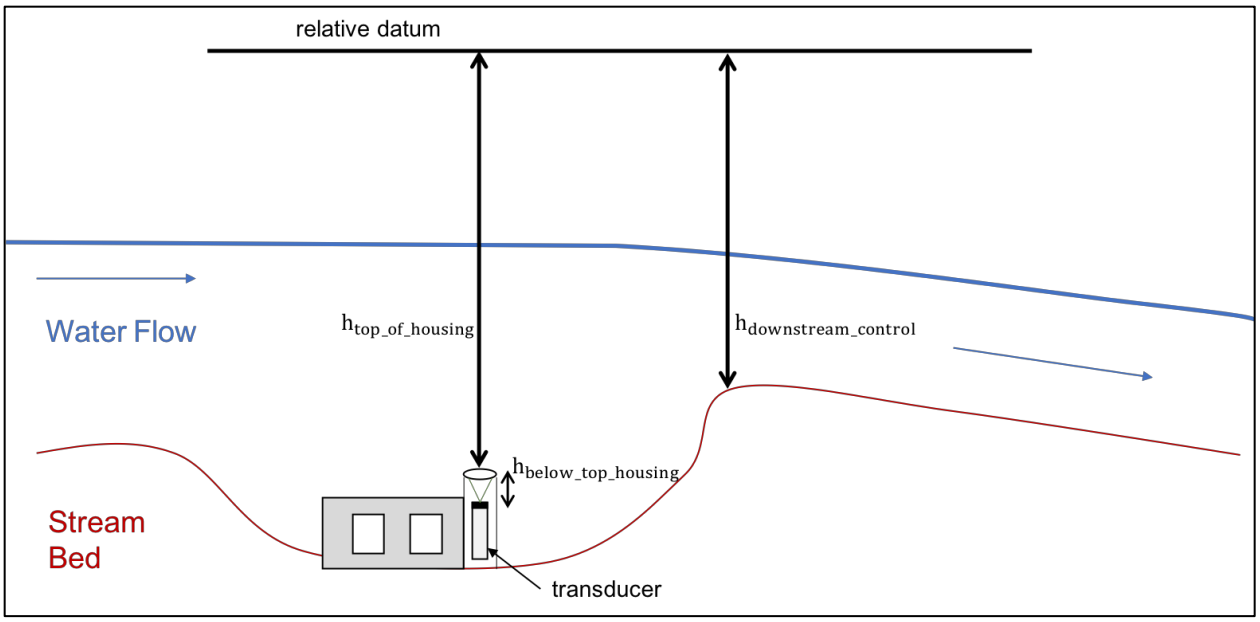

Figure 2.7. Schematic stream cross section showing elevations of the top of the PVC housing ($h_{top\_of\_housing}$) and the downstream control ($h_{downstream\_control}$) relative to a local vertical datum and the distance of the transducer below the top of the PVC housing ($h_{below\_top\_housing}$).

2.3.3 Field Discharge Measurements and Uncertainty

Discharge was measured ten times at Round Pond Brook and nine times at each of the other five monitoring stations, during a range of discharge conditions throughout the study period. The majority of discharge measurements were performed using the velocity-area method (Herschy 1985, Harrelson et al. 1994; Figure 2.8). The mid-section method was used to sum the section discharge measured for each of 20-25 verticals across the width of the stream:

$$Q_{velocity-area} = \sum_{i=1}^{m}\left(\left(\frac{b_{i+1}-b_{i-1}}{2}\right)\cdot d_i \cdot \bar{v}_i\right) \qquad \text{Equation 2.3}$$

where $Q_{velocity-area}$ is the discharge [m^3 sec^{-1}], m represents the number of verticals across the width of the stream, b_{i+1} and b_{i-1} represent the lateral locations of the two adjacent verticals on either side of vertical i [m], d represents the depth of vertical i [m], and $\bar{v}$ represents the mean velocity of water flow at vertical i [m]. Point velocity measurements were obtained using a SonTek Flowtracker Acoustic Doppler Velocimeter (ADV) attached to a top-set wading rod, which sampled at 1 Hz for 40 sec. For most verticals, the mean velocity was estimated using a

single point measurement at sixth-tenths water column depth. Discharge was high at Round Pond Brook, Back Creek B, and Mountain Cove Brook on 4/8/18, so point measurements were obtained at two- and eight-tenths water column depth at the deepest verticals and then averaged to produce the mean velocity $\bar{v}$.

Figure 2.8 Measuring discharge using the velocity area method at Mountain Cove Brook on 1/19/17.

For each discharge measurement calculated using the velocity-area method, relative uncertainty ($\varepsilon_{Q\_velocity-area}$) was calculated by adding relative random uncertainty (ε'_Q) to relative systematic uncertainty (ε''_Q) in quadrature (Herschy 1985):

$$\varepsilon_Q = \pm\left(\varepsilon'^2_Q + \varepsilon''^2_Q\right)^{\frac{1}{2}} \quad \text{Equation 2.4}$$

Random uncertainty was calculated as,

$$\varepsilon'_Q = \pm\left[\varepsilon'^2_m + \frac{1}{m}\cdot\left(\varepsilon'^2_b + \varepsilon'^2_d + \varepsilon'^2_e + \varepsilon'^2_p + \varepsilon'^2_c\right)\right]^{\frac{1}{2}} \quad \text{Equation 2.5}$$

where ε'_m is the relative random uncertainty associated with using a limited number of verticals, m is the number of verticals, ε'_b is the random uncertainty associated with the width measurement, ε'_d is the random uncertainty associated with the depth measurement, ε'_e is the

random uncertainty associated with the 40 sec required to measure the mean velocity, $\varepsilon'_{\mathrm{p}}$ is the random uncertainty associated with the number of points measured on each the vertical, and $\varepsilon'_{\mathrm{c}}$ is the random uncertainty associated with the velocity measurement from the ADV. Systematic uncertainty was calculated as,

$$\varepsilon''_{\mathrm{Q}} = \pm\left(\varepsilon''^{2}_{\mathrm{b}} + \varepsilon''^{2}_{\mathrm{d}} + \varepsilon''^{2}_{\mathrm{c}}\right)^{\frac{1}{2}} \qquad \text{Equation 2.6}$$

where ε''_{b} is the fractional systematic uncertainty associated with the measuring tape used to measure width between verticals, ε''_{d} is the percent systematic uncertainty associated with the wading rod used to measure the depth of a vertical, and $\varepsilon''_{\mathrm{c}}$ is systematic uncertainty associated with the velocity measurement from the ADV. For values used for each uncertainty term, see Table 2.2.

Table 2.2 Values used to calculate relative uncertainties associated with a single discharge measurement using the velocity-area method (cf. Herschy 1985), where m represents the number of verticals used in the measurement.

$\varepsilon'_{\mathrm{m}}$	$\varepsilon'_{\mathrm{b}}$	$\varepsilon'_{\mathrm{d}}$	$\varepsilon'_{\mathrm{e}}$	$\varepsilon'_{\mathrm{p}}$	$\varepsilon'_{\mathrm{c}}$	ε''_{b}	ε''_{d}	$\varepsilon''_{\mathrm{c}}$
4 (m >= 25) 5 (m < 25 and m > 14) 6 (m <= 15)	0.1	1.0	40 (Q <= 0.05) 22 (Q >= 0.1 and v <= 0.199) 12 (Q >= 0.2 and v <= 0.299) 7 (Q >= 0.3 and v <= 0.399) 6 (Q >= 0.4)	15	1	0.5	0.5	1

Discharge at Fernald's Brook A on 7/26/17, 12/8/17, and 10/13/17 and at Mountain Cove Brook on 10/13/17 was too low to obtain water velocity measurements using the ADV. Instead, low-flow discharge (Q) was estimated by collecting stream flow into a two-gallon plastic container for a known time. Depending on flow, collection times ranged between two and twenty seconds. Discharge was measured for two or three trials, which were then averaged. At Fernald's Brook A, low-flow discharge was measured at a small water fall. At Mountain Cove Brook, low-flow discharge was measured at the downstream side at each of two parallel road culverts, which were added together for each trial. Uncertainty with low-flow discharge

measurements using this technique was estimated at 30%, based on the standard deviation of repeated trials.

2.3.4 Stage-Discharge Rating Curves

Stage-discharge rating curves were constructed at each monitoring station using the periodic discharge measurements and the stage measured by the transducer at the same time. The stage-discharge relation was expressed as a power law:

$$\log(Q) = \log(C \cdot h^n) = \log(C) + \log(h)^n = \log(C) + n \cdot \log(h) \quad \text{Equation 2.7}$$

where Q represents discharge, h represents stage above zero flow, and C and n are fitting constants, which were identified from the best-fit straight line of $\log(Q)$ as a function of a $\log(h)$ with y-intercept $\log(C)$ and slope n.

At five of the six monitoring stations, all paired discharge and stage measurements were given equal weight. The Pawtuckaway River had eight low-flow stage-discharge pairs and only one high-flow measurement. Therefore, to fit the curve closer to the one high-flow measurement, which was obtained on 1/19/18, the high stage-discharge measurement was weighted twenty times more than the other measurements, to produce a curve that more accurately represented both low and high flow at this site. A weight of twenty was selected as it provided an adequate fit of the stage-discharge rating curve through the highest stage-discharge measurement.

2.3.5 Continuous Discharge Records and Uncertainty

Each monitoring station's stage-discharge rating curve was used to transform the 5-minute continuous record of stage to a 5-mintue continuous record of discharge. Relative uncertainty associated with each measurement (i) of the transformed discharge record (ε_{rc}) was calculated as:

$$\varepsilon_{rc,i} = \pm\left(S_{mr,i}^2 + n^2 \cdot \varepsilon_{h_i}\right)^{\frac{1}{2}} \quad \text{Equation 2.8}$$

where S_{mr} represents the relative standard error of the mean stage-discharge relation at the 95% confidence level, n represents the stage-discharge rating curve exponent, and ε_{h_i} represents the relative error associated with each stage measurement h_i, which was calculated by dividing the absolute error associated with each stage measurement (0.005 m) by the magnitude of the stage measurement. S_{mr} was calculated for each measurement (i) of stage in the continuous stage record (h):

$$S_{mr,i} = S_e \left[\frac{1}{N} + \frac{(\ln(h_i) - \ln(\bar{h}))^2}{\sum(\ln(h_j) - \ln(\bar{h}))^2}\right]^{\frac{1}{2}} \quad \text{Equation 2.9}$$

where S_e represents the standard error of the estimate, N is the number of stage-discharge measurement pairs used to construct the stage-discharge rating curve, h_j represents each measurement of stage used to construct the stage-discharge rating curve, and $\bar{h}$ represents the mean stage for stage measurements used in the construction of the rating curve. The standard error S_e was calculated as:

$$S_e = t\left[\frac{\sum\left(\frac{Q_j - Q_c}{Q_c}\right)^2}{N-2}\right]^{\frac{1}{2}} \quad \text{Equation 2.10}$$

where t represents the Student's t correction (a value of 2 was used to provide 95% confidence intervals), Q_j represents each measurement of discharge used to construct the stage-discharge rating curve, and Q_c represents discharge taken from the rating curve corresponding to Q_j.

Since rating curve uncertainty (ε_{rc}, Equation 2.8), which ranged from 30.8% to 368%, was larger than the uncertainty associated with each individual discharge measurement (ε_Q, Equation 2.7), which ranged from 7.67% to 30%, only ε_{rc} was used in estimating uncertainty with the discharge record at each monitoring station. Each discharge record measurement was multiplied by ε_{rc} and either added or subtracted to the discharge value to obtain 95% confidence limits for the discharge record.

2.3.6 Discharge Record Gap Filling and Uncertainty

Only Back Creek B, Round Pond Brook, and Mile Brook had continuous 5-minute stage records that covered the whole study period (5/19/17-5/18/18). Gaps in the continuous stage record at Mountain Cove Brook, Fernald's Brook A, and Pawtuckaway River occurred resulting from traducer removals, lost data files, or transducers that failed to record data. During late August 2017, beavers constructed a dam immediately downstream of the monitoring location at Mountain Cove Brook, which dramatically altered the stage-discharge relationship. Stage data at Mountain Cove Brook after 8/13/17 were discarded, and the transducer was removed on 10/13/17. Also during late August 2017, large quantities of sand eroded from a recently graded dirt road formed a sand delta in Fernald's Brook A, which engulfed the monitoring location. Stage data at Fernald's Brook A after 8/12/17 were discarded, and the transducer was removed on 10/13/17. Other stage data gaps occurred because transducer at Fernald's Brook A was not deployed until 5/22/17 14:30, Pawtuckaway River stage data from 8/3/17 13:40 to 8/24/17 16:00 were accidentally written over, and the transducer at Mountain Cove Brook failed to record data from 6/1/17 13:15 to 6/19/17 10:30.

Linear regression between runoff (Runoff) at a monitoring station that contained gaps (y) with another monitoring station with a complete record (x) was used to interpolate missing data at Mountain Cove Brook, Fernald's Brook A, and Pawtuckaway River. Runoff at each monitoring station was calculated as:

$$\mathrm{Runoff} = \frac{\mathrm{Q}}{\mathrm{Area}} \qquad \text{Equation 2.11}$$

where Q is discharge [$m^3\ s^{-1}$] and Area is upstream drainage area [m^2] at the monitoring station. The best-fit regression line was calculated for periods when data were available at both sites using a least-squares fitting method (Taylor 1982) and given as,

$$\mathrm{Runoff_y} = \mathrm{A} + \mathrm{B} \cdot \mathrm{Runoff_x} \qquad \text{Equation 2.12}$$

where A and B are constants. The relative uncertainty of interpolated discharge ($\varepsilon_{\mathrm{Runoff_y}}$) was calculated by adding in quadrature the relative uncertainty associated with the runoff regression line ($\varepsilon_{\mathrm{rl}}$) and the relative uncertainty associated with the runoff/discharge ($\varepsilon_{\mathrm{rc,x}}$) from the monitoring station with a complete record. The uncertainty associated with the runoff regression line $\varepsilon_{\mathrm{rl}}$ was calculated by finding the uncertainty ε_A and ε_B associated, respectively, with the regression constants A and B:

$$\varepsilon_A = \varepsilon_{\mathrm{Runoff_y}} \cdot \left(\frac{\sum \mathrm{Runoff_x}}{N \cdot \sum \mathrm{Runoff_x^2} - (\sum \mathrm{Runoff_x})^2}\right)^{\frac{1}{2}} \quad \text{Equation 2.13}$$

$$\varepsilon_B = \varepsilon_{\mathrm{Runoff_y}} \cdot \left(\frac{N}{N \cdot \sum \mathrm{Runoff_x^2} - (\sum \mathrm{Runoff_x})^2}\right)^{\frac{1}{2}} \quad \text{Equation 2.14}$$

where $\varepsilon_{\mathrm{Runoff_y}}$ is the relative uncertainty of interpolated runoff and N is the number of runoff measurements used in the regression. The uncertainty of interpolated runoff $\varepsilon_{\mathrm{Runoff_y}}$ was in turn calculated as:

$$\varepsilon_{\mathrm{Runoff_y}} = \left(\frac{1}{N-2} \cdot \sum_{i=1}^{N} \left(\mathrm{Runoff_{y,i}} - A - B \cdot \mathrm{Runoff_{x,i}}\right)^2\right)^{\frac{1}{2}} \quad \text{Equation 2.15}$$

Finally, $\varepsilon_{\mathrm{rl}}$ was calculated as,

$$\varepsilon_{\mathrm{rl}} = \frac{(A+B \cdot \mathrm{Runoff_x}) \pm [(A \pm 2 \cdot \varepsilon_A) + (B \pm 2 \cdot \varepsilon_B) \cdot \mathrm{Runoff_x}]}{(A+B \cdot \mathrm{Runoff_x})} \quad \text{Equation 2.16}$$

Gaps at Mountain Cover Brook from 6/1/17 13:15 to 6/19/17 10:30 and 8/14/17 to 5/18/18 were filled through a linear regression of Mountain Cove Brook runoff with Back Creek B runoff (Figure 2.9). Gaps at Fernald's Brook A from 5/19/17 to 5/22/17 and 8/12/2017 to 5/18/18 were filled through a linear regression of Fernald's Brook A runoff with Round Pond Brook runoff (Figure 2.10). Discharge gaps of discharge at Pawtuckaway River from 8/3/17 13:40 to 8/24/17 16:00 were filled through a linear regression of Pawtuckaway River runoff with Mile Brook runoff (Figure 2.11).

To examine how well these runoff regression lines estimated discharge, discharge measurements obtained on 10/13/17, 12/8/17, 1/18/19, and 4/8/18 after Mountain Cove Brook and Fernald's Brook A records ended were compared to the discharge estimated from runoff regression lines. On these four dates, the regression lines tended to overpredict low runoff while underpredicting higher runoff at both sites. No discharge measurements were obtained at either Pawtuckaway River or Mile Brook during the period of missing Pawtuckaway River data. The regression between Fernald's Brook A and Round Pond Brook exhibited a closer linear relationship ($r^2 = 0.77$) compared to the regressions between Mountain Cove Brook and Back Creek B ($r^2 = 0.36$) and Pawtuckaway River and Mile Brook ($r^2 = 0.53$), however no regressions were found to be linear ($p << 0.05$). Also, the relative uncertainty associated with the runoff regression lines (ε_{rl}) were very small (ranging from 1.2% to 1.8%). Therefore, uncertainty associated with gap-filled discharge by regressions was undoubtedly underestimated.

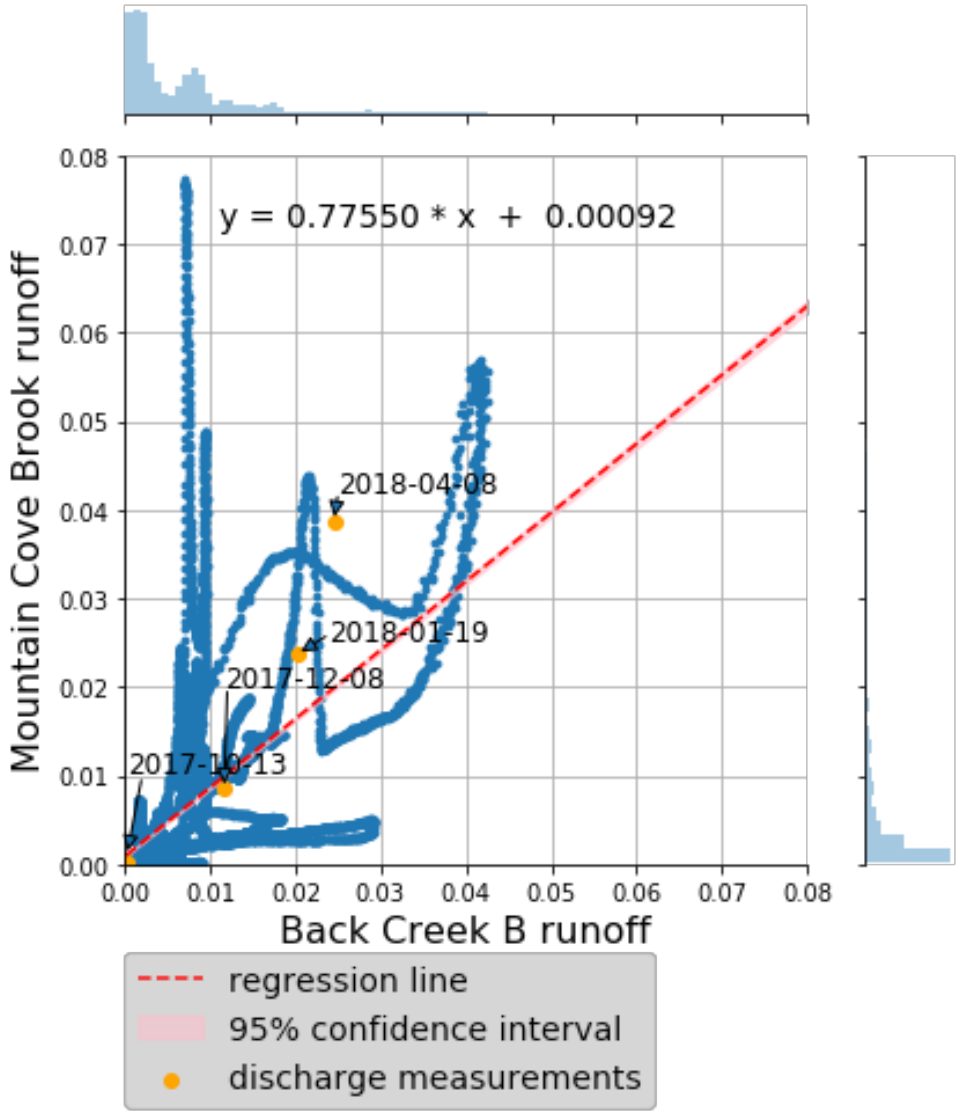

Figure 2.9 Best fit linear regression line of Mountain Cove Brook runoff (discharge normalized by drainage area) to Back Creek B runoff from 5/19/17 0:00 to 2017-06-01 13:15 and 2017-06-19 10:30 to 2017-08-13 0:00. Blue circles represent runoff measurements from the continuous 5-minute runoff record used to construct the regression line. Orange circles represent field discharge measurements during the period when Mountain Cover Brook runoff was estimated using the regression line. In the regression equation, y represents Mountain Cove Brook runoff and x represents Back Creek B runoff. Histograms along the x and y axis show the distribution of runoff data values used to construct the regression line.

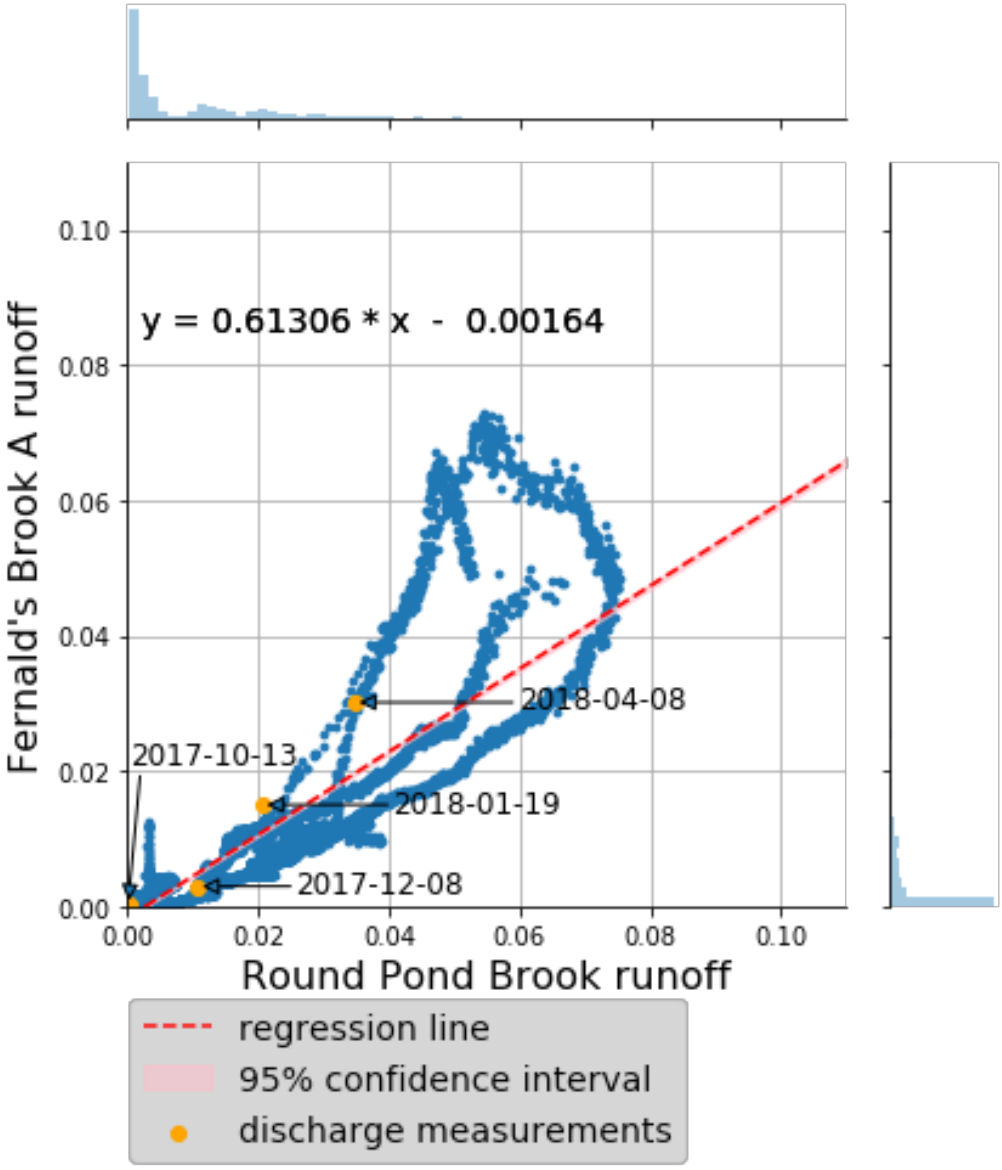

Figure 2.10 Best fit linear regression line of Fernald's Brook A runoff (discharge normalized by drainage area) to Round Pond Brook runoff from 5/22/17 14:30 to 2018-08-12 0:00. Blue circles represent runoff measurements from the continuous 5-minute runoff record used to construct the regression line. Orange circles represent field discharge measurements during the period when Fernald's Brook A runoff was estimated using the regression line. In the regression equation, y represents Fernald's Brook A runoff and x represents Round Pond Brook runoff. . Histograms along the x and y axis show the distribution of runoff data values used to construct the regression line.

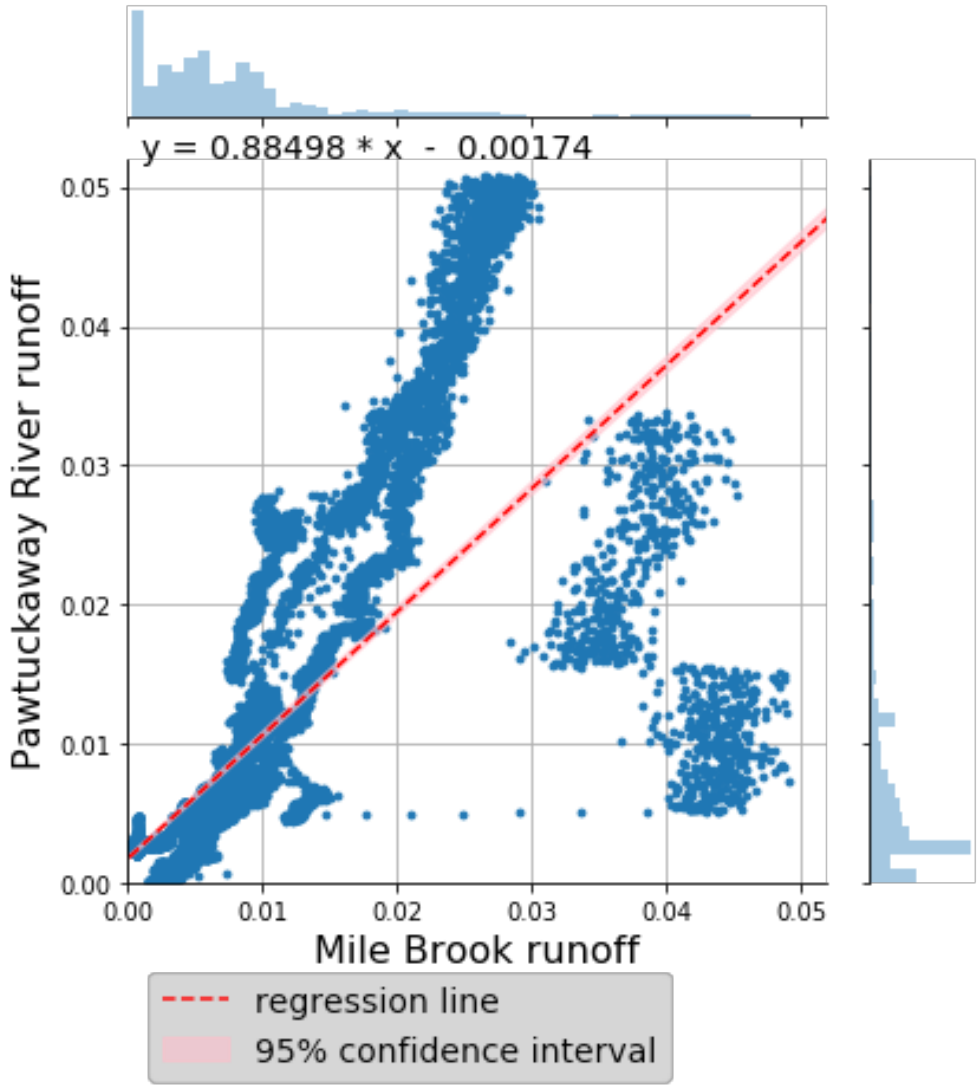

Figure 2.11 Best fit linear regression line of Pawtuckaway River runoff (discharge normalized by drainage area) to Mile Brook runoff from 2017-05-19 0:00 to 2017-08-03 0:00. Blue circles represent runoff measurements from the continuous 5-minute runoff record used to construct the regression line. In the regression equation, y represents Pawtuckaway River runoff and x represents Mile Brook runoff. Histograms along the x and y axis show the distribution of runoff data values used to construct the regression line.

2.3.7 Grab Sample Measurements of N Concentration

At each of the eight monitoring stations, water samples were collected during baseflow on 5/23/17, 7/26/17, 10/13/17, 12/8/17, 1/19/18, and 4/8/18 a from the middle of the stream at mid-depth using a syringe that was first rinsed three times with stream water. For reservoir samples and at the two USGS gauges, a rinsed two-gallon bucket with an attached rope was used in collection of surface water. All samples that were collected were assumed to be represented of the average N concentration along the stream cross section and that each stream was well mixed. Samples were then passed through an ashed filter into an acid-washed bottle, which was rinsed three times and then filled with approximately 50 mL of stream water. Samples were placed on ice in a cooler and kept in a freezer until being brought to the Water Quality Analysis Lab at the University of New Hampshire. Samples were analyzed for NO_2^- plus NO_3^- using colorimetric analysis following EPA #353.2, NH_4^+ using colorimetric analysis following EPA #353.1, and TDN using high temperature oxidation with chemiluminescent detection.

To estimate uncertainty on N solute concentrations ($\varepsilon_{N_{conc}}$), NO_3^- standards were diluted from a Dionex Five Anion Standard solution with a NO_3^- concentration of 100 mg L^{-1} and submitted to the lab alongside water samples collected in the field. Three diluted standards of NO_3^- concentration 0.045 mg L^{-1} were prepared and submitted with water samples taken on 10/13/17, two standards of NO_3^- concentration 0.090 mg L^{-1} were prepared and submitted with water samples taken on 12/8/17, and four standards of NO_3^- concentration 0.090 mg L^{-1} were prepared and submitted with water samples taken on 1/19/18 and 4/8/18. Once results were received back from the lab, a relative error was calculated for each standard based on the deviation between the lab's measurements and the known concentration of the prepared standard. The mean error of the nine standards was calculated as 13% and used to estimate uncertainty associated with N solute concentration measurements from the lab (Table 2.3).

Table 2.3 Prepared and measured nitrate standards that were used to estimate error of N solute concentration measurements analyzed at the Water Quality Analysis Laboratory at UNH.

Date Submitted	Prepared NO_3^- [mg N/L]	Measured NO_3^-+ NO_2^- [mg N/L]	Relative Error
2017-10-13	0.0451	0.0536	0.190
2017-10-13	0.0451	0.0469	0.040
2017-10-13	0.0451	0.0510	0.131
2017-12-08	0.0903	0.0968	0.072
2017-12-08	0.0903	0.0976	0.081
2018-04-08	0.0903	0.1216	0.347
2018-04-08	0.0903	0.1000	0.108
2018-04-08	0.0903	0.0944	0.045
2018-04-08	0.0903	0.1043	0.155
		Mean =	0.130

2.3.8 Estimates of N Flux at Monitoring Stations

N solute concentrations obtained from water samples collected on the six sampling dates were linearly interpolated to the rest of the year. N solute concentrations sampled on 5/23/17 were assumed equal to concentrations on 5/19/17 and solute concentrations sampled on 4/8/18 were assumed equal to concentrations on 5/18/18. N solute mass fluxes [kg N (5 min)$^{-1}$] were calculated at 5-minute intervals for each monitoring station ($\mathrm{N_{Flux\_measured}}$) as the product of discharge (Q) [m^3 s^{-1}] and N solute concentration ($\mathrm{N_{conc.}}$) [mg N L^{-1}].

$$\mathrm{N_{Flux\_measured}} = \mathrm{Q} \cdot \mathrm{N_{conc.}} \cdot 0.3 \qquad \text{Equation 2.17}$$

Relative uncertainties for N solute mass fluxes ($\mathcal{E}_{\mathrm{N_{flux}}}$) were calculated by adding relative uncertainties from the discharge record ($\mathcal{E}_{\mathrm{rc}}$) and N solute concentrations ($\mathcal{E}_{\mathrm{N_{conc}}}$) in quadrature.

$$\mathcal{E}_{\mathrm{N_{flux}}} = \left(\mathcal{E}_{\mathrm{rc}}^2 + \mathcal{E}_{\mathrm{N_{conc}}}^2\right)^{\frac{1}{2}} \qquad \text{Equation 2.18}$$

2.3.9 Tributary Discharge and N Inputs at Unmonitored Tributaries

Measurements of monthly total discharge ($\mathrm{M\_Q_{measured}}$ [m^3]) and N solute mass flux ($\mathrm{M\_N_{Flux\_measured}}$ [kg N]) at monitored tributaries were extrapolated to calculate monthly total discharge ($\mathrm{M\_Q_{extrap}}$) and N solute mass flux ($\mathrm{M\_N_{Flux\_extrap}}$) for the remaining nine unmonitored tributaries based on drainage area and similar land cover (Area; Table 2.1 and 2.4),

$$\mathrm{M\_Q_{extrap,k}} = \mathrm{M\_Q_{measured,i}} \cdot \left(\frac{\mathrm{Area_k}}{\mathrm{Area_i}}\right) \quad \text{Equation 2.19}$$

$$\mathrm{M\_N_{Flux\_extrap,k}} = \mathrm{M\_N_{Flux\_measured,i}} \cdot \left(\frac{\mathrm{Area_k}}{\mathrm{Area_i}}\right) \quad \text{Equation 2.20}$$

where k and i represent unmonitored and monitored tributaries respectively. Uncertainties calculated for discharge ($\mathcal{E}_{\mathrm{rc}}$) and N flux ($\mathcal{E}_{\mathrm{N_{flux}}}$) from each monitored tributary were applied to unmonitored tributaries listed in Table 2.4 .

Table 2.4 Table relating monitored tributaries and the tributaries to which discharge and N flux measurements were extrapolated.

Monitored Tributary	Unmonitored Tributaries
Back Creek B	Back Creek A Fundy Brook Cove Fernald's Brook B
Mountain Cove Brook	Loon Brook A Loon Brook B
Round Pond Brook	Burnham's Marsh North Burnham's Marsh South
Fernald's Brook A	White's Grove Brook Gove Dam Brook

2.4 Nearshore N Inputs from SWAT Modeling

2.4.1 SWAT Model Overview

A semi-distributed numerical model, the Soil and Water Assessment Tool (SWAT 2012; Neitsch et al. 2011), was used to estimate DON and NO_3^- inputs to the reservoir from nearshore groundwater seepage and overland runoff at Pawtuckaway Lake during the study period. SWAT has been shown to be a useful tool at modeling the hydrology within smaller catchments containing reservoirs (Lui et al. 2014), compares well to other physically-based fully distributed models (Epelde et al. 2016), and has shown to be effective at estimating nutrient loading (Vigerstol and Aukema 2011). Given input data including topography, soil type, and land cover, SWAT creates subbasins based on user-defined stream outlets, and hydrologic response units (HRUs) within each subbasin that lump together areas with similar soil, slope, and land cover characteristics. It then uses geospatial meteorological input data such as precipitation, air temperature, and relative humidity as well as N loading rates to route water and N solutes through the created HRUs at a daily time step. Each HRU has a set of default parameters that can be customized to better represent specific hydrologic and N solute transport dynamics in the subbasin. For this project, 15 subbasins and 1150 HRUs, with 20 to 300 HRUs in each subbasin, were created in ArcSWAT 2012 10.19 before being exported to the SWAT Calibration and Uncertainty Program (SWAT-CUP; Abbaspour 2015). SWAT-CUP was used to calibrate, validate, and estimate uncertainty on the hydrology and N transport within the watershed. Hydrology and N transport within the watershed were simulated from 1/1/2015 to 4/30/2018 with 1/1/2015 to 12/31/2016 used as a warmup period.

2.4.2 SWAT Input Data

A 7.5' USGS Digital Elevation Model was used along with user-defined subbasin outlets to divide the Pawtuckaway Lake watershed into 15 subbasins. Of these, 13 were inflowing tributaries and the remaining two contained the reservoir with a northern subbasin discharging

at Drowns Dam and a southern subbasin discharging at Dolloff Dam (Figure 2.12, Table 2.1). Reservoir subbasins are represented as a hypothetical reach with all water stored at the subbasin outlet. Nearshore water and N inputs to each reservoir were quantified within the two reservoir subbasins through the difference between water and N inputs from inflowing tributary subbasins and water and N outputs of the hypothetical reservoir reach.

The Soil Survey Geographic database (SSURGO) for New Hampshire was used for soil classifications. Land cover information came from data sets generated in 2015 (southeastern two thirds of the watershed; 1998 (northwestern one third of the watershed). Land cover data was reclassified using SWAT classifications (Table 2.5). Impervious surface parameters, the impervious fraction and the connected impervious fraction, were manually lowered for low density and medium-low density land cover classifications to better represent the rural residential properties along the shores of Pawtuckaway Lake (Table 2.6).

Daily precipitation and air temperature data from the NOAA National Climate Data Center (NCDC) gauge in Epping and relative humidity and wind speed from the NOAA weather gauge in Concord were used as meteorological inputs (Figure 2.4). Solar radiation data was simulated using the SWAT climatology weather generator using the WGEN_US_COOP_1990_2006 statistical database (Neisch 2011). Mean annual atmospheric N deposition from 1994 to 2006 was estimated from the Environmental Protection Agency (EPA) Clean Air Status and Trends Network (CASTNET) for the region (Arnold et al. 2012). Wet deposition was calculated in SWAT as the product of the volume of precipitation and user-specified N solute concentration in precipitation, which was estimated from CASTNET digital deposition maps as 1 mg N L^{-1} for NO_3^- and 0.2 mg N L^{-1} for NH_4^+ (Arnold et al. 2012). Dry deposition was calculated as an annual areal loading rate and was also estimated from CASTNET digital N deposition maps as 0.2 kg N ha^{-1} yr^{-1} for NO_3^- and 0.4 kg N ha^{-1} yr^{-1} for NH_4^+ (Arnold et al. 2012).

SWAT does not represent water storage in subbasins containing wetlands and ponds unless specified by the user. Therefore, user defined wetlands and ponds were manually added to tributary subbasins that contained wetlands and ponds (subbasins: 1, 6, 7, 11, and 13) to represent more realistic baseflows. Wetland and pond input data included estimates of the fraction of the subbasin that drains to the waterbody, the surface area [ha], and the volume of water stored [m^3] (Table 2.7) which were obtained through the USGS National Hydrography Dataset Version 2 (NHDPLUSv2; USGS 2013) data and NHDES bathymetry (NHDES 2015).

Daily manure loading from cows at Fernald's dairy farm was estimated by multiplying the manure loaded from a single cow (35 kg N cow^{-1} day^{-1}) by the 170 cows residing at the dairy farm (Conroy and Standish 2013; USDA 1995). Pasture land cover outside of Fernald's dairy farm was assumed to be horse pastures, for which horse manure inputs were estimated as 10 kg N ha^{-1} day^{-1} (Penn 1992).

Septic systems were assumed to be conventional systems with a drainage field. Septic system density was estimated for each land cover classification based on residential density (Table 2.8) and all septic parameters were kept as default values.

Residential fertilizer was assumed to only be applied to urban medium-low density land cover classification. For medium-low density land cover in nearshore subbasins, fertilizer application was estimated at 20 kg N ha^{-1} yr^{-1} based on fertilizer N application amounts obtained from interview with residents and commercial lawn care companies in the Lamprey River watershed (Ruddy et al. 2006). Based on visual assessment of lawn characteristics and low density of lawns, fertilizer application in tributary subbasins was estimated at 3 kg N ha^{-1} yr^{-1}.

2.4.3 SWAT Model Calibration

Modeled discharge (Q_{Mod}) at the Back Creek B, Round Pond Brook, Mountain Cove Brook, and Fernald's Brook A subbasins was calibrated to daily mean field measured discharge (Q_{Obs}) from 5/19/17 to 12/31/17. Eighteen hydrologic parameters were calibrated using the

Sequential Uncertainty Fitting (SUFI2) algorithm (Abbaspour 2015) to minimize a user-defined objective function, which was the sum of squared residuals (SSR) given as,

$$\mathrm{SSR} = \sum(\mathrm{Q_{Obs}} - \mathrm{Q_{Mod}})^2 \qquad \text{Equation 2.21}$$

Final SSR values for the tributaries were: 0.07 m^3 for Back Creek B, 0.03 m^3 for Round Pond Brook, 0.5 m^3 for Mountain Cove Brook, and 0.005 m^3 for Fernald's Brook A. The range of final hydrologic parameter values from calibration are given in Table 2.9.

There were insufficient field measurements of N solute concentration to use the SUFI2 algorithm for N calibration. Therefore, three N transport parameters were manually adjusted until modeled daily mean N solute concentration were the same order of magnitude as field measurements obtained at each sampling station on 5/23/2017, 7/26/2017, 10/13/2017, and 12/8/2017.

After automated and manual calibration, SWAT-CUP simulated discharge and N flux for the 15 subbasins from 1/1/2015 to 4/30/2018 for 200 iterations. Each iteration used a randomly selected combination of hydrologic and N transport parameters from the calibrated ranges to provide uncertainty in model output associated with parameter selection.

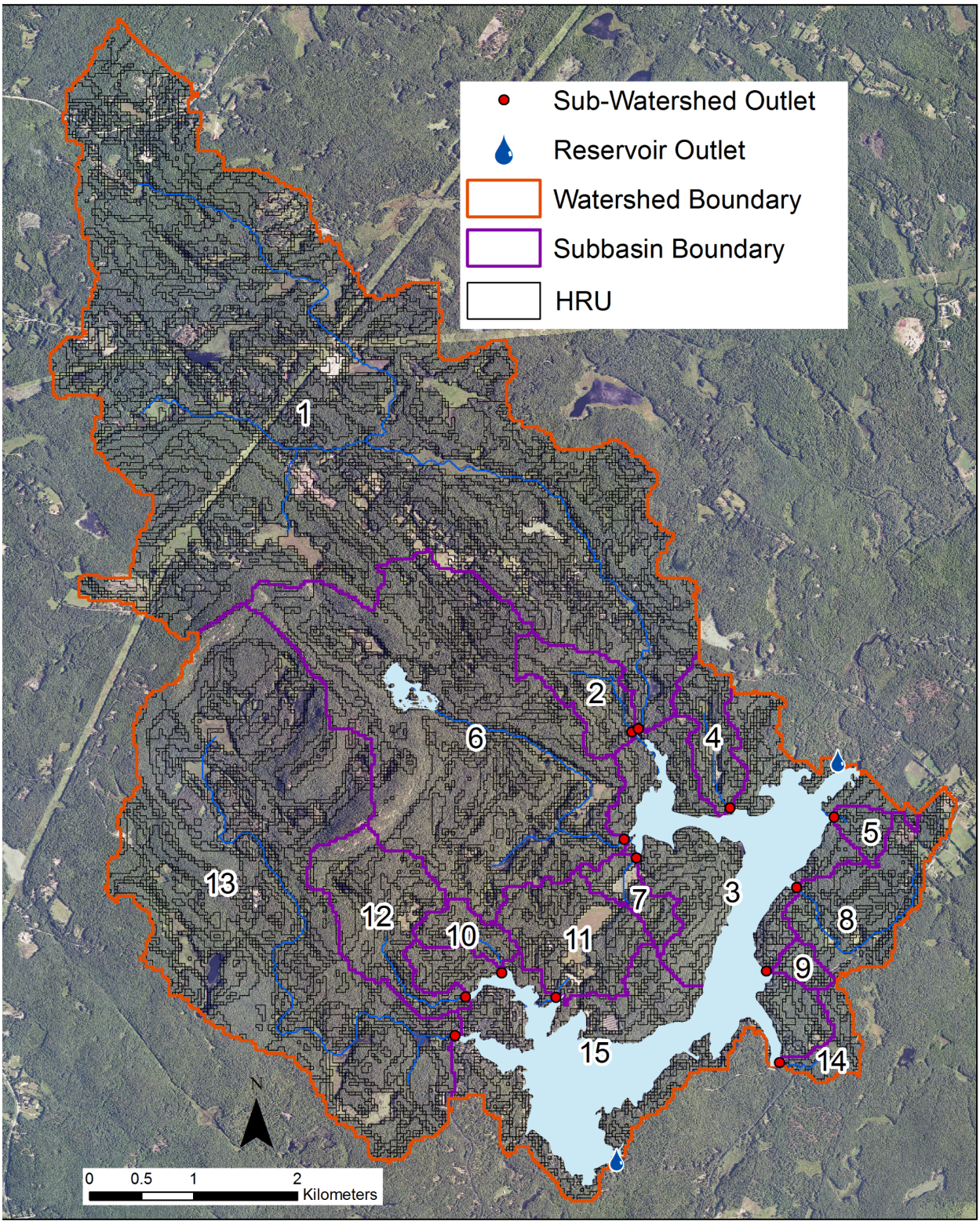

Figure 2.12 Pawtuckaway Lake watershed SWAT 2012 subbasins and hydrologic response unites (HRUs) created in ArcSWAT. Numbered subbasin names can be found in Table 2.1.

Table 2.5 Source land cover reclassified to SWAT land cover classification.

Year	Source Land Cover	SWAT Land Cover	Reasoning/True use
1998	Forest	Mixed Forest	
1998	Agriculture	Pasture	Primarily livestock pasture
1998	Barren	Range Grass	Powerline cuts
1998	Industrial/Commercial	Urban (Industrial)	Electrical substation
1998	Houses/Subdivisions	Urban (Medium-Low Density)	
1998	Transportation/Roads	Urban (Transportation)	
1998	Wetlands	Wetlands	
1998	Water	Water	
2015	Beaches and River Banks	Barren	Pawtuckaway Beach
2015	Disturbed Land	Barren	
2015	Other Barren	Barren	
2015	Forest	Mixed Forest	
2015	Agriculture	Pasture	Fernald's Dairy
2015	Other Agriculture	Pasture	Fernald's Dairy
2015	Maintained Open Areas	Range Grass	Fields and overgrown pastures
2015	Communication	Urban (Industrial)	Cell Tower
2015	Outdoor Recreation	Urban (Low Density)	Pawtuckaway Campground
2015	Single Family/Duplex	Urban (Medium-Low Density)	
2015	Road	Urban (Transportation)	
2015	Parking	Urban (Transportation)	
2015	Auxiliary Transportation	Urban (Transportation)	
2015	Water	Water	
2015	Wetlands	Wetlands	

Table 2.6 Manually adjusted urban land cover parameters.

Land Cover Type	Impervious fraction	Connected Impervious fraction
Urban (Low Density)	0.05	0.02
Urban (Medium Low Density)	0.1	0.05
Urban (Transportation)	0.98 (Default)	0.85

Table 2.7 Pond and wetland characteristics obtained from USGS NHDPLUSv2 and NHDES bathymetry data used in SWAT to represent ponds and wetlands.

SWAT subbasin	Waterbody Type	Fraction of subbasin area that drains into waterbody	Principle Surface Area (ha)	Principle Volume (m^3)
1	Wetland	0.2	20	200
6	Pond	0.15	10	4000
6	Wetland	0.15	20	200
7	Wetland	0.4	1.5	150
11	Wetland	0.5	20	200
13	Wetland	0.1	20	200

Table 2.8 Septic density values for various subbasin and land cover types.

Land Cover	Subbasins	Septic Density (systems/km^2)
Non-low density or medium-low density residential	All	0.001
Low-density residential	All	10
Medium-low density residential	Reservoir	45
Medium-low density residential	Tributary	20

Table 2.9 Hydrologic and N transport parameters and final calibration values for SWAT.

Parameter	units	Description	Calibrated Minimum	Calibrated Maximum
NFIXMX.bsn	[kg N ha^{-1}]	Maximum daily nitrogen fixation	5	15
SDNCO.bsn	[-]	Denitrification threshold water content	0.6	0.8
NPERCO.bsn	[-]	Nitrate percolation coefficient	0.05	0.25
CDN.bsn	[-]	Denitrification rate coefficient	1.2	1.6
CN2.mgt	[-]	Runoff function	-0.6	0
ALPHA_BF.gw	[day^{-1}]	Baseflow alpha factor	0.65	0.8
GW_DELAY.gw	[-]	Time for water to enter shallow aquifer after leaving soil profile	-0.8	-0.35
GWQMN.gw	[mm H_2O]	Depth of water in shallow aquifer for return flow to occur	100	1500
RCHRG_DP.gw	[-]	Fraction of percolation that enters the deep aquifer	0	0
SOL_AWC.sol	[mm H_2O mm $soil^{-1}$]	Available water capacity of soil layer	0.7	1
ESCO.hru	[-]	Soil evaporation compensation factor	0.01	0.3
EPCO.hru	[-]	Plant uptake compensation factor	0.8	0.9
SURLAG.bsn	[-]	Surface Runoff Lag Coefficient	0.6	0.9
GW_REVAP.gw	[-]	Revap coefficient	0.6	0.8
SFTMP.bsn	[C°]	Temperature at which snow and rain are equally likely to occur	.12	1
SMTMP.bsn	[C°]	Minimum temperature for snowmelt to occur	0.49	0.55
SMFMX.bsn	[mm H_2O $(C°)^{-1}$ day^{-1}]	Maximum rate of snowmelt	4.3	5.1
SMFMN.bsn	[mm H_2O $(C°)^{-1}$ day^{-1}]	Minimum rate of snowmelt	2	2.6
TIMP.bsn	[-]	Impact of previous days snowpack temperature on the current days snowpack temperature	0.4	0.6
SNOCOVMX.bsn	[mm H_2O]	Minimum snow water content that corresponds to 100% snow cover	0.75	0.85
SNO50COV.bsn	[-]	Fraction of SNOCOVMX that corresponds to 50% snow cover	0.4	0.5

2.5 Atmospheric N Inputs and Uncertainty

Direct annual wet and dry TDN, DON, and DIN atmospheric deposition to Pawtuckaway Lake was estimated using measurements of N deposition at Thompson Farm in Durham, NH for calendar years 2004 to 2009 (Daley et al. 2010). Thompson Farm measurements, given as an annual areal loads [kg N ha^{-1} yr^{-1}], were normalized by total annual precipitation measured at the NOAA weather gauge USC00272800 in Epping, NH (Figure 2.4) and averaged for 2004 to 2009 (Table 2.10). An annual areal load for the study period was then calculated through the product of total precipitation measured at the NOAA weather station from 5/19/17 to 5/18/18 (1038.4 mm) with the precipitation-normalized annual averaged areal load from Thompson Farm. Direct annual atmospheric N deposition to the reservoir was calculated through the product of the annual areal load for the study period and the reservoir surface area (297 ha). Uncertainty of N deposition estimates were obtained at 95% confidence intervals through calculating N solute deposition using two standard deviations of the Thompson Farm measurements.

The proportion of NO_3^- and NH_4^+ in DIN deposition was estimated using estimates of NO_3^- and NH_4^+ deposition from the ClimCalc model developed for New England and New York (Ollinger et al. 2001) for the Pawtuckaway Lake area. ClimCalc is an online model that requires basic geographic and topographic inputs such as latitude, longitude, elevation, and slope to estimate annual wet and dry inorganic deposition based on a regional gradient of deposition developed using data from the National Atmospheric Deposition Program/National Trends Network (NADP/NTN). ClimCalc input data for Pawtuckaway Lake included: latitude = 43.09, longitude = -71.14, elevation = 83.33 m, and slope = 0. ClimCal estimates that of total DIN deposition for the Pawtuckaway Lake area, 73.67% is NO_3^- and 26.33% is NH_4^+ (Table 2.11).

Table 2.10 Historic measurements of wet dissolved inorganic nitrogen (DIN), wet dissolved organic nitrogen (DON), and wet and dry total dissolved nitrogen (TDN) deposition measured at Thompson Farm in Durham, NH for calendar years 2004 to 2009. Historic total annual precipitation measurements were obtained from the NOAA weather gauge in Epping, NH.

Calendar Year	Precipitation [mm]	Wet DIN [kg N ha^{-1} yr^{-1}]	Wet DON [kg N ha^{-1} yr^{-1}]	Wet TDN [kg N ha^{-1} yr^{-1}]	Dry TDN [kg N ha^{-1} yr^{-1}]	Total TDN [kg N ha^{-1} yr^{-1}]
2004	1199.13	3.89	0.34	4.23	2.45	6.68
2005	1532.38	5.10	0.35	5.35	3.10	8.45
2006	1679.70	4.48	0.31	4.79	2.78	7.57
2007	1189.99	4.05	0.34	4.29	2.49	6.78
2008	1583.94	6.10	0.48	6.58	3.82	10.40
2009	1280.41	4.29	0.15	4.44	2.57	7.01
Mean	1410.93	4.65	0.33	4.95	2.87	7.82

Table 2.11 Estimates of total annual wet and dry nitrate (NO_3^-) and ammonium (NH_4^+) from ClimCalc model for Pawtuckaway Lake area.

NO_3^- [kg N ha^{-1} yr^{-1}]		NH_4^+ [kg N ha^{-1} yr^{-1}]	
Wet	Dry	Wet	Dry
2.9	1.83	1.25	0.43

2.6 N Mass Balance, Retention, and Uncertainty

To quantify annual N retention at Pawtuckaway Lake, a mass balance was constructed for the reservoir from 5/19/17 to 5/18/18. N loaded to Pawtuckaway Lake ($\mathrm{N_{inputs}}$) was calculated through the summation of all N sources:

$$\mathrm{N_{inputs}} = \mathrm{N_{Tributaries}} + \mathrm{N_{Nearshore}} + \mathrm{N_{Atmosphere}} \quad \text{Equation 2.22}$$

where $\mathrm{N_{Tributaries}}$ represents loading from inflowing tributaries, $\mathrm{N_{Nearshore}}$ represents loading from inflowing groundwater and from nearshore overland runoff, and $\mathrm{N_{Atmosphere}}$ represents loading from atmospheric deposition directly to the reservoir water surface. Net internal loading of N from the reservoir's bottom sediment is challenging to quantify and assumed to be negligible in this analysis. N leaving the reservoir ($\mathrm{N_{outputs}}$) was estimated by summing the N flux exiting the lake at the two dam outlets ($\mathrm{N_{DamOutlets}}$),

$$N_{outputs} = N_{DamOutlets}$$ Equation 2.23

N leaving the reservoir via groundwater was assumed negligible for this analysis. Other biological N fluxes to or from the reservoir from migrating insects, water fowl, and fish were also assumed negligible. N species monitored during the study period were total dissolved nitrogen (TDN), ammonium (NH_4^+), nitrite (NO_2^-) plus nitrate (NO_3^-), and dissolved organic nitrogen (DON) which was calculated by taking the difference between TDN and DIN. Annual reservoir N retention (R_N) was then calculated through the difference of N_{inputs} and $N_{outputs}$ expressed as a fraction of N_{inputs}:

$$R_N = \frac{(N_{inputs} - N_{outputs})}{N_{inputs}}$$ Equation 2.24

Uncertainty associated with annual N retention measurements ($\mathcal{E}_{R_N}$) was estimated through first adding the absolute uncertainties of all N inputs in quadrature and then calculating N retention using the upper and lower bounds of N inputs and outputs.

Chapter 3: Field Results and Discussion

This chapter presents results of the annual water and N balance used to calculate annual N retention at Pawtuckaway Lake from 5/19/17 to 5/18/18.

3.1. Pawtuckaway Lake Water Balance

Over the study period, the Pawtuckaway watershed received 1038.4 mm of rainfall (Table 3.1). The most rainfall occurred in October 2017 and April 2018 (Table 3.1). Therefore, the study year was slightly drier than average, as annual rainfall was 10.4 % lower than the average annual rainfall (1159.5 mm) over the previous 20 years.

Runoff at the four monitored tributaries all exhibited a flashy response to rainfall events, with steep rising and recession limbs that are consistent with other steep-sloped headwater streams (Figure 3.1). Monitored tributary runoff varied temporally throughout the year with the greatest flow occurring in late winter and spring and the lowest flow occurring in late summer (Figure 3.2). Of total tributary inflow to Pawtuckaway Lake, 48% occurred at Back Creek B, 20% occurred at Round Pond Brook, 18% occurred at Mountain Cove Brook, 2% occurred at Fernald's Brook A, and 12% came from the nine unmonitored tributaries with the largest discharge event coinciding with the largest rainfall event in mid-April (Figure 3.1).

Discharge at the two monitored outlet streams (Pawtuckaway River and Mile Brook) was influenced by the management of the dams upstream. Since there were no relief pulses released as part of the Instream Flow Management Program from either dam during the study period, all dam outlet management was either during the fall drawdown, during the spring when water levels were raised back to full pool, or to release additional storm runoff following rain events (Wayne Ives, NHDES, personal communication on 7/12/2018). Dam management resulted in a decrease in reservoir storage during the fall and an increase in reservoir storage during the spring.

Discharge was high at both outlets during and after the annual fall drawdown. Fall drawdown began at Drowns Dam on 10/10/17, however the majority of water left between 10/30/17 to 11/20/17 (Figure 3.2, Table 3.2; NHDES 2018). Fall drawdown also began at Dolloff Dam when stop logs were removed on 10/10/17, with additional logs removed on 10/17/17, 10/24/17, 11/14/17, and 11/20/17 (Figure 3.3; Table 3.3; NHDES 2018). To alleviate potential flooding following large rainfall events, stop logs were removed on 5/27/17 and 4/17/18 at Drowns Dam and 4/17/18 at Dolloff Dam. Winter runoff of Mile Brook was less variable compared to Pawtuckaway River runoff, which may have been due to errors in transducer stage measurements as a result of observed ice buildup on the surface of the stream above the transducer at Mile Brook.

The annual water balance for the reservoir is shown in Figure 3.4, Table 3.4, and Table 3.5. The four monitored tributaries were the greatest source of inflow to the reservoir (63.6% of inflow), while unmonitored tributaries, nearshore runoff plus groundwater seepage, and direct precipitation to the reservoir contributed 8.6%, 14.8%, and 13.0% of total inflow respectively (Table 3.4). Mile Brook, Pawtuckaway River, and free water evaporation from the reservoir's water surface accounted for 40.9%, 48.6%, and 10.5% of total outflow from the reservoir respectively (Table 3.5). Monthly totals of evaporation estimates obtained by NHDES for 12/1/1991 – 11/30/1992 were used (NHDES 1995). Overall, total annual inflow to the reservoir (23,727 $\pm$ 4,282 [1000 m^3] or 440 $\pm$ 80 [mm], Table 3.4) was greater than total annual outflow (18,146 $\pm$ 10,052 [1000 m^3] or 336 $\pm$ 188 [mm], Table 3.4), however since there was no observed change in reservoir pool level at the start and end of the study period, annual change in reservoir storage was assumed zero (Figures 3.2 and 3.3). Because the residual between reservoir inflow and outflow was highest during winter and spring months, when transducers at the dam outlets were observed to have been affected by ice buildup, the majority of the residual

most likely stems from an underprediction of outflow during these months caused by ice and inadequacies in both outlet stage-discharge curves to represent higher flows.

The annual runoff coefficient (discharge/precipitation) for the Pawtuckaway Lake watershed was calculated as 0.29, which falls within the expected range for a predominately forested watershed (Chow 1962).

To characterize how water is stored and released at Pawtuckaway Lake during the recreation season and the recreation off-season, hourly reservoir release normalized by mean hourly release for the study period was plotted against the relative active storage volume normalized by the maximum active storage volume (Figure 3.5). The resulting curve indicates that discharge is released at a much greater rate at lower reservoir storage levels during the recreation off-season and that water is retained during the recreation season until the reservoir is at full pool.

Table 3.1 Monthly totals of rainfall from 2017-05-19 to 2018-05-18 measured at NOAA weather station USC00272800 in Epping, NH.

Month	Monthly total [mm]	Fraction of total
May 19th, 2017 - May 31st, 2017	51.3	4.9%
Jun 2017	82.5	7.9%
Jul 2017	91.0	8.8%
Aug 2017	87.9	8.5%
Sep 2017	59.7	5.7%
Oct 2017	139.4	13.4%
Nov 2017	42.9	4.1%
Dec 2017	69.3	6.7%
Jan 2018	70.9	6.8%
Feb 2018	98.3	9.5%
Mar 2018	89.7	8.6%
Apr 2018	140.0	13.5%
May 1st, 2017 - May 18th, 2017	15.5	1.5%
Total	1038.4	

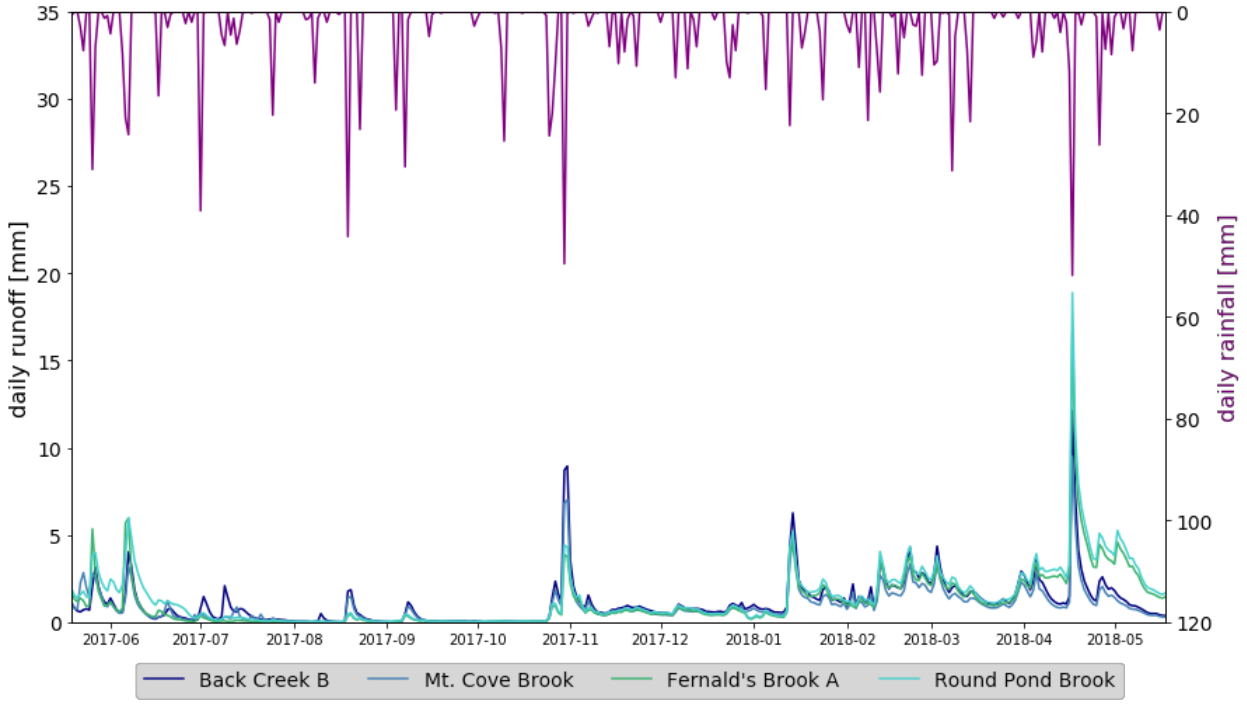

Figure 3.1 Daily runoff for the four monitored tributaries and daily rainfall from 2017-05-19 to 2018-05-18. Rainfall measurements are from NOAA weather station USC00272800 in Epping, NH.

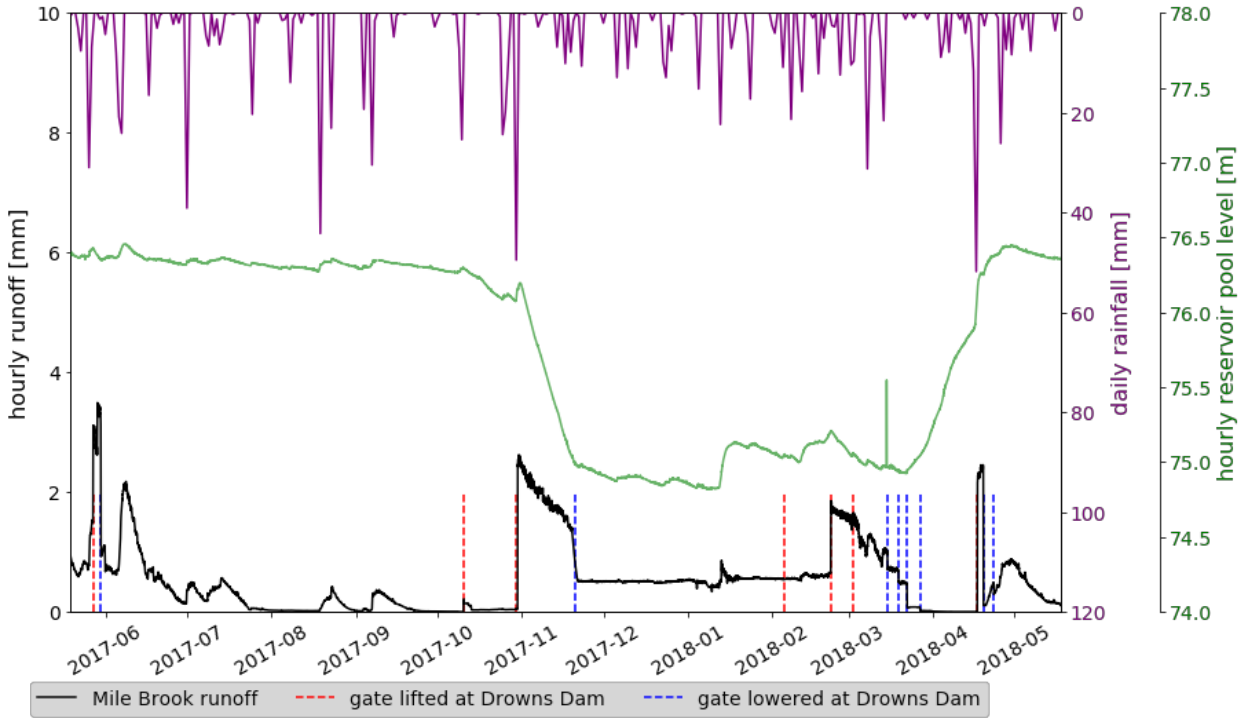

Figure 3.2 Daily runoff for Mile Brook, daily rainfall, and reservoir pool level for Pawtuckaway Lake (in meters above sea level) from 5/19/17 to 5/18/18. Rainfall measurements are from NOAA weather station USC00272800 in Epping, NH. Vertical dashed lines show timing of documented stop log gate adjustments at Drowns Dam.

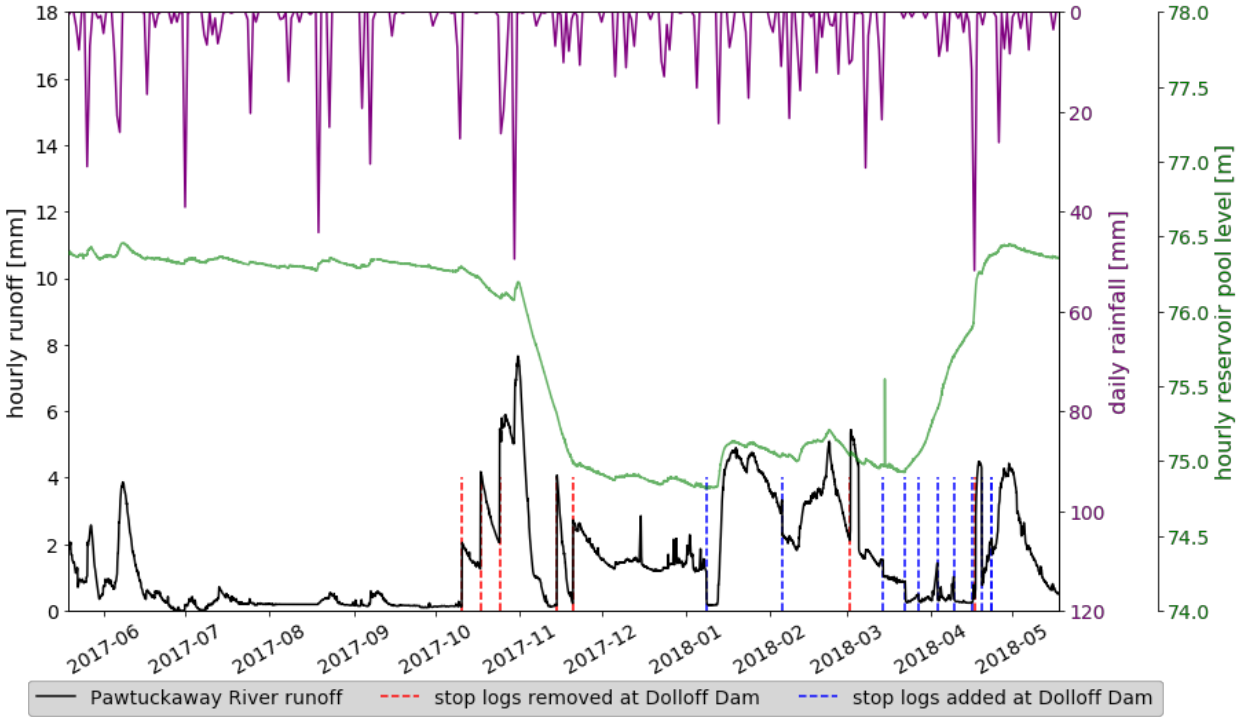

Figure 3.3 Daily runoff for the Pawtuckaway River, daily rainfall, and reservoir pool level for Pawtuckaway Lake (in meters above sea level) from 5/19/17 to 5/18/18. Rainfall measurements are from NOAA weather station USC00272800 in Epping, NH. Vertical dashed lines show timing of documented stop log adjustments at Dolloff Dam.

Table 3.2 Stop log gate management at the Drowns Dam outlet by NHDES (information provided by Wayne Ives, NHDES) showing the height to which the gate is raised above the lake bottom where a gate height of 0" indicates that the gate is closed.

Date Time	Gate height
5/27/17 14:00	10"
5/30/17 10:30	0"
10/10/17 16:00	1"
10/30/17 12:00	24"
11/20/17 11:45	4"
2/5/18 11:30	9"
2/22/18 14:30	27"
3/2/18 12:30	40"
3/15/18 11:00	12"
3/19/18 12:00	8"
3/22/18 14:35	2"
3/27/18 9:30	1"
4/17/18 9:50	24"
4/19/18 15:20	1"
4/23/18 12:00	0"

Table 3.3 Stop log management at the Dolloff Dam outlet by NHDES (information provided by Wayne Ives, NHDES) showing the number of stop logs absent from each bay where 0 indicates all stop logs are present and reservoir is at full pool.

Date Time	Bay 1	Bay 2	Bay 3
10/10/17 15:30	1	1.5	1
10/17/17 11:45	2	2.5	2
10/24/17 13:00	3	3.5	3
11/14/17 14:00	6	7.5	6
11/20/17 11:15	8	8.5	8
1/8/18 11:00	8	8	8
2/5/18 9:15	7	8.5	7
3/2/18 10:00	8	8.5	8
3/2/18 11:00	7	8.5	7
3/14/18 11:30	6	7.5	6
3/22/18 14:10	6	6.5	6
3/27/18 10:00	6	6	6
4/3/18 10:30	4	4	4
4/9/18 9:30	2	2	2
4/16/18 10:30	1	1	1
4/17/18 10:10	2	2	2
4/19/18 16:00	0	1	0
4/23/18 11:30	0	0	0

Table 3.4 Monthly totals of water inputs to Pawtuckaway Lake from 5/19/17 to 5/18/18. May 2017 only includes 5/19/17 through 5/31/17 and May 2018 only includes 5/1/18 to 5/18/18. Inputs include both monitored and unmonitored tributaries, overland runoff and groundwater seepage (Nearshore), and direct precipitation to the reservoir's water surface (Precip).

	Water Volume [10^3 m^3]														
	Months													Total Annual	Mean Monthly
Inputs	5-17	6-17	7-17	8-17	9-17	10-17	11-17	12-17	1-18	2-18	3-18	4-18	5-18		
Back Creek B	336 ± 109	496 ± 185	318 ± 128	160 ± 92	106 ± 60	522 ± 323	593 ± 195	474 ± 158	1,016 ± 334	1,244 ± 403	1,146 ± 363	1,549 ± 517	314 ± 104	8,273 ± 2971	689 ± 248
Mountain Cove Brook	206 ± 138	202 ± 94	66 ± 44	54 ± 37	39 ± 23	186 ± 117	211 ± 70	169 ± 57	360 ± 119	440 ± 143	406 ± 129	548 ± 183	112 ± 37	2,999 ± 1191	250 ± 99
Round Pond Brook	187 ± 121	355 ± 230	39 ± 29	20 ± 17	19 ± 16	91 ± 74	166 ± 103	133 ± 83	316 ± 208	427 ± 281	394 ± 252	914 ± 691	346 ± 240	3,407 ± 2345	284 ± 195
Fernald's Brook A	23 ± 23	32 ± 32	3 ± 3	2 ± 2	2 ± 2	11 ± 9	21 ± 13	17 ± 10	41 ± 27	55 ± 36	51 ± 32	119 ± 90	45 ± 31	422 ± 329	35 ± 27
Unmonitored tributaries	114 ± 68	166 ± 104	39 ± 20	24 ± 12	18 ± 10	89 ± 47	120 ± 68	96 ± 55	216 ± 124	277 ± 161	255 ± 149	464 ± 290	145 ± 96	2,023 ± 1203	167 ± 100
Nearshore	496 ± 112	333 ± 72	121 ± 93	58 ± 24	44 ± 5	86 ± 31	108 ± 32	71 ± 13	181 ± 181	446 ± 119	879 ± 193	698 ± 45	-	3,522 ± 971	294 ± 81
Precip	152 ± 15	245 ± 25	270 ± 27	261 ± 26	177 ± 18	414 ± 41	127 ± 13	206 ± 21	210 ± 21	292 ± 29	266 ± 27	415 ± 42	46 ± 5	3,082 ± 308	257 ± 26
Total Inflow	1,514 ± 252	1,829 ± 170	856 ± 170	579 ± 107	405 ± 70	1,399 ± 358	1,346 ± 244	1,166 ± 197	2,340 ± 476	3,181 ± 551	3,397 ± 523	4,707 ± 935	1,008 ± 283	23,727 ± 4,282	1,977 ± 357

Table 3.5 Monthly totals of water outputs from Pawtuckaway Lake from 5/19/17 to 5/18/18. May 2017 only includes 5/19/17 through 5/31/17 and May 2018 only includes 5/1/18 to 5/18/18. Outputs include both dam outlets (Mile Brook and Pawtuckaway Lake) and evaporation from the reservoir's surface (Evap). ΔS represents the change in reservoir storage and Residual represents the difference between Total Inflow from Table 3.4 and Total Outflow and ΔS.

	Water Volume [10^3 m^3]														
	Months													Total Annual	Mean Monthly
Outputs	5-17	6-17	7-17	8-17	9-17	10-17	11-17	12-17	1-18	2-18	3-18	4-18	5-18		
Mile Brook	669 ± 428	915 ± 515	299 ± 175	92 ± 71	117 ± 87	181 ± 158	1,566 ± 1,027	595 ± 291	626 ± 308	872 ± 473	832 ± 528	424 ± 394	235 ± 125	7,423 ± 4,580	619 ± 382
Pawtuckaway River	266 ± 198	479 ± 428	128 ± 107	119 ± 82	105 ± 92	1,251 ± 1,699	903 ± 930	716 ± 499	1,489 ± 1,846	1,440 ± 1,572	707 ± 689	764 ± 824	461 ± 366	8,828 ± 9,374	736 ± 781
Evap	89	515	449	346	247	162	0	0	0	0	0	0	89	1,897	159
Total Outflow	1,024 ± 472	1,909 ± 670	876 ± 205	557 ± 108	469 ± 127	1,594 ± 1,706	2,468 ± 1,389	1,311 ± 578	2,115 ± 1,872	2,312 ± 1,642	1,539 ± 868	1,188 ± 913	785 ± 387	18,146 ± 10,433	1,513 ± 869
ΔS	-63	-72	-100	-9	-45	-335	-3,755	-162	+597	+27	+498	+3,573	-262	-108	-9
Residual	-553	+8	-80	-31	+19	-140	-2,633	-17	+372	-842	-1,360	+54	-485	-5,688	-474

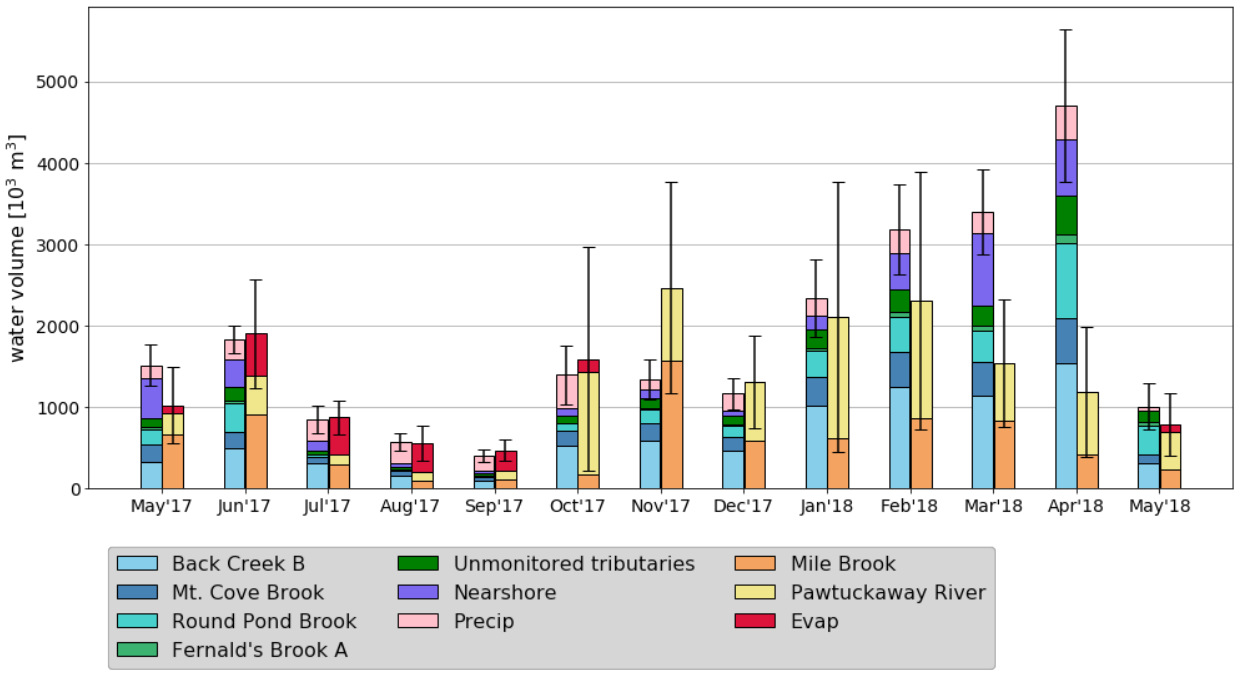

Figure 3.4 Monthly totals of tributary inflow (Back Creek B, Mountain Cove Brook, Round Pond Brook, Fernald's Brook A, and nine unmonitored tributaries) and overland runoff and groundwater seepage (Nearshore), and direct precipitation into the reservoir (Precip) to outflow from Mile Brook, Pawtuckaway River, and evaporation from the reservoir's surface (Evap) from Pawtuckaway Lake. May'17 only includes 5/19 through 5/31 and May'18 only includes 5/1 to 5/18.

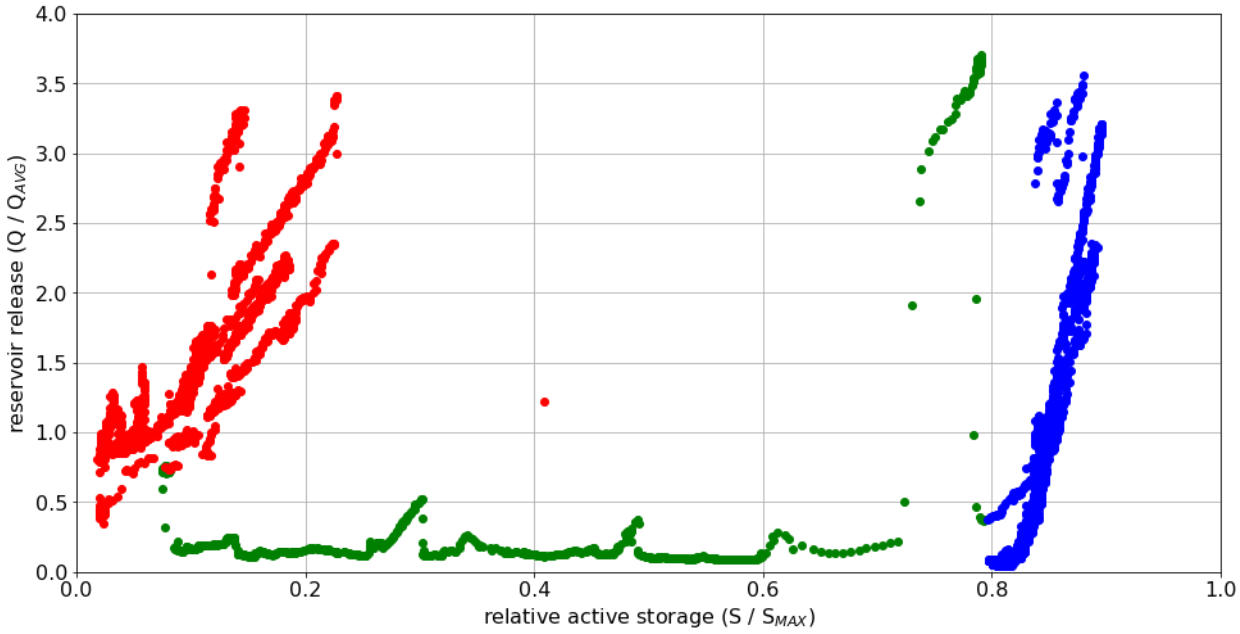

Figure 3.5 Hourly reservoir release (Q) normalized by mean annual hourly reservoir release (Q_{AVG}) compared to relative active reservoir storage (S) normalized by the maximum relative reservoir storage (S_{MAX}) for Pawtuckaway Lake from 5/19/17 to 5/18/18. Blue dots represent reservoir outflow during the recreation season once reservoir pool level was full (5/19/17 to 10/9/17 and 4/20/18 to 5/18/17), red dots represent reservoir outflow after the fall drawdown and throughout the recreation off-season (11/20/17 to 3/22/18), and green dots represent when stop logs were put back in early spring to raise reservoir water level to full pond (3/19/18 to 4/19/18).

3.2 Monitored Tributary and Dam Outlet N Solute Concentrations

The concentration of N solutes varied both spatially and temporally at all sampling sites around Pawtuckaway Lake (Tables 3.6 and 3.7). On average, N solute concentrations were highest at Fernald's Brook A (Tables 3.6 and 3.7), likely due to the runoff from cow pastures at the farm upstream, with concentrations peaking in winter, when biological N uptake is lowest. Conversely, TDN and DON concentrations peaked at Back Creek B, Round Pond Brook, and Mountain Cove Brook in the fall (Tables 3.6 and 3.7), while TDN concentrations were lowest at Back Creek B, Mountain Cove Brook, Fernald's Brook A during the summer and lowest at Round Pond Brook during the spring (Table 3.6). On average, DON made up the largest portion of TDN at Back Creek B (83.5%), Round Pond Brook (81.5%) and Fernald's Brook A (61.5%) while almost being in equal proportion to DIN at Mountain Cove Brook (50.8%).

NO_3^- and NH_4^+ concentrations remained relatively constant at Round Pond Brook and Back Creek B year-round, while there was more seasonal variability in both solutes at Fernald's Brook A and Mountain Cove Brook (Tables 3.6 and 3.7). NO_3^- and NH_4^+ concentrations peaked in winter at Fernald's Brook A and in spring at Mountain Cove Brook (Tables 3.6 and 3.7). NO_3^- made up most of DIN at Fernald's Brook A (92.3% of DIN on average), Back Creek B (83.6% of DIN on average), and Round Pond Brook (80.3% of DIN on average). NH_4^+ concentrations were highest at Mountain Cove Brook, as NH_4^+ concentration peaked in the fall and made up 40.3% of DIN on average. NH_4^+ concentrations were also relatively high at Mile Brook (34.9% of DIN on average), while NH_4^+ made up a smaller portion of DIN (20.7%) at Pawtuckaway River. Mean annual NO_3^- concentrations at all monitoring sites, excluding Fernald's Brook A, were an order of magnitude greater than measurements obtained by NHDES from 12/1/1991 – 11/30/1992 (Table 3.8), which might be the result of potentially higher N concentrations groundwater that have accumulated over the past 25 years. N concentrations obtained on 5/23/17, excluding N concentration obtained at Round Pond Brook, were all close to detection limits, while N concentrations obtained on 4/8/2018 were all consistently higher. Therefore, N concentrations obtained on 5/23/17 should be interpreted with caution.

All N solute concentrations, excluding DON, were on average higher downstream of the Dolloff Dam outlet (Pawtuckaway River) than measurements obtained just upstream within the reservoir (Tables 3.6 and 3.7). This suggests there were additional N sources introduced downstream of the dam outlet such as N groundwater inputs from either septic tanks or fertilizer use from the surrounding residential homes.

N solute concentration-discharge relationships showed weak diluting relationships (negative correlation) for TDN, NO_3^-, and DON, at Fernald's Brook A (Figure 3.6 A, B, D), TDN and DON at Mountain Cove Brook (Figure 3.7 A, D), and for all N solutes at Round Pond Brook (Figure 3.9). NO_3^- concentration-discharge relationship at Mountain Cove Brook showed a

flushing relationship (positive correlation; Figure 3.7 B). NH_4^+ concentration-discharge relationships at Fernald's Brook A and Mountain Cove Brook showed a chemo-static (constant) relationship (Figures 3.6 C and 3.7 C), while at Mile Brook and Pawtuckaway River is showed a flushing relationship (Figures 3.10 C and 3.11 C). All other N solute concentration-discharge relationships were inconclusive. All concentration-discharge regressions were found not to be statistically significant except for NH_4^+ concentration-discharge relationships at Mile Brook ($p = 0.01$; Table 3.13) and Pawtuckaway River ($p = 0.007$; Table 3.14).

Table 3.6 Seasonality of total dissolved nitrogen (TDN) and nitrate (NO_3^-) concentration at each sampling station. Summer measurements were obtained on 5/13/17 and 7/26/17, fall measurements were obtained on 10/13/17, winter measurements were obtained on 12/8/17 and 1/19/17, and spring measurements were obtained on 4/8/17.

	TDN [mg N L^{-1}]					NO_3^- [mg N L^{-1}]				
Tributary	Annual Mean	Summer	Fall	Winter	Spring	Annual Mean	Summer	Fall	Winter	Spring
Back Creek B	0.285	0.134	0.554	0.352	0.183	0.038	0.022	0.080	0.037	0.030
Mountain Cove Brook	0.143	0.019	0.249	0.198	0.178	0.033	0.009	0.050	0.024	0.082
Round Pond Brook	0.281	0.285	0.457	0.242	0.176	0.041	0.047	0.070	0.028	0.029
Fernald's Brook A	0.979	0.328	0.524	1.738	1.222	0.356	0.123	0.120	0.658	0.458
Dam Outlets										
Mile Brook	0.295	0.239	0.233	0.411	0.239	0.044	0.053	0.010	0.049	0.053
Pawtuckaway River	0.221	0.122	0.092	0.285	0.419	0.068	0.058	0.010	0.043	0.197
In-reservoir	0.174	0.024	0.060	0.272	0.244	0.026	0.004	0.010	0.038	0.041

Table 3.7 Seasonality of ammonium (NH_4^+) and dissolved organic nitrogen (DON) concentration at each sampling station. Summer measurements were obtained on 5/13/17 and 7/26/17, fall measurements were obtained on 10/13/17, winter measurements were obtained on 12/8/17 and 1/19/17, and spring measurements were obtained on 4/8/17.

	NH_4^+ [μg N L^{-1}]					DON [mg N L^{-1}]				
Tributary	Annual Mean	Summer	Fall	Winter	Spring	Annual Mean	Summer	Fall	Winter	Spring
Back Creek B	8.7	4.5	19.1	11.9	0.0	0.239	0.022	0.080	0.037	0.030
Mountain Cove Brook	21.1	9.0	82.5	4.1	18.0	0.089	0.009	0.050	0.024	0.082
Round Pond Brook	8.8	11.0	2.5	12.2	4.0	0.231	0.047	0.070	0.028	0.029
Fernald's Brook A	28.4	15.5	1.3	62.6	13.0	0.595	0.123	0.120	0.658	0.458
Dam Outlets										
Mile Brook	28.6	15.0	9.2	59.8	13.0	0.222	0.053	0.010	0.049	0.053
Pawtuckaway River	10.5	4.0	14.6	18.3	8.0	0.142	0.058	0.010	0.043	0.197
In-reservoir	7.2	3.0	10.4	9.8	3.0	0.141	0.004	0.010	0.038	0.041

Table 3.8 Seasonality of nitrate (NO_3^-) concentration at each sampling station for the study period (5/19/17 - 5/18/18) and measurements taken by New Hampshire Department of Environmental Services (NHDES) from 12/1/1991 to 11/30/1992. For 5/19/17 - 5/18/18, summer measurements were obtained on 5/13/17 and 7/26/17, fall measurements were obtained on 10/13/17, winter measurements were obtained on 12/8/17 and 1/19/17, and spring measurements were obtained on 4/8/17.

	NO_3^- [mg N L^{-1}]									
	5/19/17 - 5/18/18					NHDES 1995				
Tributary	Annual Mean	Summer	Fall	Winter	Spring	Annual Mean	Summer	Fall	Winter	Spring
Back Creek B	0.285	0.134	0.554	0.352	0.183	0.02	0.03	0.04	< 0.02	< 0.02
Mountain Cove Brook	0.143	0.019	0.249	0.198	0.178	0.03	0.03	0.04	0.03	< 0.02
Round Pond Brook	0.281	0.285	0.457	0.242	0.176	0.04	0.07	0.04	< 0.02	< 0.02
Fernald's Brook A	0.979	0.328	0.524	1.738	1.222	2.44	0.09	0.04	12.00	0.03
Dam Outlets										
Mile Brook	0.295	0.239	0.233	0.411	0.239	0.08	0.06	0.08	0.17	0.04
Pawtuckaway River	0.221	0.122	0.092	0.285	0.419	0.06	0.04	0.06	0.13	0.03

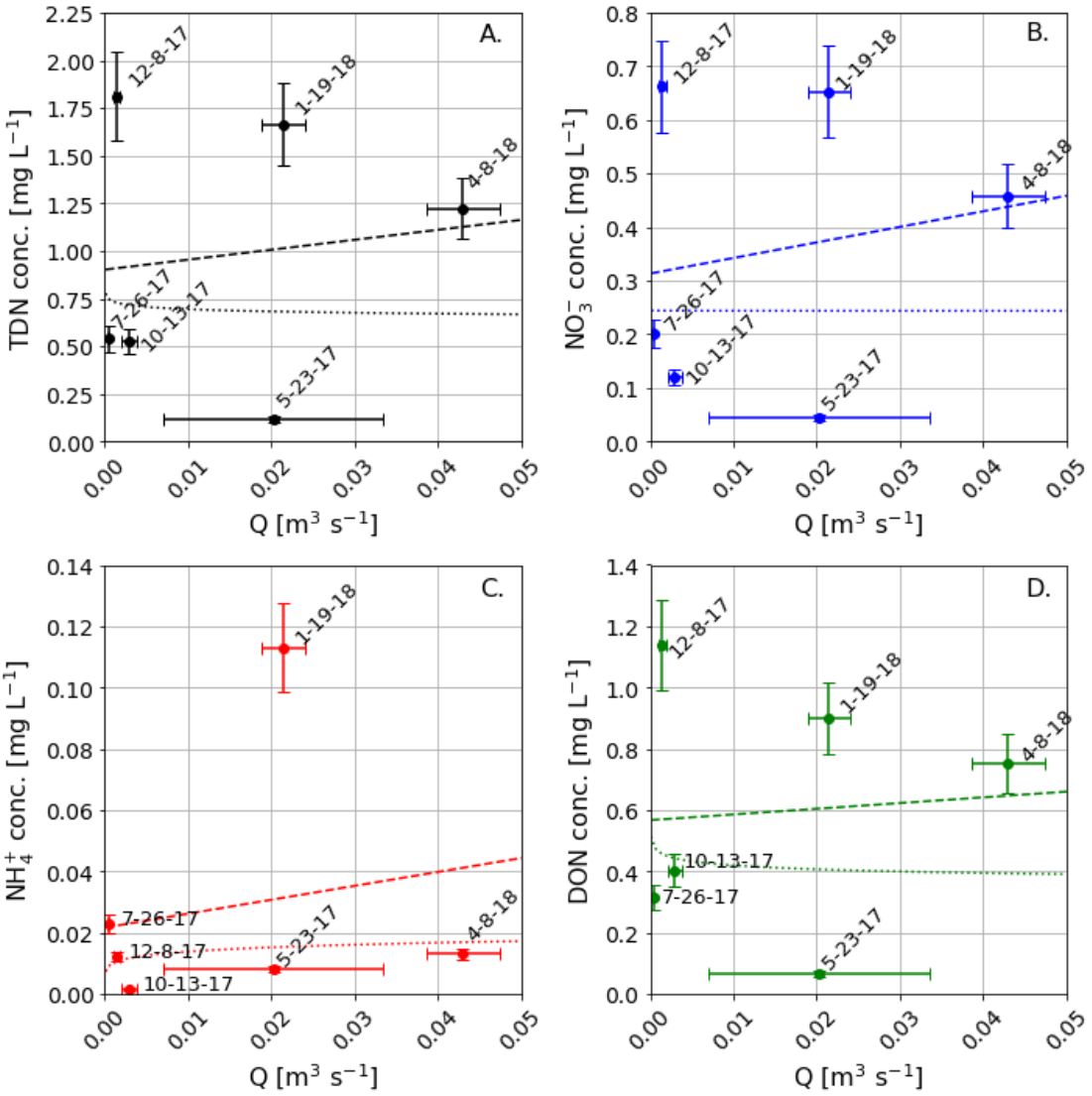

Figure 3.6 Relationship between total dissolved nitrogen (TDN; A.), nitrate (NO_3^-; B.), ammonium (NH_4^+; C.), and dissolved organic nitrogen (DON; D.) concentration and discharge (Q) at Fernald's Brook A. Error bars represent the uncertainty associated with each discharge and nitrogen concentration measurement. Dashed lines and dotted curves represent the best fit linear regression line and power law curve of the relationship respectively. Regression line and power law equations can be found in Table 3.9.

Table 3.9 Best fit regression equations to the relationship between total dissolved nitrogen (TDN), nitrate (NO_3^-), ammonium (NH_4^+), and dissolved organic nitrogen (DON) concentration (y) and discharge (x) at Fernald's Brook A from 5/19/17 – 5/18/18.

N species	Linear Regression	r^2	p value	Power Law	r^2	p value
TDN	$y = 5.21 \cdot x + 0.90$	0.016	0.811	$y = 0.62 \cdot x^{-0.025}$	0.002	0.934
NO_3^-	$y = 2.90 \cdot x + 0.31$	0.031	0.735	$y = 0.24 \cdot x^{-0.004}$	< 0.001	0.999
NH_4^+	$y = 0.45 \cdot x + 0.02$	0.032	0.732	$y = 0.03 \cdot x^{0.138}$	0.030	0.740
DON	$y = 1.86 \cdot x + 0.57$	0.006	0.884	$y = 0.34 \cdot x^{-0.044}$	0.006	0.883

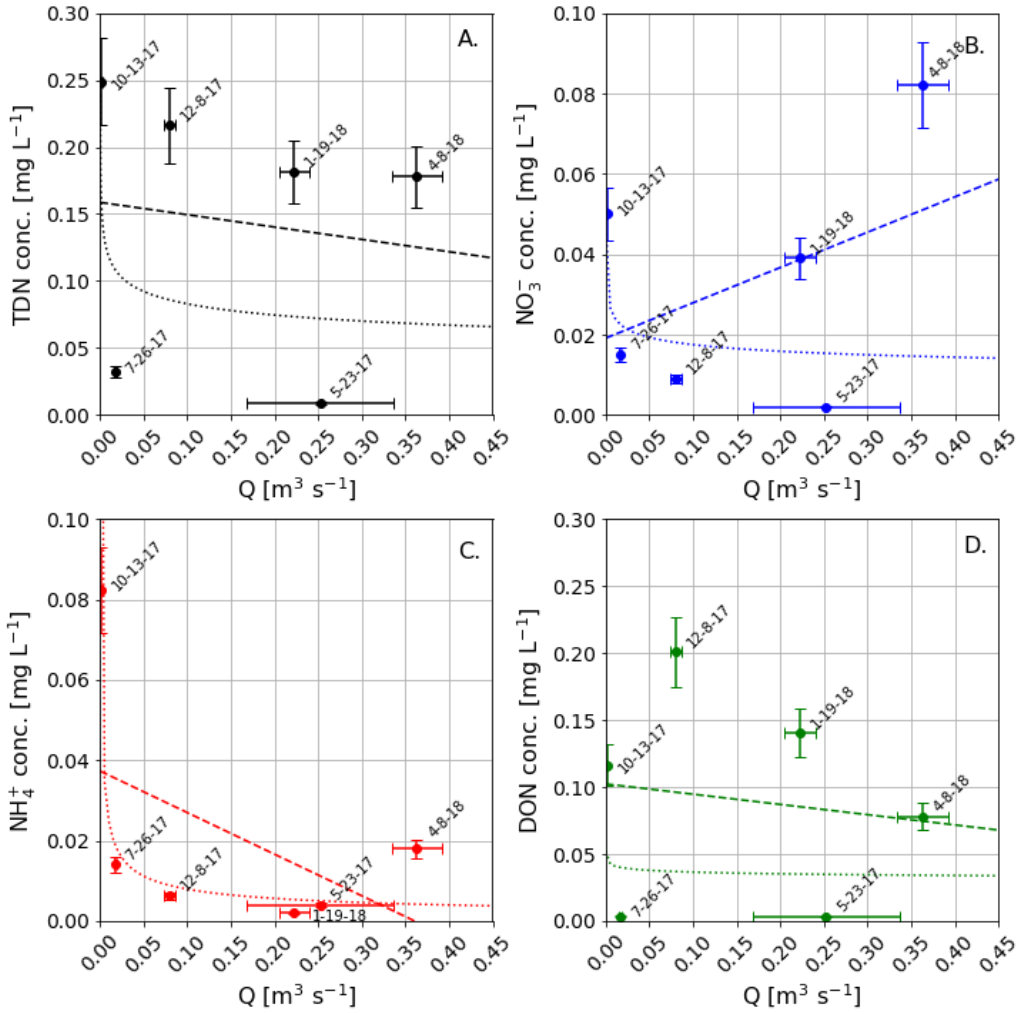

Figure 3.7 Relationship between total dissolved nitrogen (TDN; A.), nitrate (NO_3^-; B.), ammonium (NH_4^+; C.), and dissolved organic nitrogen (DON; D.) concentration and discharge (Q) at Mountain Cove Brook. Error bars represent the uncertainty associated with each discharge and nitrogen concentration measurement. Dashed lines and dotted curves represent the best fit linear regression line and power law curve of the relationship respectively. Regression line and power law equations can be found in Table 3.10.

Table 3.10 Best fit regression equations to the relationship between total dissolved nitrogen (TDN), nitrate (NO_3^-), ammonium (NH_4^+), and dissolved organic nitrogen (DON) concentration (y) and discharge (x) at Mountain Cove Brook from 5/19/17 – 5/18/18.

N species	Linear Regression	r^2	p value	Power Law	r^2	p value
TDN	$y = -0.09 \cdot x + 0.16$	0.018	0.799	$y = 0.053 \cdot x^{-0.153}$	0.053	0.660
NO_3^-	$y = 0.087 \cdot x + 0.02$	0.177	0.406	$y = 0.013 \cdot x^{-0.142}$	0.044	0.689
NH_4^+	$y = -0.13 \cdot x + 0.04$	0.239	0.324	$y = 0.003 \cdot x^{-0.497}$	0.059	0.074
DON	$y = -0.076 \cdot x + 0.90$	0.020	0.7887	$y = 0.032 \cdot x^{-0.052}$	0.002	0.918

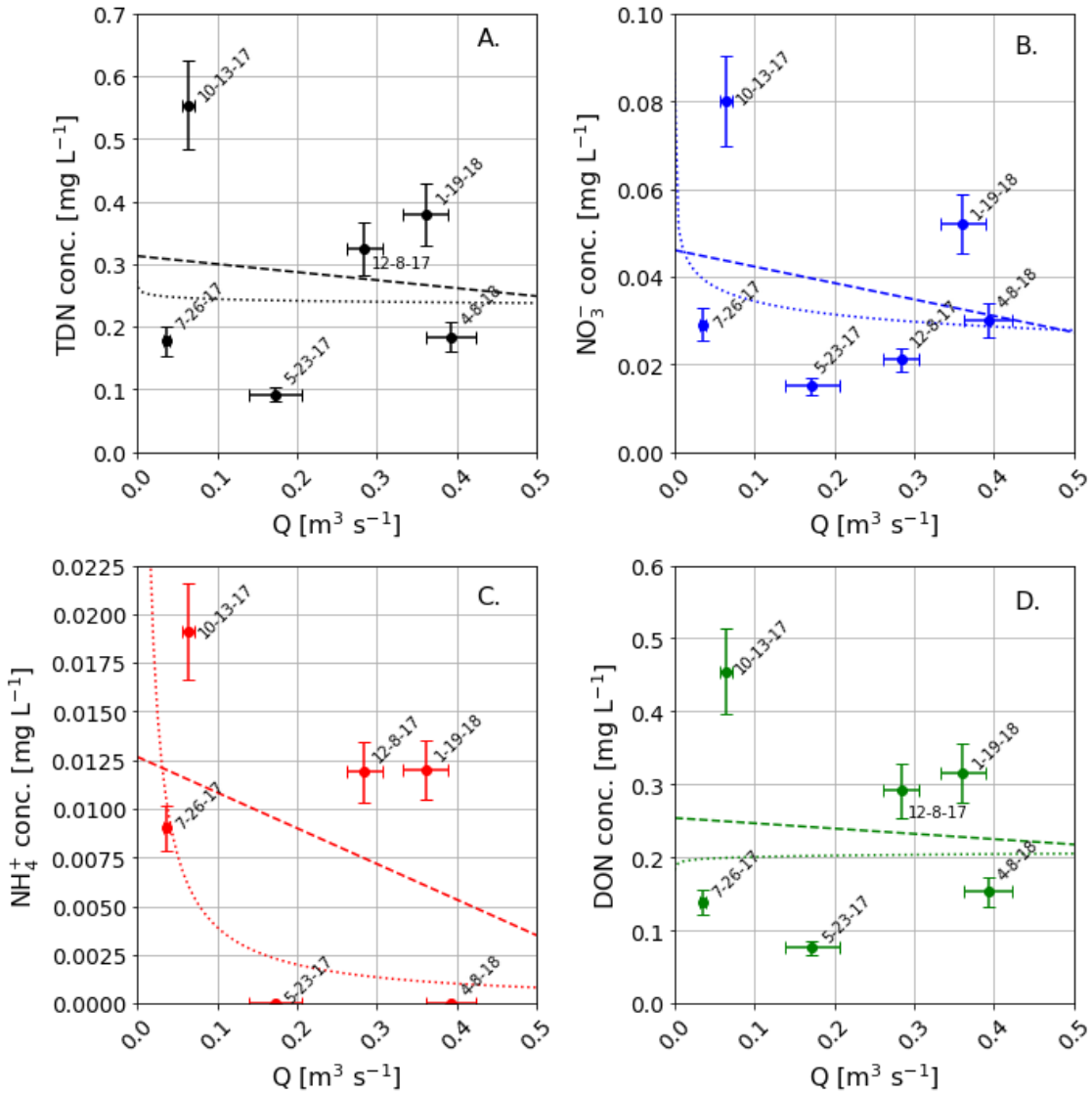

Figure 3.8 Relationship between total dissolved nitrogen (TDN; A.), nitrate (NO_3^-; B.), ammonium (NH_4^+; C.), and dissolved organic nitrogen (DON; D.) concentration and discharge (Q) at Back Creek B. Error bars represent the uncertainty associated with each discharge and nitrogen concentration measurement. Dashed lines and dotted curves represent the best fit linear regression line and power law curve of the relationship respectively. Regression line and power law equations can be found in Table 3.11.

Table 3.11 Best fit regression equations to the relationship between total dissolved nitrogen (TDN), nitrate (NO_3^-), ammonium (NH_4^+), and dissolved organic nitrogen (DON) concentration (y) and discharge (x) at Back Creek B from 5/19/17 – 5/18/18.

N species	Linear Regression	r^2	p value	Power Law	r^2	p value
TDN	$y = -0.128 \cdot x + 0.31$	0.013	0.828	$y = 0.235 \cdot x^{-0.016}$	< 0.001	0.963
NO_3^-	$y = -0.030 \cdot x + 0.05$	0.055	0.655	$y = 0.025 \cdot x^{-0.134}$	0.047	0.679
NH_4^+	$y = -0.018 \cdot x + 0.01$	0.136	0.470	$y = 0.0004 \cdot x^{-0.972}$	0.146	0.454
DON	$y = -0.072 \cdot x + 0.25$	0.006	0.883	$y = 0.207 \cdot x^{-0.014}$	< 0.001	0.969

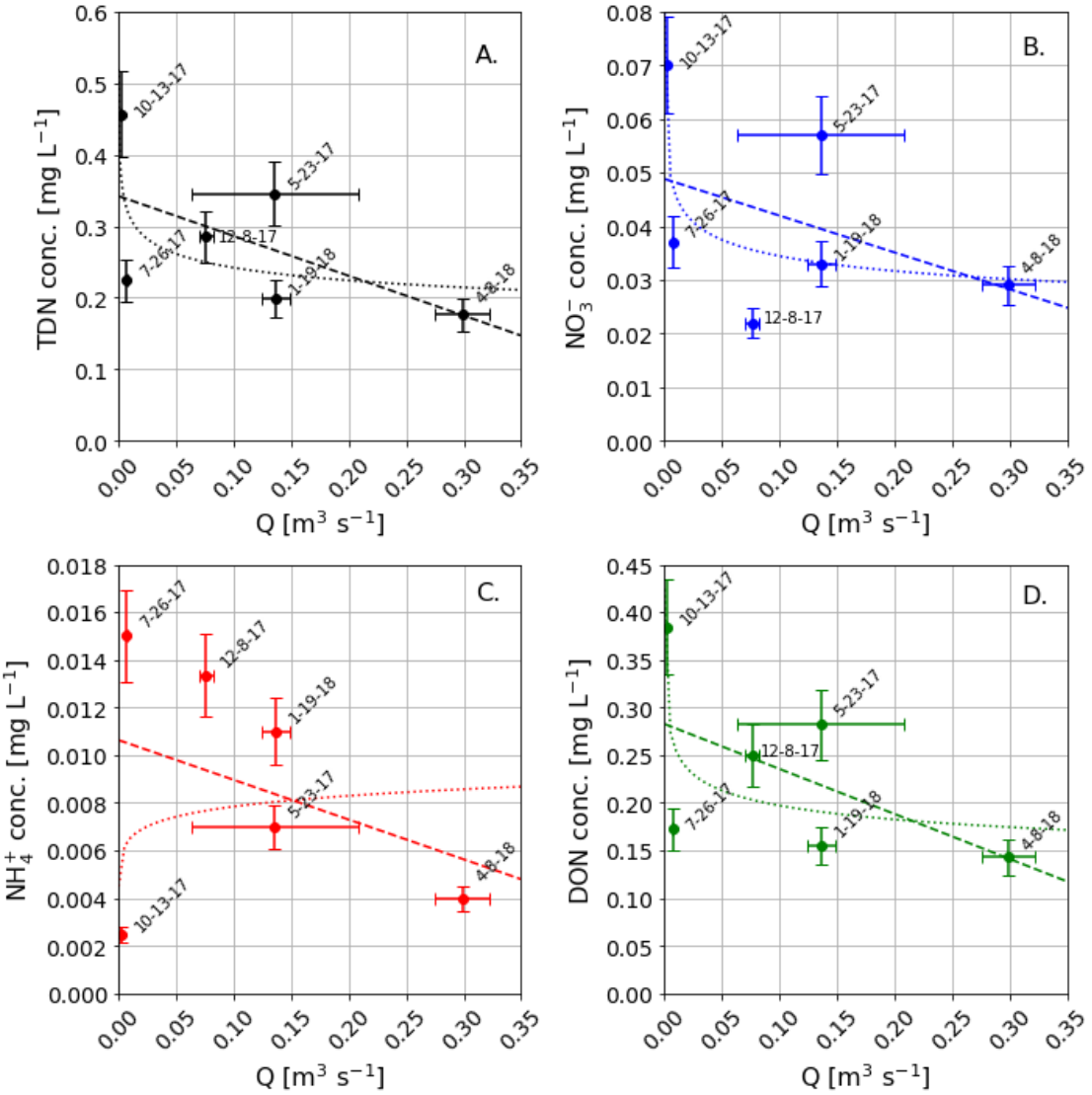

Figure 3.9 Relationship between total dissolved nitrogen (TDN; A.), nitrate (NO_3^-; B.), ammonium (NH_4^+; C.), and dissolved organic nitrogen (DON; D.) concentration and discharge (Q) at Round Pond Brook. Error bars represent the uncertainty associated with each discharge and nitrogen concentration measurement. Dashed lines and dotted curves represent the best fit linear regression line and power law curve of the relationship respectively. Regression line and power law equations can be found in Table 3.12.

Table 3.12 Best fit regression equations to the relationship between total dissolved nitrogen (TDN), nitrate (NO_3^-), ammonium (NH_4^+), and dissolved organic nitrogen (DON) concentration (y) and discharge (x) at Round Pond Brook from 5/19/17 – 5/18/18.

N species	Linear Regression	r^2	p value	Power Law	r^2	p value
TDN	$y = -0.557 \cdot x + 0.34$	0.333	0.230	$y = 0.187 \cdot x^{-0.111}$	0.363	0.206
NO_3^-	$y = -0.069 \cdot x + 0.05$	0.168	0.418	$y = 0.026 \cdot x^{-0.121}$	0.306	0.255
NH_4^+	$y = -0.016 \cdot x + 0.01$	0.129	0.480	$y = 0.009 \cdot x^{-0.081}$	0.049	0.673
DON	$y = -0.472 \cdot x + 0.28$	0.309	0.251	$y = 0.153 \cdot x^{-0.111}$	0.314	0.247

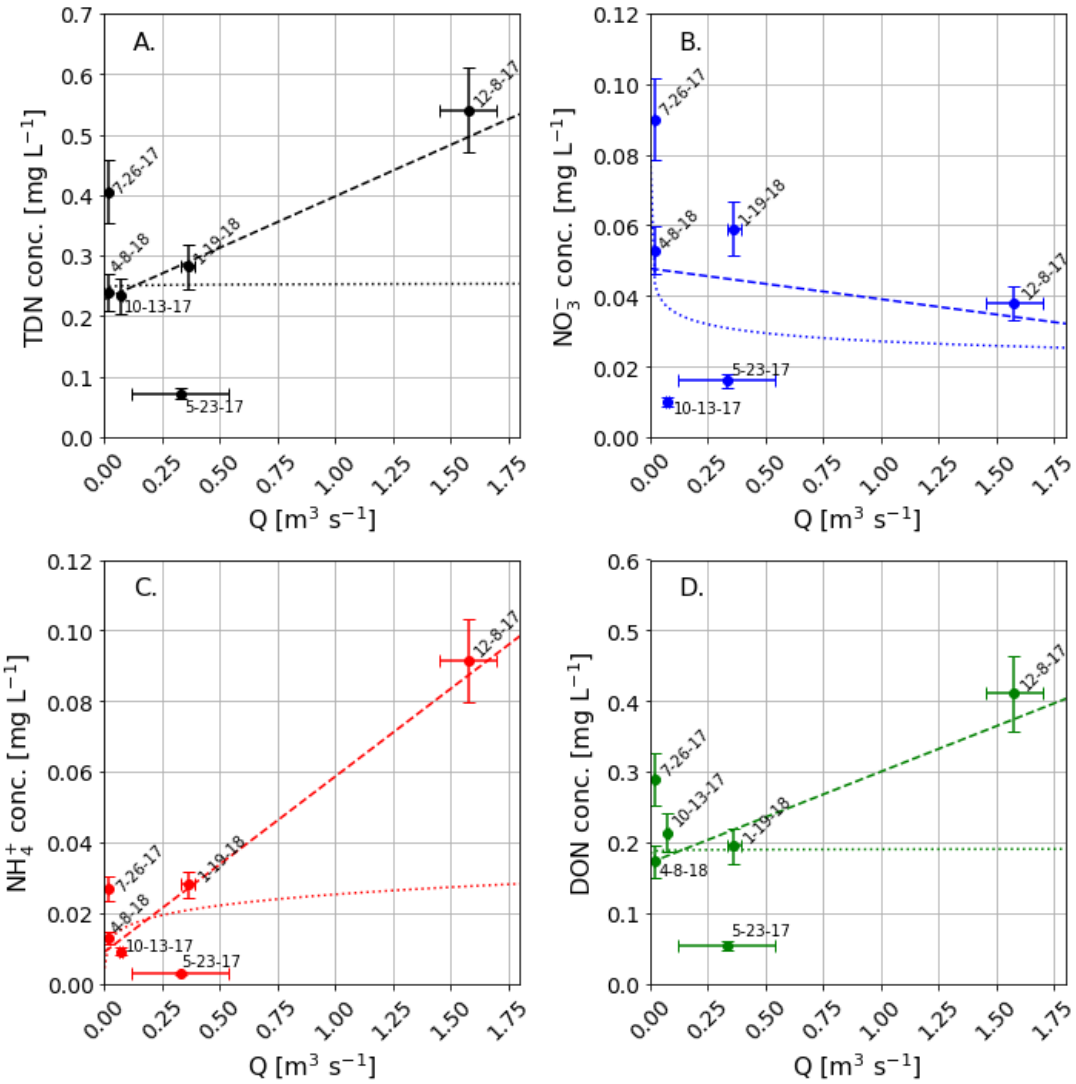

Figure 3.10 Relationship between total dissolved nitrogen (TDN; A.), nitrate (NO_3^-; B.), ammonium (NH_4^+; C.), and dissolved organic nitrogen (DON; D.) concentration and discharge (Q) at Mile Brook. Error bars represent the uncertainty associated with each discharge and nitrogen concentration measurement. Dashed lines and dotted curves represent the best fit linear regression line and power law curve of the relationship respectively. Regression line and power law equations can be found in Table 3.13.

Table 3.13 Best fit regression equations to the relationship between total dissolved nitrogen (TDN), nitrate (NO_3^-), ammonium (NH_4^+), and dissolved organic nitrogen (DON) concentration (y) and discharge (x) at Mile Brook from 5/19/17 – 5/18/18.

N species	Linear Regression	r^2	p value	Power Law	r^2	p value
TDN	$y = 0.169 \cdot x + 0.22$	0.399	0.178	$y = 0.253 \cdot x^{-0.004}$	< 0.001	0.983
NO_3^-	$y = -0.008 \cdot x + 0.05$	0.030	0.740	$y = 0.027 \cdot x^{-0.118}$	0.063	0.631
NH_4^+	$y = 0.049 \cdot x + 0.009$	0.841	0.010	$y = 0.025 \cdot x^{0.191}$	0.087	0.570
DON	$y = 0.130 \cdot x + 0.17$	0.414	0.169	$y = 0.190 \cdot x^{0.003}$	< 0.001	0.987v

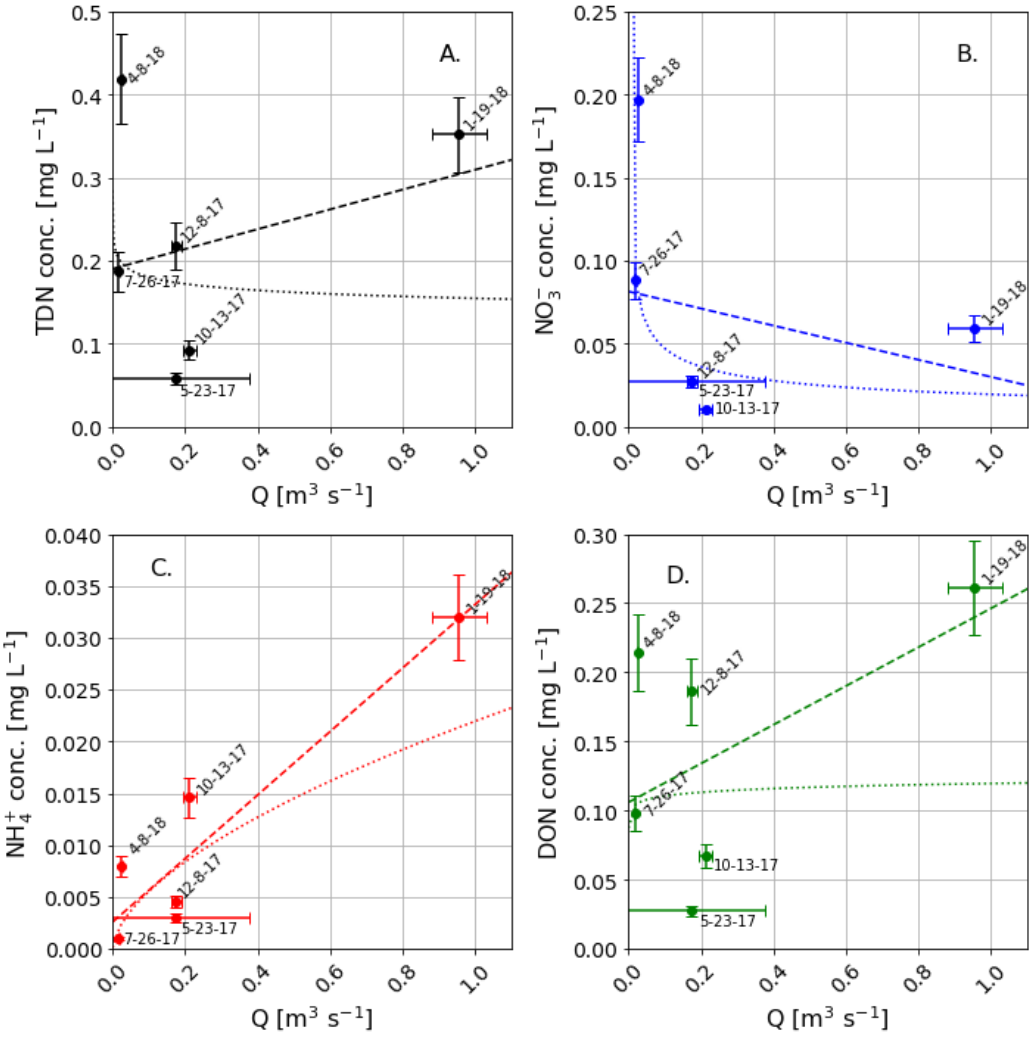

Figure 3.11 Relationship between total dissolved nitrogen (TDN; A.), nitrate (NO_3^-; B.), ammonium (NH_4^+; C.), and dissolved organic nitrogen (DON; D.) concentration and discharge (Q) at Pawtuckaway River. Error bars represent the uncertainty associated with each discharge and nitrogen concentration measurement. Dashed lines and dotted curves represent the best fit linear regression line and power law curve of the relationship respectively. Regression line and power law equations can be found in Table 3.14.

Table 3.14 Best fit regression equations to the relationship between total dissolved nitrogen (TDN), nitrate (NO_3^-), ammonium (NH_4^+), and dissolved organic nitrogen (DON) concentration (y) and discharge (x) at Pawtuckaway River from 5/19/17 – 5/18/18.

N species	Linear Regression	r^2	p value	Power Law	r^2	p value
TDN	$y = 0.119 \cdot x + 0.19$	0.086	0.571	$y = 0.154 \cdot x^{-0.066}$	0.016	0.808
NO_3^-	$y = -0.051 \cdot x + 0.08$	0.068	0.617	$y = 0.019 \cdot x^{-0.384}$	0.302	0.258
NH_4^+	$y = 0.031 \cdot x + 0.002$	0.863	0.007	$y = 0.022 \cdot x^{0.598}$	0.537	0.098
DON	$y = 0.140 \cdot x + 0.11$	0.288	0.272	$y = 0.119 \cdot x^{0.034}$	0.003	0.911

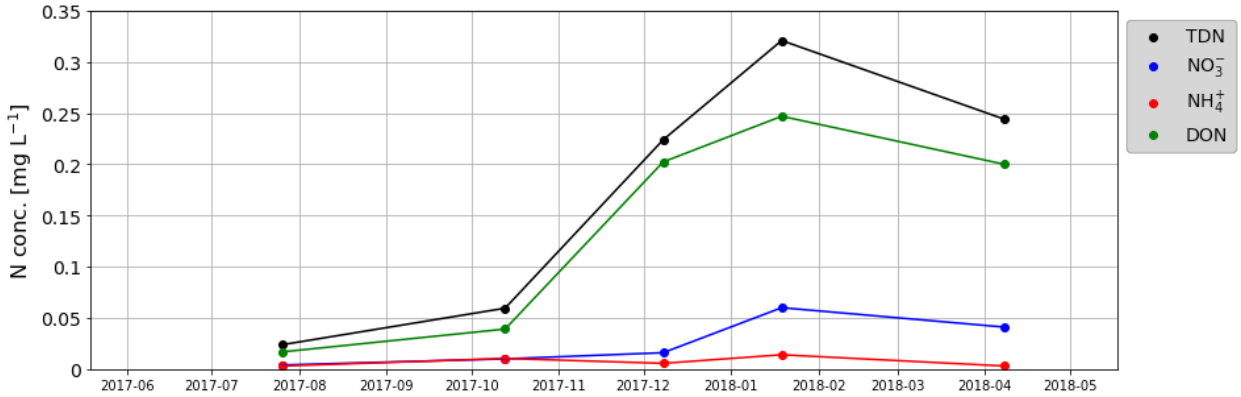

Figure 3.12 Measurements of total dissolved nitrogen (TDN), nitrate (NO_3^-), ammonium (NH_4^+), and dissolved organic nitrogen (DON) concentration obtained in the reservoir above the Dolloff Dam outlet.

3.3 Tributary and Dam Outlet N Flux

Over the study year (5/19/17 to 5/18/18), 4,372 ± 1,100 kg N of TDN was loaded to Pawtuckaway Lake from tributaries, of which 923 ± 230 kg N was NO_3^- (20.88% of TDN), 178 ± 41 kg N was NH_4^+ (4.07% of TDN), and 3,281 ± 850 kg N was DON (75.03% of TDN; Tables 3.15 – 3.18). Back Creek B was the single largest contributor of tributary TDN flux (1971 ± 760 kg N, 45.16% of total tributary TDN flux), while Fernald's Brook A had the highest TDN load per area (351 ± 270 kg N km^{-2}, Table 3.19). Monthly N fluxes to Pawtuckaway Lake were greatest for all N solutes during winter and spring months (1/1/18 to 4/31/18; Figures 3.12 – 3.15), which coincided with the most inflow during the study period (Figure 3.4). Total annual tributary NO_3^- flux to Pawtuckaway Lake (923 ± 230 kg N) was much lower than NHDES measurements of total annual tributary NO_3^- flux to Pawtuckaway Lake from 12/1/1991 to 11/30/1992 (3,384 kg N; Table 3.20; NHDES 1995). However, this offset is mostly dominated by a large difference in loading from the Fernald's Brook A tributary between this study period and that of the early '90s (Table 3.20). This could be due to a reduction in the concentration of NO_3^- in runoff as a result of improved manure management at Fernald's dairy farm upstream, or due to failure to estimate wintertime inputs with short duration but very high magnitude. NHDES estimates for Fernald's

Brook A were large relative to other tributaries as a result of one very high NO_3^- concentration measurement during December 1991 (12.00 mg L^{-1}, NHDES 1995). Measurements of total annual tributary NO_3^- flux were greater at Back Creek B, Mountain Cove Brook, and Round Pond Brook compared to those from 12/1/1991 to 11/30/1992 (Table 3.21; NHDES 1995).

Over the study year, total TDN flux leaving Pawtuckaway Lake via the dam outlets was 4,581 $\pm$ 3,000 kg N, of which 1,017 $\pm$ 760 kg N was NO_3^- (22.21% of TDN), 357 $\pm$ 210 kg N was NH_4^+ (7.79% of TDN), and 3,206 $\pm$ 2,000 kg N was DON (70.0% of TDN) (Tables 3.14 - 3.17). Over the study year, 53.09% of total TDN flux leaving Pawtuckaway Lake (2,432 $\pm$ 2,600 kg N) left via the Dolloff Dam outlet (Pawtuckaway River), while the remaining 46.91% (2,149 $\pm$ 1,400 kg N) left via the Drowns Dam outlet (Mile Brook). TDN, NH_4^+, and DON flux leaving the reservoir was highest during and after the fall drawdown (November) and cold weather during winter (January and February; Figures 3.13 – 3.16). NO_3^- flux was also high during the winter and remained high throughout the spring (Figure 3.14). Annual NO_3^- flux leaving Pawtuckaway Lake (1,017 $\pm$ 760 kg N, Table 3.14) was less than NO_3^- flux leaving Pawtuckaway Lake from 12/1/1991 to 11/30/1992 (2,318 kg N, Table 3.21, NHDES 1995).

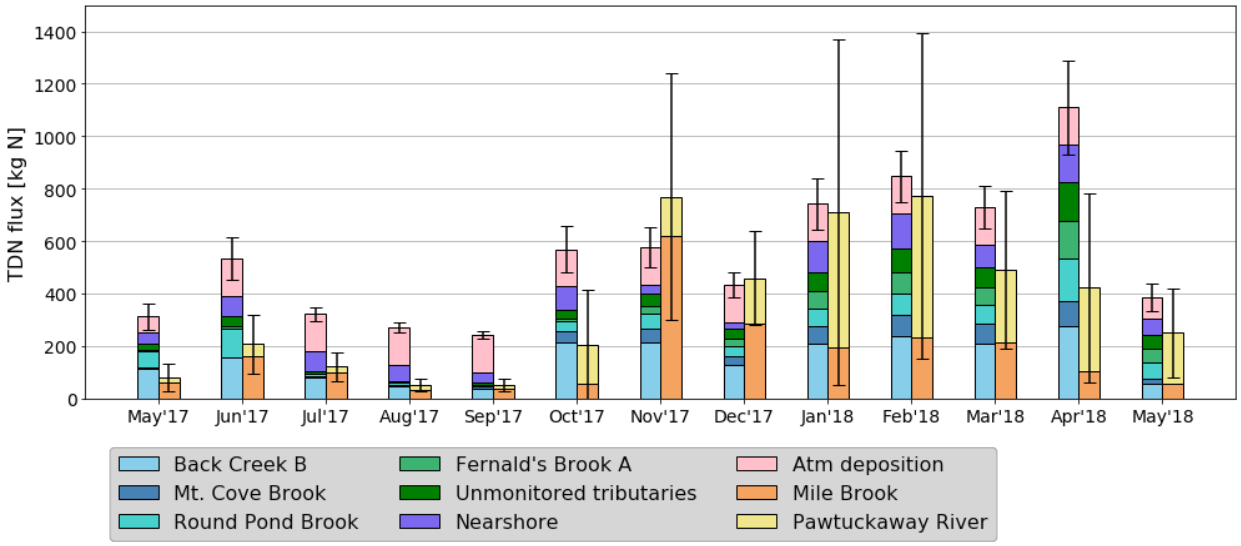

Figure 3.13 Monthly totals of total dissolved nitrogen (TDN) flux loaded to and leaving Pawtuckaway Lake. Sources of TDN loading to Pawtuckaway include monitored tributaries (Back Creek B, Mountain Cove Brook, Round Pond Brook, and Fernald's Brook A), unmonitored tributaries, nearshore runoff and groundwater (Nearshore), and atmospheric deposition (Atm deposition). TDN fluxes leaving Pawtuckaway Lake include Mile Brook and Pawtuckaway River. May'17 only includes May 19th through May 31st and May'18 only includes May 1st to May 18th.

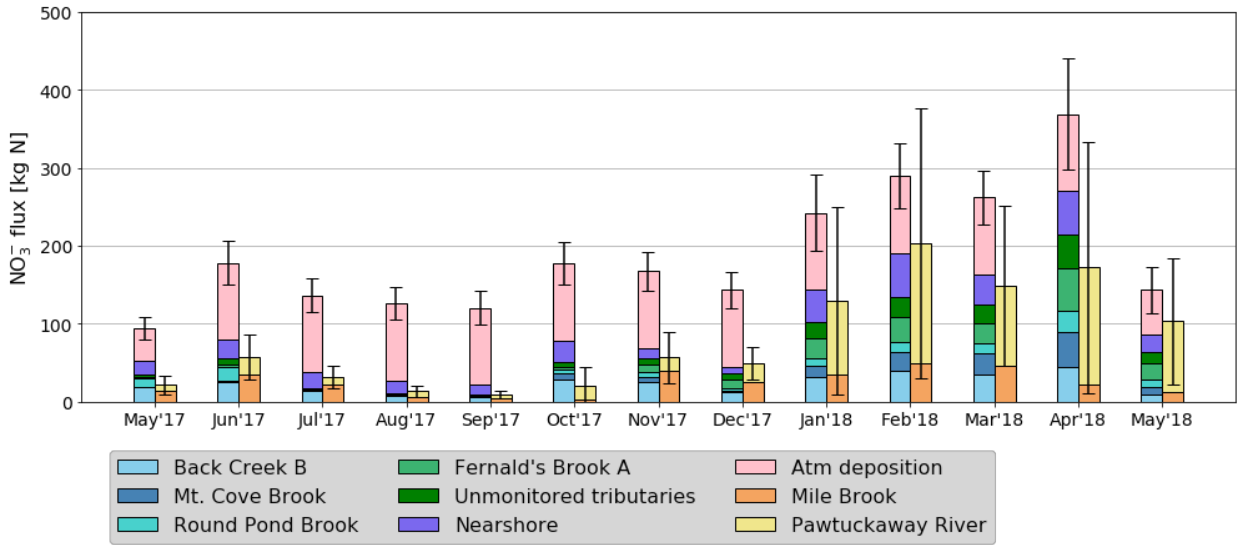

Figure 3.14 Monthly totals of nitrate (NO_3^-) flux loaded to and leaving Pawtuckaway Lake. Sources of NO_3^- loading to Pawtuckaway include monitored tributaries (Back Creek B, Mountain Cove Brook, Round Pond Brook, and Fernald's Brook A), unmonitored tributaries, nearshore runoff and groundwater (Nearshore), and atmospheric deposition (Atm deposition). NO_3^- fluxes leaving Pawtuckaway Lake include Mile Brook and Pawtuckaway River. May'17 only includes May 19th through May 31st and May'18 only includes May 1st to May 18th.

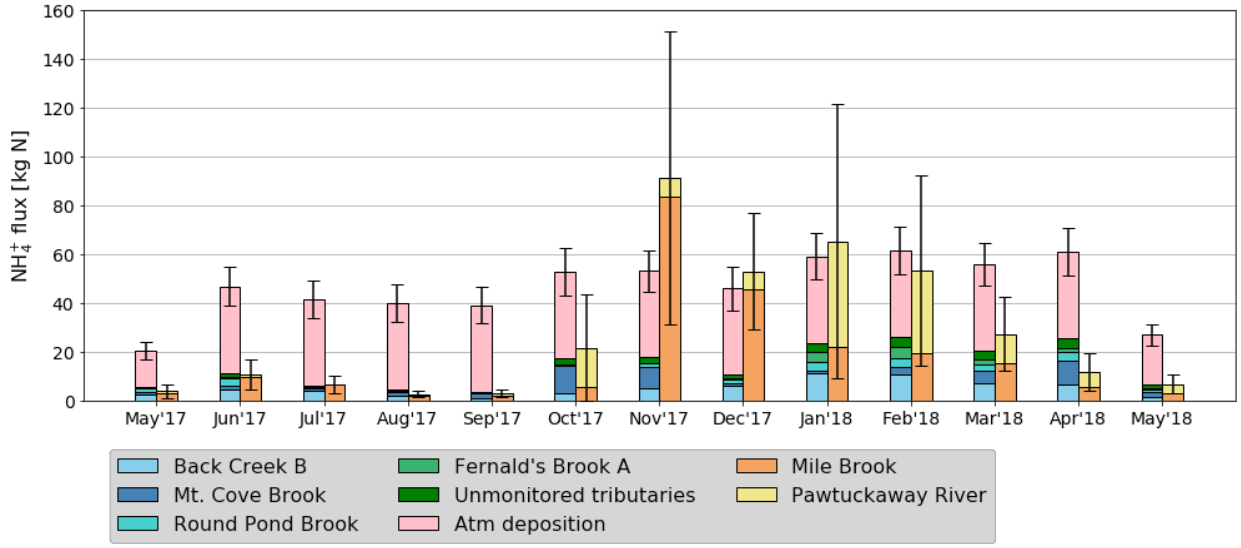

Figure 3.15 Monthly totals of ammonium (NH_4^+) flux loaded to and leaving Pawtuckaway Lake. Sources of NH_4^+ loading to Pawtuckaway include monitored tributaries (Back Creek B, Mountain Cove Brook, Round Pond Brook, and Fernald's Brook A), unmonitored tributaries, and atmospheric deposition (Atm deposition). NH_4^+ fluxes leaving Pawtuckaway Lake include Mile Brook and Pawtuckaway River. May'17 only includes May 19th through May 31st and May'18 only includes May 1st to May 18th.

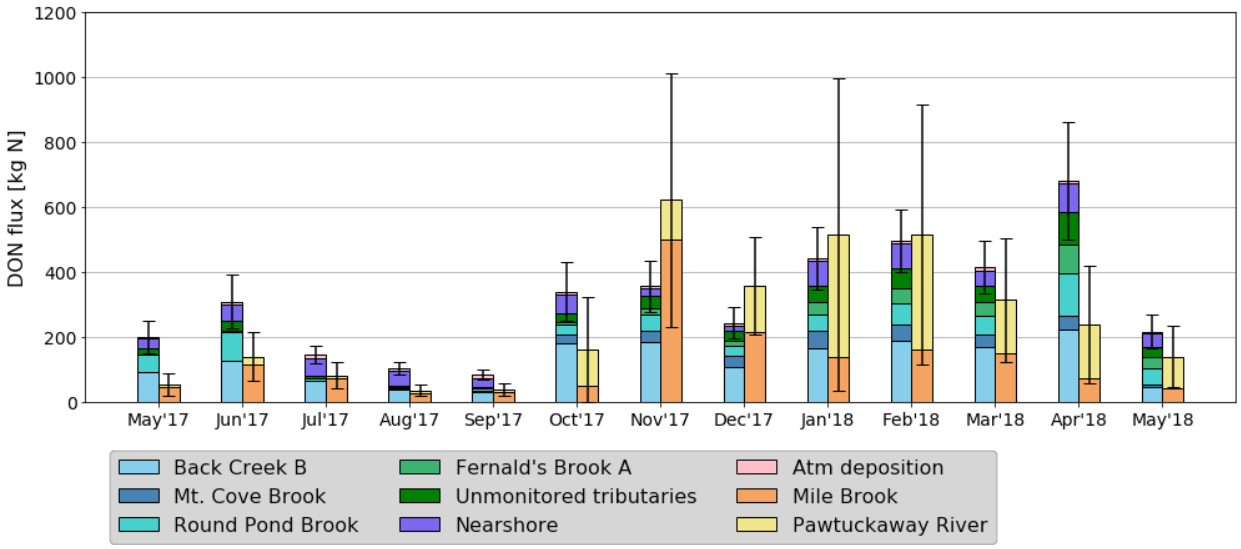

Figure 3.16 Monthly totals of dissolved organic nitrogen (DON) flux loaded to and leaving Pawtuckaway Lake. Sources of DON loading to Pawtuckaway include monitored tributaries (Back Creek B, Mountain Cove Brook, Round Pond Brook, and Fernald's Brook A), unmonitored tributaries, nearshore runoff and groundwater (Nearshore), and atmospheric deposition (Atm deposition). DON fluxes leaving Pawtuckaway Lake include Mile Brook and Pawtuckaway River. May'17 only includes May 19th through May 31st and May'18 only includes May 1st to May 18th.

Table 3.15 Monthly total dissolved nitrogen (TDN) flux to and from Pawtuckaway Lake from tributaries and the two dam outlets respectively. 5-17 only includes May 19th through May 31st and 5-18 only includes May 1st to May 18th.

	TDN flux [kg N]														
N Inputs	5-17	6-17	7-17	8-17	9-17	10-17	11-17	12-17	1-18	2-18	3-18	4-18	5-18	Total Annual	Mean Monthly
Back Creek B	114 ± 40	155 ± 57	81 ± 30	47 ± 18	38 ± 16	212 ± 109	215 ± 76	127 ± 45	210 ± 78	237 ± 84	210 ± 72	273 ± 110	55 ± 19	1,974 ± 760	164 ± 63
Mountain Cove Brook	2 ± 2	3 ± 2	2 ± 1	5 ± 2	6 ± 3	44 ± 23	49 ± 17	35 ± 13	66 ± 25	79 ± 28	73 ± 25	98 ± 40	20 ± 7	486 ± 190	41 ± 16
Round Pond Brook	64 ± 43	110 ± 77	10 ± 7	6 ± 4	7 ± 5	37 ± 28	60 ± 38	36 ± 23	65 ± 45	81 ± 56	72 ± 48	161 ± 137	61 ± 44	769 ± 560	64 ± 47
Fernald's Brook A	3 ± 6	7 ± 15	1 ± 2	1 ± 1	1 ± 1	10 ± 8	26 ± 17	30 ± 19	68 ± 47	83 ± 57	69 ± 46	145 ± 125	55 ± 40	500 ± 380	42 ± 32
Unmonitored tributaries	24 ± 16	41 ± 30	8 ± 4	6 ± 3	6 ± 3	35 ± 21	50 ± 25	38 ± 20	74 ± 43	90 ± 52	78 ± 44	146 ± 110	49 ± 33	645 ± 400	54 ± 38
Nearshore	46 ± 5	75 ± 9	77 ± 11	61 ± 7	41 ± 3	87 ± 10	33 ± 1	24 ± 3	116 ± 81	134 ± 35	86 ± 6	144 ± 51	63 ± 7	987 ± 228	82 ± 19
Atmospheric Deposition	60 ± 13	143 ± 31	143 ± 31	143 ± 31	143 ± 31	143 ± 31	143 ± 31	143 ± 31	143 ± 31	143 ± 31	143 ± 31	143 ± 31	83 ± 18	1,713 ± 370	143 ± 31
Total	313 ± 63	534 ± 110	322 ± 45	269 ± 37	242 ± 36	568 ± 120	576 ± 97	433 ± 67	742 ± 140	847 ± 140	731 ± 110	1,110 ± 250	386 ± 78	6,534 ± 1,200	590 ± 100
N Outputs															
Mile Brook	62 ± 50	161 ± 100	100 ± 53	32 ± 20	35 ± 21	58 ± 50	622 ± 450	285 ± 140	194 ± 99	232 ± 140	212 ± 129	101 ± 70	56 ± 30	2,149 ± 1,400	172 ± 110
Pawtuckaway River	17 ± 13	45 ± 40	21 ± 18	19 ± 15	13 ± 12	145 ± 200	148 ± 150	175 ± 120	516 ± 650	540 ± 600	279 ± 270	320 ± 350	193 ± 170	2,432 ± 2,600	203 ± 220
Total	79 ± 52	206 ± 110	121 ± 56	51 ± 25	49 ± 24	203 ± 210	770 ± 470	459 ± 180	711 ± 660	772 ± 620	491 ± 300	421 ± 360	239 ± 170	4,581 ± 3,000	382 ± 250

Table 3.16 Monthly nitrate (NO_3^-) flux to and from Pawtuckaway Lake from tributaries and the two dam outlets respectively. 5-17 only includes May 19th through May 31st and 5-18 only includes May 1st to May 18th.

	NO_3^- flux [kg N]														
N Inputs	5-17	6-17	7-17	8-17	9-17	10-17	11-17	12-17	1-18	2-18	3-18	4-18	5-18	Total Annual	Mean Monthly
Back Creek B	18.8 ± 6.6	25.5 ± 9	13.3 ± 5	7.6 ± 2.9	6 ± 2.5	29.2 ± 15	25.9 ± 9.2	11.9 ± 4.2	32.3 ± 12	39 ± 14	34.7 ± 12	45 ± 18	9.1 ± 3.2	298 ± 110	24.8 ± 9.0
Mountain Cove Brook	0.5 ± 0.4	1.2 ± 0.6	0.8 ± 0.5	1.4 ± 0.6	1.4 ± 0.6	7.1 ± 3.7	5.6 ± 2.1	2.8 ± 1.0	13.5 ± 5.0	24 ± 8.6	28 ± 9.6	44.6 ± 18	9.2 ± 3.2	141 ± 54	11.8 ± 4.0
Round Pond Brook	10.5 ± 7.1	18.1 ± 13	1.6 ± 1.2	0.9 ± 0.7	1.1 ± 0.8	5.2 ± 3.9	7.2 ± 4.6	3.3 ± 2.1	10 ± 7.0	13.5 ± 9.3	11.9 ± 7.9	26.5 ± 23	10 ± 7.3	120 ± 87	10 ± 7.2
Fernald's Brook A	1.2 ± 2.2	2.8 ± 5.5	0.5 ± 0.6	0.4 ± 0.3	0.3 ± 0.2	3.1 ± 2.3	8.9 ± 5.6	11 ± 6.9	26 ± 18	32.1 ± 22	26.4 ± 18	54.5 ± 47	21 ± 15	188 ± 140	15.7 ± 12
Unmonitored tributaries	4.4 ± 3.3	7.6 ± 6.5	1.6 ± 1.0	1.1 ± 0.6	1.1 ± 0.6	5.9 ± 3.7	8.8 ± 4.8	7.4 ± 4.3	20 ± 12	26 ± 16	23.3 ± 13	45 ± 33	15 ± 10	167 ± 110	13.9 ± 9.0
Nearshore	18 ± 3.0	24 ± 3.0	20 ± 1.0	16 ± 1.0	12 ± 1.0	28 ± 4.0	12 ± 1.0	8 ± 1.0	41 ± 36	56 ± 16	39 ± 5.0	55 ± 13	22 ± 3.0	351 ± 40	29.3 ± 3.3
Atmospheric Deposition	41.1 ± 9	98.8 ± 21	98.8 ± 21	98.8 ± 21	98.8 ± 21	98.8 ± 21	98.8 ± 21	98.8 ± 21	98.8 ± 21	98.8 ± 21	98.8 ± 21	98.8 ± 21	57.4 ± 12	1,186 ± 250	98.8 ± 21
Total	94.5 ± 14	178 ± 28	137 ± 22	216 ± 21	121 ± 21	177 ± 27	167 ± 25	143 ± 23	242 ± 49	289 ± 42	262 ± 35	369 ± 71	185 ± 29	2,451 ± 340	204 ± 29
N Outputs															
Mile Brook	13.7 ± 11	35.7 ± 22	22.0 ± 12	5.8 ± 3.6	4.8 ± 2.8	3.2 ± 2.8	39 ± 28	35.1 ± 13	35 ± 18	49.5 ± 30	45.9 ± 28	22.5 ± 15	12.4 ± 6.6	315 ± 190	26.3 ± 16
Pawtuckaway River	7.8 ± 5.9	21.2 ± 19	10 ± 8.5	7.9 ± 6.3	4.2 ± 3.6	16.8 ± 24	17.8 ± 18	23.9 ± 17	94.5 ± 120	154.2 ± 170	103.1 ± 99	150 ± 160	90.9 ± 81	702 ± 740	58.5 ± 61
Total	21.5 ± 12	56.9 ± 29	32 ± 15	13.7 ± 7.3	9 ± 4.6	20 ± 24	56.9 ± 33	49 ± 21	129.7 ± 120	203.7 ± 173	149 ± 103	172.5 ± 161	103.3 ± 81	1,017 ± 760	84.8 ± 63

Table 3.17 Monthly total and mean and annual total ammonium (NH_4^+) flux to and from Pawtuckaway Lake from tributaries and the two dam outlets respectively. 5-17 only includes May 19th through May 31st and 5-18 only includes May 1st to May 18th.

	NH_4^+ flux [kg N]														
N Inputs	5-17	6-17	7-17	8-17	9-17	10-17	11-17	12-17	1-18	2-18	3-18	4-18	5-18	Total Annual	Mean Monthly
Back Creek B	2.49 ± 0.87	4.60 ± 1.7	4.16 ± 1.6	1.79 ± 0.70	0.79 ± 0.32	2.97 ± 1.5	5.02 ± 1.8	6.01 ± 2.1	11.21 ± 4.2	10.53 ± 3.7	7.10 ± 2.5	6.32 ± 2.6	1.26 ± 0.44	64.25 ± 24	5.35 ± 2.0
Mountain Cove Brook	0.91 ± 0.74	1.41 ± 0.66	0.80 ± 0.49	1.91 ± 0.79	2.17 ± 0.94	11.27 ± 5.8	8.65 ± 3.1	1.06 ± 0.40	1.04 ± 0.40	3.43 ± 1.2	5.25 ± 1.8	9.76 ± 4.0	2.02 ± 0.70	49.76 ± 21	4.15 ± 1.7
Round Pond Brook	1.38 ± 0.94	3.31 ± 2.3	0.51 ± 0.37	0.22 ± 0.17	0.14 ± 0.11	0.50 ± 0.38	1.41 ± 0.90	1.69 ± 1.1	3.46 ± 2.4	3.59 ± 2.5	2.44 ± 1.6	3.70 ± 3.2	1.39 ± 1.0	23.77 ± 17	1.98 ± 1.4
Fernald's Brook A	0.20 ± 0.37	0.39 ± 0.77	0.06 ± 0.07	0.03 ± 0.03	0.02 ± 0.02	0.05 ± 0.04	0.15 ± 0.10	0.54 ± 0.30	4.17 ± 2.9	4.21 ± 2.9	2.27 ± 1.5	1.63 ± 1.4	0.58 ± 0.40	14.31 ± 11	1.19 ± 0.9
Unmonitored tributaries	0.76 ± 0.61	1.55 ± 1.2	0.56 ± 0.31	0.55 ± 0.25	0.51 ± 0.24	2.52 ± 1.3	2.40 ± 0.97	1.24 ± 0.63	3.76 ± 2.3	4.24 ± 2.5	3.16 ± 1.6	3.98 ± 2.4	1.09 ± 0.62	26.33 ± 15	2.19 ± 1.2
Nearshore	-	-	-	-	-	-	-	-	-	-	-	-	-	-	-
Atmospheric Deposition	14.8 ± 3.1	35.3 ± 7.5	35.3 ± 7.5	35.3 ± 7.5	35.3 ± 7.5	35.3 ± 7.5	35.3 ± 7.5	35.3 ± 7.5	35.3 ± 7.5	35.3 ± 7.5	35.3 ± 7.5	35.3 ± 7.5	20.5 ± 4.4	424 ± 90	35.3 ± 7.5
Total	20.5 ± 3.5	46.8 ± 8.1	41.6 ± 7.7	40.0 ± 7.6	39.0 ± 7.6	53.0 ± 9.7	53.0 ± 8.4	46.0 ± 9.0	59.0 ± 9.7	62.0 ± 9.6	55.7 ± 8.6	60.9 ± 9.8	26.8 ± 4.6	602 ± 99	50.4 ± 8.2
N Outputs															
Mile Brook	2.99 ± 2.5	9.58 ± 5.9	6.48 ± 3.5	1.93 ± 1.2	1.88 ± 1.1	5.80 ± 5.1	83.33 ± 59	45.39 ± 23	21.83 ± 11	19.40 ± 12	15.37 ± 9.4	5.51 ± 3.8	3.05 ± 1.6	223 ± 140	18.55 ± 12
Pawtuckaway River	0.78 ± 0.60	1.17 ± 1.1	0.18 ± 0.15	0.57 ± 0.45	0.99 ± 0.89	15.86 ± 21	8.0 ± 8.7	7.50 ± 5.3	43.44 ± 55	34.01 ± 37	11.94 ± 12	6.18 ± 6.7	3.69 ± 3.3	134 ± 150	11.19 ± 13
Total	3.77 ± 2.6	10.75 ± 6.0	6.66 ± 3.5	2.50 ± 1.3	2.87 ± 1.4	21.66 ± 22	91.32 ± 60	52.89 ± 24	64.27 ± 56	53.41 ± 39	27.32 ± 15	11.70 ± 7.7	6.74 ± 3.7	357 ± 210	29.74 ± 18

Table 3.18 Monthly total and mean and annual total dissolved organic nitrogen (DON) flux to and from Pawtuckaway Lake from tributaries and the two dam outlets respectively. 5-17 only includes May 19th through May 31st and 5-18 only includes May 1st to May 18th.

	DON flux [kg N]														
N Inputs	5-17	6-17	7-17	8-17	9-17	10-17	11-17	12-17	1-18	2-18	3-18	4-18	5-18	Total Annual	Mean Monthly
Back Creek B	93 ± 33	124 ± 46	63 ± 24	38 ± 16	32 ± 13	180 ± 84	184 ± 66	109 ± 38	167 ± 61	187 ± 66	168 ± 58	222 ± 86	45 ± 16	1,612 ± 610	134 ± 51
Mountain Cove Brook	0.6 ± 0.5	0.6 ± 0.3	0.2 ± 0.2	2.1 ± 0.9	2.8 ± 1	26 ± 12	34 ± 12	31 ± 11	52 ± 19	52 ± 18	40 ± 14	43 ± 17	9.0 ± 3	295 ± 110	25 ± 9
Round Pond Brook	52 ± 35	89 ± 62	7.8 ± 5.5	4.7 ± 3.5	5.8 ± 4.5	31.6 ± 23	51 ± 33	31 ± 20	51 ± 35	64 ± 44	58 ± 38	131 ± 110	50 ± 36	625 ± 450	52 ± 37
Fernald's Brook A	1.8 ± 2.8	4.2 ± 7.8	0.8 ± 0.9	0.7 ± 0.5	0.8 ± 0.6	6.9 ± 4.9	17 ± 11	18 ± 11	37 ± 25	47 ± 32	41 ± 27	90 ± 74	33 ± 25	298 ± 230	25 ± 19
Unmonitored tributaries	19 ± 12	31 ± 22	6.1 ± 3.2	4.1 ± 2.3	4.2 ± 2.4	26.8 ± 15	38.5 ± 20	29 ± 15	51 ± 28	60 ± 34	52 ± 29	97 ± 72	33 ± 23	452 ± 280	38 ± 23
Nearshore	29 ± 3	51 ± 8	57 ± 11	45 ± 7	29 ± 3	59 ± 7	22 ± 1	16 ± 2	75 ± 51	78 ± 23	47 ± 2	90 ± 41	40 ± 5	638 ± 90	53 ± 8
Atmospheric Deposition	3.5 ± 1.7	8.5 ± 4	8.5 ± 4	8.5 ± 4	8.5 ± 4	8.5 ± 4	8.5 ± 4	8.5 ± 4	8.5 ± 4	8.5 ± 4	8.5 ± 4	8.5 ± 4	5 ± 2.3	102 ± 48	8.5 ± 4
Total	199 ± 50	308 ± 81	143 ± 27	103 ± 18	83 ± 15	339 ± 90	355 ± 78	218 ± 48	442 ± 97	497 ± 97	415 ± 81	682 ± 180	215 ± 52	4,022 ± 850	336 ± 71
N Outputs															
Mile Brook	45.24 ± 35	115.81 ± 72	70.79 ± 38	24.30 ± 15	28.43 ± 17	48.57 ± 41	499.24 ± 370	214.01 ± 110	137.33 ± 70	162.70 ± 97	150.59 ± 93	73.37 ± 55	40.57 ± 22	1,611 ± 1,000	134.25 ± 86
Pawtuckaway River	7.98 ± 6.0	22.66 ± 20	11.09 ± 9.6	10.64 ± 8.5	8.30 ± 7.4	112.41 ± 150	122.40 ± 130	143.15 ± 100	378.46 ± 470	352.17 ± 390	163.59 ± 160	163.53 ± 170	98.74 ± 91	1,595 ± 1,700	132.93 ± 142
Total	53.22 ± 36	138.47 ± 75	81.88 ± 39	34.95 ± 17	36.72 ± 19	160.97 ± 160	621.64 ± 390	357.15 ± 150	515.79 ± 480	514.87 ± 400	314.19 ± 190	236.90 ± 180	139.31 ± 94	3,206 ± 2,000	267.17 ± 170

Table 3.19 Annual total and areal flux of total dissolved nitrogen (TDN), dissolved inorganic nitrogen (DIN), nitrate (NO_3^-), ammonium (NH_4^+), and dissolved organic nitrogen (DON) to Pawtuckaway Lake from the four monitored tributaries from 5/19/17 to 5/18/18.

		TDN		DIN		NO_3^-		NH_4^+		DON	
Monitored Tributary	Drainage area [km^2]	Annual flux [kg N]	Areal flux [kg km^{-2}]	Annual flux [kg N]	Areal flux [kg km^{-2}]	Annual flux [kg N]	Areal flux [kg km^{-2}]	Annual flux [kg N]	Areal flux [kg km^{-2}]	Annual flux [kg N]	Areal flux [kg km^{-2}]
Back Creek B	20.65	1,974.57 ± 760	95.61 ± 37	362.64 ± 134	17.54 ± 6.5	298.39 ± 110	14.44 ± 5.3	64.25 ± 24	3.11 ± 1.2	1,611.93 ± 610	78.05 ± 30
Mountain Cove Brook	9.38	483.08 ± 187	51.50 ± 20	189.82 ± 75	20.39 ± 8.0	140.14 ± 54	14.93 ± 5.8	49.68 ± 21	5.30 ± 2.2	293.26 ± 110	31.26 ± 12
Round Pond Brook	6.70	769.92 ± 560	114.85 ± 84	143.83 ± 104	21.43 ± 16	120.05 ± 87	17.91 ± 13	23.77 ± 17	3.55 ± 2.5	626.09 ± 450	93.40 ± 67
Fernald's Brook A	1.43	499.99 ± 380	351 ± 270	202.39 ± 151	141.94 ± 110	188.07 ± 140	131.90 ± 98	14.31 ± 11	10.04 ± 7.7	297.61 ± 230	208.71 ± 160

Table 3.20 Annual total dissolved nitrogen (TDN), dissolved inorganic nitrogen (DIN), nitrate (NO_3^-), ammonium (NH_4^+), and dissolved organic nitrogen (DON) flux to Pawtuckaway Lake from the extrapolated tributaries from 5/19/17 to 5/18/18.

Minor Tributary	Annual TDN flux [kg N]	Annual DIN flux [kg N]	Annual NO_3^- flux [kg N]	Annual NH_4^+ flux [kg N]	Annual DON flux [kg N]
Back Creek A	34.181	6.281	5.167	1.114	27.899
Fundy Brook Creek	56.663	10.412	8.566	1.846	46.25
Fernald's Brook B	24.218	4.45	3.661	0.789	19.768
Loon Cove Brook A	65.914	25.911	19.169	6.742	40.002
Loon Cove Brook B	28.834	11.334	8.385	2.949	17.498
Burnham's Marsh North	51.183	49.599	7.983	41.616	1.583
Burnham's Marsh South	139.493	26.0736	21.7586	4.315	113.419
White's Grove Brook	257.127	104.046	96.73	7.316	153.081
Gove Dam Brook	91.942	37.204	34.588	2.616	54.737

Table 3.21 Total annual nitrate (NO_3^-) flux measurements at tributaries and dam outlets from 5/19/17 to 5/18/18 compared to total annual flux measurements obtained by NHDES from 12/1/91 to 11/30/92 (NHDES 1995).

Tributary	Annual NO_3^- Load [kg N]	
	5/19/17 - 5/18/18	NHDES 1995
Back Creek B	297.93	141.85
Mountain Cove Brook	141.47	128.50
Round Pond Brook	119.85	53.70
Fernald's Brook A	188.07	2898.13
Back Creek A	5.17	28.59
Fundy Brook Creek	8.58	10.68
Fernald's Brook B	3.67	4.66
Loon Cove Brook A	18.99	22.65
Loon Cove Brook B	8.31	18.26
Burnham's Marsh North	8.00	35.04
Burnham's Marsh South	21.79	7.65
White's Grove Brook	67.84	4.12
Gove Dam Brook	24.26	30.34
Total	913.24	3384.17
Dam Outlet		
Mile Brook	315	532
Pawtuckaway River	702	1,786
Total	1,017	2,318

3.4 N Loading from Atmospheric Deposition and the Near Shore N Loading from SWAT

Total direct atmospheric TDN deposition to Pawtuckaway Lake's water surface for the study period was estimated to be 1,713 ± 370 kg of N, with 1,186 ± 250 kg of N from NO_3^- (69.38% of TDN), 424 ± 90 kg of N from NH_4^+ (24.76% of TDN), and 102 ± 48 kg of N from DON (5.96% of TDN).

SWAT estimates of nearshore N loading from 5/1/17 to 4/30/18 were 988 ± 228 kg of N from TDN, of which 35.45 % was NO_3^- (350 ± 87 kg N) and 64.55% was DON (638 ± 162 kg N; Table 3.22). SWAT assumed that nearshore loading of NH_4^+ was negligible. N nearshore loading was highest in winter and spring months 1/1/18 to 4/30/18 (Table 3.22), which is consistent with when field-measured tributary N loading was highest (Figures 3.13 – 3.16). SWAT nearshore TDN, NO_3^-, and DON loading estimates were 20.1%, 25.8%, and 14.3% of total modeled TDN, NO_3^-, and DON flux respectively to Pawtuckaway Lake (Table 3.21). SWAT estimates of total NO_3^- flux to Pawtuckaway Lake (2,442 ± 890 kg N) were similar to estimates of total field-measured NO_3^- flux for this study (2,449 ± 351 kg N). However, SWAT estimates of total TDN flux to Pawtuckaway Lake (4,916 ± 1,200 kg N) were much lower than field-measured estimates of total TDN flux to the reservoir for this study (7,073 ± 1,200 kg N), primarily because total DON flux to the reservoir (2,442 ± 890 kg N) was underestimated by the model compared to field-measured estimates from this study (4,021 ± 870 kg N). Since SWAT was calibrated for hydrology and manually matched for DON concentration during 5/1/17 to 12/31/17 when DON concentrations tended to be lower (Table 3.18, Figure 3.16). This led to an underestimation of DON concentration and DON flux from 1/1/18 to 4/30/18 when field-measured DON flux loaded to Pawtuckaway Lake was highest (Table 3.18, Figure 3.16).

Table 3.22 Nearshore flux, total flux, and percent of nearshore flux that makes up total flux of total dissolved nitrogen (TDN), dissolved organic nitrogen (DON), and nitrate (NO_3^-) to Pawtuckaway Lake from the Soil and Water Assessment Tool (SWAT) model for 5/1/17 to 4/30/18.

		TDN			DON			NO_3^-		
		Nearshore flux [kg N]	Total flux [kg N]	% of total flux	Nearshore flux [kg N]	Total flux [kg N]	% of total flux	Nearshore flux [kg N]	Total flux [kg N]	% of Total flux
2017	5	109 ± 12	533 ± 320	20.5%	69 ± 8	276 ± 190	25.0%	40 ± 5	257 ± 150	15.7%
	6	75 ± 9	326 ± 210	23.0%	51 ± 8	209 ± 160	24.4%	24 ± 3	117 ± 64	20.4%
	7	77 ± 11	319 ± 230	24.1%	57 ± 11	217 ± 160	26.2%	20 ± 1	102 ± 75	19.7%
	8	61 ± 7	261 ± 190	23.4%	45 ± 7	140 ± 41	32.4%	16 ± 1	122 ± 150	13.1%
	9	41 ± 3	191 ± 150	21.6%	29 ± 3	93 ± 15	31.2%	12 ± 1	98 ± 130	12.5%
	10	87 ± 10	465 ± 420	18.7%	59 ± 7	210 ± 56	28.2%	28 ± 4	255 ± 370	10.9%
	11	33 ± 1	160 ± 97	20.8%	22 ± 1	73 ± 4	29.6%	12 ± 1	87 ± 95	13.3%
	12	24 ± 3	114 ± 90	20.7%	16 ± 2	54 ± 8	29.4%	8 ± 1	60 ± 83	12.9%
2018	1	116 ± 81	651 ± 840	17.8%	75 ± 51	338 ± 320	22.1%	41 ± 36	313 ± 560	13.2%
	2	134 ± 35	771 ± 380	17.4%	78 ± 23	355 ± 160	22.1%	56 ± 16	417 ± 254	13.4%
	3	86 ± 6	409 ± 130	21.0%	47 ± 2	165 ± 39	28.2%	39 ± 5	244 ± 97	16.1%
	4	144 ± 51	717 ± 430	20.1%	90 ± 41	345 ± 250	26.1%	55 ± 13	372 ± 210	14.6%
Total		987 ± 100	4,917 ± 1,200	20.1%	638 ± 90	2,475 ± 530	25.8%	351 ± 40	2,444 ± 800	14.3%

3.5 Reservoir N Retention Results and Discussion

Of total TDN flux to Pawtuckaway for the study period (7,073 ± 1,200 kg N), 52.7% came from the monitored tributaries (3,729 ± 1,000 kg N), 9.12% came from unmonitored tributaries (645 ± 400 kg N), 24.21% came from direct atmospheric deposition (1,712 ± 370 kg N), and 13.97% came from nearshore loading (987 ± 230 kg N; Figure 3.17). During the same period, a total of 4,581 ± 3,000 kg N was measured leaving the lake in river outflow. Therefore, annual TDN retention for the study period was 0.35 ± 0.21 (Table 3.23). Of the N solutes that make up TDN, NO_3^- had the highest annual retention of 0.58 ± 0.26, followed by DIN retention (0.55 ± 0.27), and NH_4^+ retention (of 0.41 ± 0.32; Table 3.23). DON had the lowest retention and highest uncertainty (0.2 ± 0.52; Table 3.23), which may indicate that Pawtuckaway Lake is a source of DON rather than a sink.

Estimates of annual TDN retention were lower than estimates from Daley et al. 2010 (0.91) for the portion of the Pawtuckaway Lake watershed draining downstream of the Dolloff Dam outlet. However, the Daley et al. 2010 estimates included both terrestrial and aquatic retention, whereas this study only estimated retention occurring within the reservoir. Annual TDN retention measured at Pawtuckaway Lake was similar to TDN retention measured for a reservoir in a peatland catchment in the UK (0.21 – 0.31; Edokpa et al. 2016). However, Edokpa et al. 2016 found higher DON retention (0.39 – 0.55) and lower DIN retention (0.06 – 0.13) compared this study.

NHDES estimates NO_3^- retention from 12/1/1991 to 11/30/1992 as 0.315 (Figure 3.18), however this only accounted for tributary NO_3^- inputs to Pawtuckaway and did not include estimates of nearshore loading or atmospheric deposition (NHDES 1995). Estimates of annual N retention within Pawtuckaway Lake from the Seitzinger et al. (2002) empirical model were 0.69 (using a mean depth of 3.3 m and a hydraulic residence time of 1.71 yr; NHDES 1995).

This study's estimates of NO_3^- and DIN retention were lower than predicted by Seitzinger et al. 2002, but still fell within the range of uncertainty (Figure 3.18, Table 3.23). However, both TDN and DON retention estimates were lower (Figure 3.18, Table 3.23). Estimates of annual NO_3^- and DIN retention from this study may have been lower than estimates from the Seitzinger relationship since only 6 N concentration measurements were obtained during baseflow. Thus, N fluxes to the reservoir from tributaries during storm flow may have been overestimated since in-stream N concentration typically dilutes during storm events (Koenig et al. 2017). Estimates of annual total nitrogen retention at Pawtuckaway Lake (0.18) from the SPARROW model developed for the northeastern United States (Moore et al. 2004) fell on the low end of TDN uncertainty from this study (Figure 3.18) which shows the limitation of large regional scale models to accurately represent N loads, residence times, and fluxes for smaller scale catchments.

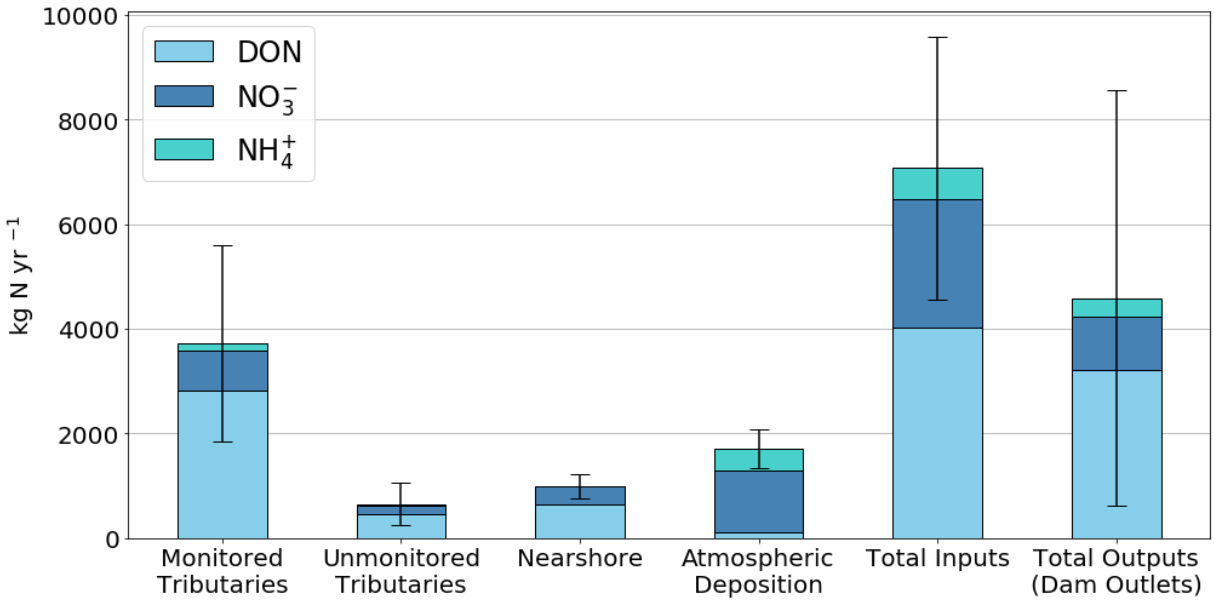

Figure 3.17 Total annual dissolved organic nitrogen (DON), nitrate (NO_3^-), ammonium (NH_4^+), and total dissolved nitrogen (the summation of DON, NO_3^-, and NH_4^+) fluxes into (tributaries, nearshore loading, and atmospheric deposition) and leaving (dam outlets) Pawtuckaway Lake from 5/19/2017 to 5/18/2018. Error bars are shown at 95% confidence intervals.

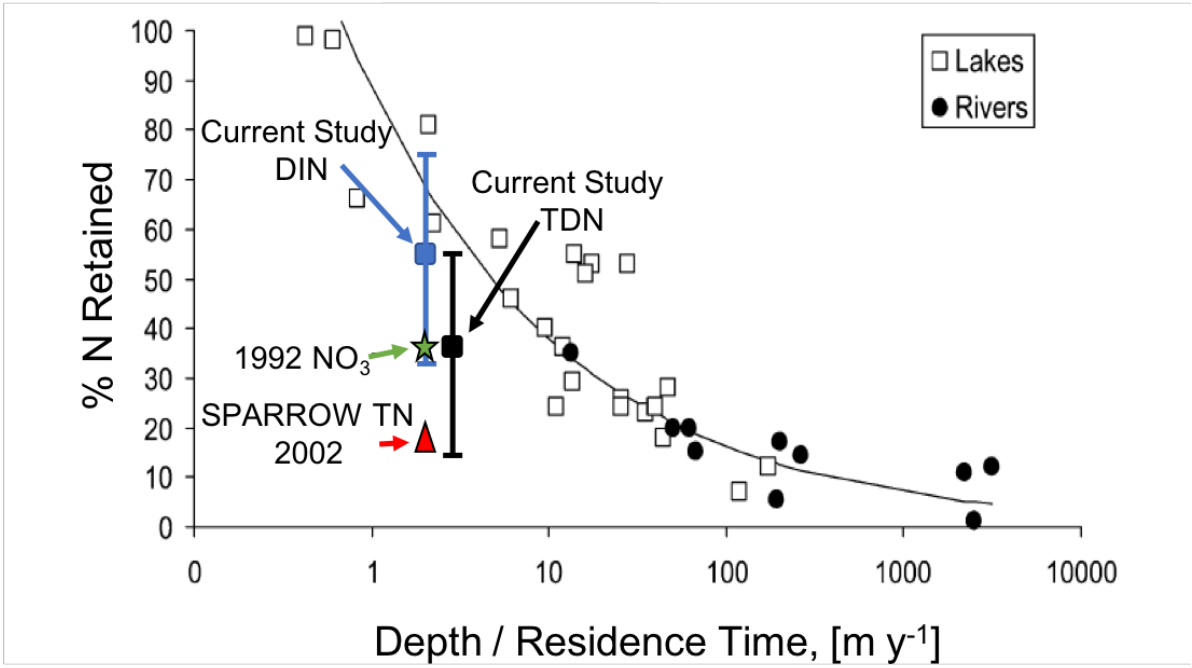

Figure 3.18 Estimates of the percentage of N removed in waterbodies versus the ratio of water depth to residence time (modified from Seitzinger et al. 2002). Blue and black square and error bars show dissolved inorganic nitrogen (DIN) and total dissolved nitrogen (TDN) retention within Pawtuckaway Lake from 5/19/2017 to 5/18/2018. The green star shows nitrate (NO_3^-) retention measurements taken by NHDES at Pawtuckaway Lake (NHDES 1995). The red triangle show retention estimates of total nitrogen (TN) retention from the SPARROW model developed for the northeastern U.S. on the reach containing Pawtuckaway Lake (Moore et al. 2004).

Table 3.23 Annual total dissolved nitrogen (TDN), dissolved inorganic nitrogen (DIN), nitrate (NO_3^-), ammonium (NH_4^+), and dissolved organic nitrogen (DON) retention for Pawtuckaway Lake from 5/19/2017 to 5/18/2018.

TDN R	DIN R	NO_3^- R	NH_4^+ R	DON
0.35 ± 0.21	0.55 ± 0.27	0.58 ± 0.26	0.41 ± 0.32	0.2 ± 0.52

3.6 N Flux from the Pawtuckaway Lake Watershed

TDN, DIN, and DON flux from the Pawtuckaway Lake watershed normalized to watershed area was lower on all sampling dates compared to the upper and lower Lamprey River watershed (Table 3.24). Although the upper Lamprey River watershed and the Pawtuckaway Lake watershed have similar land use, the upper Lamprey River watershed has

higher areal N fluxes. This suggests that Pawtuckaway Lake is an important waterbody in the Lamprey River watershed in regard to mitigating N flux within the watershed and to Great Bay. Area-normalized TDN, DIN, and DON flux from the upper Lamprey River watershed was lower than the lower Lamprey River watershed except for on 4/8/18 which may indicate high in-channel and terrestrial N uptake during the spring when nitrogen demand from plants for growth is greatest.

Table 3.24 A synoptic comparison of total dissolved nitrogen (TDN), dissolved inorganic nitrogen (DIN), and dissolved organic nitrogen (DON) loading from the Pawtuckaway watershed and the upper (at USGS gauge 01073319) and lower Lamprey River watershed (at USGS gauge 01073500).

	Pawtuckaway watershed (drainage area = 54 km^2)			upper Lamprey River watershed (drainage area = 144 km^2)			lower Lamprey River watershed (drainage area = 479 km^2)		
Date	TDN flux [kg km^{-2}]	DIN flux [kg km^{-2}]	DON flux [kg km^{-2}]	TDN flux [kg km^{-2}]	DIN flux [kg km^{-2}]	DON flux [kg km^{-2}]	TDN flux [kg km^{-2}]	DIN flux [kg km^{-2}]	DON flux [kg km^{-2}]
5/23/17	0.0361	0.0128	0.0232	0.2783	0.0852	0.1930	0.4313	0.1525	0.2788
7/26/17	0.0264	0.0096	0.0167	0.1055	0.0336	0.0719	0.1814	0.0559	0.1255
10/13/17	0.0437	0.0097	0.0340	0.0326	0.0132	0.0194	0.1658	0.0840	0.0819
12/8/17	0.2590	0.0555	0.2035	0.4656	0.1304	0.3353	0.8642	0.2616	0.6026
1/19/18	0.4320	0.1178	0.3142	1.1418	0.4101	0.7318	1.3306	0.4256	0.9050
4/8/18	0.0535	0.0261	0.0273	2.1154	0.8206	1.2949	1.3591	0.4673	0.8918

Chapter 4: FrAMES Modeling Methods

4.1 FrAMES Model Background

The Framework for Aquatic Modeling in the Earth System (FrAMES) numerical model (Wollheim et al 2008, Stewart et al. 2011) was used to explore hydrology and DIN retention within the Lamprey River watershed, and determine how these quantities may change in response to changes in climate, land use, and dam management. FrAMES, which is developed and maintained by the Water Systems Analysis Group at the University of New Hampshire, is a spatially distributed hydrologic model that simulates water temperature, water storage, and solute concentrations throughout a watershed. FrAMES simulates hydrology using the Water Balance Model (WBM; Wisser et al. 2010), water temperature using the River Temperature Re-equilibration Model (RTRM; Dingman 1972), and nitrogen transport and retention by both the river network (Wollheim et al. 2008) and reservoirs (Seitzinger et al. 2002).

FrAMES is a distributed model that parses a watershed into equal-area grid cells at the same spatial resolution as a given input river network. It then uses additional geospatial input data to simulate the vertical exchange of water between the Earth's atmosphere and the ground surface, and the horizontal movement of water and DIN within each grid cell, at a daily time step. Even though a daily time step averages over sub-daily hydrological processes such as snowpack and transpiration dynamics and may not be appropriate for smaller catchments (where sub-daily runoff routing becomes more important), it was chosen to model river flow within the Lamprey River watershed as a typical flood wave takes several days to peak and attenuate on the lower Lamprey River mainstem. Required input data include gridded time series information, such as daily precipitation and air temperature; gridded static layers such as land use cover; and geospatial databases such as wastewater treatment plant and dam locations. For the river network, FrAMES uses a Simulated Topological Network (STN) built from a digital elevation model to provide river flow direction exiting each grid cell. Flow routing of

water downstream was then determined using the Linear Reservoir Routing method using a constant flow velocity. Prior to running the model, all spatially gridded input data was first rescaled to match the spatial resolution of the STN using proximal interpolation. Also, all dammed reservoirs were snapped to a grid cell along the STN using a search algorithm based on the known upstream drainage area for each reservoir. FrAMES then used a spin-up phase to estimate initial water and DIN storage in each pool within each grid cell prior to the first day of the model run. This spin-up phase ran the first year of the model simulation five times sequentially, then took an ensemble average of water and DIN in each storage pool. See appendix B for additional information on water and DIN routing in FrAMES.

4.2 Model Application Overview

FrAMES was used to quantify how the presence and management of a network of dams affects river discharge and DIN retention within the Lamprey River watershed, both for contemporary and for projected climate and land use conditions. Following calibration for hydrology, DIN loading, and DIN retention, water and DIN transport were modeled within the watershed using either contemporary land use and climate (for water years 1996 to 2015) or projected land use and climate for a late century period (water years 2080 to 2099). For both periods, dam presence and dam management alternatives were explored and compared to current conditions within the watershed.

4.3 Model Input Data

4.3.1 River Network

A single simulated topological river network (STN; Feteke et al. 2001) was used to represent the Lamprey River watershed for all climate, land use, and dam management scenarios (Figure 4.1). This STN was developed by the Conservation Science Program of the World Wildlife Fund's Shuttle Elevation Derivatives at multiple scales project (Hydro SHEDS; Lehner et al. 2008) and is based on elevation data obtained from the National Aeronautics and

Space Administration's (NASA) Shuttle Radar Topography Mission. The network is at approximately 0.5 km resolution and was edited to match USGS National Hydrography flow lines (NHDPLUS Version 2). At this resolution, the Lamprey River watershed was parsed into 3,486 uniform grid cells (areas approximately 0.25 km^2).

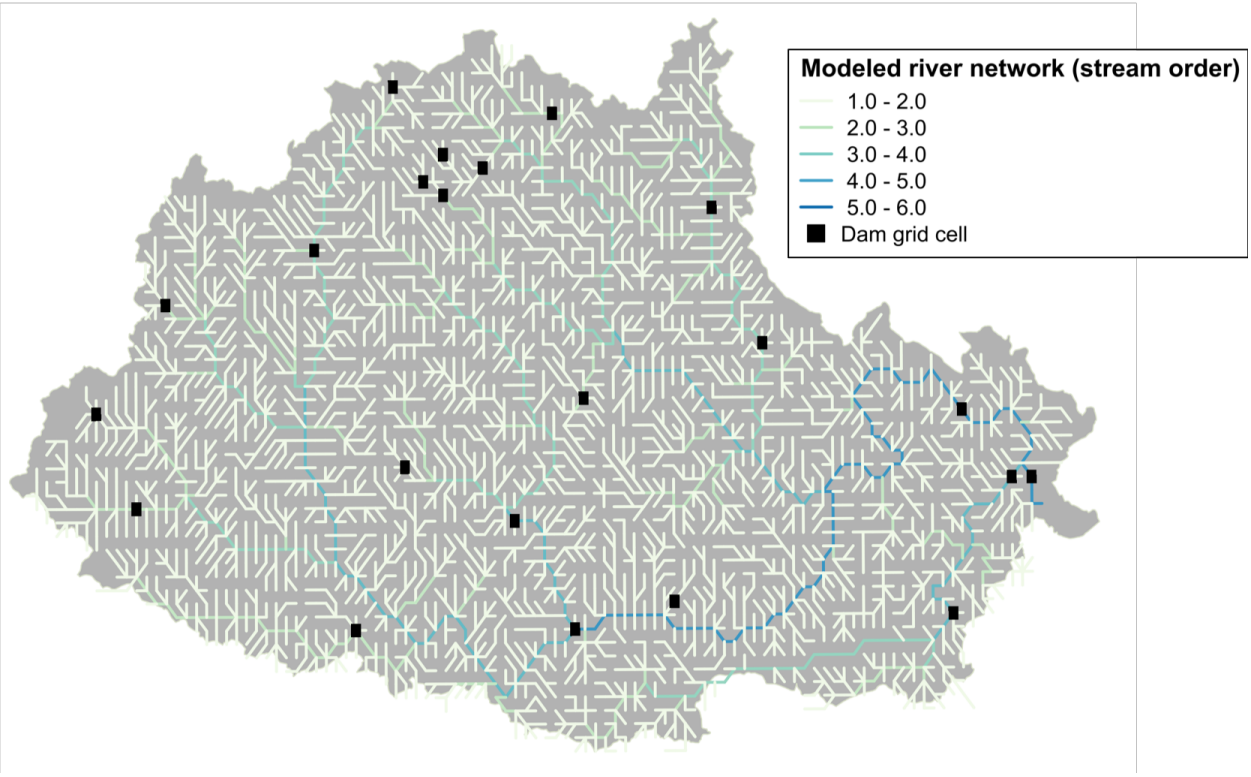

Figure 4.1 Figure of the simulated topological network (STN) for the Lamprey River watershed used in FrAMES. Grey watershed outline is from NHDPlusV2 delineation of the Lamprey River watershed.

4.3.2 Dam Management

Dams are added to the Simulated Topological Network using a geospatial dam database which provides reservoir location, maximum reservoir volume, reservoir surface area, upstream drainage area, and dam management type (Table 1.1). If a grid cell contains a dam, the amount of outflow released from the impoundment depends on the dam management type, a long-term average outflow at that grid cell, and the reservoir water storage level (Grogan et al. 2017). Dam management types are represented as either managed (controlled outflow) or unmanaged

(uncontrolled outflow). Managed dams are further categorized depending on their designated purpose and are assigned one of six operating types: generic, flood control, hydroelectric, irrigation, water supply, or recreation. For managed reservoirs, outflow released downstream from the impoundment ($outflow$) is calculated using a bimodal log/exponential function based on reservoir storage (S),

$$outflow = \begin{cases} Q_{avg} \cdot [Q_{min} + a \cdot \ln(1 + c \cdot S)] & \text{if } S < S_{opt} \\ Q_{avg} \cdot [B + b \cdot (S - S_{opt})^{p}] & \text{if } S \geq S_{opt} \end{cases} \quad \text{Equation 4.1}$$

where,

$$a = \frac{1 - Q_{min}}{\ln(1 + c \cdot S_{opt})} \quad \text{Equation 4.2}$$

$$b = \frac{4}{(1 - S_{opt} + d)^{p} - d^{p}} \quad \text{Equation 4.3}$$

$$B = S_{opt} - b \cdot d^{p} \quad \text{Equation 4.4}$$

where Q_{avg} [$m^3\ s^{-1}$] is the 5-year running average for annual outflow at the grid cell, Q_{min} is the minimum release allowed normalized by the long-term annual mean discharge for that location, S is the reservoir storage level [fraction of maximum reservoir capacity], and S_{opt} is the optimal reservoir storage level for the reservoir [fraction of maximum reservoir capacity]. Parameters c and p are set depending on dam purpose while a, b, B, and d are calculated. Table 4.1 and Figure 4.2 list parameter values and show reservoir outflow/storage curves for reservoirs operating for flood control and water supply respectively. Dams operating for recreation normally keep reservoir levels high during summer for boating, swimming, and fishing and low during winter and spring to allow for dock maintenance and accommodate extra runoff due to storms and snow melt. Therefore, dams with the operating type of recreation use parameters for water supply during May – October and flood control during November – April (Table 4.1; Figure 4.2).

Unmanaged dams are treated as small spillway dams where outflow over the spillway crest is calculated as,

$$outflow = \begin{cases} Q_{avg} \cdot \left(\frac{\sqrt{1+\beta \cdot S_e}-1}{\sqrt{\sqrt{1+\beta \cdot S_d}-1}} \right)^{1.6} & \text{if } fld \geq 0 \\ Q_{avg} \cdot \left(\frac{S_e}{S_d}\right)^{1.6} & \text{if } fld = 0 \end{cases} \quad \text{Equation 4.5}$$

where,

$$\beta = \frac{4 \cdot fld}{res_{Area}} \quad \text{Equation 4.6}$$

and,

$$S_e = H \cdot res_{Area} \cdot (1 + fld \cdot H) \quad \text{Equation 4.7}$$

where Q_{avg} [m^3 s^{-1}] is the 5-year running average for annual outflow at the grid cell, S_d [m^3] is the reservoir storage when water level is at the spillway crest, S_e [m^3] is the effective reservoir storage when water level is above the spillway crest, H [m] is the 5-year running average of water level reservoir depth [m] in the grid cell, fld [m^{-1}] is the reservoir area flooding rate (default of 0.3), and res_{Area} [m^2] is the surface area of the reservoir at the spillway crest. Unmanaged reservoir outflow curves are shown for different reservoir area flooding rates in Figure 4.3.

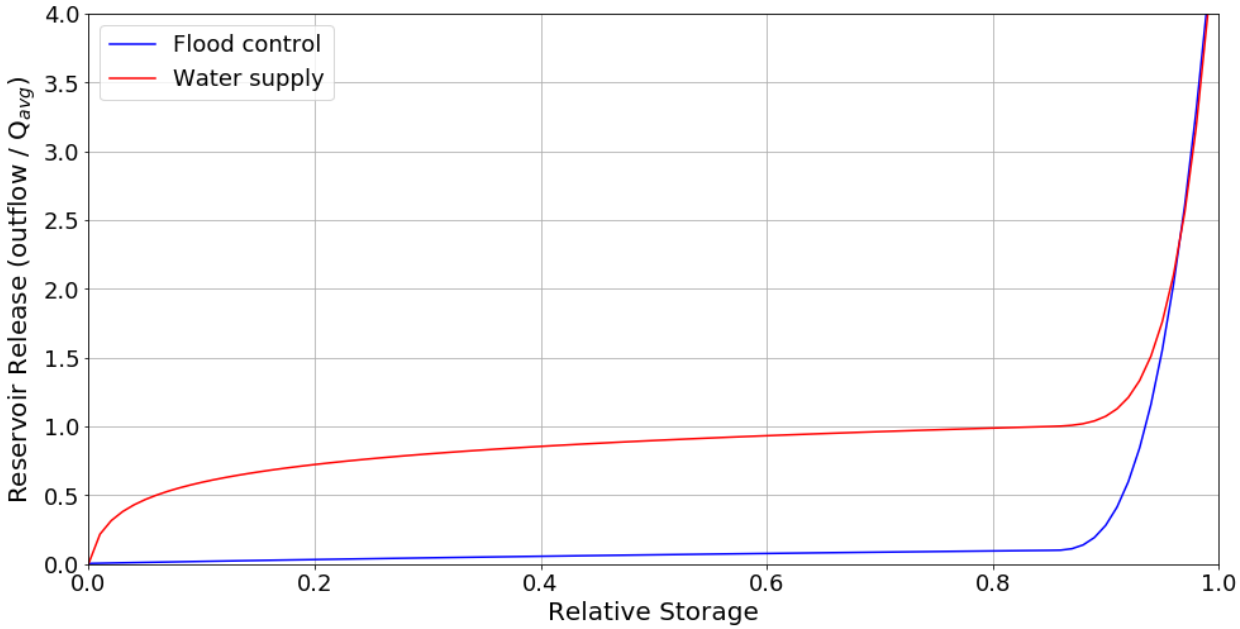

Figure 4.2 Reservoir outflow/storage curves for managed dams with operating types of flood control and water supply. Reservoir outflow is normalized by the 5-year running average, Q_{avg}, for annual outflow at the grid cell and relative reservoir storage is given as a fraction of maximum reservoir capacity.

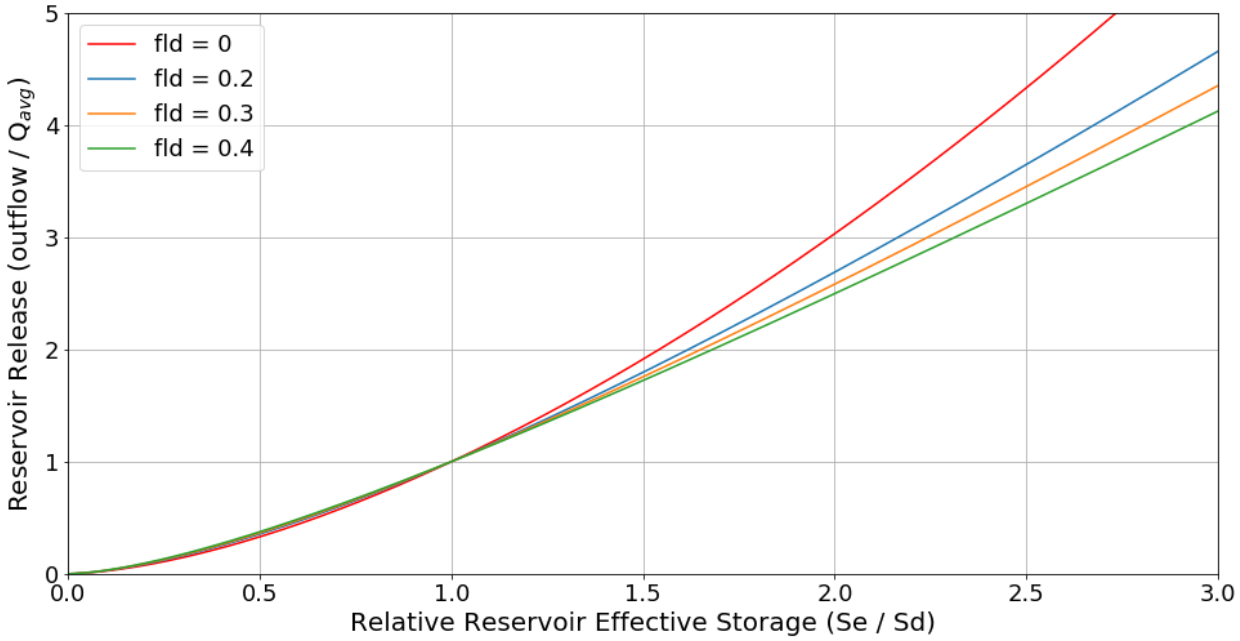

Figure 4.3 Reservoir outflow/storage curves for unmanaged dams with different reservoir flooding area rates (fld). Reservoir outflow is normalized by the 5-year running average, Q_{avg}, for annual outflow at the grid cell, S_e [m^3] is the effective reservoir storage when water level is above the spillway crest, and S_d [m^3] is the reservoir storage when water level is at the spillway crest.

Table 4.1 Parameter values used to model different reservoir management types.

Management Type	c	p	Q_{min}	S_{opt}	fld
Unmanaged Spillway	-	-	-	-	0.3
Managed for Flood Control	100	170	0.005	0.85	-
Managed for Water Supply	1	6	0.005	0.85	-

4.3.3 Contemporary Climate and Land Use

Contemporary meteorological input data included precipitation and air temperature data developed by METDATA (Abatzoglou et al. 2013) from a reanalysis of high temporal resolution data with high spatial resolution data into a daily 4-km resolution gridded dataset. METDATA mean total annual precipitation and mean maximum 1-day rainfall for water years 1996 to 2015 were 9.71% and 7.05% lower, respectively, at the same location compared to historic observations obtained at the NOAA weather gauge USC00272800 in Epping (Figure 4.4). This underrepresentation of precipitation amount and intensity may have contributed to an underrepresentation of in modeled discharge.

METDATA mean annual air temperature for water years 1996 to 2015 was 1.01% lower than historic air temperature measured at the NOAA weather gauge for the same period (Figure 4.5). Daily cloud cover, wind speed, wind direction, relative humidity, as well as leaf area index data were used from the Modern-Era Retrospective analysis for Research and Applications version 2 (MERRA-2) (Gelaro et al. 2017). MERRA-2 reanalysis used satellite observations to produce gridded data at approximately 50 km resolution. Soil water capacity data was used from the Harmonized World Soil Database at approximately 11 km resolution (2012, Harmonized World Soil Database version 1.2). The New Hampshire Land Cover (NHLC) database was used to obtain contemporary land cover including agriculture, development, impervious surfaces, open water surfaces, wetlands, and population density (Thorn et al. 2017;

Figure 1.5, Table 1.3) at a resolution of 30 meters. The skewness index of human land cover (development + agriculture) for the year 2005 was calculated as 0.911 (cf. Mineau et al. 2015). DIN point source loading within the watershed was estimated for the wastewater treatment plant located along the Lamprey River mainstem in Epping based on the population served (4,960 people) by the plant (with 20g of DIN per person per day, Van Drecht et al. 2009), the treatment type (tertiary) obtained from the Environmental Protection Agency (USEPA 2008), and the fraction of DIN removed before being discharged into the Lamprey River (80% DIN removed, Van Drecht et al. 2009) .

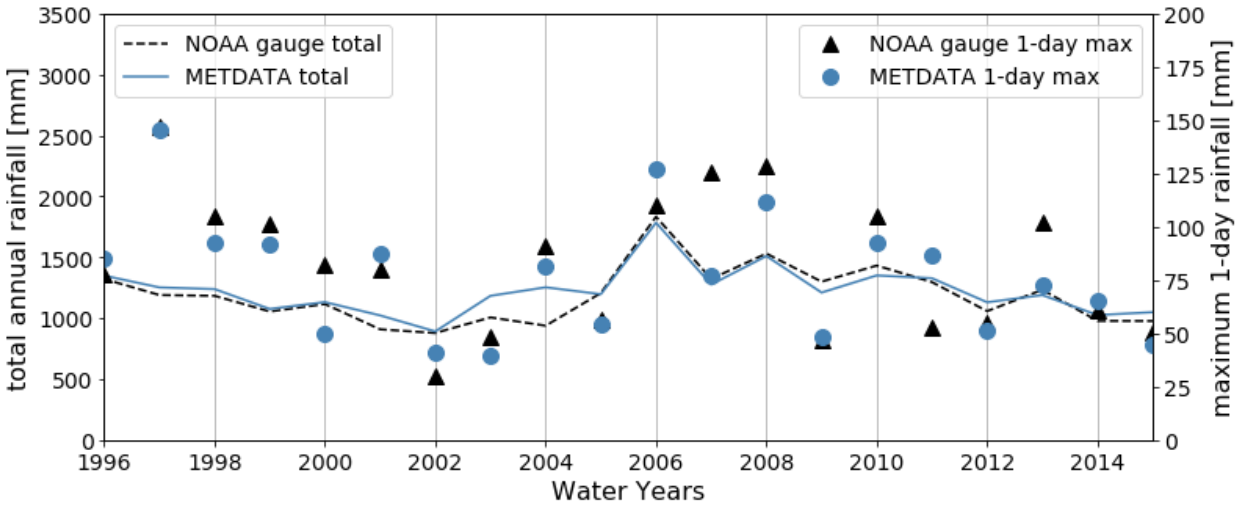

Figure 4.4 Historic total annual rainfall and maximum 1-day rainfall from METDATA and measured at the NOAA weather gauge USC00272800 in Epping for water years 1996 to 2015.

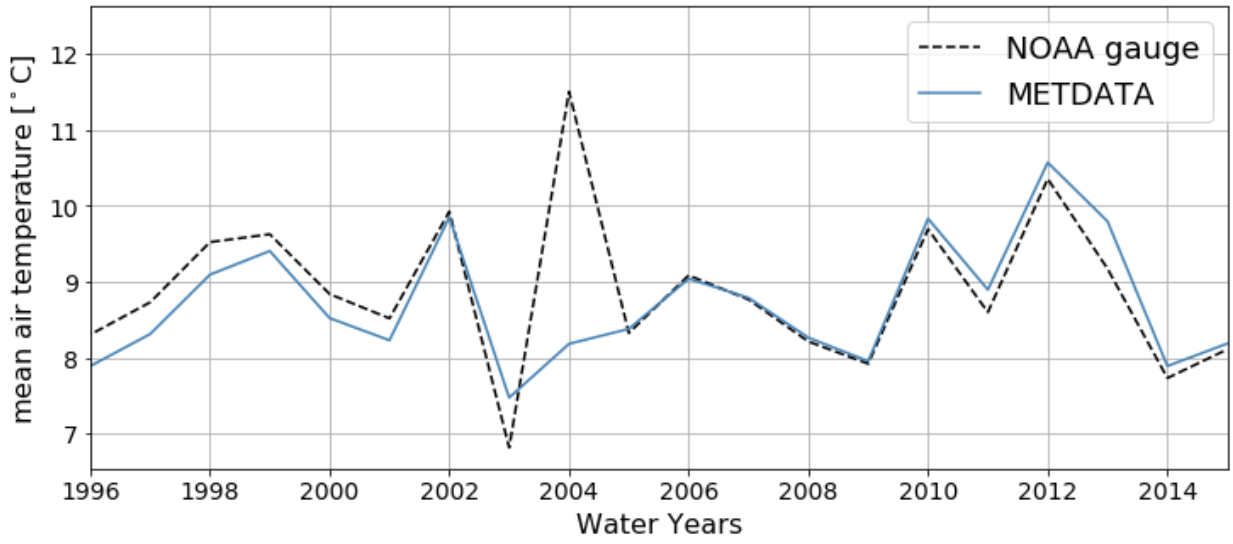

Figure 4.5 Historic annual mean air temperature from METDATA (averaged over the watershed) and measured at the NOAA weather gauge USC00272800 in Epping for water years 1996 to 2015.

4.3.4 Future Climate and Land Use

For late century climate, daily precipitation and air temperature projections were chosen from an ensemble of five statistically downscaled global climate models (GCM; Table 4.2) that were run under a high emissions scenario developed from the Coupled Model Intercomparison Project phase 5 (CMIP5). The high emissions scenario, Representative Concentration Pathway (RPC) 8.5, forecasts that the concentration of radiative forcings, which is the difference between the solar radiation absorbed by the Earth and the radiation that is reflected back to space at the tropopause, will be 8.5 times that of pre-industrial levels by 2100. GCM projections were previously downscaled to a local resolution of approximately 6 km for the Northeast United States using the Localized Constructed Analogs method (LOCA; Pierce et al. 2014).

Under emissions scenario RPC 8.5, LOCA GCMs project that annual mean air temperature will increase within the Lamprey River watershed by 4.6°C (from 7.6°C to 12.2°C) from water years 2007 to 2015 to water years 2080 to 2099 (Figure 4.6). LOCA GCMs project that median total annual rainfall will increase by 4.6% (1140 mm to 1195.5 mm) and 1-day and

7-day rainfall intensity will increase by 6.9% and 7.6 % respectively from 2007 to 2015 to 2080 to 2099 (Figures 4.7 – 4.9). The five LOCA GCMs total mean annual rainfall compares well to historic observation for water years 2007 to 2015 (Figure 4.7). However, rainfall intensity, particularly maximum 1-day rainfall, is underrepresented during this time period. Therefore, scenarios using late-century climate were compared to a baseline scenario that was calculated using the ensemble average of five LOCA GCMs for water years 2007 to 2015.

No future projections were available for cloud cover, wind speed, wind direction, relative humidity, or leaf area index; therefore, daily climatology estimates for each were obtained from the MERRA-2 contemporary data (calendar years 1980 to 2015). Daily climatology estimates of climate variables are based on day of year and long-term averages for the contemporary period. Similarly, soil-available water capacity and canopy height data layers were unchanged between contemporary and future scenarios.

A published regional land cover projection, the Backyard Amenities scenario (Thorn et al. 2017), was used to estimate future agriculture, development, impervious surfaces, open water surfaces, and population density. This land cover scenario predicts that development within the Lamprey River watershed will be characterized by dispersed development along with increased residential land cover and impervious surfaces, and a decrease in agriculture by the year 2100 (Figure 4.10, Table 4.3). This scenario was chosen as it represents a large amount of development, impervious surfaces, and increased transportation energy consumption which would be consistent with the high emissions scenario (RCP 8.5) also chosen. The skewness index of human land cover (development + agriculture) for the year 2090 was calculated as 0.978.

Table 4.2 Name, institution, and references of the five statistically downscaled global climate models whose projections of precipitation and air temperature were used for late century climate scenarios.

Model Name	Institution	Main Reference(s)
ACCESS1-0	Commonwealth Scientific and Industrial Organization (CSIRO) and Bureau of Meteorology (BOM), Australia	Bi et al. 2013b, Dix et al. 2013
CESM1-CAM5	NSF-DOE-NCAR	Hurrell et al. 2013
GFLD-ESM2G	NOAA Geophysical Fluid Dynamics Laboratory	Dunne et al. 2012, Dunne et al. 2013
HadGEM2-ES	UK Met Office Hadley Centre	Collins et al. 2011, Martin et al. 2011
MIROC-ESM	University of Tokyo, National Institute for Environmental Studies, and Japan Agency for Marine-Earth Science and Technology	Watanabe et al. 2011

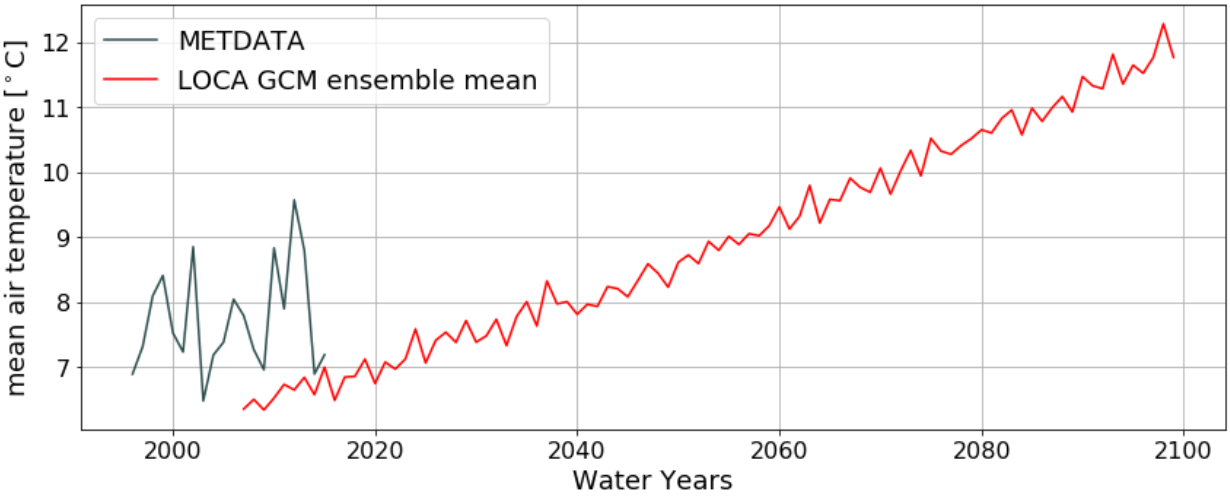

Figure 4.6 Historic annual mean air temperature from METDATA (water years 1996 - 2015) and mean late century projections (water years 2007 - 2099) of air temperature from five LOCA downscaled global climate models (GCM) in the Lamprey River watershed.

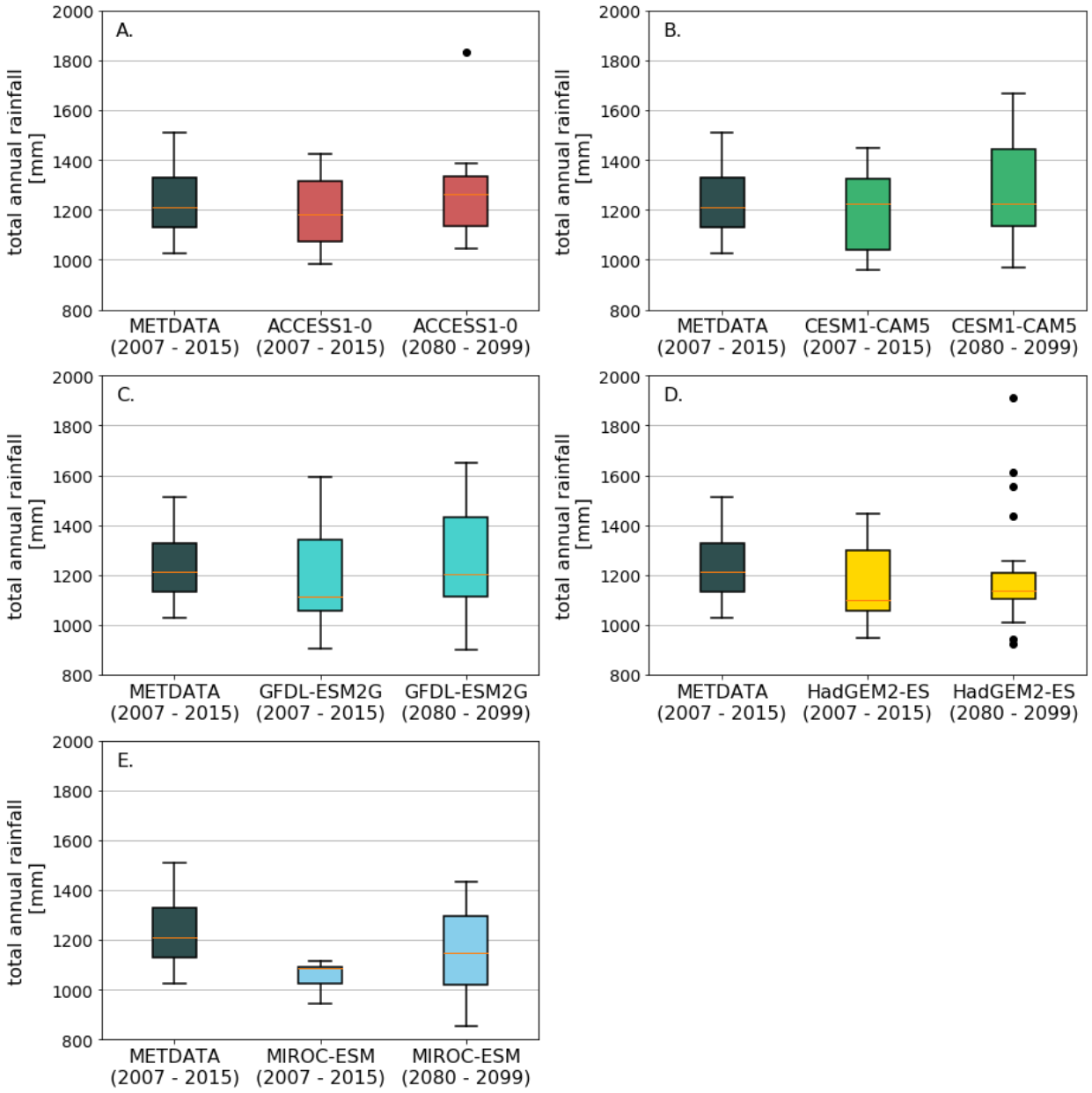

Figure 4.7 Boxplots of historic total annual rainfall from METDATA (water years 2007 - 2015) and projected total annual rainfall from LOCA downscaled global climate models ACCESS1-0 (A.), CESM1-CAM5 (B.), GFDL-ESM2G (C.), HadGEM2-ES (D.), and MIROC-ESM (E.) for water years 2007 – 2015 and water years 2080 – 2099. Orange lines indicate the median, boxes range from the first and third quartiles, whiskers extend to 1.5 the interquartile range, and data points outside whiskers are plotted as circles.

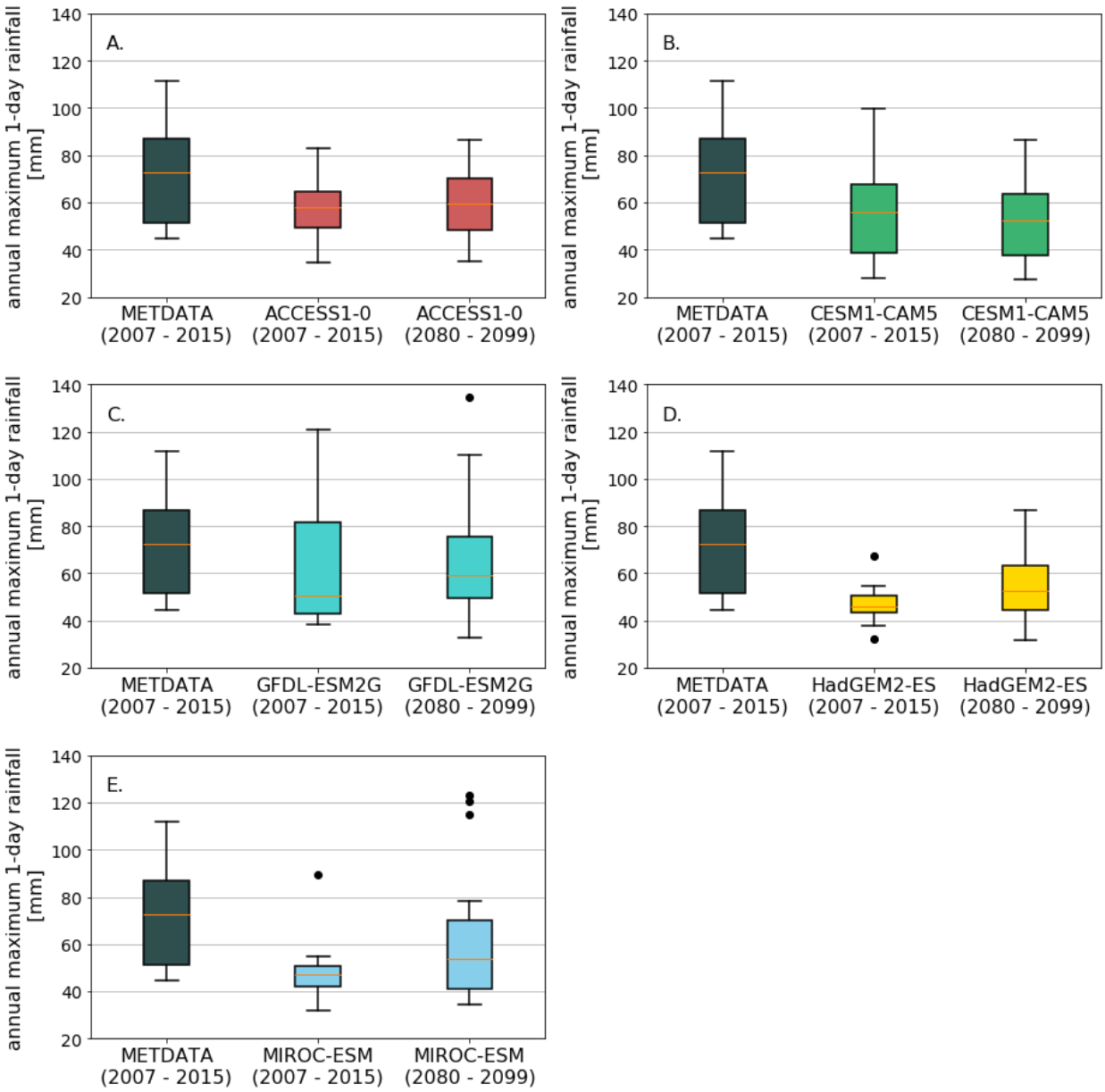

Figure 4.8 Boxplots of historic annual maximum 1-day rainfall from METDATA (water years 2007 - 2015) and projected maximum 1-day rainfall from LOCA downscaled global climate models ACCESS1-0 (A.), CESM1-CAM5 (B.), GFDL-ESM2G (C.), HadGEM2-ES (D.), and MIROC-ESM (E.) for water years 2007 – 2015 and water years 2080 – 2099. Orange lines indicate the median, boxes range from the first and third quartiles, whiskers extend to 1.5 the interquartile range, and data points outside whiskers are plotted as circles.

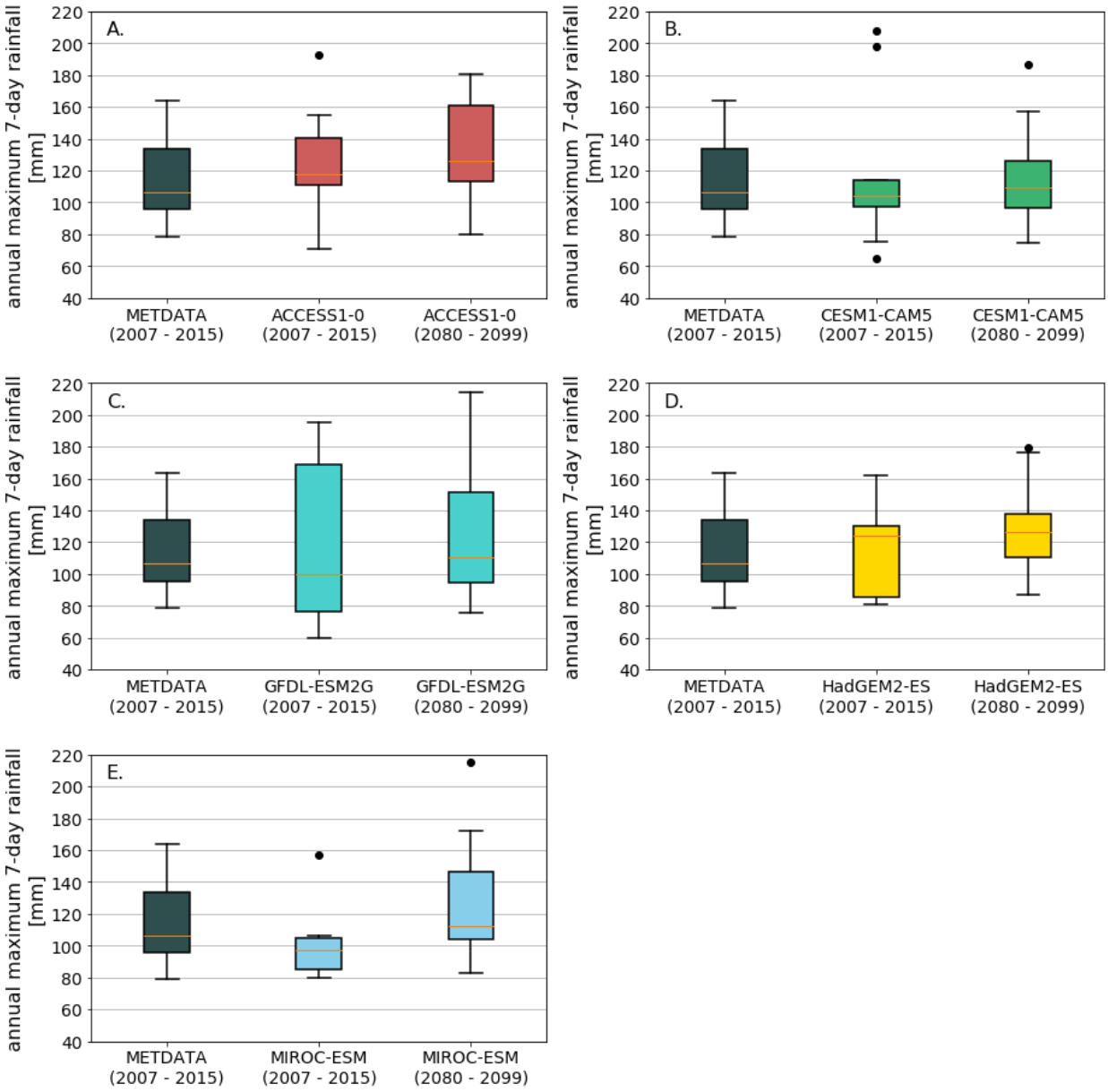

Figure 4.9 Boxplots of historic annual maximum 7-day rainfall from METDATA (water years 2007 - 2015) and projected maximum 7-day rainfall from LOCA downscaled global climate models ACCESS1-0 (A.), CESM1-CAM5 (B.), GFDL-ESM2G (C.), HadGEM2-ES (D.), and MIROC-ESM (E.) for water years 2007 – 2015 and water years 2080 – 2099. Orange lines indicate the median, boxes range from the first and third quartiles, whiskers extend to 1.5 the interquartile range, and data points outside whiskers are plotted as circles.

Table 4.3 Projected land cover for the Lamprey River watershed. Source: Thorn et al 2017.

	Land Cover					
Year	Agriculture (%)	Development (%)	Impervious (%)	Forest (%)	Water (%)	Wetland (%)
2020	6.7	8.4	2.6	69.1	1.8	13.9
2030	6.5	11.6	3.2	66.2	1.8	13.9
2040	6.3	14.3	3.7	63.7	1.8	13.9
2050	6.0	17.4	4.3	60.8	1.8	13.9
2060	5.6	21.5	5.0	57.3	1.8	13.9
2070	4.9	27.2	6.1	52.2	1.8	13.9
2080	4.0	34.8	7.6	45.5	1.8	13.9
2090	2.9	42.5	9.2	39.0	1.8	13.9
2100	1.9	51.0	10.8	31.5	1.8	13.9

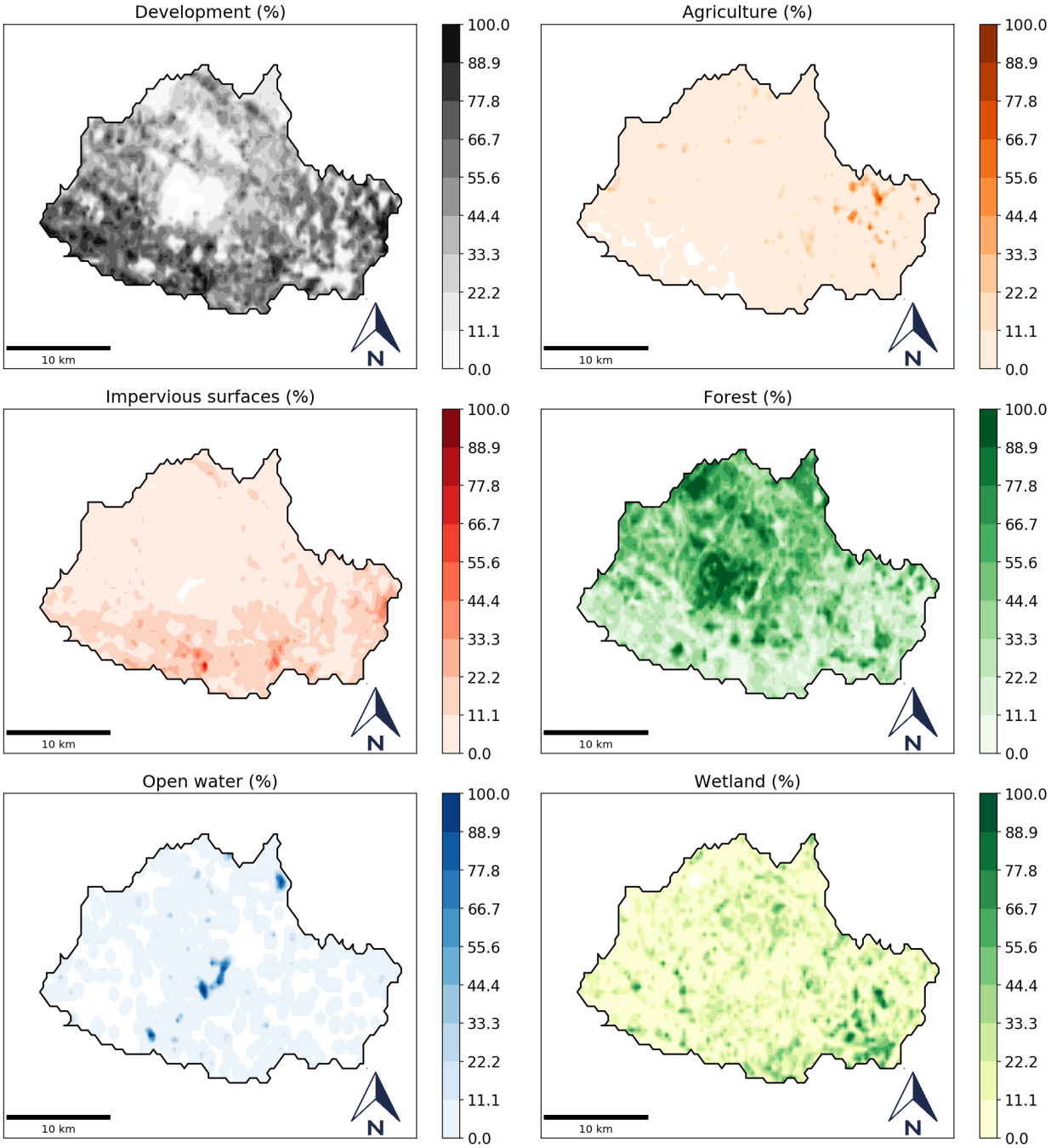

Figure 4.10 Projected land cover of the Lamprey River watershed for year 2090. Source: Thorn et al 2017.

4.4 Model Calibration

4.4.1 Hydrologic calibration methods

Water years 2000 to 2009 were used for the hydrologic calibration period. This time period contained two large flooding events in May 2006 and April 2007 (daily discharge of 8400 cfs and 7590 cfs respectively). The successive five water years (2010 to 2015) were used as the validation period. This period contained a large flood event in 2010 (mean daily discharge of 6550 cfs).

Calibrated hydrologic parameters comprised the soil moisture drying rate (α [-]), the fraction of surplus that infiltrates groundwater ($\mathrm{infiltr}$ [-]), the fraction of groundwater that exits to baseflow (β [-]), and the drainage rate ($\mathrm{RhRt2}$ [-]) and maximum capacity (RRPMax [mm]) of the surface runoff retention pool. A Python 2.x script using the BasinHopping function from the SciPy optimize library (Jones et al. 2001) was used to minimize the SSR objective function for the calibration period through calibrating these five hydrologic parameters (Figure 4.9). The BasinHopping function utilizes a Metropolis Hastings approach, which is comprised of "inner iterations" to find local objective function minima and stochastic perturbations, or "hopping iterations," to find global objective function minima in parameter space. Default hydrologic parameter values were determined using FrAMES default values, and parameter value selection was constrained during calibration by providing minimum and maximum bounds for each parameter (Table 4.3). Parameter bounds were selected based on reasonable values for implementation of the model. A delta (Δ) value and tolerance (tol) value were also assigned to each hydrologic parameter (Table 4.3). The delta indicates how far in either direction a parameter value could be adjusted during an inner iteration (Figure 4.9), while the tolerance value indicates how far in either direction a parameter value could be adjusted during a hopping iteration (Figure 4.9).

A BasinHopping function with 300 hopping iterations was used for the hydrologic calibration. See Figure 4.9 for a visual representation of the calibration procedure.

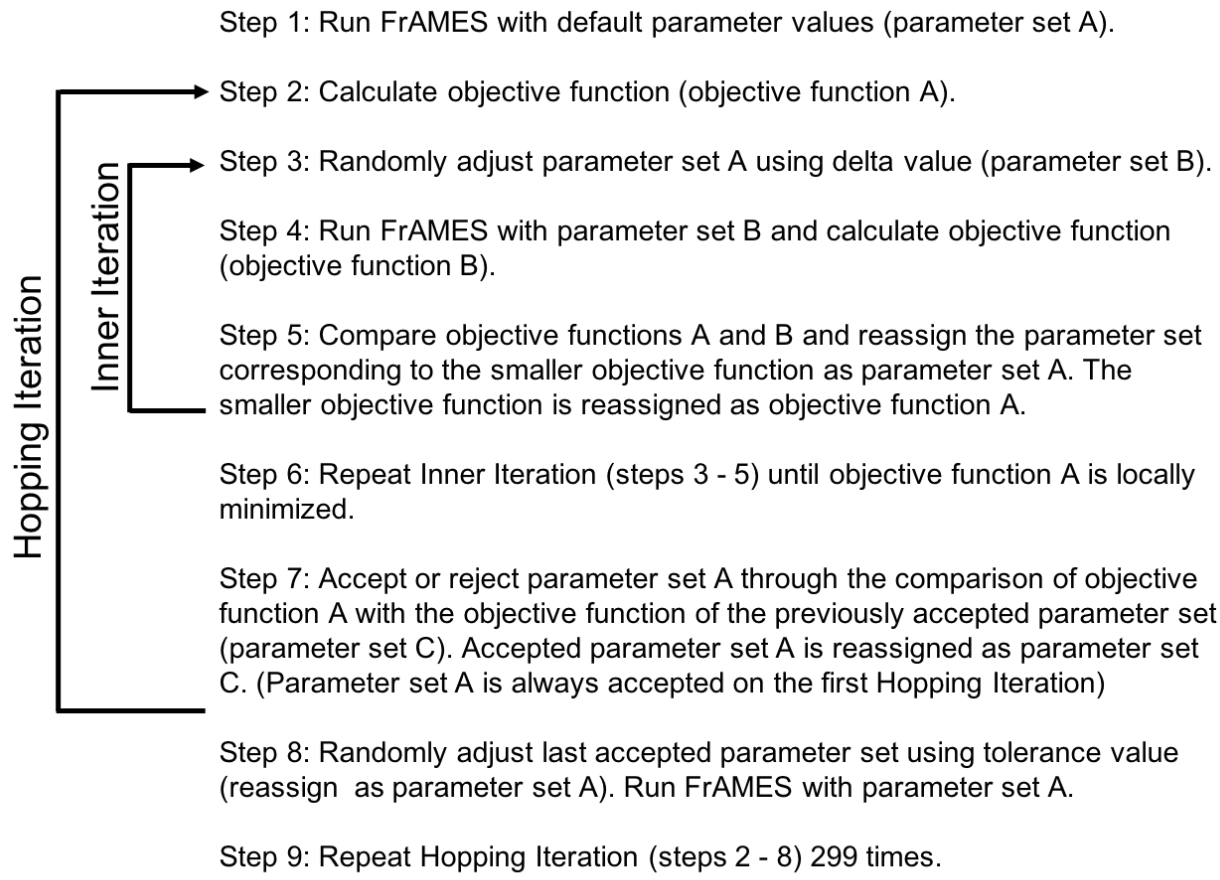

Figure 4.11 Flow chart of the Python 2.x script used to calibrate the five hydrologic parameters (parameter set). All accepted parameters sets (parameter set C) were stored in order to create a posterior joint distribution used in assessing parameter uncertainty.

Local minimization was achieved when the fractional difference between successive objection functions [i.e., objective functions B ($\mathrm{Obj_B}$) and A ($\mathrm{Obj_A}$)] was below $1 \cdot 10^{-8}$ (Figure 4.8, Step 5),

$$\frac{\mathrm{Obj_B} - \mathrm{Obj_A}}{\mathrm{Maximum}} \leq 1 \cdot 10^{-8} \qquad \text{Equation 4.1}$$

where $\mathrm{Maximum}$ is a function that is the maximum value of either $\mathrm{Obj_B}$, $\mathrm{Obj_A}$, or 1. After the objective function was locally minimized (Figure 4.8, Step 6) during the first hopping iteration, the parameter set was accepted. For the other 299 hopping iterations, after local objective function minimization was achieved, the parameter set was accepted if the difference between

the objective function and the previously accepted parameter set's objective function was less than a temperature value of 0.5; otherwise, the parameter set was rejected. The temperature value was chosen because multiple preliminary BasinHopping function tests using a temperature value of 0.5 converged to similar hydrologic parameter values. After 300 hopping iterations, all accepted parameter sets were combined into a joint posterior distribution and used in the hydrologic uncertainty analysis.

To closely match discharge across the entire flow regime, the flow duration curve of historic observations of daily discharge measured at USGS gauge 01073500 (Packer's Falls near Newmarket, NH) was compared to the flow duration curve of modeled discharge for the hydrologic calibration period (Table 4.4). Flow duration curves were calculated for both modeled and observed flow duration curves by assigning a rank (Rank) to each daily discharge measurement for the period from highest to lowest. Exceedance probabilities (EP) were then calculated for each rank,

$$\mathrm{EP} = \frac{\mathrm{Rank}}{\mathrm{N}+1} \qquad \text{Equation 4.2}$$

where N is the total number of daily discharge measurements. Then, 26 evaluation points along the flow duration curve were selected based on equal intervals of water volume (Westerberg, et al. 2011; Figure 4.10). Modeled ($\mathrm{Q_{Mod}}$) and observed ($\mathrm{Q_{Obs}}$) daily discharge at each evaluation point were log-transformed, in order to give more weight to low flow residuals, then the sum of squares residuals (SSR) was calculated as follows:

$$\mathrm{SSR} = \sum[\log(\mathrm{Q_{Obs}}) - \log(\mathrm{Q_{Mod}})]^2 \qquad \text{Equation 4.3}$$

This sum of squares residuals (SSR) was used as an objective function to calculate a goodness of fit between modeled daily discharge and observed daily discharge.

Two additional metrics were used to compare modeled to observed flow duration curves during the calibration and validation period. The first metric was the percentage of total observed discharge conserved ($\%Q_{conserved}$),

$$\%Q_{conserved} = \left[\frac{\sum Q_{mod}}{\sum Q_{obs}}\right] \cdot 100 \qquad \text{Equation 4.4}$$

where $\%Q_{conserved} > 100$ indicates there was an excess of discharge and $\%Q_{conserved} < 100$ indicates there was insufficient discharge. The second metric was the Nash-Sutcliffe efficiency coefficient (NSE; Nash and Sutcliffe 1970), which is calculated as,

$$NSE = 1 - \frac{\sum[Q_{Mod} - Q_{obs}]^2}{\sum[Q_{obs} - \overline{Q}_{obs}]^2} \qquad \text{Equation 4.5}$$

where $\overline{Q}_{obs}$ represents the mean of observed daily discharge. NSE values can range from -∞ to 1. An NSE of 1 indicates modeled mean daily discharge perfectly matches observations, while a negative value indicates that the mean of observed mean daily discharge provides more accuracy than modeled discharge.

Table 4.3 Optimized hydrologic parameter default, bounds (min and max), delta (Δ), and tolerance (tol) values that were used during hydrologic calibration.

Parameter	default	min	max	Δ	tol
α [-]	5.0	1.05	19.99	0.08	2.0
infiltr [-]	0.5	0.09	0.91	0.035	0.25
β [-]	0.0167	0.0001	0.35	0.035	0.01
RhRt2 [-]	0.056	0.0001	1.0	0.035	0.05
RRPMax [mm]	30	0.0005	150.0	0.035	25.0

Table 4.4 Values of 26 evaluations points used during the hydrologic calibration across the flow duration curve.

Evaluation	Exceedance	Evaluation	Exceedance
1	0.0003041	14	0.1700858
2	0.0028293	15	0.1951909
3	0.0080119	16	0.2226646
4	0.0151238	17	0.2529276
5	0.0234031	18	0.2862475
6	0.0334119	19	0.3241754
7	0.0451473	20	0.3672061
8	0.0583296	21	0.4168571
9	0.0729865	22	0.4748304
10	0.0891395	23	0.5453163
11	0.1067518	24	0.6377737
12	0.1258386	25	0.7796548
13	0.1469162	26	0.9996958

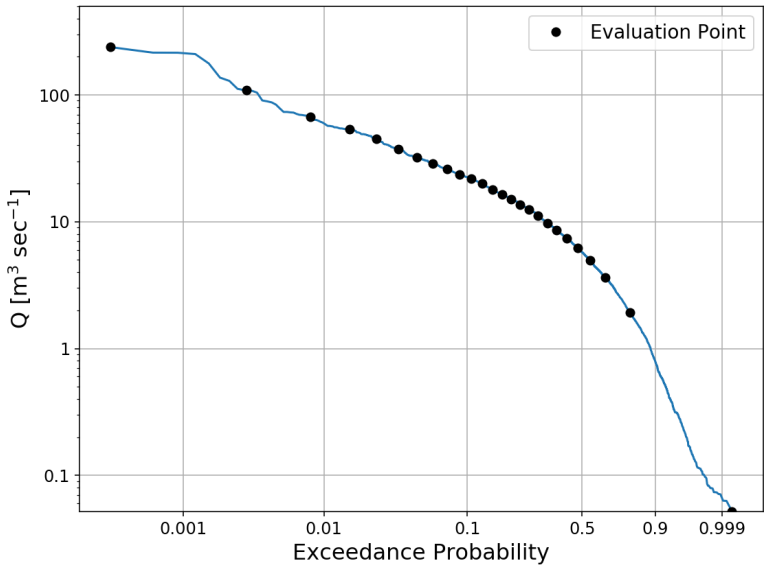

Figure 4.12 The 26 evaluation points used during hydrologic calibration across the flow duration curve of historic observations of mean daily discharge (Q) at USGS gauge # 01073500 near Newmarket, NH for water years 2000 to 2009.

4.4.2 Hydrologic Calibration Results

The flow duration curves from the ensemble of modeled mean daily discharge captures most of the observed flow duration curve at USGS gauge 01073500 for the calibration period (Figure 4.11 A), which is reflected by a mean NSE of 0.538. The flow duration curves from the ensemble of modeled mean daily discharge for the validation period had a mean NSE of 0.406 (Figure 4.11B). During both periods, modeled discharge tended to under-predict observed higher flows (Figure 4.11A,B) and over-predict lower flows for the calibration period (Figure 4.11A) and under-predict low flows for the validation period (Figure 4.11B). The highest observed flows, which occurred in the spring (Figure 4.12), were underpredicted, likely as a result of modeling runoff on a daily time step or an underprediction of the amount of water stored in snowpack during the winter. In order to better capture the highest observed flows, sub-daily runoff modeling becomes more important. Modeled low flows were both under- and overpredicted compared to observations due to a large variability of water volume released at reservoirs upstream during periods of low flow. The mean percentage of total observed discharge conserved ($\%\mathrm{Q}_{\mathrm{conserved}}$) for the calibration and validation periods were 89.07% and 88.18% respectively with little variation between each model output in the ensemble of accepted parameter sets. This underestimation of total modeled water volume was likely the result of an underestimation in total annual precipitation used as model input compared to actual total annual precipitation.

Hydrologic calibration yielded 16 accepted parameter sets with objective function values ranging from 2.165 $m^3\ s^{-1}$ to 14.569 $m^3\ s^{-1}$. None of the optimal parameter values were at the minimum or maximum of the specified parameter rangers, suggesting that optimization had not been constrained by the choice of allowable ranges. Parameters α, $\mathrm{infiltr}$, β, all exhibited similar sensitivity relative to the best value, while the surface runoff retention pool parameters $\mathrm{RhRt2}$ and RRPMax had a larger relative range of values (Table 4.5).

Table 4.5 Hydrologic parameter ranges and best values after calibration. Best values are from the hydrologic parameter set with the lowest objective function.

Parameter symbol	Parameter name	Best value	Calibrated minimum	Calibrated maximum
α [-]	soil moisture drying rate	9.806507	5.462000	12.784976
infiltr [-]	fraction of surplus that infiltrates groundwater	0.476529	0.254142	0.674074
β [-]	fraction of groundwater that exits to baseflow	0.025998	0.018546	0.033651
RhRt2 [-]	drainage rate of runoff retention pool	0.183238	0.141149	0.511640
RRPMax [mm]	max capacity of runoff retention pool	4.466693	0.0005	41.328097

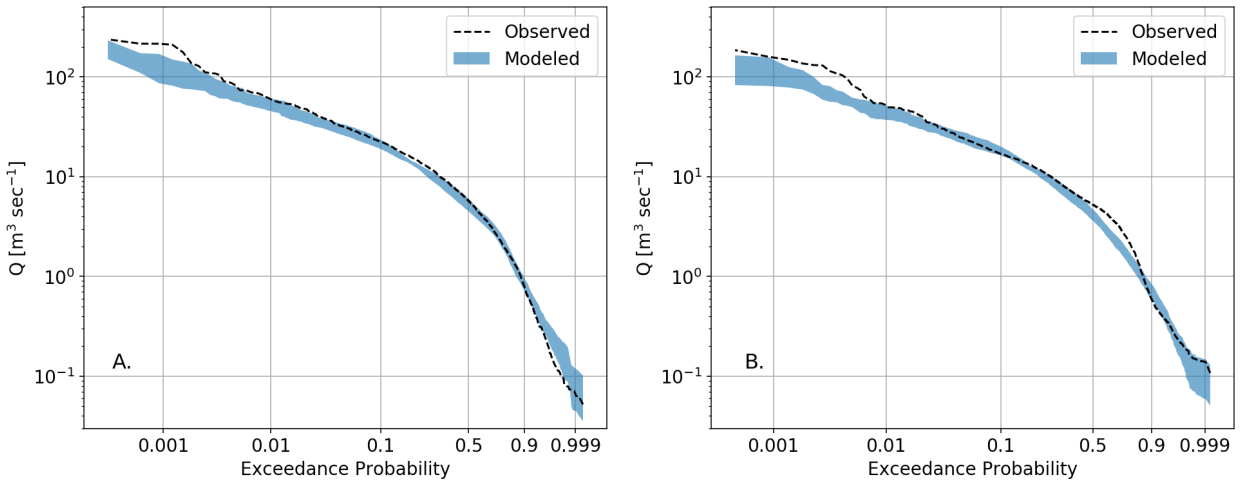

Figure 4.13 Observed and modeled flow duration curves of mean daily discharge (Q) at USGS gauge 01073500 for (A) water years 2000 to 2009 and (B) water years 2010 to 2015. The modeled flow duration curves span the ensemble of model output using the 16 accepted hydrologic parameter sets.

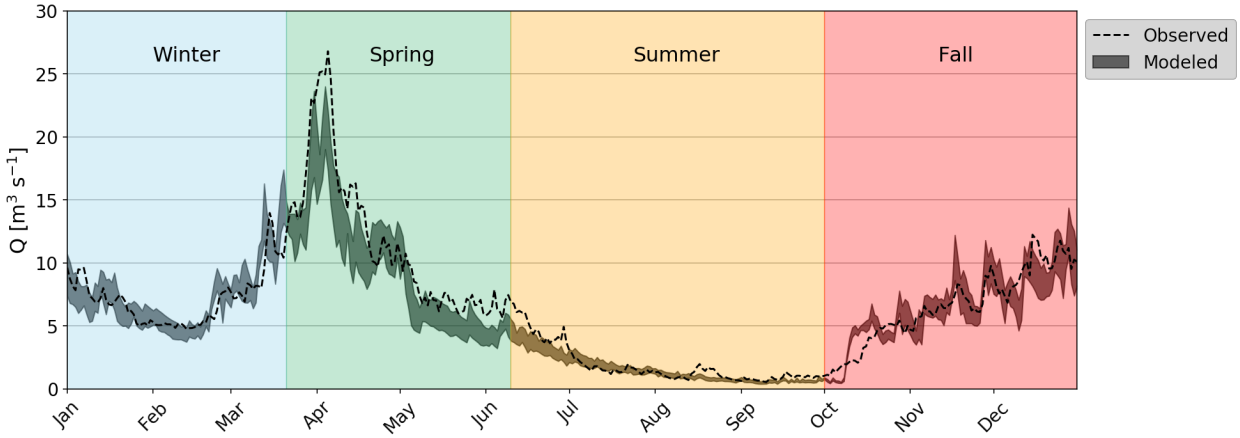

Figure 4.14 Observed and modeled median daily discharge (Q) for day of year at USGS gauge 01073500 for water years 2000 to 2015.

4.4.3 DIN loading Calibration

Modeled DIN loading was calibrated using weekly historical measurements of DIN concentration ($\mathrm{DIN_{Conc}}$) taken by the NH Water Resources Research Center at UNH at five headwater tributaries with varying human land use (HLU; agriculture + development) throughout the watershed (Table 4.6). The DIN loading logistic function (Figure 4.12) required the calibration of four parameters: the asymptote of the logistic function (Asym); the human land use range at which concentration increases (Scale); and the human land use percentage at which the inflection point occurs (Xmid) which is the discharge-dependent (Q) with an intercept ($\mathrm{Xmid_b}$) and slope ($\mathrm{Xmid_m}$).

$$\mathrm{DIN_{Conc}} = \frac{\mathrm{Asym}}{1+e^{\frac{(\mathrm{Xmid}-\mathrm{HLU})}{\mathrm{scale}}}} \qquad \text{Equation 4.6}$$

$$\mathrm{Xmid} = \mathrm{Xmid_b} + \mathrm{Xmid_m} \cdot \log(\mathrm{Q}) \qquad \text{Equation 4.7}$$

In order to calibrate parameters over a range of discharge conditions, nine monthly averaged windows between 2013 and 2015 were chosen (cf. Wollheim et al. 2008). Of these nine windows, three contained high discharge, three contained medium discharge, and three contained low discharge conditions within the watershed. Since no discharge measurements were taken at the headwater sites, mean daily discharge measurements taken downstream at USGS gauge 01073500 at Packer's Falls were averaged over each month and used to determine whether a particular window was considered a high, medium, or low discharge period. Windows with higher discharge (monthly averaged mean daily Q > 10 m^3 sec^{-1}) were April of 2013, 2014, and 2015. Medium discharge windows (monthly averaged mean daily Q < 10 m^3 sec^{-1} and > 4 m^3 sec^{-1}) were May of 2013, 2014, and 2015. Low discharge windows (monthly averaged mean daily Q < 4 m^3 sec^{-1}) were August of 2013 and June of 2014 and 2015.

A Python 3.x script using the Minimize function from the SciPy optimize library (Jones et al. 2001) was used to find the DIN loading parameter set of the best fitting logistic curve for all

nine windows. The Minimize function follows a similar approach as Steps 1 through 6 of the BasinHopping function described in the hydrologic calibration section (Figure 4.8), here using DIN concentration estimates produced by the logistic curve instead of discharge estimates produced by FrAMES as described above. Once a local minima had been reached, DIN loading parameters were saved and the minimize function terminated. The sum of squared residual between the logistic curve estimates and averaged DIN concentration measurements for each window was used as an objective function. DIN loading boundary conditions and delta values are listed in Table 4.7. Initial DIN loading parameters were originally set to Ipswich values, however it was found that the sum of squared residuals was smaller when initial DIN loading parameters were set to 0.

DIN loading calibration resulted in a minimum SSR value of 0.868 mg DIN L^{-1} using the parameter values listed in Table 4.8. This resulted in a logistic curve that estimates higher DIN concentration in terrestrial runoff within grid cells of lower human land use as compared to logistic curves previously developed for the Ipswich watershed (Figure 4.15). Differences could result from a smaller sample size of headwater sites within the Lamprey River watershed as compared to the Ipswich, the use of monthly averages of discharge and DIN concentrations as compared to synoptic measurements (Wollheim et al. 2008), or differences in the amount and spatial distribution of wetlands between watersheds.

Table 4.7 Locations and human land use (sum of agriculture and development) of first-order tributaries used to calibrate DIN loading.

Location	Human Land Use (%)	Drainage Area (km^2)
Wednesday Hill Brook	33.4	1.02
Dowst Cate Forest	13.5	7
Moonlight Brook	41.1	0.89
Rum Brook	20.9	4.9
Saddleback Mountain	0.5	0.3

Table 4.8 Parameters optimized during DIN loading calibration and final values calibrated for the Ipswich (cf. Wollheim et al. 2008) and Lamprey River watersheds.

Parameter	initial	min	max	delta	Calibrated value in Ipswich	Calibrated value in Lamprey
$Asym$	0.0	0.0	2.0	0.1	1.4	0.69
$Scale$	0.0	0.0	30	0.1	12.2	3.65
$Xmid_b$	0.0	0.0	60	0.1	40.3	13.91
$Xmid_m$	0.0	0.0	40	0.1	19.5	12.55

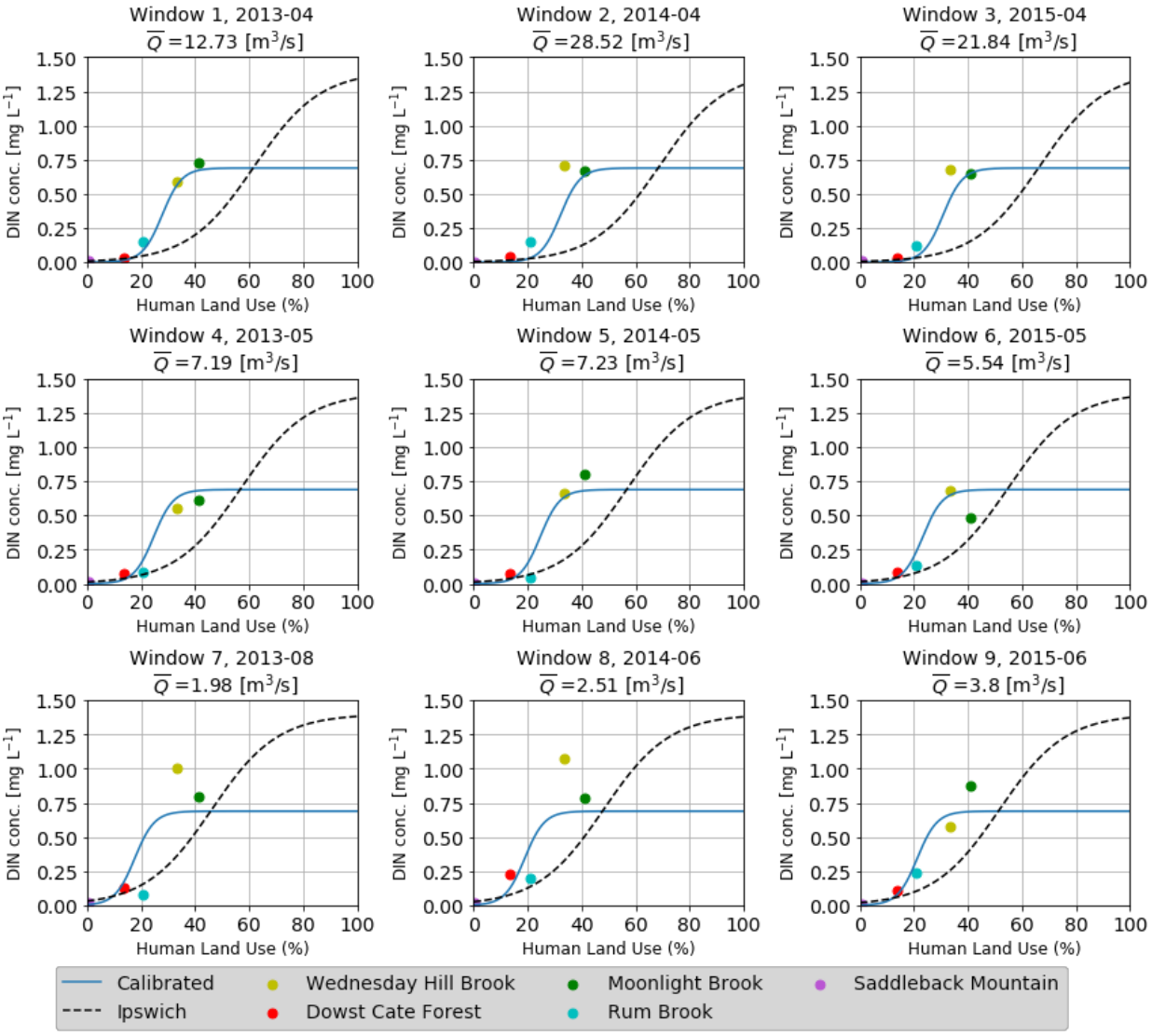

Figure 4.15 Calibration of dissolved inorganic nitrogen (DIN) concentration in runoff at five headwater sites in the Lamprey River watershed. Each panel shows a different monthly window. Markers show monthly average concentration across five different subwatersheds with different land use.

4.4.4 Modeled DIN Reservoir and River Retention

Annual DIN retention estimates from the empirical model developed by Seitzinger et al. (2002) were rescaled to daily estimates and implemented into FrAMES to represent DIN retention within reservoirs (see appendix B.14). To incorporate seasonality into reservoir DIN retention, daily estimates were scaled by a Q10 water temperature coefficient (Sierra 2012),

$$\mathrm{Q10} = 2^{\left(\frac{(T_W - Tref)\cdot Tscale}{10}\right)} \quad \text{Equation 4.8}$$

where T_w is the water temperature [°C], $Tref$ is the reference water temperature [°C], and $Tscale$ is a temperature scaling factor [-]. Q10 parameters were calibrated based on a visual comparison of modeled median mean daily instream DIN concentration for day of year and observed DIN concentration measured by WRRC at the USGS gauge 01073500 averaged for water years 2000 to 2015 (Figure 4.16). The best fit for the winter (January 1st to March 21st) and summer (June 10th to October 1st) seasons was obtained when the Q10 water temperature coefficient's reference water temperature ($Tref$) was set at 18°C and the numerator of the exponent was multiplied by a temperature scaling factor ($Tscale$) of 6. The temperature scaling factor was implemented to increase DIN retention during periods when water temperature was greater than the reference water temperature (Summer) and decrease DIN retention during periods when water temperature was less than the reference water temperature.

For FrAMES grid cells without reservoirs, the efficiency loss model (Mulholland et al. 2008) was used to calculate river channel DIN retention (R_{river}) with an uptake velocity (V_f) [m day^{-1}] that varies with both in-channel water temperature and DIN concentration. R_{river} is then calculated as,

$$R_{River} = 1 - \exp\left(-\frac{1}{V_f \cdot \frac{outflow}{river_{Area}}}\right) \quad \text{Equation 4.9}$$

where,

$$V_f = 10^{(int + \log(DIN_{outflow} \cdot slope)} \cdot \mathrm{Q10} \qquad \text{Equation 4.10}$$

where V_f is the uptake velocity of DIN [g km^{-2} d^{-1}], $river_{Area}$ [m] is the river channel area and is calculated from the channel width and height derived from empirical relationships relating discharge with reach-averaged width and depth, int [-] is the uptake velocity intercept (value of -2.975; Mulholland et al. 2008), $slope$ [-] is the slope of the uptake velocity (value of -0.493; Mulholland et al. 2008) $\mathrm{Q10}$ is a water temperature correction factor. Unlike for reservoir retention, Q10 parameters applied to river DIN retention were not calibrated and therefore the reference water temperature and temperature scaling factor were chosen as default (values of 20°C and 1.0 respectively).

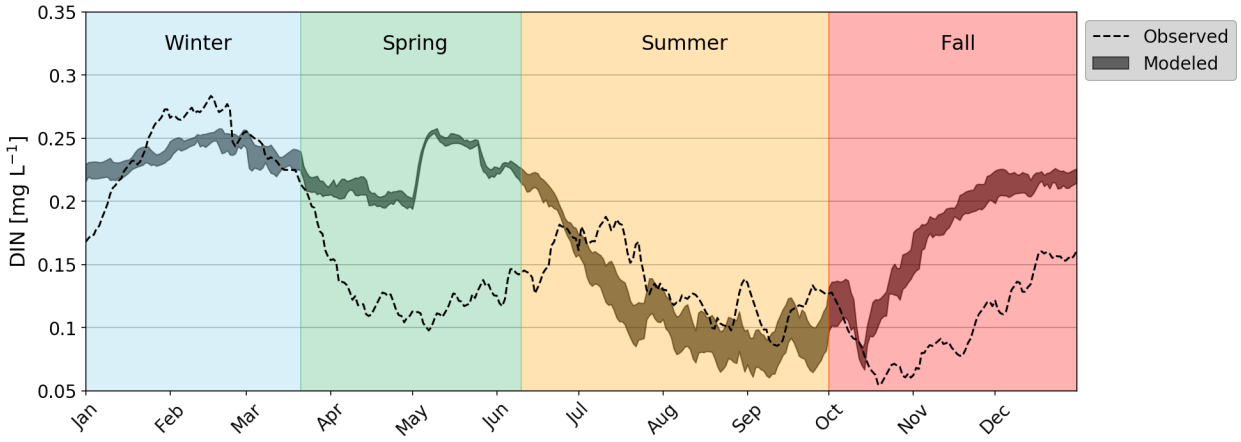

Figure 4.16 Observed and modeled median mean daily dissolved inorganic nitrogen (DIN) concentration for day of year at USGS gauge 01073500 for water years 2000 to 2015. Observed measurements were collected through weekly grab samples obtained by the WRRC at UNH and linearly interpolated to daily estimates. The range in modeled DIN concentration comes from the ensemble of model output using the 16 accepted hydrologic parameter sets.

4.4.5 DIN concentration Variability with Discharge

In order to characterize how DIN concentration varied seasonally with discharge at USGS gauge 01073500, both observed and modeled DIN concentration-discharge relationships were constructed for each season by calculating the best-fit power law relationship using a least-squares fitting (Figure 4.17). All power-law relationships exponents were found to be significantly different from zero ($p < 0.05$) except for the observed fall DIN concentration-

discharge relationship ($p = 0.083$; Table 4.9). During winter and spring, both modeled and observed DIN concentration and discharge were negatively correlated (diluting effect; Figure 4.17 A), while during summer, both modeled and observed DIN concentration-discharge relationships were positively correlated (flushing effect) during low flows, whereas during higher discharge DIN concentration appeared to plateau (Figure 4.17 C). Fall observations showed no discernable pattern while modeled DIN concentration-discharge showed a weak flushing effect. Modeled DIN concentration was therefore representative of observed DIN concentration during the winter and summer seasons, but failed to capture observed DIN concentration during the spring (March 22nd to June 9th) and fall (October 2nd to December 31st) seasons (Figure 4.16 and 4.17). This misrepresentation of DIN concentration in spring could be a result of an increase in both terrestrial and aquatic demand for DIN at the beginning of the growing season, which is not represented in the model. During the fall, the influx of carbon into the river network following leaf-out could result in an increase in DIN retention, which the model does not capture.

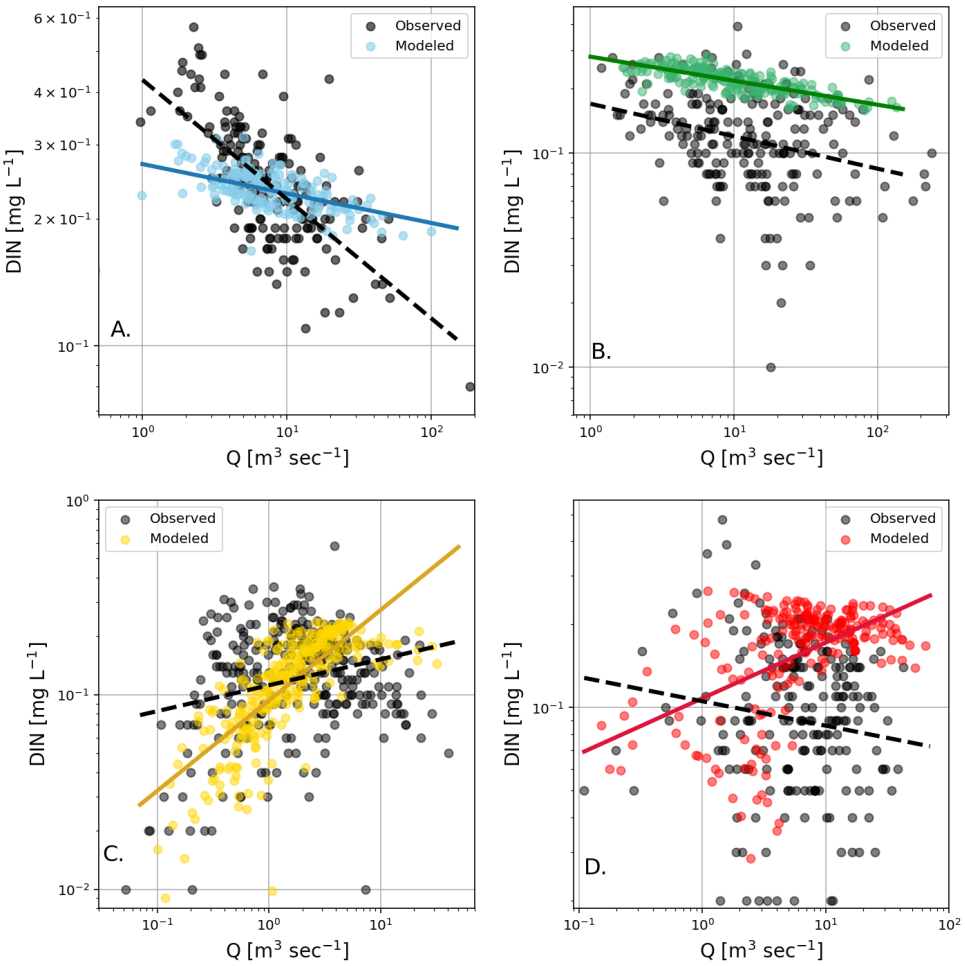

Figure 4.17 Observed and modeled dissolved inorganic nitrogen (DIN) concentration to discharge (Q) for (A) winter, (B) spring, (C) summer, and (D) fall seasons. Solid lines represent the modeled best-fit power law DIN concentration-discharge relationship and dashed lines represent the observed best-fit power law DIN concentration-discharge relationship

Table 4.9 Best-fit power laws of observed and modeled dissolved inorganic nitrogen concentration to discharge. r^2 values indicate the fraction of the variation of the relationship between dissolved inorganic nitrogen concentration and discharge explained from the power law regression curve. P values < 0.05 indicate that the power law relationship (the correlation between dissolved inorganic nitrogen concentration and discharge) is statistically significant at a 95% confidence level.

Season	Observed			Modeled		
	Power Law	r^2	p value	Power Law	r^2	p value
Winter	$0.427 \cdot x^{-0.282}$	0.466	$2.599 \cdot 10^{-26}$	$0.269 \cdot x^{-0.069}$	0.252	$5.203 \cdot 10^{-13}$
Spring	$0.169 \cdot x^{-0.151}$	0.088	$1.269 \cdot 10^{-5}$	$0.281 \cdot x^{-0.112}$	0.629	$4.385 \cdot 10^{-46}$
Summer	$0.111 \cdot x^{0.133}$	0.055	$2.740 \cdot 10^{-5}$	$0.093 \cdot x^{0.464}$	0.581	$3.194 \cdot 10^{-60}$
Fall	$0.105 \cdot x^{-0.088}$	0.013	0.083	$0.108 \cdot x^{0.201}$	0.252	$1.732 \cdot 10^{-15}$

4.4.6 Modeled DIN Flux

After hydrologic and DIN Q10 calibration and implementation of site-specific DIN loading coefficients the model successfully captures the magnitude in DIN concentration and flux during the winter and summer seasons. However, model overestimation of DIN concentration during spring and fall resulted in overestimations in DIN flux during both seasons (Figure 4.18). Due to limitations in modeling DIN flux during the spring and fall seasons, this project focused on trends in DIN flux during the winter and summer seasons.

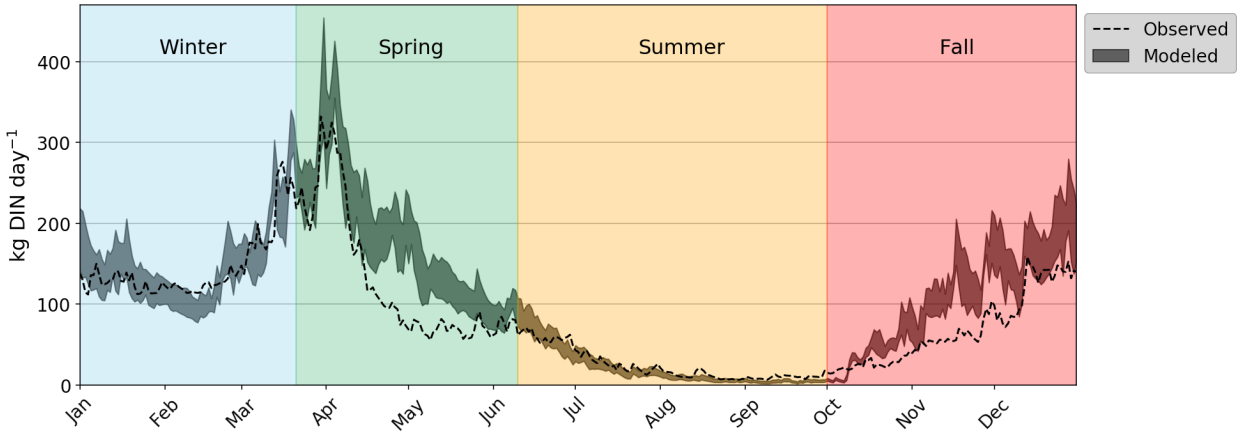

Figure 4.18 Observed and modeled median mean daily dissolved inorganic nitrogen (DIN) flux for day of year at USGS gauge 01073500 for water years 2000 to 2015. The range in modeled DIN flux comes from the ensemble of model output using the 16 accepted hydrologic parameter sets.

4.4.7 Estimation of Hydrologic Parameter Uncertainty

Model discharge uncertainty associated with parameter selection was estimated using an approximate Bayesian computation approach (Turner and Van Zandt, 2011). Thirty-six unique sets of the five calibrated hydrologic parameters were randomly sampled from the hydrologic parameter joint posterior distribution obtained in hydrologic model calibration (Figure 4.19) and used to produce an ensemble of 36 model runs for each scenario. A 95% confidence interval on model discharge was constructed from the 5th and 95th percentiles of the ensemble

of 36 runs and used to estimate uncertainty on 2-yr flood discharge magnitudes and winter and summer DIN flux.

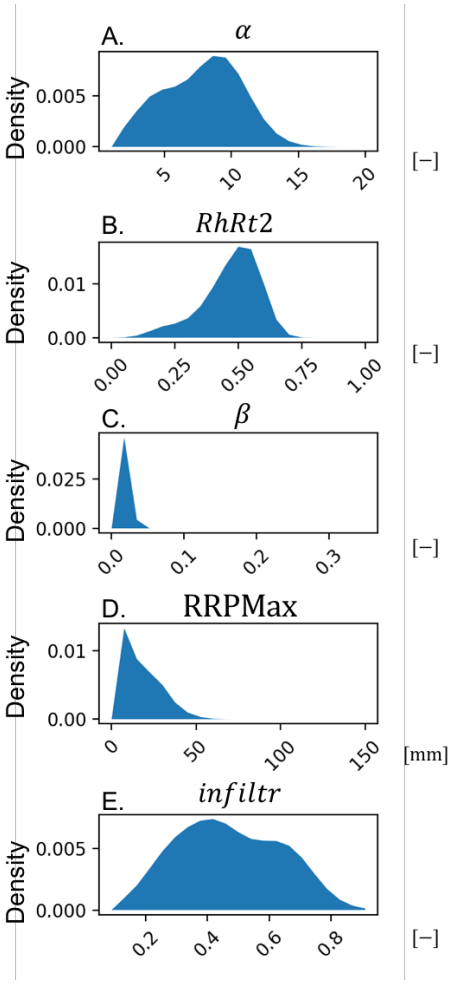

Figure 4.19 Kernel density estimation plots of calibrated hydrologic parameters (A) α, (B) $\mathrm{RhRt2}$, (C) β, (D) RRPMax, and (E) $infiltr$ obtained during hydrologic calibration and used to estimate model uncertainty associated with parameter selection.

4.5 Model Scenarios

The model was used to estimate how dams, specifically reservoir size, management, and location within the Lamprey River watershed, affected floods and seasonal DIN flux under contemporary land use and climate (for water years 1996 to 2015) and projected climate and land use (water years 2080 to 2099). Dam scenarios under contemporary climate and land use consisted of the following ten scenarios:

1. all current dams present under current management,

2. all current dams present managed for flood control,
3. all current dams present managed for water supply,
4. all dams removed,
5. small reservoirs removed, remaining dams under current management,
6. large reservoirs removed, remaining dams under current management,
7. increasing total maximum reservoir capacity within the watershed by 100 x 10^6 m^3 distributed evenly to the four dams located along the lower mainstem, so each reservoir's maximum capacity increased by 25 x 10^6 m^3
8. increasing total maximum reservoir capacity within the watershed by 500 x 10^6 m^3 distributed evenly to the four dams located along the lower mainstem, so each reservoir's maximum capacity increased by 125 x 10^6 m^3
9. increasing total maximum reservoir capacity within the watershed by 100 x 10^6 m^3 distributed evenly to the 18 dams located within the headwaters, so each reservoir's maximum capacity increased by 5.55 x 10^6 m^3
10. increasing total maximum reservoir capacity within the watershed by 500 x 10^6 m^3 distributed evenly to the 18 dams located within the headwaters, so each reservoir's maximum capacity increased by 27.77 x 10^6 m^3

Currently, five dams within the Lamprey River watershed are actively managed for recreation, and reservoir drawdown announcements are annually published by the NHDES Dams Bureau (Mendum's Pond, Dolloff Dam and Drowns Dam for Pawtuckaway Lake, and North River Pond) and the town of Raymond (Onway Lake). The remaining seventeen dams within the Lamprey River watershed were considered unmanaged and were modeled as spillway dams for each scenario using current dam management. Large reservoirs were defined as reservoirs with a maximum reservoir capacity greater than 1 x 10^6 m^3, which included five dams within the watershed: Drowns Dam, Dolloff Dam, Mendum's Pond Dam, Onway Lake

Dam, and the Macallen Dam. The remaining dams were defined as having small reservoirs. Dam and/or reservoir attributes for the modeled dams within the Lamprey River watershed were obtained from either the NID or NHDES databases and are listed in Table 1.1. In order to explore how reservoir location and reservoir storage (a proximation for residence time) affects floods and seasonal DIN fluxes the maximum reservoir capacities of either reservoirs located along the Lamprey River mainstem or in the upper watershed headwaters were increased in dam scenarios #7-10. The four mainstem dams include two currently active dams (Wiswall Dam and the Piscassic River Dam), one dam that has been breached (Wadleigh Falls Dam), and one that was removed in 2011 (Bunker Pond Dam). Dam scenarios #1, 4, 7, and 9 were also implemented under projected climate and land use together (Figure 4.20). Dam scenarios #1 and 4 were implemented also under contemporary climate and projected land use and projected climate and contemporary land use.

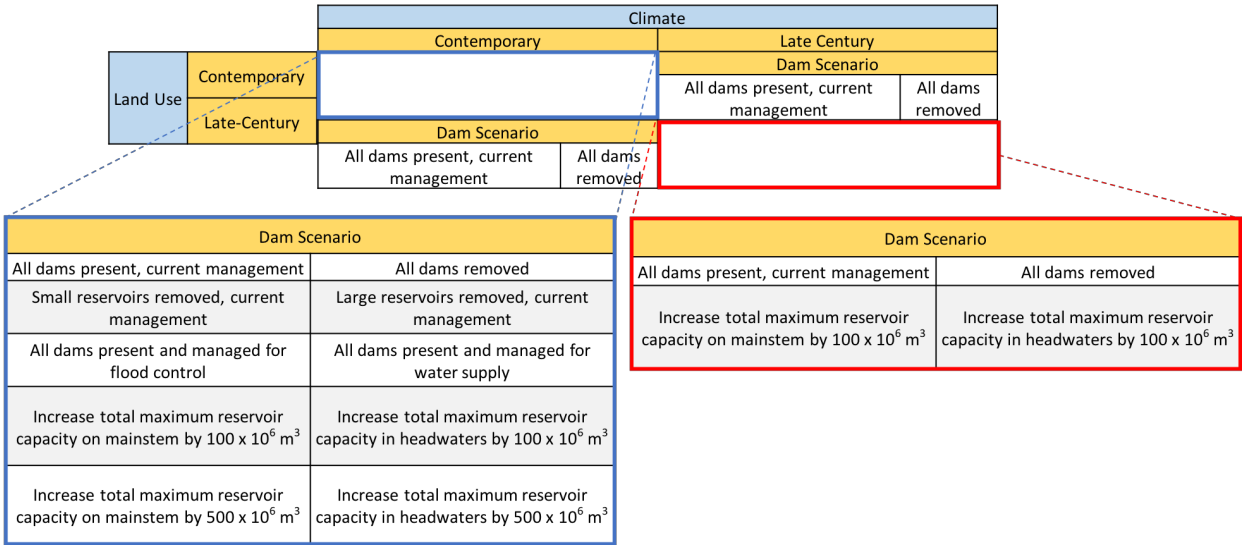

Figure 4.20 Figure of all scenarios modeled in FrAMES showing each combination of climate, land use, and dam scenario.

4.6 Comparison Metrics

High flow magnitudes, mean daily wintertime and summertime DIN flux, and DIN retention at the watershed outlet were used as metrics to compare different modeled scenarios

to current conditions. High flows were defined as the historic daily discharge exceeded only once every other year (otherwise known as the 2-yr flood event) observed at USGS gauge 01073500 (71.1 $m^3 s^{-1}$). A two-sided Mann-Whitney rank sum test was used to compare metrics for each scenario (based on the variability in the 36 model run ensemble) to current conditions to determine if comparison metrics were statistically different from current conditions (Helsel and Hirsch 2002). For each scenario, a skewness index (cf. Mineau et al. 2015) was also calculated for total mean reservoir storage within the watershed over the 20-year scenario. All scenarios using late-century climate were compared to a baseline scenario using the ensemble of five LOCA GCM climate drivers, contemporary land use, and current dam management for water years 2007 to 2015.

Chapter 5: FrAMES Modeling Results

5.1 Flood Magnitudes

5.1.1 Dam Scenarios Under Contemporary Climate & Land Use

Model results confirmed that dams attenuate floods within the Lamprey River watershed. With contemporary climate and land use and current dam management, the removal of all dams resulted in an 18.57% increase in the median 2-yr flood magnitude relative to the current dam management scenario (Figure 5.1), which was a significant increase (p=0.0015, Table 5.1). The removal of dams with large reservoirs increased the median 2-yr flood magnitude by 9.33% (Figure 5.1), which was also significant. The removal of dams with smaller reservoirs increased the median 2-yr flood magnitude by 5.2% (Figure 5.1), which is not statistically different (p=0.2303; Table 5.1). This suggests that, despite being outnumbered by approximately 3:1 and being located mostly in the headwaters, larger reservoirs help reduce flood magnitudes more so than smaller reservoirs within the Lamprey River watershed.

Model results also confirmed that dam management affects flooding within the watershed. When all dams were operated under flood control management, 2-yr flood magnitudes were not statically different (p=0.9955; Table 5.1), but when all dams were managed for water supply, median 2-yr flood magnitudes increased by 13.19% (Figure 5.1) and were statically different (p=0.0206; Table 5.1), likely because less reservoir capacity was available to mitigate large flow events. This suggests that dam management decisions do have a significant effect on flood magnitudes within the Lamprey. Increasing the maximum capacity of mainstem reservoirs by approximately 4 times (1.0×10^7 m^3) or approximately 20 times (5.0×10^7 m^3) had no effect on 2-yr flood magnitudes (Figure 5.1; Table 5.1). Surprisingly, increasing total reservoir capacity in headwaters by 1.0×10^7 m^3 and 5.0×10^7 m^3 decreased 2-yr flood magnitudes by 5.31% and 7.55% respectively (Figure 5.1) but was also not statistically different

(Table 5.1), suggesting that altering dam management within the dam network had more of an impact on high flows than increasing the size of the dam network's reservoir capacity.

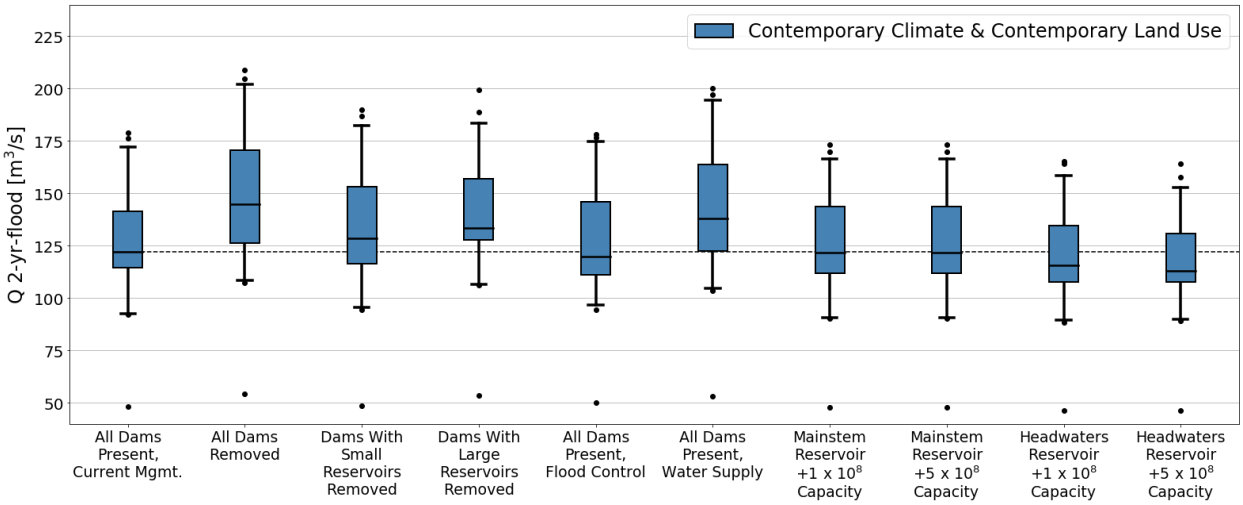

Figure 5.1 Median mean daily discharge (Q) of the 2-year flood at the Lamprey River watershed outlet for water years 1996 to 2015 for dam scenarios under contemporary climate and land use conditions. Whisker bars represent to 5th and 95th percentiles of the Monte Carlo ensemble for each dam scenario. Outliers are given as circles.

Table 5.1 Results of the Mann-Whitney U test for statistical significance between modeled mean daily 2-yr flood discharge at the Lamprey River watershed outlet for two scenarios. Scenarios were compared against the contemporary climate and land use scenario with all dams under current management.

Climate	Land Use	Dam Scenario	Mann-Whitney U Statistic	p value
Contemporary	Contemporary	All Dams Removed	366	0.0015
Contemporary	Contemporary	Dams With Small Reservoirs Removed	541	0.2303
Contemporary	Contemporary	Dams With Large Reservoirs Removed	454	0.0293
Contemporary	Contemporary	All Dams Flood Control	647	0.9955
Contemporary	Contemporary	All Dams Water Supply	442	0.0206
Contemporary	Contemporary	Increased Mainstem Reservoir +1.0 x10⁸ Capacity	692	0.6242
Contemporary	Contemporary	Increased Mainstem Reservoir +5.0 x10⁸ Capacity	692	0.6242
Contemporary	Contemporary	Increased Headwaters Reservoir +1.0 x10⁸ Capacity	763	0.1972
Contemporary	Contemporary	Increased Headwaters Reservoir +5.0 x10⁸ Capacity	783	0.1298

5.1.2 Dam Scenarios Under Late-Century Climate and/or Land Use

Late-21st-century land use did not significantly affect 2-yr flood magnitudes compared contemporary land use, when dams were present in the watershed and climate was unchanged from contemporary conditions (Table 5.2). However, removing all dams within the watershed during late-century land use increased the median 2-yr flood by 25.08% (Figure 5.2), which was significantly different from the 2-yr flood with all dams with contemporary land use ($p << 0.05$; Table 5.2) and increased the median 2-yr flood by 6.5% compared to all dams removed with contemporary land use.

Late-21st-century climate decreased the median 2-yr flood by 6.50% (Figure 5.2), when dams were present in the watershed and contemporary land use was maintained. This finding of flood reduction is somewhat surprising, since precipitation is predicted to increase, but increased mean annual air-temperature will also increase evapotranspiration, thus reducing runoff. Thus, predicted increases in temperature appear to be more important than predicted increases in precipitation. With all dams removed and late-century projections of climate and contemporary land use, 2-yr floods increased by 13.11% (Figure 5.2) and was statistically different compared to the baseline global climate model scenario ($p=0.0367$; Table 5.2). Of the four scenarios using late-century projections for both climate and land use, only the scenario with all dams removed resulted in an increase in 2-yr floods (+18.34%; Figure 5.2) when compared to the baseline global climate model scenario.

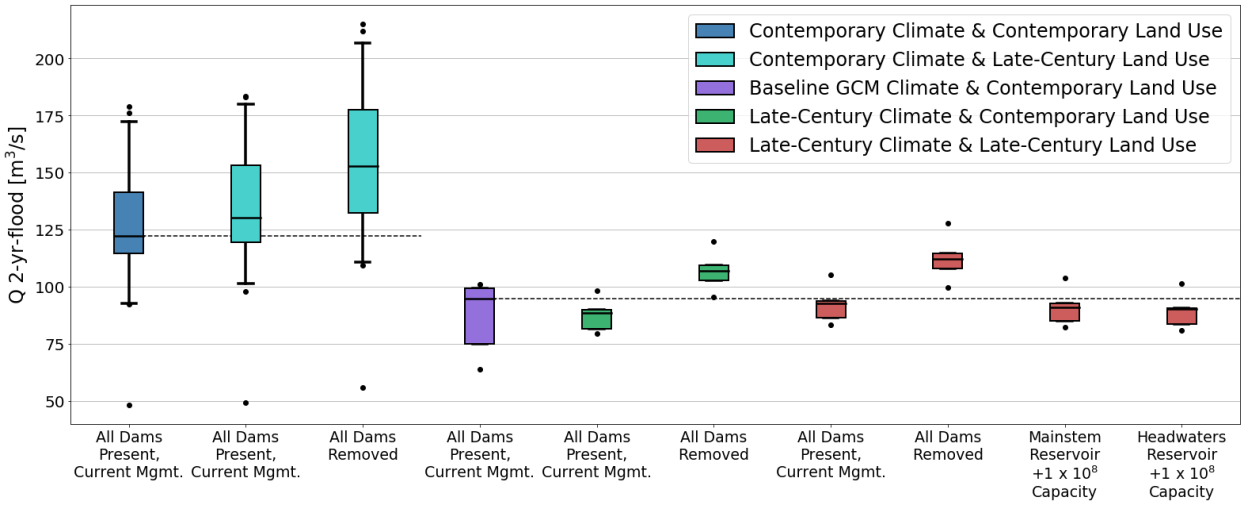

Figure 5.2 Median mean daily discharge (Q) of the 2-year flood at the Lamprey River watershed outlet for dam scenarios under contemporary, baseline global climate model (GCM) projections, late-century GCM-projected climate, and contemporary and late-century projected land use conditions. Whisker bars represent the 5th and 95th percentiles of the Monte Carlo ensemble for each dam scenario. Outliers are given as circles.

Table 5.2 Results of the Mann-Whitney U test for statistical significance between modeled mean daily 2-yr flood discharge at the Lamprey River watershed outlet between different scenarios. Scenarios in yellow were compared against the contemporary climate and land use scenario with all dams under current management, while scenarios in green were compared against the baseline global climate model climate and contemporary land use scenario and with all dams under current management.

Climate	Land Use	Dam Scenario	Mann-Whitney U Statistic	p value
Contemporary	Late-Century	All Dams, Current Mgmt.	522	0.1575
Contemporary	Late-Century	All Dams Removed	298	8.279×10^{-5}
Late-Century	Contemporary	All Dams, Current Mgmt.	14	0.8345
Late-Century	Contemporary	All Dams Removed	2	0.0367
Late-Century	Late-Century	All Dams, Current Mgmt.	12	1.0
Late-Century	Late-Century	All Dams Removed	1	0.0215
Late-Century	Late-Century	Increased Mainstem Reservoir +1.0 x10^8 Capacity	12	1.0
Late-Century	Late-Century	Increased Headwaters Reservoir +1.0 x10^8 Capacity	12	1.0

5.2 Winter DIN Load, Flux, and Retention

5.2.1 Dam Scenarios Under Contemporary Climate & Land Use

Contemporary climate and land use resulted in wintertime DIN loading of 276 kg day^{-1} to the Lamprey River river network. Model results confirmed that the aquatic network retained some portion of this loading, though the amount retained depended on reservoir size and dam management. Comparisons of different dam scenarios to current dam management conditions under contemporary climate and land use within the Lamprey River watershed revealed that removing all dams in the network increased median wintertime DIN flux by 13.91% (Figure 5.3 A), which was statistically significant ($p=1.874 \times 10^{-21}$, Table 5.3) which corresponded 59% loss of DIN retention within the watershed (Figure 5.3 B). This suggests that the 22 dams within the Lamprey River watershed are providing a significant reduction in DIN flux to Great Bay during winter, which is the season with the second highest observed flux.

Model results show that reservoir size and location within the watershed affected wintertime DIN flux. The removal of dams with smaller reservoirs within the watershed increased median wintertime DIN flux by 5.27% ($p=4.350 \times 10^{-10}$), as opposed to the removal of all dams with large reservoirs which increased median wintertime DIN flux by 8.15% ($p=1.404 \times 10^{-5}$; Figure 5.3 A; Table 5.3). Similar to flood attenuation, larger reservoirs reduced watershed DIN flux more than smaller reservoirs and therefore increased watershed DIN retention more (Figure 5.3 B). Unlike for flood attenuation, dam management did not affect wintertime DIN flux: all dams operating for flood control or water supply did not alter wintertime DIN flux compared to current operations (Table 5.3). Among the tested dam scenarios, the largest reduction in wintertime DIN flux and the largest increase in wintertime DIN retention occurred when the maximum capacity of mainstem reservoirs was increased by 1.0×10^7 m^3 and 5.0×10^7 m^3. This decreased median wintertime DIN flux by 47.14% ($p=1.53 \times 10^{-131}$) and 84.53% ($p=1.139 \times 10^{-}$

^{236}) respectively (Figure 5.3 A). Increasing the maximum capacity of headwater reservoirs had a similar but smaller effect on decreasing wintertime DIN flux than increasing the maximum capacity of mainstem reservoirs (Figure 5.3 A; Table 5.3). Thus, wintertime DIN flux seemed to depend most strongly on reservoir capacity, especially capacity located downstream of DIN sources.

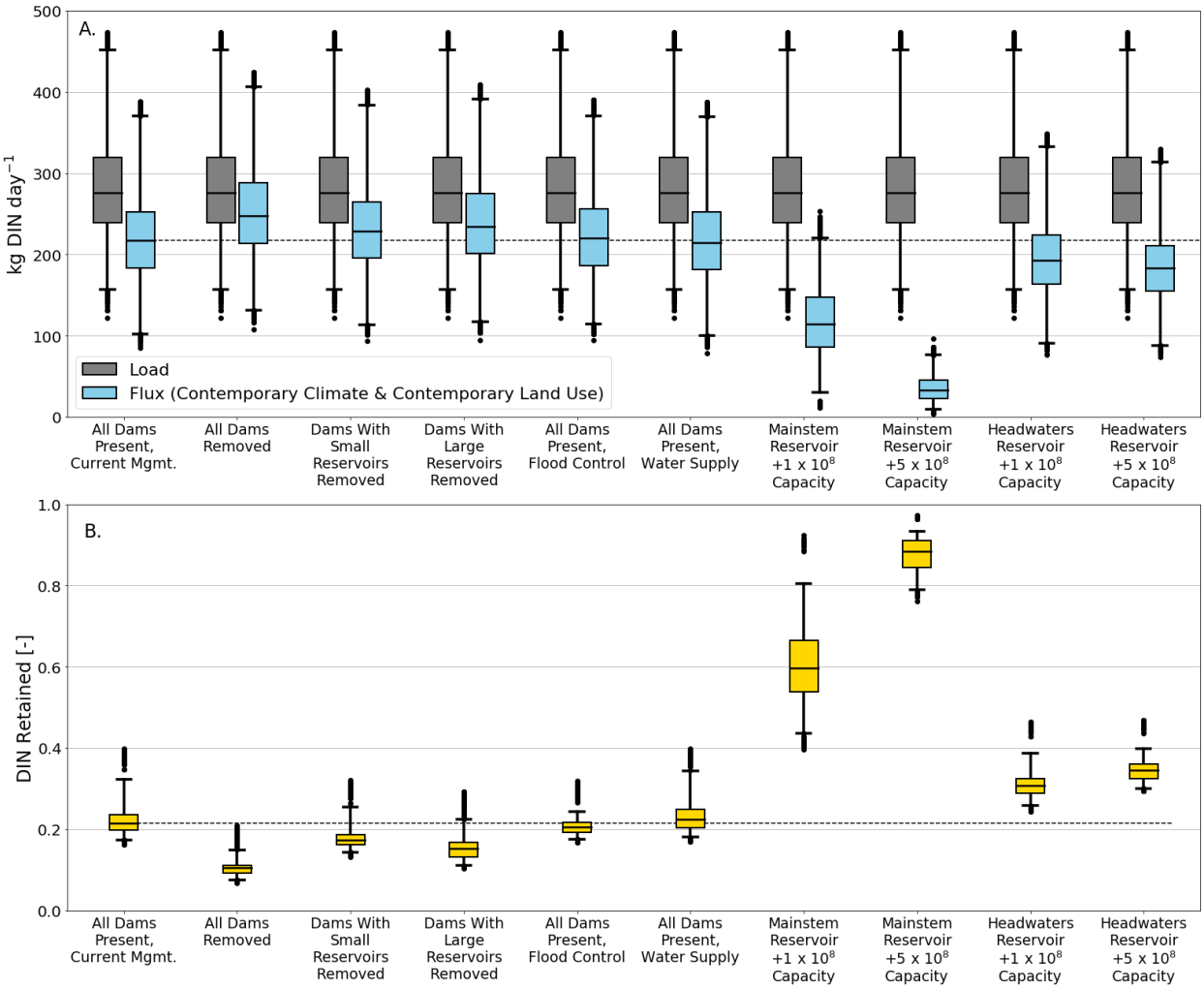

Figure 5.3 Wintertime (1/1 – 3/21) daily (A) DIN load and flux and (B) retention for the Lamprey River watershed averaged over water years 1996 to 2015 under contemporary climate and land use conditions. Whisker bars represent 5th and 95th percentiles of the Monte Carlo ensemble for each dam management scenario. Outliers are given as circles.

Table 5.3 Results of the Mann-Whitney U test for statistical significance between modeled wintertime daily DIN flux at the Lamprey River watershed outlet compared with the contemporary climate and land use scenario with all dams under current management.

Climate	Land Use	Dam Scenario	Mann-Whitney U Statistic	p value
Contemporary	Contemporary	All Dams Removed	184152	1.874×10^{-21}
Contemporary	Contemporary	Dams With Small Reservoirs Removed	224932	1.404×10^{-5}
Contemporary	Contemporary	Dams With Large Reservoirs Removed	209959	4.350×10^{-10}
Contemporary	Contemporary	All Dams Flood Control	247554	0.140
Contemporary	Contemporary	All Dams Water Supply	267471	0.294
Contemporary	Contemporary	Increased Mainstem Reservoir $+1.0 \times 10^8$ capacity	451752	1.53×10^{-131}
Contemporary	Contemporary	Increased Mainstem Reservoir $+5.0 \times 10^8$ capacity	518385	1.139×10^{-236}
Contemporary	Contemporary	Increased Headwaters Reservoir $+1.0 \times 10^8$ capacity	325308	5.351×10^{-17}
Contemporary	Contemporary	Increased Headwaters Reservoir $+5.0 \times 10^8$ capacity	350663	4.509×10^{-31}

5.2.2 Dam Scenarios Under Late-Century Climate and/or Land Use

Late-21st-century land use increased median wintertime DIN loading by 148.12% compared to contemporary climate and land use. This increased DIN flux by 127.97% with all dams present and 166.05% when all dams were removed (Figure 5.4 A) With additional DIN loading as a result of late-century land use, total watershed median wintertime mean daily DIN retention was 23.41% more efficient (Figure 5.4 B), but this still resulted in a larger increase in DIN flux to the coast. This suggests that under late-century projections of land use, the network of dams in the Lamprey River watershed helps to mitigate expected increases in wintertime DIN flux to Great Bay.

Late-21st-century climate decreased median wintertime DIN loading by 2.55% for contemporary land use compared to baseline global climate. However, there was higher DIN load variability that resulted from higher variability in late-century projected runoff, which as a result caused overall DIN loading to increase (Figure 5.4 A). Despite increases in wintertime DIN loading, median wintertime DIN flux was unchanged for late-century climate ($p=0.780$; Table 5.4). This was likely due to the model assumption that increased wintertime mean air temperatures resulted in an increase in biological activity, which translated into a slight increase in median DIN retention (Figure 5.4 B). Removing all dams under these same conditions significantly increased wintertime DIN flux ($p=0.003$; Table 5.4).

The combination of both late-century climate and land use significantly increased wintertime DIN flux compared to the baseline global climate model scenario, except for when maximum reservoir capacity was increased for mainstem dams (Figure 5.4 A; Table 5.4).

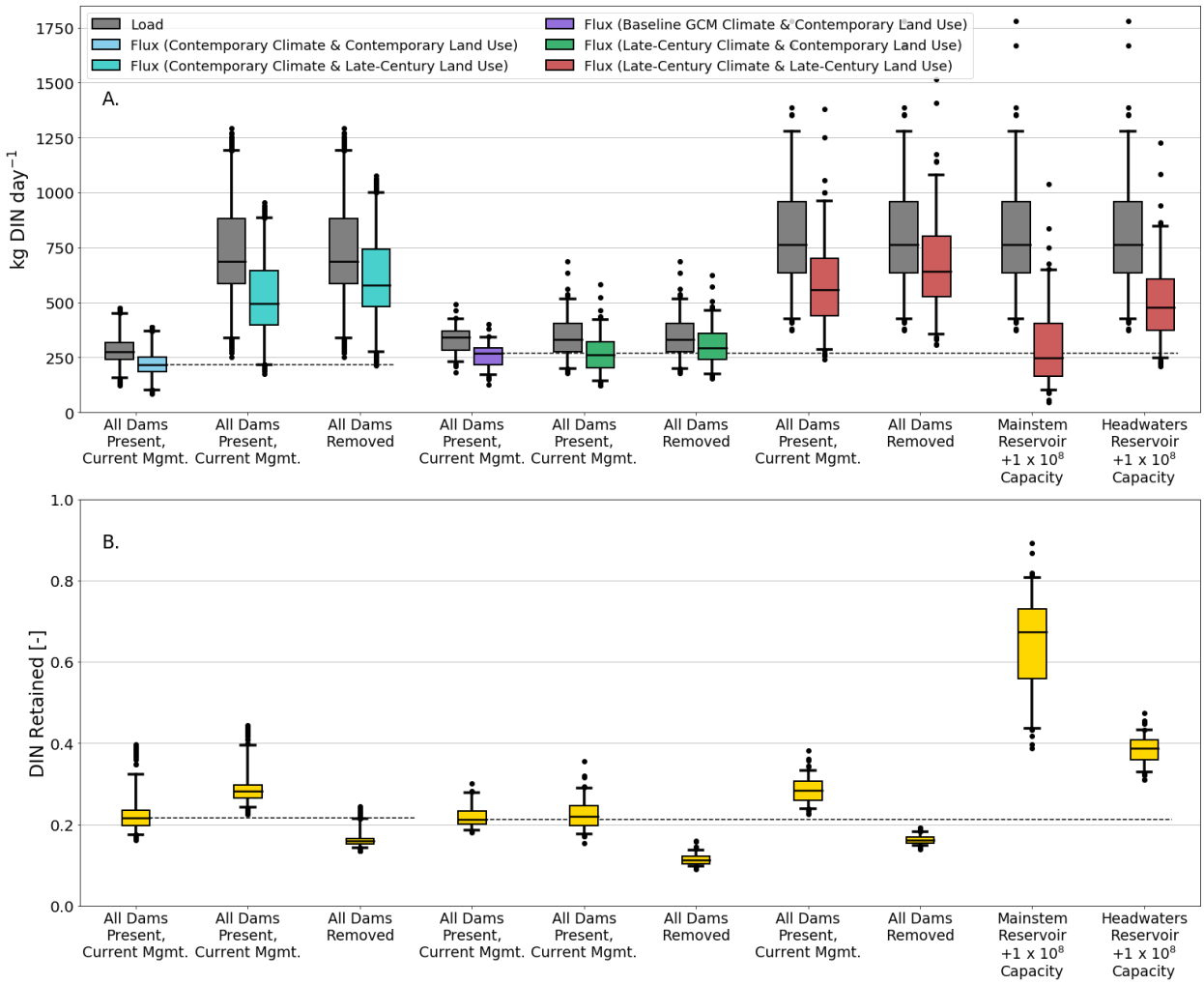

Figure 5.4 Wintertime (1/1 – 3/21) daily (A) DIN load and flux and (B) retention for the Lamprey River watershed for dam scenarios under contemporary, baseline global climate model (GCM) projected, late-century GCM projected climate and contemporary and late-century projected land use conditions. Whisker bars represent the 5th and 95th percentiles of the Monte Carlo ensemble for each dam scenario. Outliers are given as circles.

Table 5.4 Results of the Mann-Whitney U test for statistical significance between modeled daily wintertime DIN flux at the Lamprey River watershed outlet of different scenarios. Scenarios in yellow were compared against the contemporary climate and land use scenario with all dams under current management, while scenarios in green were compared against the baseline global climate model climate and contemporary land use scenario and with all dams under current management.

Climate	Land Use	Dam Scenario	Mann-Whitney U Statistic	p value
Contemporary	Late-Century	All Dams, Current Mgmt.	39472	1.106×10^{-170}
Contemporary	Late-Century	All Dams Removed	15272	7.223×10^{-210}
Late-Century	Contemporary	All Dams, Current Mgmt.	2184	0.780
Late-Century	Contemporary	All Dams Removed	1552	0.003
Late-Century	Late-Century	All Dams, Current Mgmt.	201	2.046×10^{-18}
Late-Century	Late-Century	All Dams Removed	42	3.937×10^{-21}
Late-Century	Late-Century	Increased Mainstem Reservoir +1.0 $\times 10^8$ capacity	2145	0.655
Late-Century	Late-Century	Increased Headwaters Reservoir +1.0 $\times 10^8$ capacity	393	2.119×10^{-15}

5.3 Summer DIN Load, Flux, and Retention

5.3.1 Dam Scenarios Under Contemporary Climate & Land Use

Comparisons of different dam scenarios under contemporary climate and land use within the Lamprey River watershed revealed that removing the network of dams increased median summertime DIN flux by 46.13% ($p=3.964 \times 10^{-31}$, Figure 5.5 A; Table 5.5). The dam network provides an additional 36.13% of DIN retention within the watershed (Figure 5.5 B) during the summer. This reduction of summertime DIN flux provided by the network of dams within the Lamprey River watershed is particularly important because summer is the time of year where Great Bay is most vulnerable to eutrophication. The removal of both dams with small reservoirs and dams with large reservoirs within the watershed had a similar effect on DIN flux in the summer as in the winter (Figure 5.5 A; Table 5.5). In addition, unlike for wintertime DIN flux, differences in dam operation affected summertime flux: operating all dams for flood control and water supply both significantly increased summertime mean daily DIN flux ($p=1.409 \times 10^{-23}$ and $p=0.0235$ respectively; Table 5.5). As with winter, the largest reduction in summertime mean daily DIN flux and largest increase in summertime mean daily DIN retention occurred when the maximum capacity of mainstem reservoirs was increased by 1.0×10^7 m^3 and 5.0×10^7 m^3. This decreased median summertime mean daily DIN flux by 57.66% ($p=3.494 \times 10^{-78}$) and 86.01% ($p=1.877 \times 10^{-191}$) respectively (Figure 5.5 A). Increasing the maximum capacity of headwater reservoirs also had a similar but smaller effect on decreasing summertime mean daily DIN flux than increasing the maximum capacity of mainstem reservoirs (Figure 5.5 A; Table 5.5).

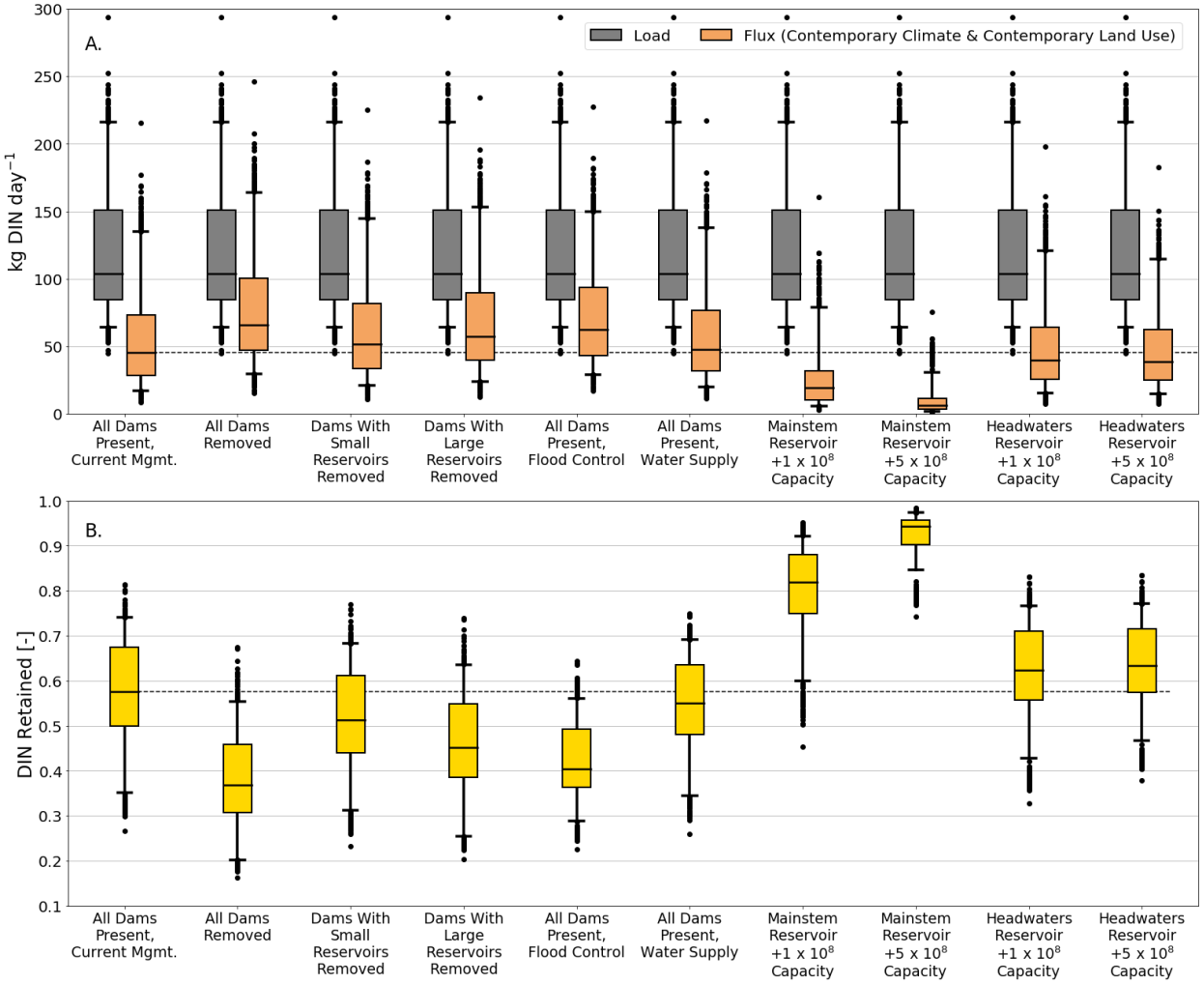

Figure 5.5 Summertime (6/10 – 10/1) daily (A) DIN load and flux and (B) retention for the Lamprey River watershed for water years 1996 to 2015 for dam scenarios under contemporary climate and land use conditions. Whisker bars represent to 5th and 95th percentiles of the Monte Carlo ensemble for each dam scenario. Outliers are given as circles.

Table 5.5 Results of the Mann-Whitney U test for statistical significance between modeled summertime daily DIN flux at the Lamprey River watershed outlet compared with the contemporary climate and land use scenario with all dams under current management.

Climate	Land Use	Dam Scenario	Mann-Whitney U Statistic	p value
Contemporary	Contemporary	All Dams Removed	167650	3.964×10^{-31}
Contemporary	Contemporary	Dams With Small Reservoirs Removed	226405	3.232×10^{-5}
Contemporary	Contemporary	Dams With Large Reservoirs Removed	199391	3.446×10^{-14}
Contemporary	Contemporary	All Dams Flood Control	180239	1.409×10^{-23}
Contemporary	Contemporary	All Dams Water Supply	241330	0.0235
Contemporary	Contemporary	Increased Mainstem Reservoir $+1.0 \times 10^{8}$ capacity	406889	3.494×10^{-78}
Contemporary	Contemporary	Increased Mainstem Reservoir $+5.0 \times 10^{8}$ capacity	492068	1.877×10^{-191}
Contemporary	Contemporary	Increased Headwaters Reservoir $+1.0 \times 10^{8}$ capacity	287286	0.0004
Contemporary	Contemporary	Increased Headwaters Reservoir $+5.0 \times 10^{8}$ capacity	294345	8.415×10^{-8}

5.3.2 Dam Scenarios Under Late-Century Climate and/or Land Use

Late-21st-century land use increased median summertime DIN loading by 124.52% compared to contemporary land use. This increase in loading resulted in increases of median summertime mean daily DIN flux by 142.30% with all dams and 242.39% when all dams were removed (Figure 5.6A) Under late-century land use conditions with all dams under current management, total watershed median summertime mean daily DIN retention decreased by 6.46% (Figure 5.6B). This suggests that the network of dams in the Lamprey River watershed may be able to help buffer summertime N inputs contributed by future watershed development.

Late-21st-century climate decreased median DIN loading by 31.83% and increased median DIN retention by 11.31% when compared to the baseline global climate model scenario ($p=0.007$; Table 5.6). This decrease in summertime DIN flux and increase in DIN retention was likely the result of higher summertime mean instream water temperatures from late-century climate. Removing all dams under the same conditions did not result in a significant difference in summertime mean daily DIN flux ($p=0.479$; Table 5.6).

Unlike wintertime DIN flux, summertime DIN flux was significantly different for all scenarios using both late-century climate and land use compared to the baseline global climate model scenario (Figure 5.6A; Table 5.6).

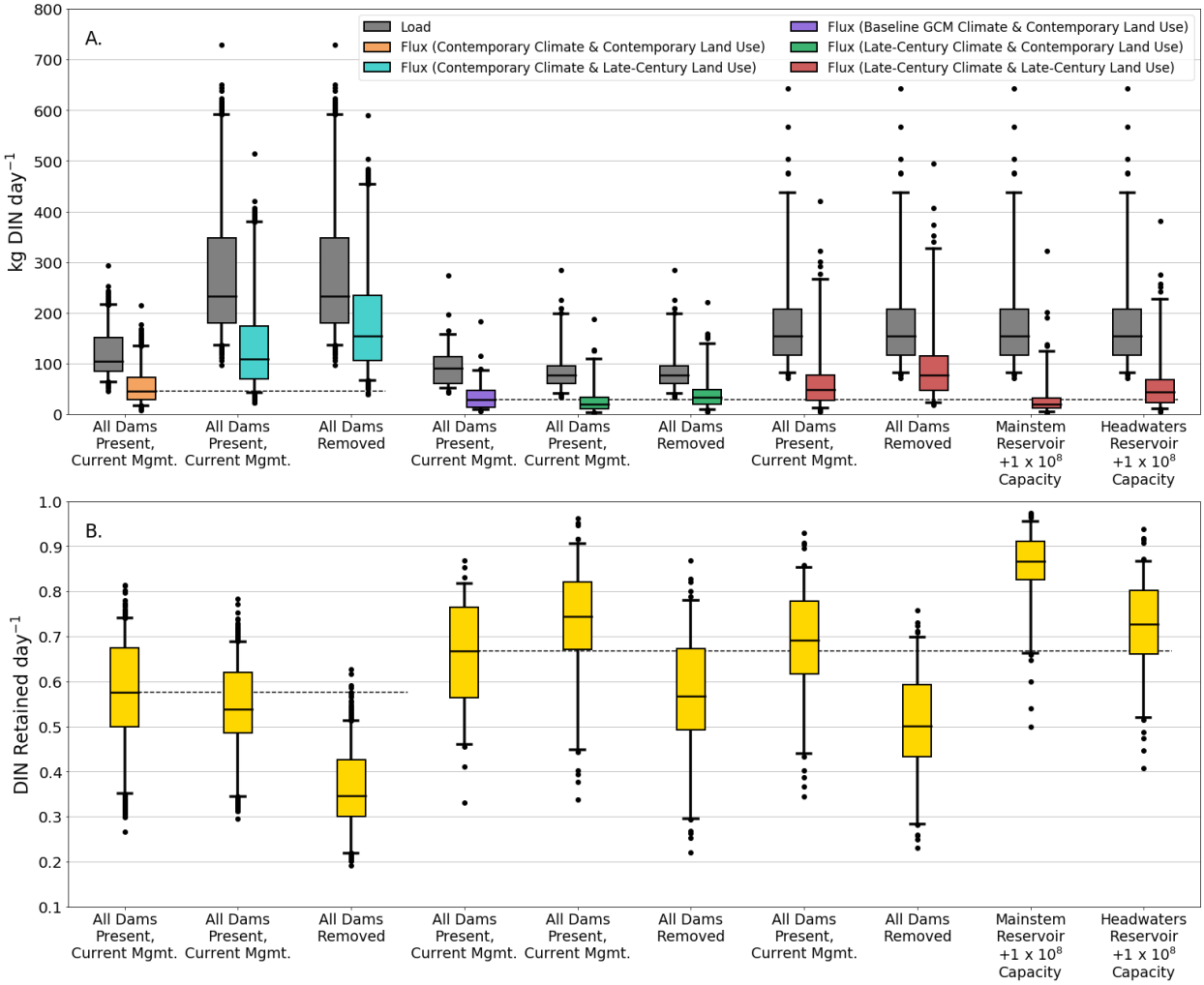

Figure 5.6 Summertime (6/10 – 10/1) daily (A) DIN load and flux and (B) retention for the Lamprey River watershed for dam scenarios under contemporary, baseline global climate model (GCM) projected, late-century GCM projected climate and contemporary and late-century projected land use conditions. Whisker bars represent the 5th and 95th percentiles of the Monte Carlo ensemble for each dam scenario. Outliers are given as circles.

Table 5.6 Results of the Mann-Whitney U test for statistical significance between modeled daily summertime DIN flux at the Lamprey River watershed outlet of two scenarios. Scenarios in yellow were compared against the contemporary climate and land use scenario with all dams under current management, while scenarios in green were compared against the baseline global climate model climate and contemporary land use scenario and with all dams under current management.

Climate	Land Use	Dam Scenario	Mann-Whitney U Statistic	p value
Contemporary	Late-Century	All Dams, Current Mgmt.	92005	1.160×10^{-99}
Contemporary	Late-Century	All Dams Removed	41645	2.304×10^{-167}
Late-Century	Contemporary	All Dams, Current Mgmt.	2880	0.007
Late-Century	Contemporary	All Dams Removed	2084	0.479
Late-Century	Late-Century	All Dams, Current Mgmt.	1525	0.002
Late-Century	Late-Century	All Dams Removed	795	5.095×10^{-10}
Late-Century	Late-Century	Increased Mainstem Reservoir +1.0 $x10^8$ capacity	2797	0.020
Late-Century	Late-Century	Increased Headwaters Reservoir +1.0 $x10^8$ capacity	1684	0.016

Chapter 6: Conclusions

6.1 Summary

This study found that field measurements of DIN retention at Pawtuckaway Lake were reasonably predicted by the RivR-N empirical model developed by Seiztinger et al. (2002). RivR-N was then implemented in a distributed coupled hydrological and biogeochemical model, FrAMES, to estimate DIN retention within all reservoirs within the Lamprey River watershed. Model results suggest that, under current management, the existing network of 22 dams provides significant seasonal DIN flux mitigation as well as flood attenuation. Large dams within the watershed were found to provide the most seasonal DIN flux mitigation and flood attenuation. Dam management also had an effect, as flooding increased when all dams were managed for water supply dams and summer DIN flux increased when all dams were managed for flood control. Different spatial distributions of large dams within the river network showed that seasonal DIN flux was reduced the most when there were larger dams on the lower mainstem and flood attenuation was greatest when there were larger dams in the headwaters. Modeling the watershed under projected climate and land use showed how the network of dams can help mitigate increases in flood magnitudes and seasonal DIN fluxes that are expected as a result of climate and land use change.

6.2 Comparing Results to other Watershed Models

DIN retention provided by just the river network accounted for 0.11 and 0.21 of winter and summer DIN retention respectively. These results were lower but similar in magnitude to FrAMES modeled annual DIN retention (0.15 – 0.33) for the Ipswich River watershed in Massachusetts (Wollheim et al. 2008). However, in the Ipswich, human development is skewed towards the headwaters (skewness index of 1.09; Mineau et al. 2015), which provides more opportunity for DIN loaded to the river network to be retained.

Seitzinger calculated N retention for sixteen watersheds in the eastern U.S. using the RivR-N model and found that reservoirs had a minimal effect on annual N removal. However, the majority of the watersheds modeled were very large (median drainage area of approximately 12,000 km^2) compared to the Lamprey River watershed (549 km^2) and had a much lower density of dams within their river networks as smaller run of river reservoirs were not included. Results from the SPARROW model developed for the northeastern United States showed that reservoirs were not statistically significant at reducing annual TN fluxes to the coast (Moore et al. 2004), however like Seitzinger et al. 2002, only large reservoirs (reservoir surface areas > 2 km^2) were examined. This study modeled a smaller watershed and showed that cumulative effect of a dam network, most of which were smaller run-of-river, dams does have a significant effect on seasonal DIN removal.

6.3 Suggestions for Future Field Work

For field measurements, the uncertainty with the stage-discharge rating curve at each monitoring station dominated the uncertainty with N fluxes and N retention estimates for this study. Therefore, to reduce this uncertainty future studies should obtain more discharge measurements throughout the study period and at higher flows, and consider installing permanent control structures. Herschey (1985) recommended that at least thirty discharge measurements be obtained to accurately estimate uncertainty with each limb of the stage-discharge rating curve at each gauging station. Ice build-up above the transducers in winter also contributed to stage uncertainty. Future studies should use strategies to prevent ice build-up such as the deployment of heaters at the gauging site.

No attempt was made here to estimate the uncertainty associated with the infrequency of N solute concentration measurements at each monitoring station (N = 6), which was likely a substantial source of error. Therefore, it is recommended that future reservoir N retention studies obtain N solute concentrations through the use of high resolution in-situ sensors

(Wollheim et al. 2017). With higher a frequency of N concentration measurements, regressions between N concentration and discharge could be used to interpolate and extend N concentration measurements for the rest of the year (Edokpa et al. 2016) and used to quantity uncertainty using the standard error of the regression line (Haggard et al. 2003). For this study relative uncertainties were used to propagate errors associated with N concentration measurements, however absolute errors have been used in similar studies (Oliver et al. 2014).

During this study, samples were obtained during baseflow, therefore the effects of storm flow on N concentration were not estimated. Since a large portion of N flux occurs during storm events, the manner in which N concentration changes during storm events is important to estimate N fluxes accurately over long-time scales. Therefore, it is recommended that future studies also obtain N solute concentrations during storm events as well as baseflow.

6.4 Sources of Model Error and Suggestions for Future Modeling

Every numerical model depends on the assumptions made during model construction. Using FrAMES to explore reservoir N retention is limited by our limited understanding of reservoir N retention, and in particular the potential for saturation at high DIN concentrations. The capacity of river channels to retain N has been found through tracer studies to decrease N concentration increases (Mulholland et al. 2008). Since the RiVR-N model utilized in FrAMES to represent N retention in reservoirs does not account for this potential saturation kinetics, seasonal reservoir DIN retention may be overestimated, especially in winter and for scenarios with overall increased DIN loading within the watershed.

This study estimated hydrologic model uncertainty associated with hydrologic parameter selection for all scenarios and uncertainty with global climate model forcings for scenarios using late-century climate. Other known model error sources were not estimated, such as the uncertainty associated with other input data, observations used in calibration, and structural model deficiencies (Sadegh and Vrugt 2013). Future modeling efforts should include estimates

from these other model error sources. Uncertainty associated with DIN loading and reservoir retention parameters were also not quantified, but could be an even greater source of error than hydrologic uncertainty.

Flood and seasonal DIN flux/retention metrics were only examined at the watershed outlet, however future modeling could instead examine how dams affect these metrics further upstream within the watershed, especially where flooding might be a greater concern. In the Lamprey River watershed, TN is predominately comprised of dissolved N, however in watersheds where particulate N is found in greater quantity (Filoso and Palmer 2011), reservoirs could be even more efficient at retaining N.

Field observations of reservoir release at Pawtuckaway Lake over a year reveal that dam operations follow a similar pattern to the reservoir storage release curves implemented in FrAMES (Figure 6.1). However, observed release during both the recreation season and off-season was more variable and occurred at lower reservoir storage levels compared to the model representation, likely as a result of active dam management through stop log and gate adjustment. Future modeling could fit reservoir storage-release curves to field observations to better represent reservoir operations. This again shows the need for complementary field measurements to improve and validate modeling results. Field measurements at Pawtuckaway Lake also showed that DON is a larger component of TDN than DIN, therefore by only modeling DIN a large portion of N flux within the river network is not accounted for. Future modeling should incorporate DON as well as dissolved organic carbon (DOC) fluxes and how DOC limits N retention to better capture N dynamics during the fall season.

As population density increases in the watershed under late-century land use projections, one unknown is the potential construction of sewer lines and wastewater treatment plants. Since the relationship between human land use and DIN loading was calibrated to current DIN loading conditions, in which the majority of residents within the Lamprey River

watershed are on septic systems, the introduction of sewer would likely shift DIN loading spatially from non-point sources to point sources. Therefore, future modeled land use scenarios should consider examining the effect of adding additional DIN point sources within the watershed or denitrifying onsite wastewater treatment systems (Oakley et al. 2010).

DIN export from the Lamprey River watershed depends upon the spatial distribution of both DIN loading and sinks. DIN retention provided by the dam network within the Lamprey River watershed depended on the spatial distribution of reservoir storage (sinks) and the amount of total storage in relation to human land use (loading). Figure 6.2 shows that as total water volume stored within the watershed increases, summertime DIN retention also increases and summertime DIN export decreases. However, in addition to total volume of water stored in the watershed, the location of water stored within the river network also determines seasonal DIN flux. Figure 6.3 shows additional DIN retention provided by the dam network is highest when the distribution of reservoir storage is skewed towards the watershed outlet. Figure 6.4 shows a proposed relationship between DIN retention provided by the dam network and the distributions of reservoir storage and human land use within the watershed using a skewness index (Mineau et al. 2015). Dam network DIN retention is highest when human land use is skewed towards the headwaters and reservoir storage is skewed towards the outlets, thus increasing the likelihood that DIN loaded to the river network will be processed by the reservoirs in the network. Conversely, dam network DIN retention is lowest when human land use is skewed towards the outlet and reservoir storage is skewed towards the headwaters. Therefore, future modeling should include additional scenarios using similar total watershed reservoir capacity under a range of different reservoir storage skewness and human land use skewness to better resolve this relationship.

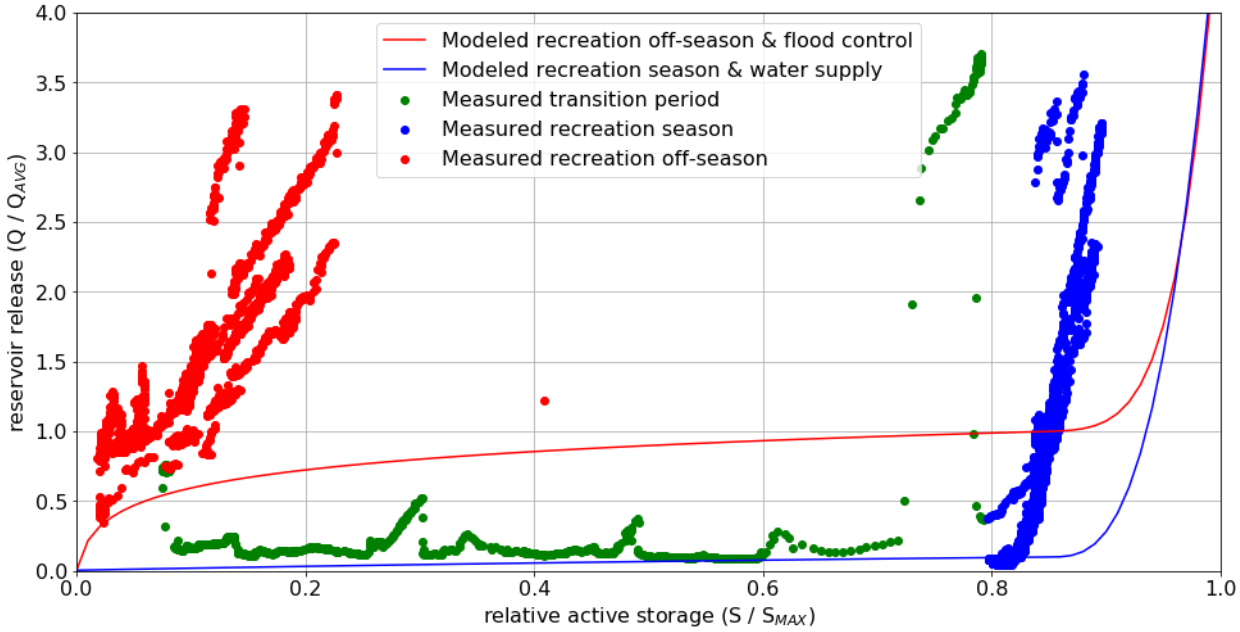

Figure 6.1 Hourly reservoir release (Q) normalized by mean annual hourly reservoir release (Q_{AVG}) compared to relative active reservoir storage (S) normalized by the maximum relative reservoir storage (S_{MAX}) for Pawtuckaway Lake from 5/19/17 to 5/18/18. The blue line indicates the reservoir release curve implemented in FrAMES for actively managed recreation dams during the recreation season and water supply dams. The red line represents the reservoir release curve implemented in FrAMES for actively managed recreation dams during the recreation off-season and flood control dams. Blue dots represent reservoir outflow during the recreation season once reservoir pool level was full (5/19/17 to 10/9/17 and 4/20/18 to 5/18/17), red dots represent reservoir outflow after the fall drawdown and throughout the recreation off-season (11/20/17 to 3/22/18), and green dots represent the transition period when stop logs were put back in early spring to raise reservoir water level to full pool (3/19/18 to 4/19/18).

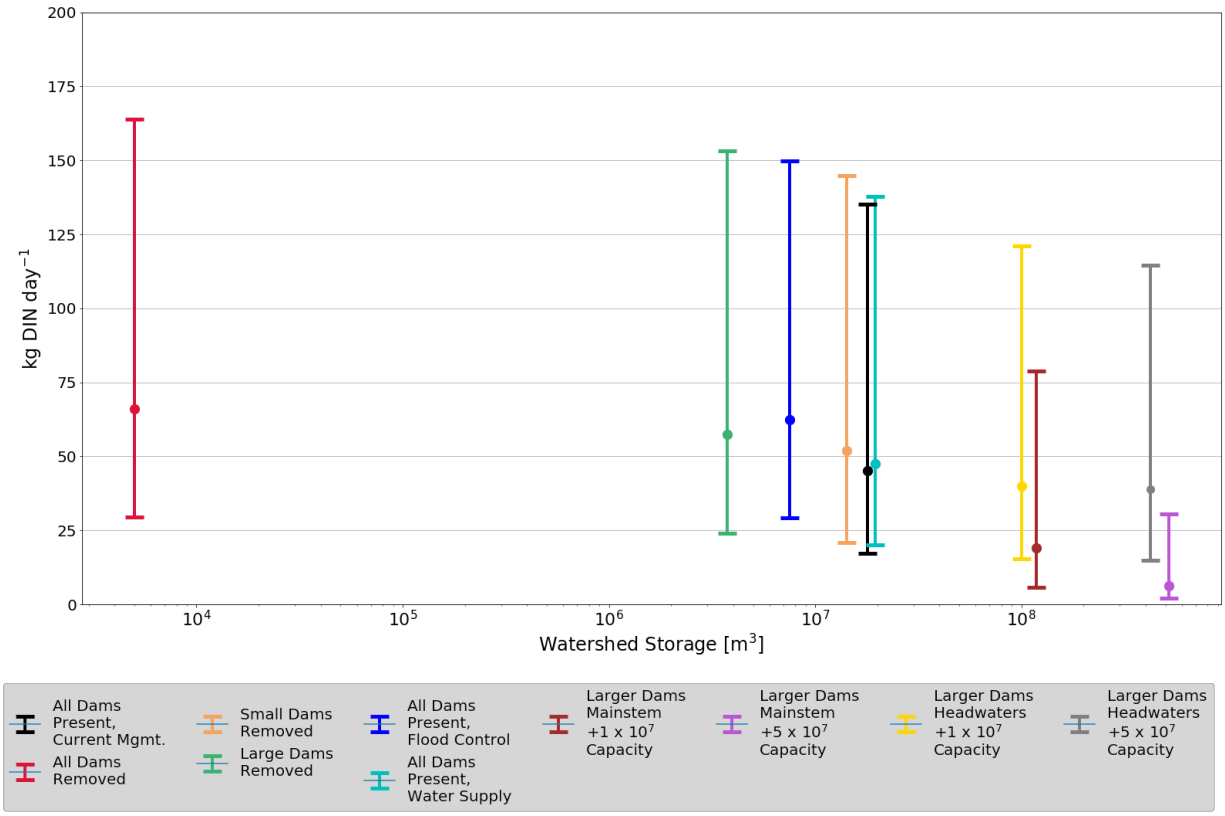

Figure 6.2 Summer DIN flux leaving the Lamprey River watershed versus total watershed water storage (river network plus reservoirs) averaged over the summer for water years 1996 to 2015 for dam management scenarios under contemporary climate and land use conditions. Error bars represent the 5th and 95th percentiles of the Monte Carlo ensemble and circles represent the median.

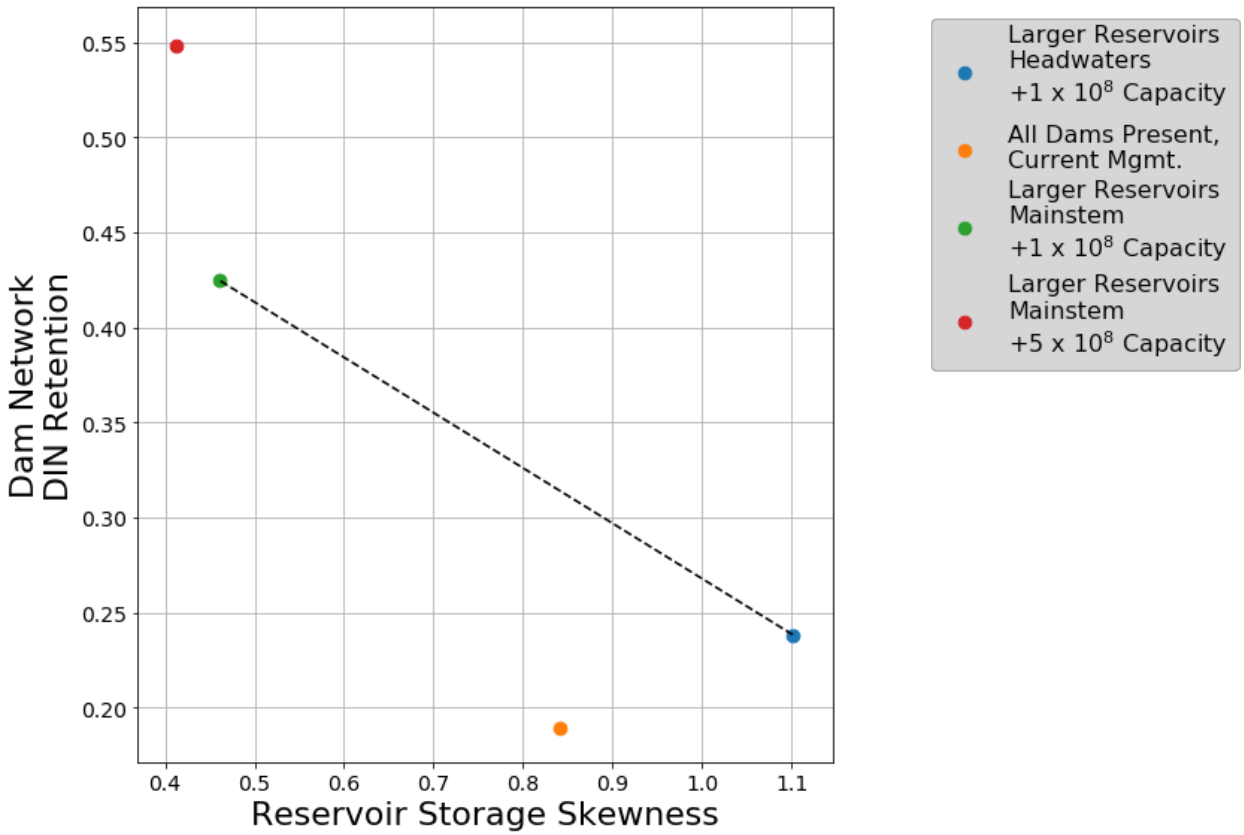

Figure 6.3 Summer DIN retention provided by the dam network within the Lamprey River watershed versus the distribution of reservoirs within the river network (reservoir storage skewness) for water years 1996 to 2015 for four dam scenarios under contemporary climate and land use conditions.

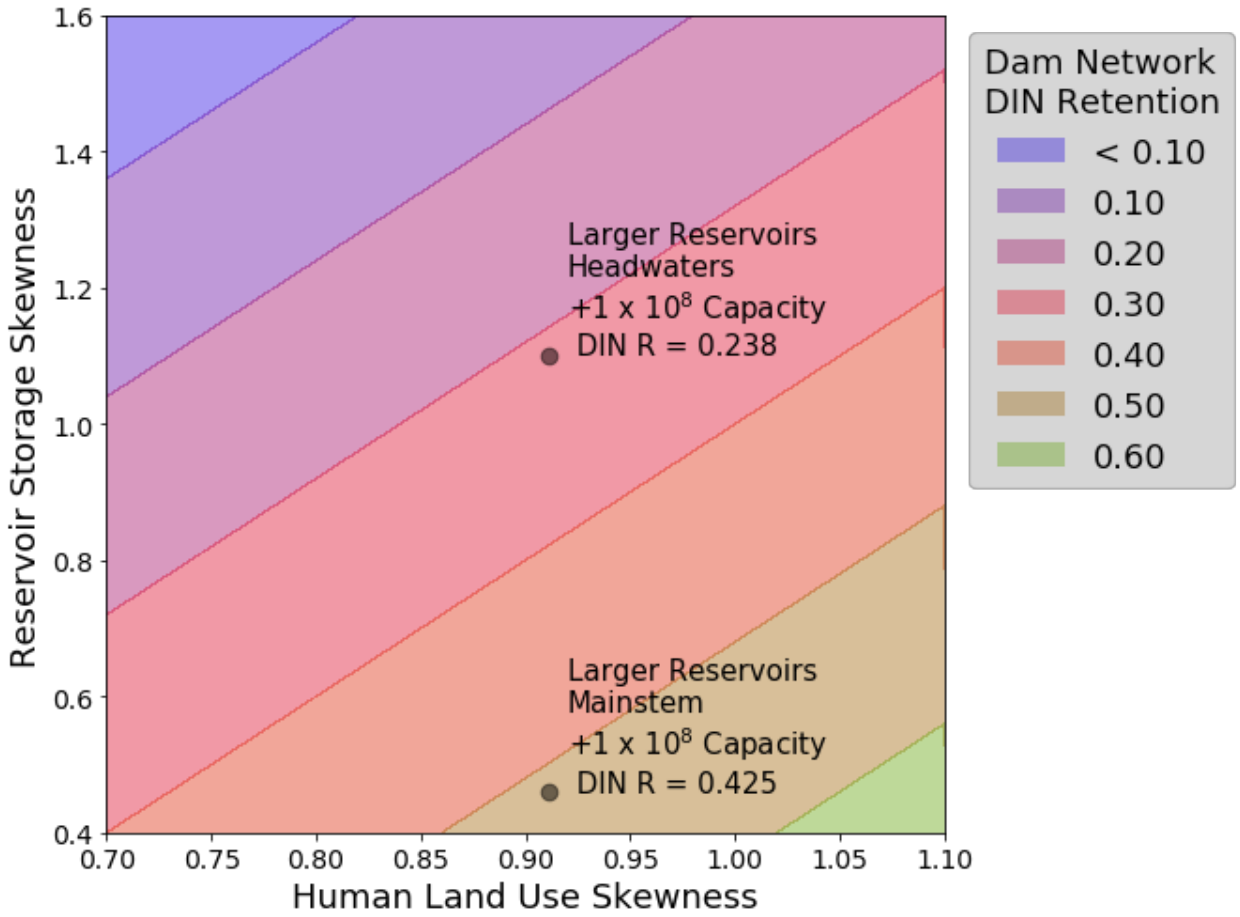

Figure 6.4. Contour plot of summer DIN retention provided by a dam network within a watershed as a function of reservoir storage skewness to human land use skewness for two scenarios of similar reservoir storage volumes for water years 1996 to 2015 under contemporary climate and land use conditions. Contour lines were constructed from the two scenarios through simple linear interpolation.

6.5 Implications for Decision Making

Numerical hydrologic modeling allows for the assessment of dam tradeoffs in the context of an entire network of dams. This study found that in the Lamprey River watershed, dams within the headwaters have the highest potential to mitigate flooding. Conversely dams along the lower mainstem have the potential to provide the most DIN retention within the dam network. Therefore, project goals should determine which dams are considered for removal or changes in management. The proposed model to predict seasonal dam network DIN retention based on reservoir storage skewness and human land use skewness (Figure 6.4) could also be

used as a framework for dam decision makers to estimate dam network DIN retention within other similar coastal watersheds.

This study examined the benefits of seasonal DIN retention and flood mitigation provided by dams and their reservoirs, however these are just two tradeoffs that influence decisions about dams. For example, within coastal watersheds, dams along the lower mainstem are often considered for removal to improve fish passage. Safety also drives dam decisions. For example, many older headwater dams within New England are classified as high-risk dams (Gold et al. 2016), where dam removal could be both a safer and less expensive option to repairs or upgrades. Aesthetics, historical and cultural significance, hydropower production, irrigation, and recreational opportunities are also a few examples of the multitude of other factors that shape dam decision making. This author recommends that seasonal DIN retention and flood mitigation provided by dams should be considered in future dam related decisions to provide a more complete understanding of all dam removal tradeoffs.

References

Abatzoglou J.T., (2013). *Development of gridded surface meteorological data for ecological application and modeling*. International Journal of Climatology, 33: 121-131.

Abbaspour K.C., (2015). *SWAT Calibration and Uncertainty Programs.* eawag:s Swiss Federal Institue of Aquatic Science and Technology.

Alexander R.B., Smith R.A., Schwartz G.E., (2000). *Effect of stream channel size on the delivery of nitrogen to the Gulf of Mexico*. Nature, 403.

Anderson D.M., Gilbert P.M., Burkholder J.M., (2002). *Harmful Algal Blooms and Eutrophication: Nutrient Sources, Composition, and Consequences*. Estuaries, 25, 4b, 704-726.

Anthony A., Atwood J., August P., Byron C., Cobb S., Foster C., Fry C., Gold A., Hagos K., Heffner L., Kellogg D.Q., Lellis-Dibble K., Opaluch J.J, Oviatt C., Pfeiffer-Herbert A., Rohr N., Smith L., Smythe T., Swift J., Vinhaterio N., (2009). *Coastal Lagoons and Climate Change: Ecological and Societal Ramifications in U.S. Atlantic and Gulf Coast Ecosystems.* Ecology and Society, 14(1): 8.

Arnold J.G., (2012). *Soil and Water Assessment Tool Input/Output Documentation.* Texas Water Resources Institute.

Ayalew T.B., Krajewski W.F., Mantilla R., (2013). *Exploring the Effect of Reservoir Storage on Peak Discharge Frequency*. Journal of Hydrologic Engineering, 18, 1697-1708.

Ayalew T.B, Krajewski W.F., Mantilla R (2015). *Insights into expected changes in regulated flood frequencies due to the spatial configuration of flood retention ponds*. Journal of Hydrologic Engineering, 51(6), 3900 – 3921.

Ayalew T.B., Krajewski W.F., Mantilla R., Wright D.B, Small S.J., (2017). *Effect of Spatially Distributed Small Dams on Flood Frequency: Insights from the Soap Creek Watershed*. Journal of Hydrologic Engineering, 22(7).

Bernhardt E.S., Likes G.E., (2002). *Dissolved Organic Carbon Enrichment Alters Nitrogen Dynamics In A Forest Stream*. Ecology, 83(6), 1689-1700.

Boyer E.W., Goodale C.L., Jawkorski N.A., (2002). *Anthropogenic nitrogen sources and relationships to riverine nitrogen export in the northeastern U.S.A.* Biogeochemistry, 57/58:137-169.

Boyer E.W., Alexander R.B., Parton W.J., Li C., Butterbach-Bahl K., Donner S.D., Skaggs R.W., Grosso S.J., (2006). *Modeling Denitrification in Terrestrial and Aquatic Ecosystems at Regional Scales*. Ecological Applications, 16(6), 2123-2142.

Burns D.A., (1998). *Retention of NO_3^- in an upland stream environment: A mass balance approach*. Biogeochemistry 40, 73-96.

Caldwell P.V., Kennen J.G., Sun G., Kiang J.E., Butcher J.B., Eddy M.C., Hay L.E., LaFontaine J.H., Hain E.F., Nelson S.A.C., McNulty S.G., (2015). *A comparison of hydrologic models for ecological flows and water availability*. Ecohydrology, 8, 1525-1546.

Campbell J. L., Driscoll C. T., Pourmokhtarian A., Hayhoe K., (2011). *Streamflow responses to past and projected future changes in climate at the Hubbard Brook Experimental Forest, New Hampshire, United States*. Water Resources Research, 47.

Cheng F.Y., Basu N.B., (2017). *Biogeochemical hotspots: Role of small water bodies in landscape nutrient processing*. Water Resources Research, 53, 5038-5056.

Chow V.T., (1962*). Hydrologic Determination of Waterway Areas for the Design of Drainage Structures in Small Drainage Basins.* Engineering Station Bulletin, 462.

Collins M.J., (2009). *Evidence for Changing Flood Risk in New England Since the Late 20th Century.* Journal of the American Water Resources Association, 45, 2, 279-290.

Conroy D., Standish B., (2013). *New Hampshire Dairy Farmer Panel – sharing expertise and ideas for the future.* Retrieved from Country Folks: *http://countryfolks.com/new-hampshire-dairy-farmer-panel-sharing-expertise-and-ideas-for-the-future/*

Craig L.S., Palmer M.A., Richardson D.C., Filoso S., Bernhardt E.S., (2008). *Stream restoration strategies for reducing river nitrogen loads*. The Ecological Society of America 6(10), 529-538.

Crossman J., Eimers M.C., Casson N.J., Burns D.A., Campbell J.L., Likens G.E., Mitchell M.J., Nelson S.J., Shanley J.B., Watmough S.A., Webster K.L., (2016). *Regional meteorological drivers and long term trend of winter-spring nitrate dynamics across watershed in northeastern North America*. Biogeochemistry, 129, 3.

Daley M., Potter J.D. (2010). *Nitrogen Assessment for the Lamprey River Watershed*. New Hampshire Water Resources Research Center.

David M.B., Wall L.G., Royer T.V., Tank J.L., (2006). *Denitrification and the Nitrogen Budget of a Reservoir in an Agricultural Landscape*. Ecological Application, 16(6), 2177-2190.

Dietrich W.E., Bellugi D.G., Sklar L.S., Stock J.D., Heimsath A. M., Roering J.J. (2003). *Geomorphic Transport Laws for Predicting Landscape Form and Dynamics*. Prediction in Geomorphology. Geophysical Monograph 135. Copyright 2003 by the American Geophysical Union 10.1029/135GM09

Doyle M.W., Harbor J.M., Stanley E.H., (2003). *Toward Policies and Decision-Making for Dam-Removal*. Environmental Management, 31, 4, 453-465.

Edokpa D.A., Evans M.G., Rothwell J.J. (2016). *Reservoirs are hotspots of nitrogen cycling in peatland catchment.* Hydrological Processes, 20, 3666-3681.

Epelde A.M., Antiguedad I., Brito D., Jauch E., Neves R., Garneau C., Sauvage, Sánchez-Pérez J. M., (2016). *Differing modeling approaches to evaluate nitrogen transport and turnover at the watershed scale.* Journal of Hydrology, 539, 478-494.

Feteke B.M., Vörösmarty C.J., Lammers R.B. (2001). *Scaling gridded river networks for macroscale hydrology: Development, analysis, and control of error.* Water Resources Research, 37(7): 1995-1967.

FitzHugh T.W., Vogel R.M., (2011). *The Impact of Dams on Flood Flows in the United States*. Research and Applications, 27, 1192-1215.

Gelaro R., McMarty W., Suarz M.J., (2017). *The Moden-Era Retrospective Analysis for Research and Application, Version 2 (MERRA-2)*. Journal of Climate.

Gold A.J., Addy K., Morrison A., Simpson M., (2016). *Will Dam Removal Increase Nitrogen Flux to Estuaries?*. Water 8, 522.

Groffman P.M., Dorsey A.M., Mayer P.M., (2005). *N processing within geomorphic structures and urban streams*. Journal of the North American Benthological Society, 24(3), 631-625.

Grogan D.S., Wisser D., Prusevich A., Lammers R.B., Frolking S., (2017). The use and re-use of unsustainable groundwater for irrigation: a global budget. Environmental Research Letters, 12, 034017.

Guswa A.J., Brauman K.A., Brown C., Hamel P., Keeler B.L., Sayre S.S., (2014). *Ecosystem services: Challenges and opportunities for hydrologic modeling to support decision making*. Water Resources Research, 50, 4535-4544.

Haggard B.E., Soerens T.S., Green W.R., Richards R.P., (2003). *Using regression methods to estimate stream phosphorus loads at the Illinois River, Arkansas.* Applied Engineering in Agriculture, 19: 187-194.

Harrelson C.C., Rawlins C.L., Potyondy J.P. (1994*). Stream channel reference sites: an illustrated guide to field technique.* Gen Tech. Rep. RM-245. Fort Collins, CO: U.S> Department of Agriculture, Forest Service, Rocky Mountain Forest and Range Experiment Station. 61 p.

Harrison J.A., Maranger R.J., Alexander R.B., Giblin A.E., Jacinthe P.A., Mayorga E., Seitzinger S.P., Sobota D.J., Wollheim W.M., (2009). *The regional and global significance of nitrogen removal in lakes and reservoirs*. Biogeochemistry, 93, 143-157.

Hayhoe, K., Wake C. P., Huntington T. G., Luo L., Schwartz M. D., Sheffield, J., Wood E., Anderson B., Bradbury J., DeGaetano A., Troy T.J., Wolfe D., (2007). *Past and future changes in climate and hydrological indicators in the US Northeast.* Climate Dynamics, 28(4), 381–407.

Helsel D.R., Hirsch R.M., (2002). *Statistical Methods in Water Resources. Techniques of Water-Resources Investigations of the United States Geological Survey*. Book 4, Hydrologic Analysis and Interpretation. http://water.usgs.gov/pubs/twri/twri4a3/

Herschy R.W. (1985). *Streamflow Measurements.* Elsevier Applied Science Publishers LTD 1985, 52 Vanderbilt Ave, New York, NY 10017

Hill, A. R., (1979). *Denitrification in the nitrogen budget of a river ecosystem.* Nature, 281, 291–292.

Hill, B. H., (1986). *The role of aquatic macrophytes in nutrient flow regulation in lotic ecosystems.* American Society for Testing and Materials, Philadelphia: 157–167.

Hirsch R.M., (1981). *Estimating probabilities of reservoir storage for the upper Delaware River basin.* Unites States Geological Survey. 81-478. Reston VA. U.S. Dept. of the Interior.

Hogkins G.A., Whitfield P.H., Burn D.H., Hannaford J., Renard B., Stahl K., Fleig A.K, Madsen H., Mediero L., Korhonen J., Murphy C., Wilson D., (2017). *Climate-driven variability in the occurrence of major floods across North America and Europe*. Journal of Hydrology, 552, 704-717.

Howard-Williams C., (1983). *Wetlands and watershed management: the role of aquatic vegetation.* Journal of the Limnological Society of Southern Africa, 9, 54–62.

Howarth R.W., Marino R., (2006). *Nitrogen as the Limiting Nutrient for Eutrophication in Coastal Marine Ecosystems: Evolving Views over Three Decades*. Limnology and Oceanography, 51, 1, 364-376.

Howarth R.W., Swaney D.P., Boyer E.W., Marino R., Jaworski N., Goodale C., (2006). *The influence of climate on average nitrogen export from larger watersheds in the Northeastern United States*. Biogeochemistry, 79, 163-186.

Huntington, T. G., (2003). *Climate warming could reduce runoff significantly in New England, USA*. Agriculture and Forest Meteorology, 117, 193 – 201.

Johnson S.E., Graber B.E., (2002). *Enlisting the Social Sciences in Decisions about Dam Removal: The application of social science concepts and principles to public decision making about whether to keep or remove dams may help achieve outcomes leading to sustainable ecosystems and other goals in the public interest*. BioScience, 52, 8, 731-738.

Jordan T.E., Correll D.L., Weller D.E., (1997). *Effects of Agriculture on Nutrients from Coastal Plain Watersheds of Chesapeake Bay*. Journal of Environmental Quality, 26, 3, 836-848.

Kellogg D.Q., Gold A.J., Cox S., Addy K., August P.V., (2010). *A geospatial approach for assessing denitrification sinks within lower-order catchments*. Ecological Engineering, 36, 1596-1606.

Koenig L.E., Shattuck M.D., Snyder L.E., Potter J.D., McDowell W.H., (2017). *Deconstructing the Effects of Flow on DOC, Nitrate, and Major Ion Interactions Using a High-Frequency Aquatic Sensor Network*. Water Resources Research, 53, 10, 655-673.

Lane S.N., Brookes C., Hardy R.J., Holden J., James T.D., Kirkby M.J., (2003). *Land management, flooding and environmental risk: New approaches to a very old question.* In: Proceedings of the CIWEM National Conference, 1–21.

Larinier M.W., (2000). *Dams and Fish Migration*. World Commission on Dams Food and Agriculture Organization of the United Nations: Roma, Italy. Fisheries Technical Paper, 419, 45-89.

Lazar J.G., Addy K., Gold A.J. Groffman P.M., McKinney R.A., Kellogg D.Q., (2015). *Beaver Ponds: Resurgent Nitrogen Sinks for Rural Watershed in the Northeastern United States*. Journal of Environmental Quality, 44, 1684-1693.

Lehner B., Verdin K., Jarvis A. (2008). *New Global Hydrograph Derived from Space born Elevation Data.* Transactions and American Geophysical Union, 89(10): 93-94.

Lejon A.G.C., Renöfält B.M., Nilsson C., (2009). *Conflicts Associated with Dam Removal in Sweden*. Ecology and Society, 14(2): 4.

Lightbody L., (2017). *Flooding Disasters Cost Billions in 2016: Impacts Hit Owners of Homes and Businesses Across the Country*. The PEW Charitable Trusts. http://www.pewtrusts.org/en/research-and-analysis/blogs/compass-points/2017/02/01/flooding-disasters-cost-billions-in-2016.

Lui P., Li L., Chen G., Rheinheimer D.E., (2014). *Parameter uncertainty analysis operating rules based on implicit stochastic optimization*. Journal of Hydrology, 514, 102-113.

Lui P., Li L., Guo S., Xiong L., Zhang W., Zhang J., Xu C., (2015). *Optimal design of seasonal flood limited water levels and its application for the Three Gorges Reservoir*. Journal of Hydrology, 527, 1045-1053.

Lui Y., Yang W., Yu Z., Lung I., Yarotski J., Elliott J., Tiessen K. (2014). *Assessing Effects of Small Dams on Stream Flow and Water Quality in an Agricultural Watershed.* Journal of Hydrologic Engineering, 19.

Magilligan F.J., Nislow K.H., (2001). *Long-Term Changes in Regional Hydrologic Regime Following Impoundment in a Humid-Climate Watershed*. Journal of the American Water Resources Association, 37, 6, 1551-1569.

Magilligan F.J., Nislow K.H., (2005). *Changes in hydrologic regime by dams*. Geomorphology, 71, 61-78.

McClain M.E., Boyer E.W., Dent C.L., Gergel S.E., Grimm N.B., Groffman P.M., Hart S.C., Harvey J.W., Johnston C.A., Mayorga E., McDowell W.H., Pinay G., (2003). *Biogeochemical Hot Spots and Hot Moments at the Interface of Terrestrial and Aquatic Ecosystems*. Ecosystems, 6, 301-312.

McLaughlin D.L., Cohen M.J., (2011). *Thermal artifacts in measurements of fine-scale water level variation*. Water Resources Research, 47(9).

Melis, T. S., Schmit L.M, Schmidt J.C., Grams P.E., Kennedy T.A., Raslton B.E., Wright S.A., (2011*), Effects of three high-flow experiments on the Colorado River ecosystem downstream from Glen Canyon Dam, Arizona*. U.S. Geological Survey Circular 1366, 147 p.

Mendoza P.A., Clark M.P., Mizkuami N., Gutmann E.D., Arnold J.R., Brekke L.D., Rajapopalan B., (2016). *How do hydrologic modeling decisions affect the portrayal of climate change impacts?*. Hydrological Processes, 30, 1071-1095.

Meyer J.L., Paul M.J., Taulbee W.K., (2005). *Stream ecosystem function in urbanizing landscapes*. Journal of the North American Benthological Society, 24(3), 602-612.

Moore R.B., Johnston C.M., Robinson K.W., Deacon J.R., (2004). *Estimation of Total Nitrogen and Phosphorus in New England Streams Using Spatially Referenced Regression Models*. U.S. Geological Survey Scientific Investigations Report 2004, 50.

Mulholland P.J., Helton A.M., Poole G.C., Hall R.O., Hamilton S.K., Peterson B.J., Tank J.L, Ashkenas L.R., Cooper L.W., Dahm C.N., Dodds W.K., Findlay S.E.G., Gregory S.V., Grimm N.B., Johnson S.L., McDowell W.H., Meyer J.J., Bernot M.J., Burgin A.J., Crenshaw C.L., Johnson L.T., Neiderlehner B.R., O'Brien J.M., Potter J.D., Sheilbley R.W., Sobota D.J., Thomas S.M., (2008). *Stream denitrification across biomes and its response to anthropogenic nitrate loading*. Nature, 452:202-205.

Nation Oceanic and Atmospheric Administration (2014). *United States Flood Loss Report – Water Year 2014*

Neitsch S.L, (2011). *Soil and Water Assessment Tool Theoretical Documentation.* Texas A&M University Systems.

New Hampshire Department of Environmental Services (1995). Connor J., Landry S. *Pawtuckaway Lake Diagnostic/Feasibility Study*.

New Hampshire Department of Environmental Services (2012). Wood M.A., Trowbridge P. *"Nitrogen, Phosphorus, and Suspended Solids Concentrations in Tributaries to the Great Bay Estuary Watershed in 2011".* PREP Publications. 8.

New Hampshire Department of Environmental Services (2015). *Bathymetry Lakes Polygons*.

New Hampshire Department of Environmental Services (2015). Thomas B., Clark F., Forbes E., *"Report of the Instream Flow Pilot Program".*

New Hampshire Department of Fish and Game (2015). Smith K. *"Presentation on River Herring in the Lamprey River".* Dec 8th, 2015.

NH Water Resources Research Center (WRRC), other acknowledgements include the NSF Experimental Program to Stimulate Competitive Research (EPSCoR) program Research Infrastructure Improvement Award EPS 1101245, and the National Science Foundation DEB-1556603. Partial funding was provided by the New Hampshire Agricultural Experiment Station. This work was supported by the USDA National Institute of Food and Agriculture McIntire-Stennis Project 1006760.

NRCC and NRCS (Northeast Regional Climate Center and Natural Resource Conservation Service). (2008). *Extreme Precipitation in New York and New England*.

Oakley, S.M., A. J. Gold and A. J. Oczkowski. (2010). *Nitrogen Control through Decentralized Wastewater Treatment: Process Performance and Alternative Management Strategies.* Ecological Engineering, 36: 1520-1531.

Oliver A.A., Dahlgren R.A., Deas M.L., (2014). *The upside-down river: Reservoirs, algal blooms, and tributaries affect temporal and spatial patterns in nitrogen and phosphorus in the Klamath River, USA*. Journal of Hydrology, 519, 164-176.

Opperman, J. J., Royte J., Banks J., Day L. R., Apse C., (2011). *The Penobscot River, Maine, USA: a basin-scale approach to balancing power generation and ecosystem restoration.* Ecology and Society, 16(3): 7.

Penn State College of Agricultural Sciences (1992). Pasture and Hay for Horses. Retrieved from Penn State Forages: www.forages.psu.edu/agfacts/agfact32.pdf

Poff L.N., Allen D.J., Bain M.B., Karr J.R., Prestegaard K.L., Ritcher B.D., Sparks R.E., Stromberg J.C., (1997). *The Natural Flow Regime A paradigm for river conservation and restoration.* BioScience, 47(11).

Piscataqua Region Estuaries Partnership (2018). *2018 State of Our Estuaries Report*. STATEOFOURESTUARIES.org

Powers S.M., Robertson D.M., Stanley E.H., (2014). *Effects of lakes and reservoirs on annual river nitrogen, phosphorus and sediment export in agricultural and forested landscapes*. Hydrological Processes, 28, 5919-5937.

Ritcher B.D., Thomas G.A., (2007). *Restoring Environmental Flows by Modifying Dam Operations*. Ecology and Society, 12, 1, 12.

Ruddy B.C., Lorenze D.L., Mueller D.K., (2006). *County-Level Estimates of Nutrient Inputs to the Land Surface of the Conterminous United States,* 1982-2001.

Saunders D.L., Kalff J., (2001). *Nitrogen retention in wetlands, lakes and rivers*. Hydrobiologia, 443, 205-212.

Seitzinger S.P., Kroeze C., (1998). *Global distribution of nitrous oxide production and N inputs in freshwater and coastal marine ecosystems*. Global Biogeochemical Cycles, 12(1), 93-113.

Seitzinger S.P., Styles R.V., Boyer E.W., Alexander R.B., Billen G., Howarth R.W., Mayer B., Van Breemen N., (2002). *Nitrogen retention in rivers:model development and application to watersheds in northeastern U.S.A.*. Biogeochemistry, 57, 58, 199-237.

Seitzinger S.P., Harrison A., Böhlke J.K., Bouwman A.F., Lowrance R., Peterson B., Tobias Van Drecht G., (2006). *Denitrification Across Landscaped and Waterscapes: A Synthesis*. Ecological Applications, 16(6), 2064-2090.

Sharma, K. D., Sorooshian, S. and Wheater, H., (2008). *Hydrological Modelling in Arid and Semi-Arid Areas.* Cambridge University Press, New York

Sierra, C.A., (2012). *Temperature sensitivity of organic matter decomposition in the Arrhenius equation: some theoretical considerations.* Biogeochemistry*,* 108: 1.

Smith R.A., Schwartz G.E., Alexander R.B., (1997). *Regional interpretation of water-quality monitoring data*. Water Resources Research, 33, 12, 2781-2798.

Stewart R.J., Wollheim W.M., Gooseff M.N., (2011). *Separation of River Network–scale Nitrogen Removal among the Main Channel and Two Transient Storage Compartments*. Water Resources Research, 47, 10.

Stewart R.J., Wollheim W.M., Miara A., Vörösmarty C.J., Fekete B., Lammers R.B., Rosenzxweig B. (2013). *Horizontal cooling towers: riverine ecosystem services and the fate of thermoelectric heat in the contemporary Northeast US*. Environmental Research Letters, 8(2).

Taylor J.R. (1982). *An Introduction to Error Analysis The Study of Uncertainties in Physical Measurements.* Second Edition. University Science Books

Thorn A.M., Wake C.P., Grimm C.D., Mitchell C.R., Mineau M.M., Ollinger S.V., (2017). *Development of scenarios for land cover, population density, impervious cover, and conservation in New Hampshire, 2010-2100*. Ecology and Society, 22(4): 19.

Todd, C.R., Ryan T., Nicol S.J., Bearlin A.R., (2005). *The impact of cold water releases on critical period of post-spawning survival and its implications for Murray cod (Maccullochella peelii peelii): a case study of the Mitta Mitta River, southeastern* Australia. River Research and Applications, 21, 1035-1052.

USEPA. (2008). *Municipal nutrient removal technologies reference document:* Vol. 1. Technical report EPA-832-R-08-006, Office of Wastewater Management, Washington D.C.

U.S. Geological Survey (1984). Rantz S.E., *Measurement and Computation of Streamflow: Volume 1. Measurements of Stage and Discharge.* Geological Survey Water-Supply Paper 2175.

U.S. Geological Survey (2013). National Hydrography Dataset available on the World Wide Web (https://nhd.usgs.gov). accessed [3/1/2018].

Van Drecht G., Bouwman A.F., Harrison J., Knoop J.M. (2009). *Global nitrogen and phosphate in urban wastewater for the period 1970 to 2050*. Global Biogeochemical Cycles, 23: GB0A03.

Vigerstoal K.L., Aukema J.E., (2011). *A comparison of tools for modeling freshwater ecosystem services.* Journal of Environmental Management, 92, 2403-2409.

Vitousek P.M., Aber J.D., Howarth R.W., Likens G.E., Matson P.M., Schindler D.W., Schlesinger W.H., Tilman D.G., (1997). *Human Alteration of the Global Nitrogen Cycle: Sources and Consequences*. Ecological Applications, 7(3), 737-750.

Vörösmarty C.J., Meybeck M., Fekete B., Sharma K., Green P., Syvitski J.P.M., (2003). *Anthropogenic sediment retention: major global impact from registered river impoundments*. Global and Planetary Change, 39, 169-190.

Wake C. P., (2013). *Assessing the Risk of 100-year Freshwater Floods in the Lamprey River Watershed of New Hampshire Resulting from Changes in Climate and Land Use*.

Wisser D., Fekete B.M., Vörösmarty C.J., (2010). *Reconstructing 20th century global hydrography: a contribution to the Global Terrestrial Network- Hydrology (GTN-H).* Hydrology and Earth System Sciences, 14(1), 1-24.

Waterline, (2017). National River Levels and Flow Forecasts. 235114 PENOBSCOT RIVER LOWER W BR, MCKAY STN, RIPOGENUS DAM. http://www.h2oline.com/default.aspx?pg=si&op=235114

Wollheim W.M., Peterson B.J., Thomas S.M., Hopkinson C.H., Vörösmarty C.J., (2008). *Dynamics of N removal over annual time periods in a suburban river network*. Journal of Geophysical Research, 113.

Zimmerman J.K.H., Letchner B.H., Nislow K.H., Lutz K.A., Magilligan F.J., (2010). *Determining the Effects of Dams on Subdaily Variation in River Flows at a Whole-Basin Scale*. Research and Applications, 26, 1246-1260.

Appendix A: Field Measurement Data

A.1 Barometric transducer field measurements

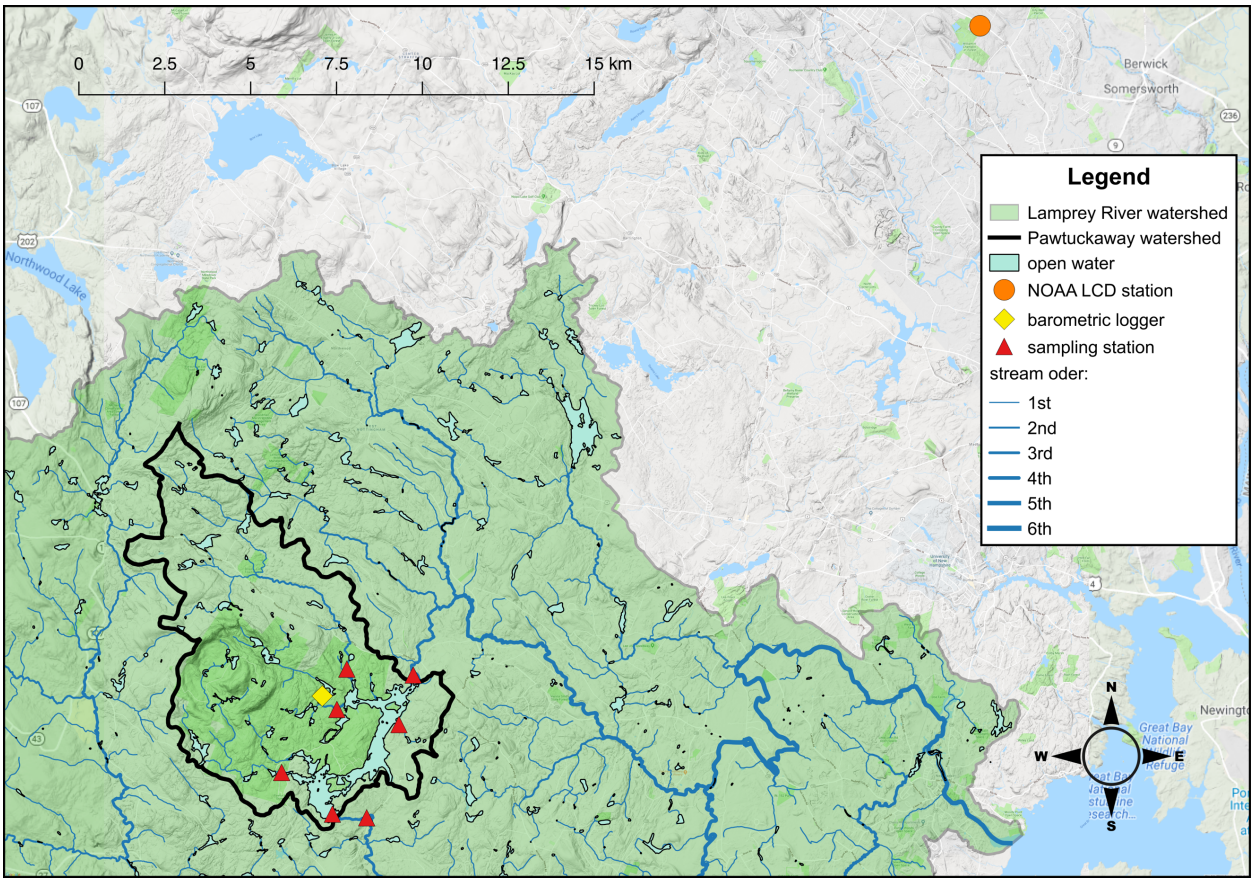

Figure A.1. Location of barometric transducer, sampling stations, and NOAA Local Climatological Data (LDC) station id WBAN:54791 at Skyhaven Airport in Rochester, NH. Background area outside of Lamprey River watershed was obtained from Google Maps.

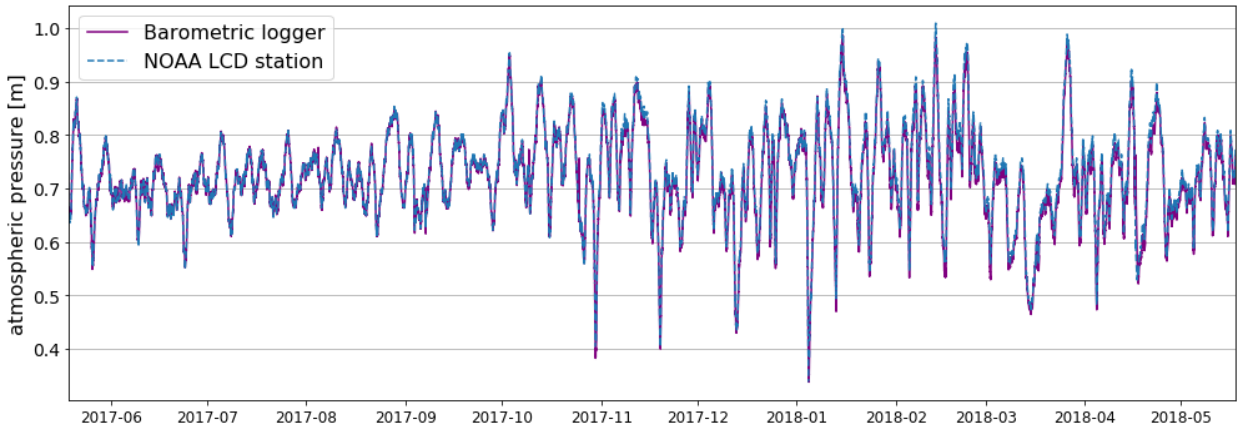

Figure A.2. Barometric transducer pressure head (recorded at 5-minute intervals) compared to daily mean pressure head measured at the NOAA Local Climatological Data (LDC) station id WBAN:54791 at Skyhaven Airport in Rochester, NH from 2017-05-19 to 2018-05-18.

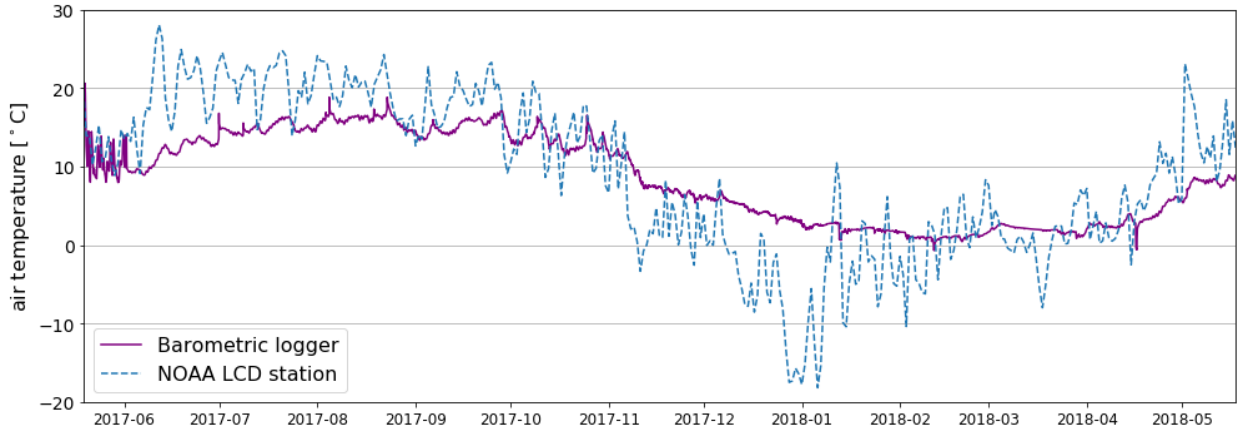

Figure A.3. Barometric transducer air temperature (recorded at 5-minute intervals) compared to daily mean air temperature measured at the NOAA Local Climatological Data (LDC) station id WBAN:54791 at Skyhaven Airport in Rochester, NH from 2017-05-19 to 2018-05-18.

Table A.1. Dates and times when barometric transducer data was trimmed and filled with linear interpolation due to data retrieval.

	Data Trimmed		# of measurements interpolated
Date	Start Time	Stop Time	
2017-06-01	16:35	17:55	17
2017-06-22	12:05	17:35	67
2017-07-14	11:15	14:55	45
2017-08-13	15:20	16:40	17
2017-09-15	10:35	13:00	30
2017-10-13	7:35	15:00	90
2018-01-19	17:25	18:30	14
2018-04-08	7:05	10:00	36
2018-05-02	15:50	17:15	18

Table A.2. Number of measurements kept and measurements trimmed and filled through linear interpolation for the Barometric transducer from 2017-05-19 to 2018-05-18.

# of measurements recorded	# of measurements interpolated	% of measurements interpolated
104499	334	0.318

A.2 Round Pond Brook field measurements

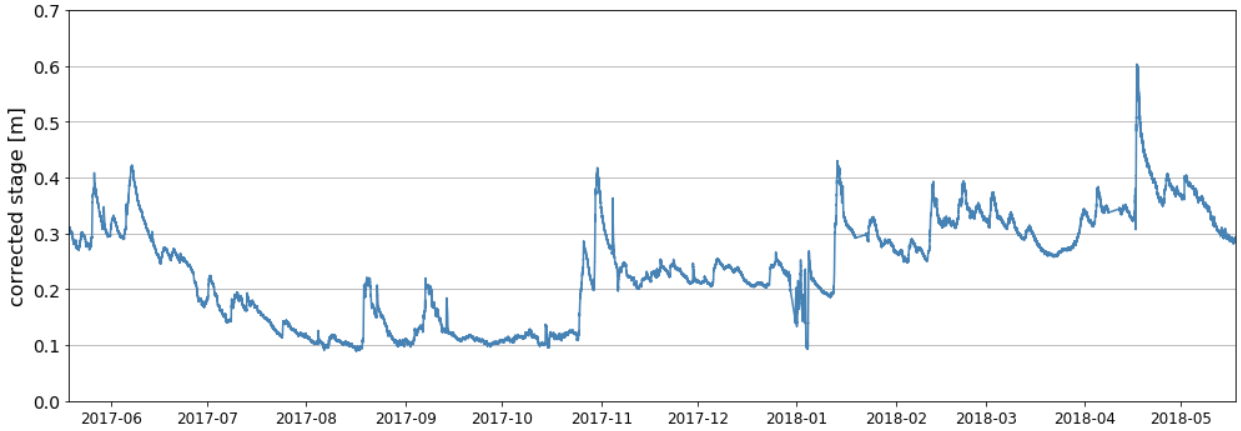

Figure A.4. Corrected stage (recorded at 5-minute intervals) at Round Pond Brook from 2017-05-19 to 2018-05-18.

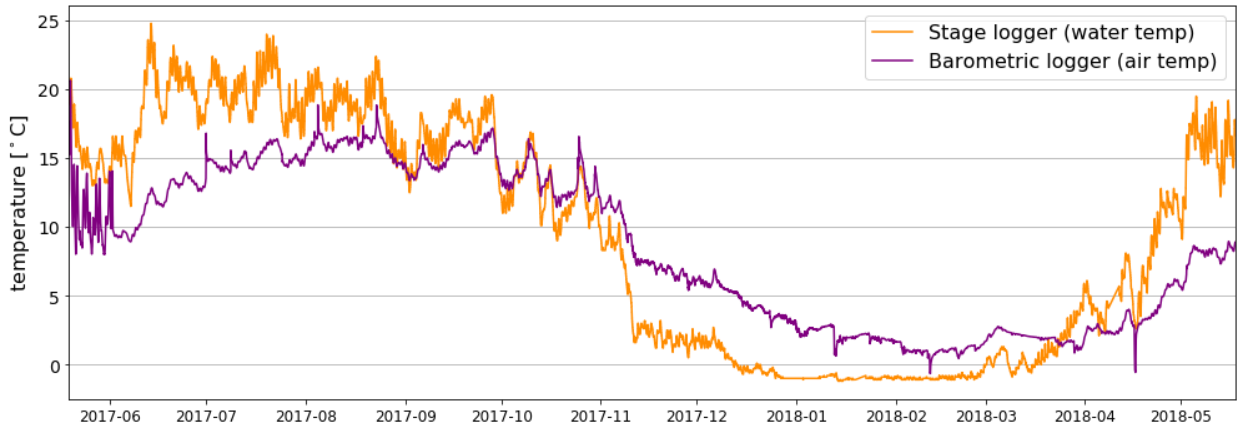

Figure A.5. Water temperature (recorded at 5-minute intervals) at Round Pond Brook compared to air temperature from the barometric logger from 2017-05-19 to 2018-05-18.

Table A.3. Dates and times when pressure transducer data was trimmed and filled with linear interpolation at Round Pond Brook.

	Data trimmed		# of measurements interpolated
Date of data retrieval	Start time	Stop time	
2017-06-01	16:45	17:50	14
2017-06-22	14:00	15:00	13
2017-06-30	20:55	23:35	33
2017-07-06	12:15	12:45	7
2017-07-14	11:25	12:00	8
2017-08-03	15:35	16:00	6
2017-09-15	10:30	11:30	13
2017-10-13	7:00	13:30	79
2018-01-19	9:20	18:20	109
2017-04-08	7:50	2017-04-11 16:00	963
2018-05-02	15:30	16:00	7

Table A.4. Dates and times when pressure transducer data was corrected for intentional and unintentional transducer relocations at Round Pond Brook.

		Correction applied to record	
Intentionally moved	Correction [m]	Start date, time	End date, time
No	-0.034	2017-06-30, 21:00	2017-07-06, 12:10
Yes	+0.16	2017-05-19, 00:00	2017-07-14, 12:00
Yes	+0.005	2017-05-19, 00:00	2017-10-13, 6:55
No	-0.04	2018-04-11, 16:00	2018-05-01, 12:13

Table A.5. Discharge measurements obtained at Round Pond Brook using the velocity-area method and corrected stage used in the construction of the stage-discharge rating curve in Figure A.6.

Date Time	m	Measured at	Q [m^3/s]	Corrected stage [m]	Q uncertainty +/- (%)
6/12/17 12:30	20	0.6 depth	0.082125	0.3056	7.88
7/7/17 15:00	21	0.6 depth	0.008138	0.1433	10.65
7/14/17 10:40	20	0.6 depth	0.034712	0.1707	10.86
7/25/17 15:30	22	0.6 depth	0.007487	0.1402	10.47
7/26/17 15:30	22	0.6 depth	0.006992	0.1377	10.47
8/8/17 11:50	28	0.6 depth	0.005067	0.1119	9.10
10/13/17 8:15	20	0.6 depth	0.002051	0.1018	11.08
12/8/17 9:00	20	0.6 depth	0.076198	0.2453	7.88
1/19/18 16:15	18	0.6 depth	0.136424	0.2925	9.21
4/8/18 7:00	21	0.6 and 0.2 & 0.8 depth	0.298635	0.3384	7.77

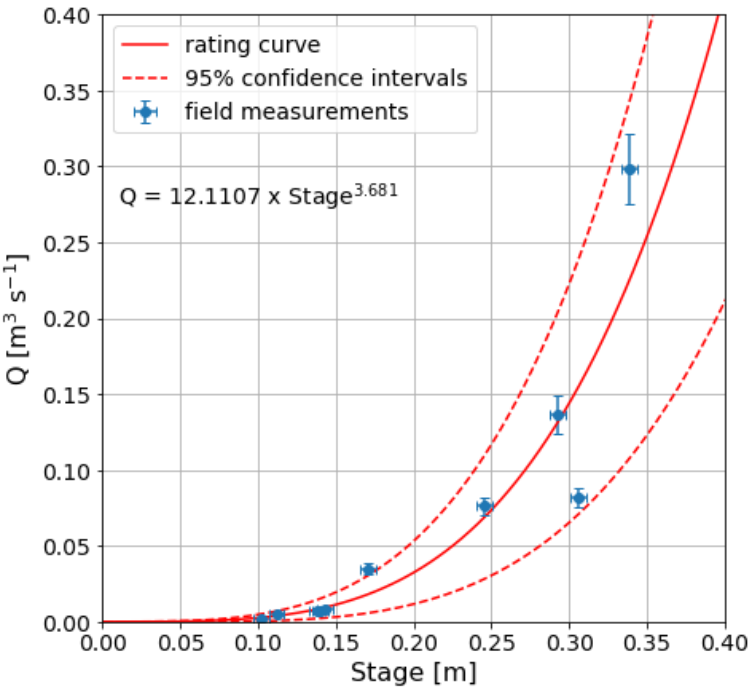

Figure A.6. Stage-discharge rating curve for Round Pond Brook. Field measurements of discharge and stage are located in Table A.5.

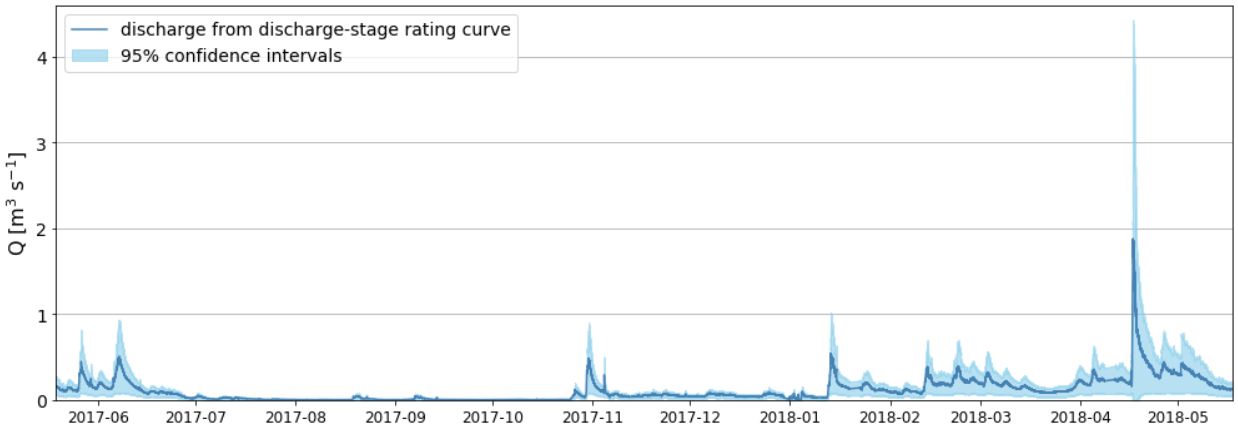

Figure A.7. Time series of discharge (Q) at 5-minute intervals for Round Pond Brook from 2017-05-19 to 2018-05-18.

Table A.6. Nitrogen solute concentration measurements obtained at Round Pond Brook.

Date	TDN [mg N/L]	DON [mg N/L]	$NO+NO_2^-$ [mg N/L]	NH_4^+ [µg N/L]
2017-05-23	0.346	0.282	0.057	7.00
2017-07-26	0.225	0.173	0.037	15.00
2017-10-13	0.457	0.385	0.070	2.50
2017-12-08	0.285	0.250	0.022	13.35
2018-01-19	0.199	0.155	0.033	11.00
2018-04-08	0.176	0.143	0.029	4.00

A.3 Back Creek B field measurements

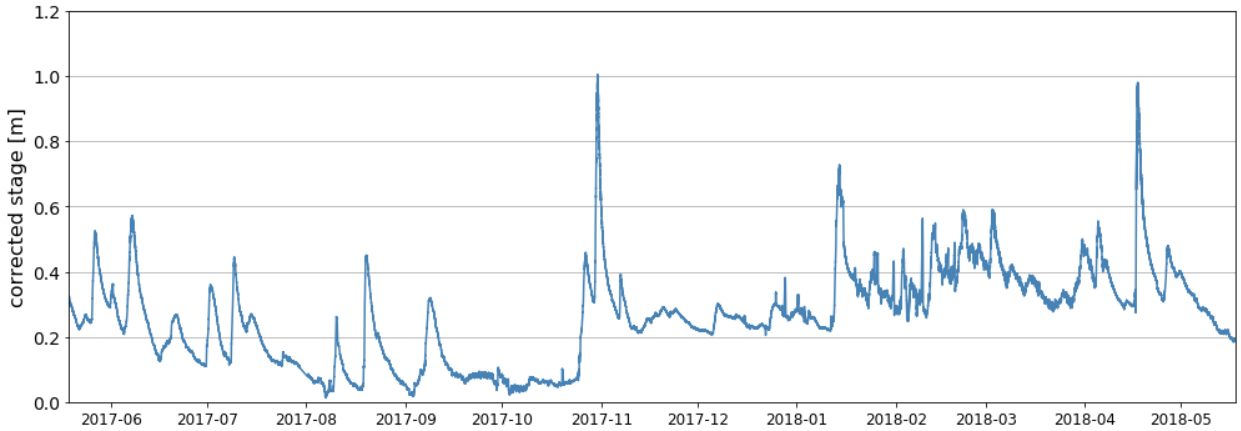

Figure A.8. Corrected stage (recorded at 5-minute intervals) at Back Creek B from 2017-05-19 to 2018-05-18.

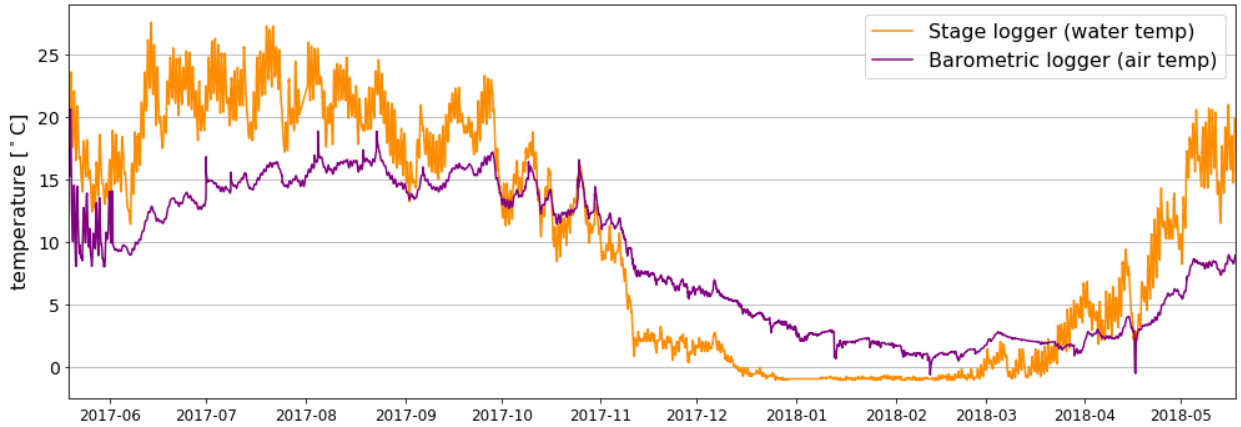

Figure A.9. Water temperature (recorded at 5-minute intervals) at Back Creek B compared to air temperature from the barometric logger from 2017-05-19 to 2018-05-18.

Table A.7. Dates and times when pressure transducer data was trimmed and filled with linear interpolation at Back Creek B.

	Data trimmed		# of measurements interpolated
Date of data retrieval	Start time	Stop time	
2017-06-01	16:00	16:30	7
2017-06-22	13:55	15:10	16
2017-07-06	9:50	9:55	2
2017-07-30	10:00	8/1/17 12:00	601
2017-08-01	13:15	15:45	31
2017-08-03	16:05	16:25	5
2017-09-15	9:45	10:35	11
2017-10-13	8:45	17:35	107
2018-01-19	16:25	16:45	5
2017-04-08	8:05	11:15	39
2018-05-02	14:40	15:30	11

Table A.8. Dates and times when pressure transducer data was corrected for intentional and unintentional transducer relocations at Back Creek B.

		Correction applied to record	
Intentionally moved	Correction [m]	Start date, time	End date, time
Yes	+0.175	2017-05-19, 00:00	2017-07-06, 10:10
Yes	+0.095	2017-05-19, 00:00	2017-08-01, 14:15

Table A.9. Discharge measurements obtained at Back Creek B using the velocity-area method and corrected stage used in the construction of the stage-discharge rating curve in Figure A.10.

Date Time	m	Measured at	Q [m^3/s]	Corrected stage [m]	Q uncertainty +/- (%)
6/12/17 14:55	20	0.6 depth	0.15697	0.241155	8.00
7/6/17 11:20	25	0.6 depth	0.047831	0.152695	9.52
7/25/17 14:00	20	0.6 depth	0.042071	0.142735	10.29
7/26/17 17:00	23	0.6 depth	0.036026	0.136075	10.86
8/8/17 14:15	20	0.6 depth	0.002691	0.037225	10.13
10/13/17 9:50	25	0.6 depth	0.009239	0.06425	11.31
12/8/17 10:40	20	0.6 depth	0.224063	0.283845	7.88
1/19/18 14:40	20	0.6 depth	0.398902	0.361175	7.88
4/8/18 10:50	21	0.6 depth	0.562348	0.392685	7.77

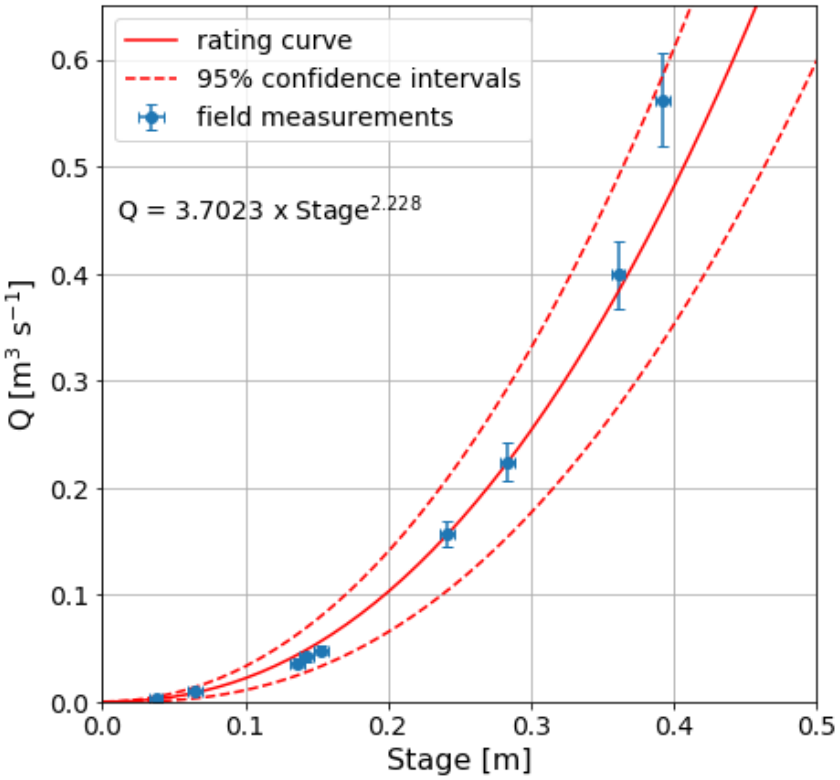

Figure A.10. Stage-discharge rating curve for Back Creek B. Field measurements of discharge and stage are located in Table A.9.

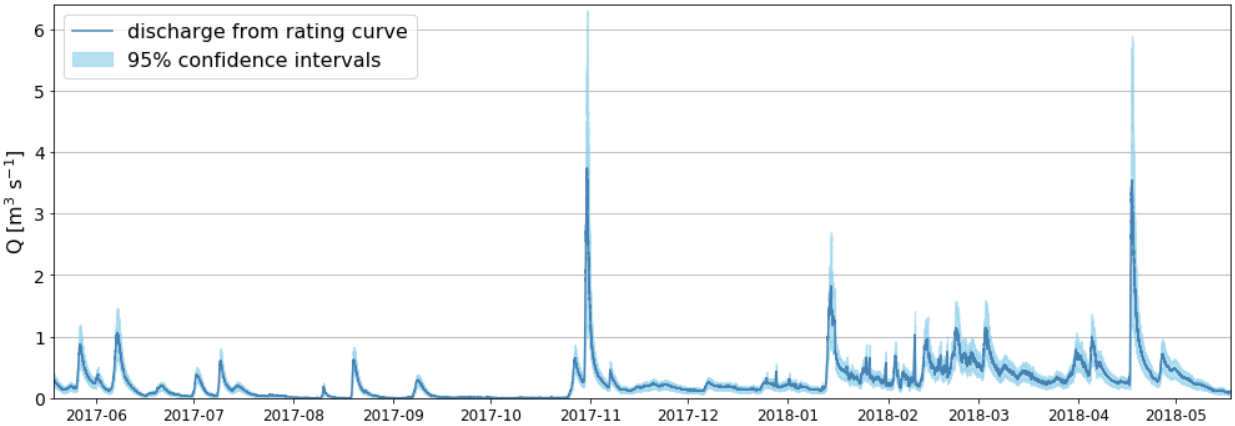

Figure A.11. Time series of discharge (Q) at 5-minute intervals for Back Creek B from 2017-05-19 to 2018-05-18.

Table A.10. Nitrogen solute concentration measurements obtained at Back Creek B.

Date	TDN [mg N/L]	DON [mg N/L]	NO3+NO2 [mg N/L]	NH4 [μg N/L]
2017-05-23	0.0915	0.077	0.015	0.00
2017-07-26	0.1769	0.139	0.029	9.00
2017-10-13	0.554	0.455	0.080	19.10
2017-12-08	0.324	0.291	0.021	11.89
2018-01-19	0.379	0.315	0.052	12.00
2018-04-08	0.183	0.153	0.030	0.00

A.4 Mountain Cove Brook field measurements

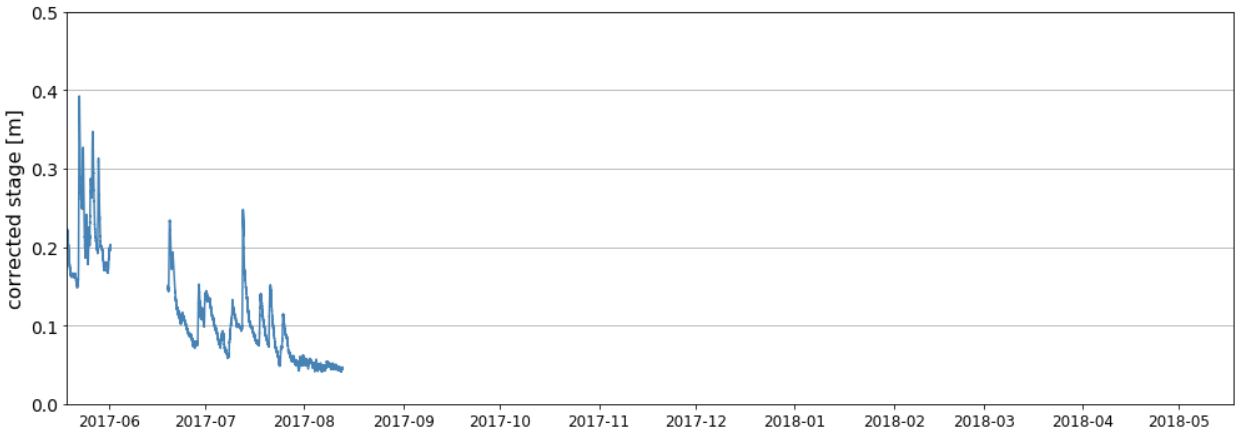

Figure A.12. Corrected stage (recorded at 5-minute intervals) at Mountain Cove Brook from 2017-05-19 to 2017-06-1 13:15 and 2017-06-19 10:30 to 2017-08-13. Data gap from 2017-06-01 13:15:00 to 2017-06-19 10:30:00 was a result of the transducer failing to record data. Stage data after 2017-08-13 was cut from the record due to upstream beaver activity.

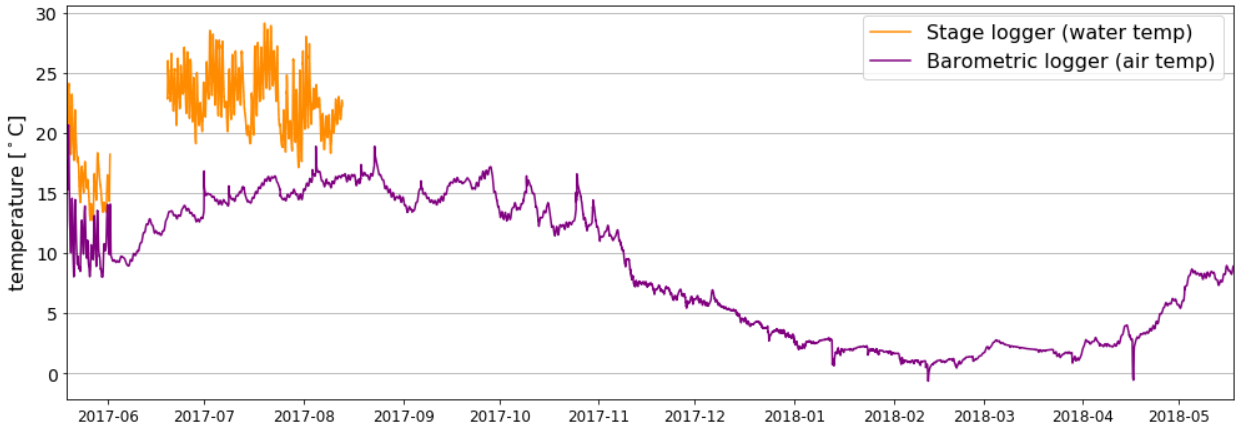

Figure A.13. Water temperature (recorded at 5-minute intervals) at Mountain Cove Brook from 2017-05-19 to 2017-06-1 13:15 and 2017-06-19 10:30 to 2017-08-13 compared to air temperature from the barometric logger from 2017-05-19 to 2018-05-18.

Table A.11. Dates and times when pressure transducer data was trimmed and filled with linear interpolation at Mountain Cove Brook.

	Data trimmed		# of measurements interpolated
Date of data retrieval	Start time	Stop time	
2017-06-01	13:05	13:35	7
2017-07-13	13:10	13:40	6
2017-08-03	10:35	12:00	18
2017-08-04	17:40	18:00	5

Table A.12. Dates and times when pressure transducer data was corrected for intentional and unintentional transducer relocations at Mountain Cove Brook.

		Correction applied to record	
Intentionally moved	Correction [m]	Start date, time	End date, time
Yes	+0.269	2017-05-19, 00:00	2017-08-03, 10:35

Table A.13. Discharge measurements obtained at Mountain Brook Cove using the velocity-area method and corrected stage used in the construction of the stage-discharge rating curve in Figure A.14.

Date Time	m	Measured at	Q [m^3/s]	Corrected stage [m]	Q uncertainty +/-(%)
6/15/17 11:30	20	0.6 depth	0.091657	0.168164	7.88
6/22/17 10:05	25	0.6 depth	0.044802	0.120635	10.86
7/13/17 12:00	20	0.6 depth	0.076523	0.16015	7.88
7/25/17 10:10	23	0.6 depth	0.024914	0.114225	10.13
7/26/17 9:30	20	0.6 depth	0.017193	0.08483	10.47
12/8/17 14:30	20	0.6 depth	0.080025	-	8.27
1/19/18 8:45	20	0.6 depth	0.222568	-	8.00
4/8/18 14:00	21	0.6 and 0.2 & 0.8 depth	0.36318	-	8.00

Table A.14. Discharge measured at the two parallel road culverts at Mountain Cove Brook using bucket technique on 10/13/17 at 15:50.

	Left culvert		Right culvert			
Trial	Volume [L]	Time [s]	Volume [L]	Time [s]	Q [m^3/s]	Q uncertainty +/- (%)
1	3.25	2	1.45	5	0.001915	30
2	3.2	2	1.45	5	0.00189	30
3	3.3	2	1.6	5	0.00197	30
Mean =					0.001925	30

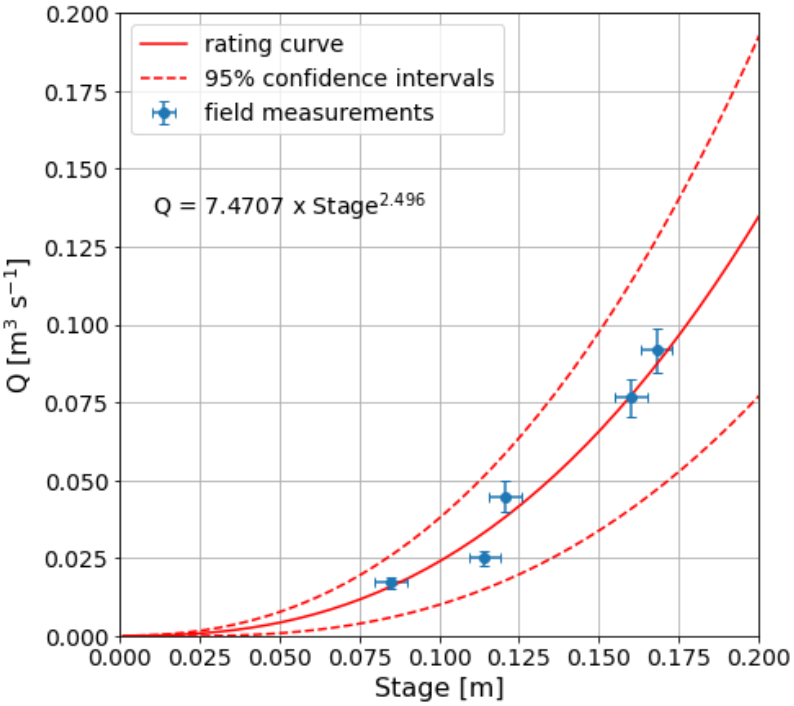

Figure A.14. Stage-discharge rating curve for Mountain Cove Brook. Field measurements of discharge and stage are located in Table A.13.

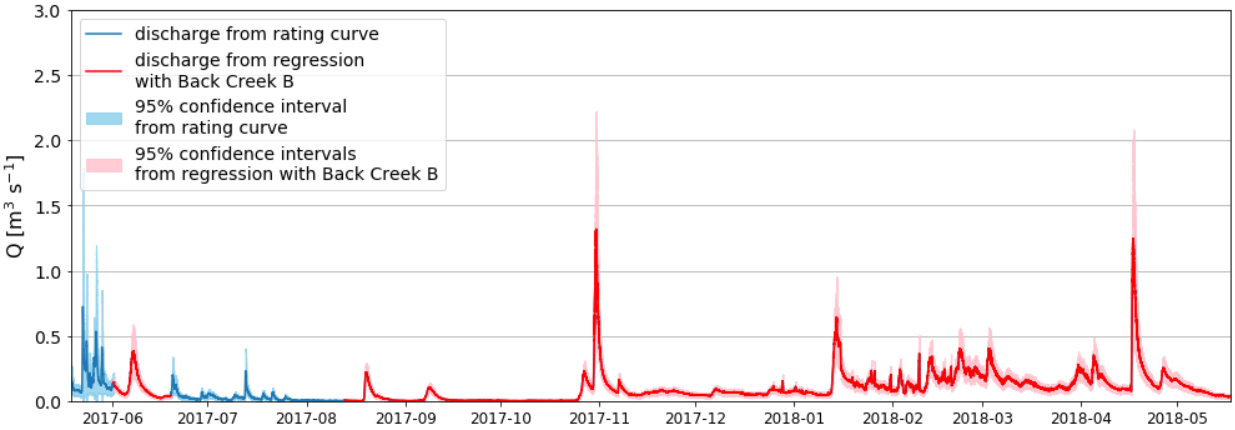

Figure A.15. Time series of discharge (Q) at 5-minute intervals at Mountain Cove Brook from 2017-05-19 to 2018-05-18.

Table A.15. Nitrogen solute concentration measurements obtained at Mountain Cove Brook.

Date	TDN [mg N/L]	DON [mg N/L]	NO3+NO2 [mg N/L]	NH4 [μg N/L]
2017-05-23	0.009	0.003	0.002	4.00
2017-07-26	0.033	0.004	0.015	14.00
2017-10-13	0.249	0.117	0.050	82.50
2017-12-08	0.216	0.201	0.009	6.26
2018-01-19	0.181	0.140	0.039	2.00
2018-04-08	0.178	0.078	0.082	18.00

A.5 Fernald's Brook A field measurements

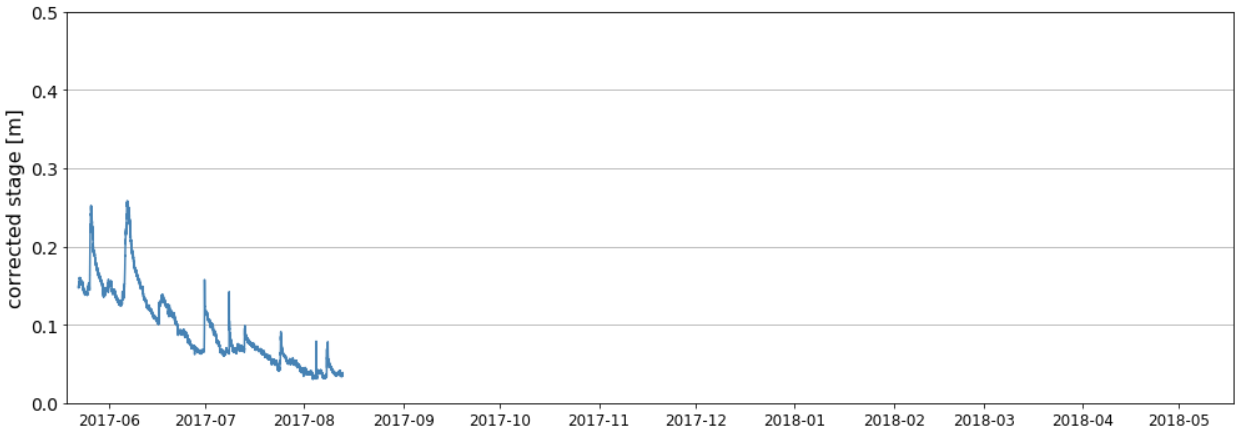

Figure A.16. Corrected stage (recorded at 5-minute intervals) at Fernald's Brook A from 2017-05-22 14:30 to 2017-08-13. Logger data after 2017-08-13 was cut from the record due to a the formation of a sand delta that buried the transducer.

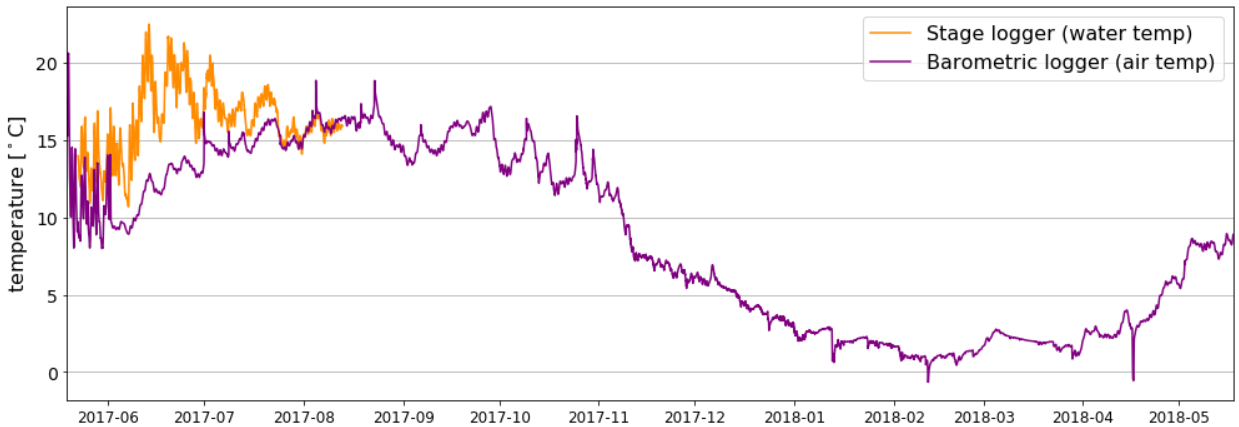

Figure A.17. Water temperature (recorded at 5-minute intervals) at Fernald's Brook A from 2017-05-22 14:30 to 2017-08-13 compared to air temperature from the barometric logger from 2017-05-19 to 2018-05-18.

Table A.16. Dates and times when pressure transducer data was trimmed and filled with linear interpolation at Fernald's Brook A.

	Data trimmed		# of measurements interpolated
Date of data retrieval	Start time	Stop time	
2017-06-01	14:05	14:45	9
2017-06-19	10:55	11:30	8
2017-07-13	11:35	11:45	3
2017-07-26	12:50	13:30	9
2017-07-27	12:10	12:30	5
2017-08-03	13:10	13:50	9

Table A.17. Dates and times when pressure transducer data was corrected for intentional and unintentional transducer relocations at Fernald's Brook A.

		Correction applied to record	
Intentionally moved	Correction [m]	Start date, time	End date, time
Yes	+0.03	2017-05-22, 14:30	2017-08-13

Table A.18. Discharge measurements obtained at Fernald's Brook A using the velocity-area method and corrected stage used in the construction of the stage-discharge rating curve in Figure A.19.

Date Time	m	Measured at	Q [m^3/s]	Corrected stage [m]	Q uncertainty +/-%
6/15/17 14:05	20	0.6 depth	0.004914	0.11008	11.08
7/13/17 10:30	20	0.6 depth	0.002954	0.089105	11.08
8/8/17 8:55	20	0.6 depth	0.001074	0.0749	10.86
1/19/18 10:55	18	0.6 depth	0.021461	-	11.86
4/8/18 14:30	24	0.6 depth	0.043026	-	10.13

Table A.19. Discharge measured at the Fernald's Brook A using bucket technique on 7/26/17 at 13:30.

Trial	Volume [L]	Time [s]	Q [m^3/s]	Q uncertainty +/- (%)
1	0.76	1.88	0.000404	30
2	0.75	2.02	0.000371	30
3	0.75	1.84	0.000408	30
Mean =			0.000394	30

Table A.20. Discharge measured at the Fernald's Brook A using bucket technique on 10/13/17 at 13:25.

Trial	Volume [L]	Time [s]	Q [m^3/s]	Q uncertainty +/- (%)
1	0.70	20	0.000035	30
2	0.60	20	0.000030	30
Mean =			0.000033	30

Table A.21. Discharge measured at the Fernald's Brook A using bucket technique on 12/8/17 at 14:45.

Trial	Volume [L]	Time [s]	Q [m³/s]	Q uncertainty +/- (%)
1	4.30	3	0.00143	30
2	4.25	3	0.00142	30
3	4.30	3	0.00143	30
Mean =			0.00143	30

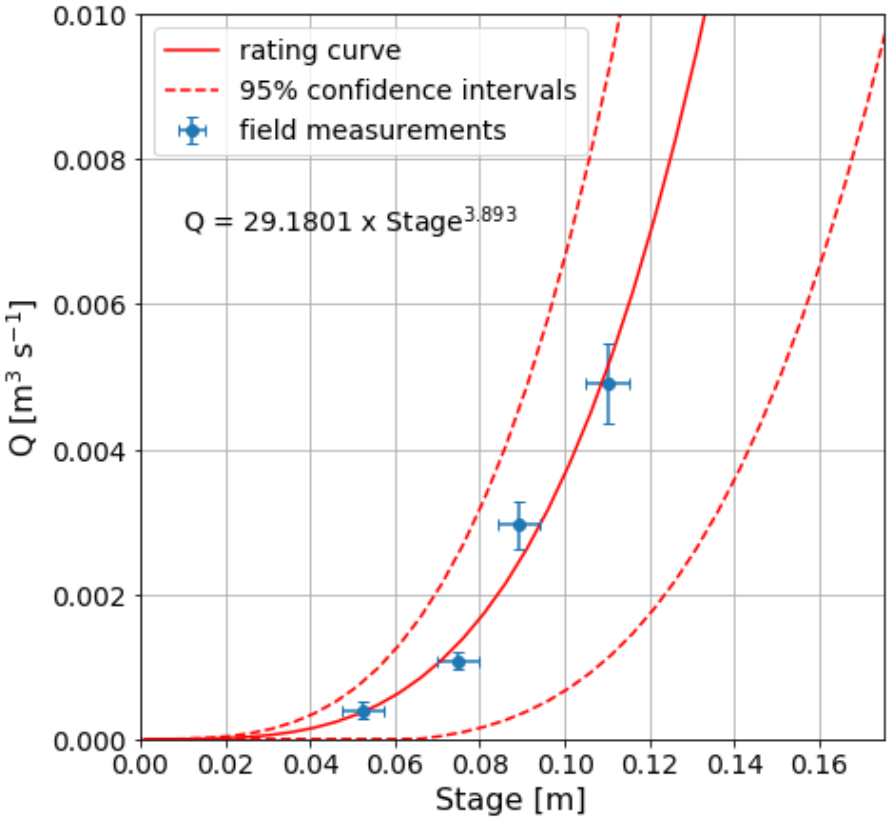

Figure A.18. Stage-discharge rating curve for Fernald's Brook A. Field measurements of discharge and stage are located in Tables A.18 - 19.

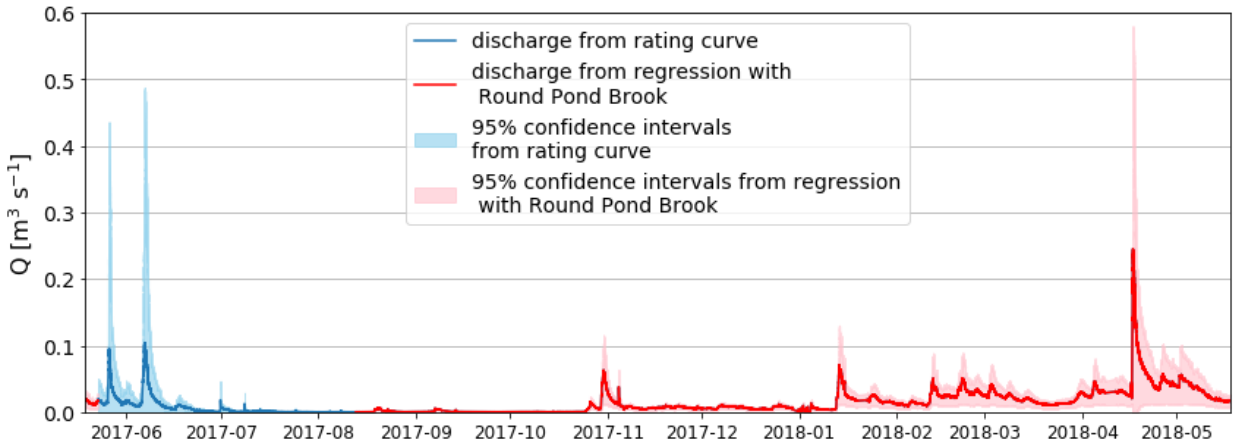

Figure A.19. Time series of discharge (Q) at 5-minute intervals at Fernald's Brook A from 2017-05-19 to 2018-05-18.

Table A.22. Nitrogen solute concentration measurements obtained at Fernald's Brook A.

Date	TDN [mg N/L]	DON [mg N/L]	NO3+NO2 [mg N/L]	NH4 [μg N/L]
2017-05-23	0.117	0.065	0.044	8.00
2017-07-26	0.539	0.314	0.202	23.00
2017-10-13	0.524	0.403	0.120	1.30
2017-12-08	1.812	1.137	0.663	12.10
2018-01-19	1.664	0.898	0.653	113.00
2018-04-08	1.220	0.749	0.458	13.00

A.6 Mile Brook field measurements

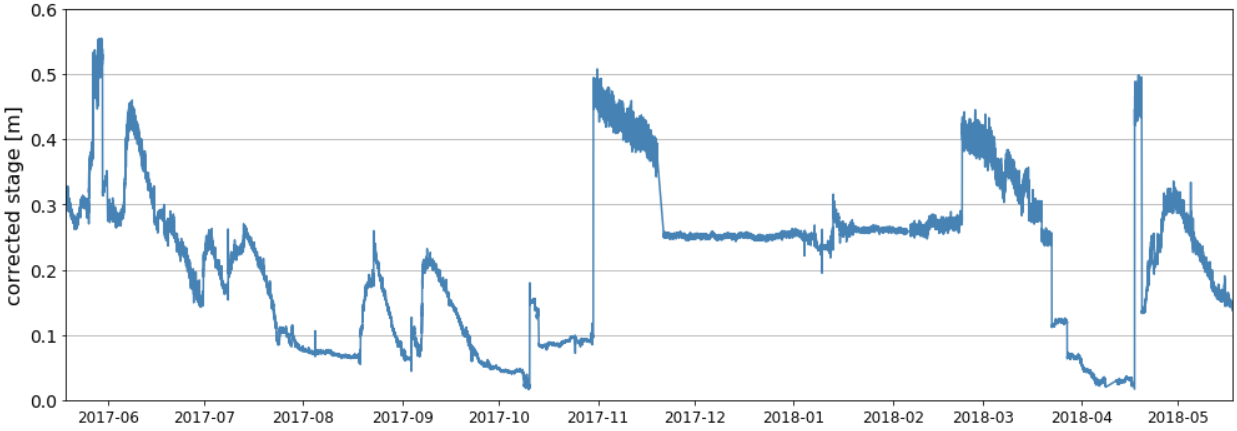

Figure A.20. Corrected stage (recorded at 5-minute intervals) at Mile Brook from 2017-05-19 to 2018-05-18.

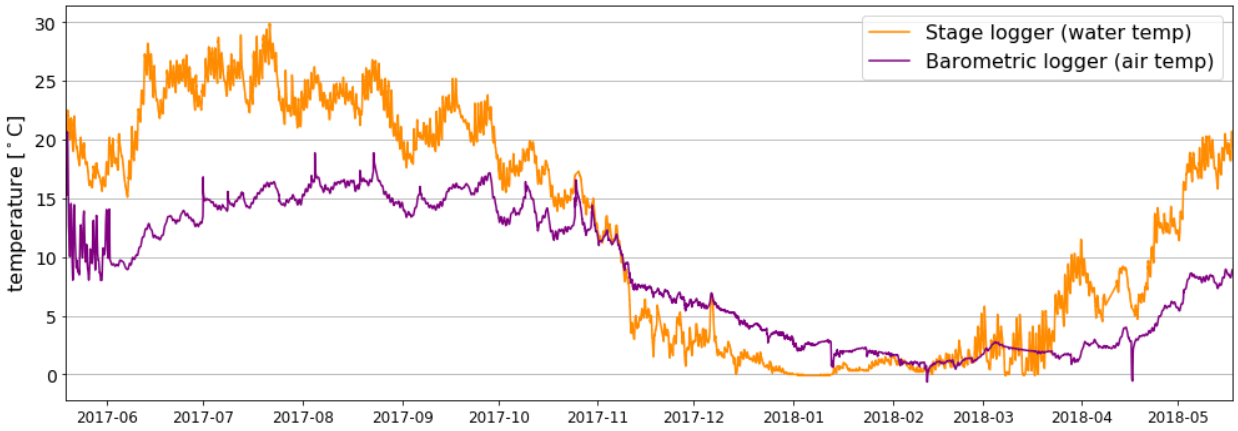

Figure A.21. Water temperature (recorded at 5-minute intervals) at Mile Brook compared to air temperature from the barometric logger from 2017-05-19 to 2018-05-18.

Table A.23. Dates and times when pressure transducer data was trimmed and filled with linear interpolation at Mile Brook.

	Data trimmed		# of measurements interpolated
Date of data retrieval	Start time	Stop time	
2017-05-23	13:25	13:50	6
2017-05-30	8:45	9:15	7
2017-05-31	20:30	23:35	38
2017-06-01	15:10	15:35	6
2017-06-15	9:45	10:00	4
2017-06-18	14:35	15:35	13
2017-06-19	11:40	12:05	6
2017-06-22	11:25	12:45	17
2017-07-27	13:35	14:40	14
2017-08-03	14:15	14:50	8
2017-08-04	17:40	17:55	4
2017-09-15	9:10	9:35	6
2017-10-09	10:25	10:45	5
2017-10-25	9:00	12:00	37
2017-11-19	13:00	11/19/17 13:00	577
2018-01-11	14:35	15:05	7
2018-01-19	12:00	15:35	44
2018-02-05	9:20	2/6/18 10:20	289
2018-04-08	9:20	4/11/18 18:00	969
2018-04-16	14:00	4/17/18 9:40	237
2018-05-02	14:15	14:50	8

Table A.24. Dates and times when pressure transducer data was corrected for intentional and unintentional transducer relocations at Mile Brook.

		Correction applied to record	
Intentionally moved	Correction [m]	Start date, time	End date, time
Yes	+0.17	2017-05-19, 00:00	2017-05-23, 13:50
No	+0.06	2017-05-27, 12:25	2017-05-30, 8:55
No	+0.046	2017-05-29, 1:05	2017-05-30, 9:05
No	+0.09	2017-05-27, 12:20	2017-05-30, 9:00
No	+0.07	2017-05-31, 20:45	2017-06-01, 14:55
Yes	+0.03	2017-05-19, 00:00	2017-06-15, 10:05
No	+0.07	2017-06-18, 15:25	2017-06-22, 12:35
No	-0.18	2017-06-19, 12:10	2017-06-22, 12:30
Yes	+0.16	2017-05-19, 00:00	2017-07-27, 14:30
Yes	+0.065	2017-05-19, 00:00	2017-08-03, 14:15
No	-0.051	2017-09-15, 9:40	2017-10-13, 11:15
No	-0.085	2017-11-21, 13:00	2018-02-05, 13:00
No	-0.01	2018-04-11, 14:40	2018-05-18, 14:40
No	+0.4	2018-04-17, 9:50	2018-04-19, 15:05

Table A.25. Discharge measurements obtained at Mile Brook using the velocity-area method and corrected stage used in the construction of the stage-discharge rating curve in Figure A.24.

Date Time	m	Measured at	Q [m^3/s]	Corrected stage [m]	Q uncertainty +/-%
6/12/17 10:00	20	0.6 depth	0.51769	0.359	8.00
6/22/17 12:30	20	0.6 depth	0.23136	0.252	7.88
7/7/17 16:20	20	0.6 depth	0.09395	0.173	7.88
7/26/17 18:00	23	0.6 depth	0.01845	0.101	10.29
8/8/17 13:00	23	0.6 depth	0.007703	0.075	10.29
10/13/17 11:30	22	0.6 depth	0.07157	0.130	7.67
12/8/17 12:00	20	0.6 depth	1.577	0.565	7.88
1/19/17 13:00	20	0.6 depth	0.36208	0.305	7.88
4/8/17 13:00	22	0.6 depth	0.01845	0.020	10.47

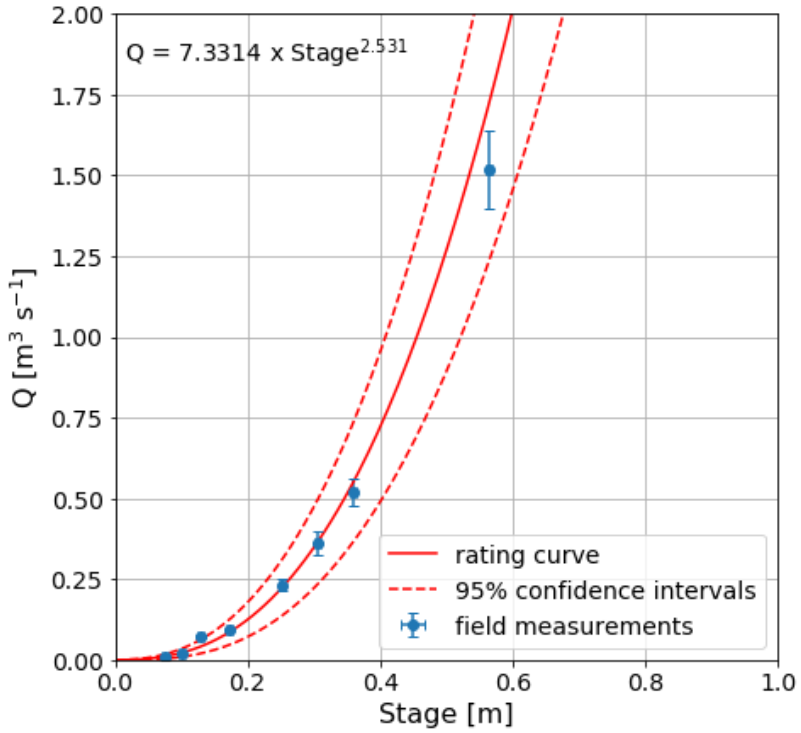

Figure A.22. Stage-discharge rating curve for Mile Brook. Field measurements of discharge and stage are located in Table A.25.

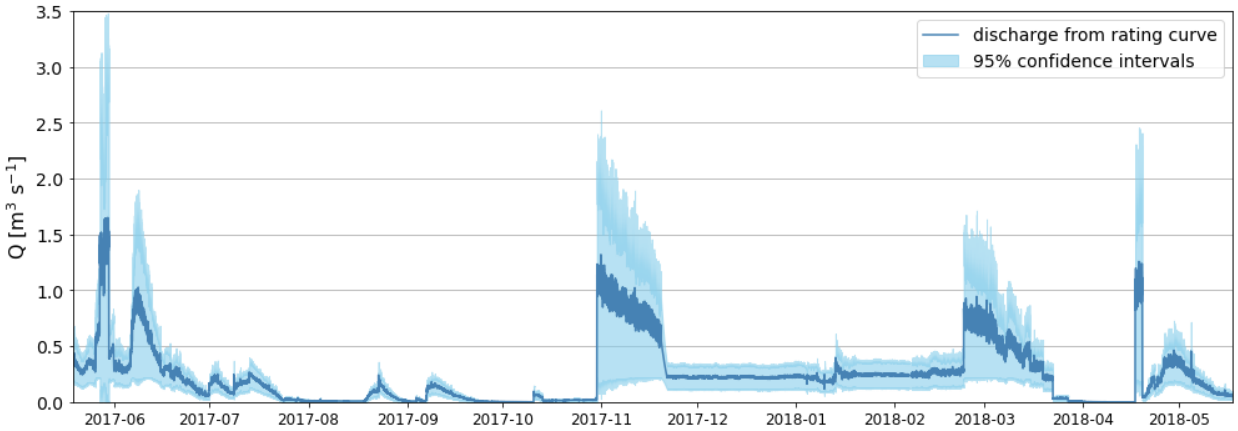

Figure A.23. Time series of discharge (Q) at 5-minute intervals at Mile Brook from 2017-05-19 to 2018-05-18.

Table A.26. Nitrogen solute concentration measurements obtained at Mile Brook.

Date	TDN [mg N/L]	DON [mg N/L]	NO3+NO2 [mg N/L]	NH4 [µg N/L]
2017-05-23	0.072	0.053	0.016	3.00
2017-07-26	0.406	0.289	0.090	27.00
2017-10-13	0.233	0.214	0.010	9.20
2017-12-08	0.540	0.410	0.038	91.59
2018-01-19	0.282	0.195	0.059	28.00
2018-04-08	0.239	0.173	0.053	13.00

A.7 Pawtuckaway River field measurements

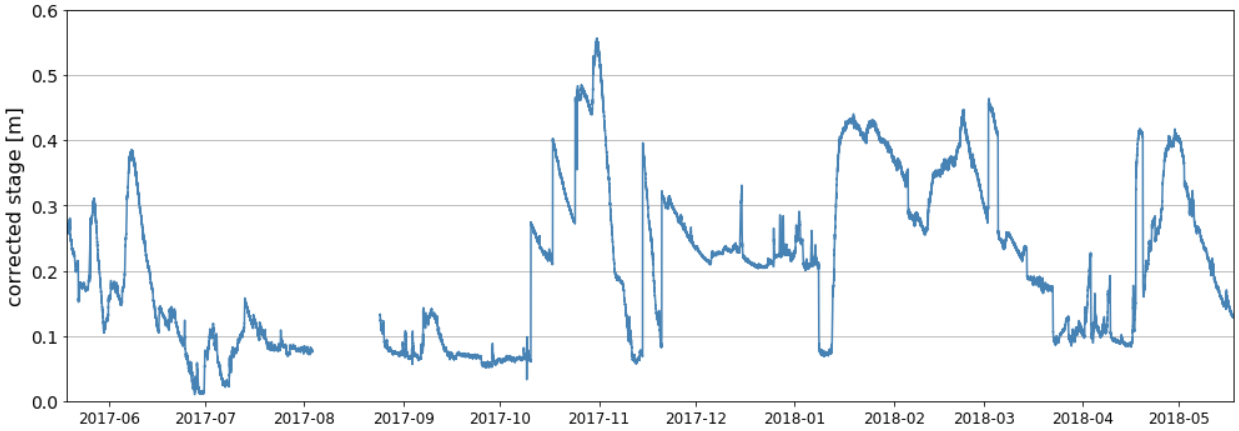

Figure A.24. Corrected stage (recorded at 5-minute intervals) at Pawtuckaway River from 2017-05-19 to 2018-05-18. Data gap exists between 2017-08-03 13:40 to 2017-08-24 16:00 from failure to download logger data.

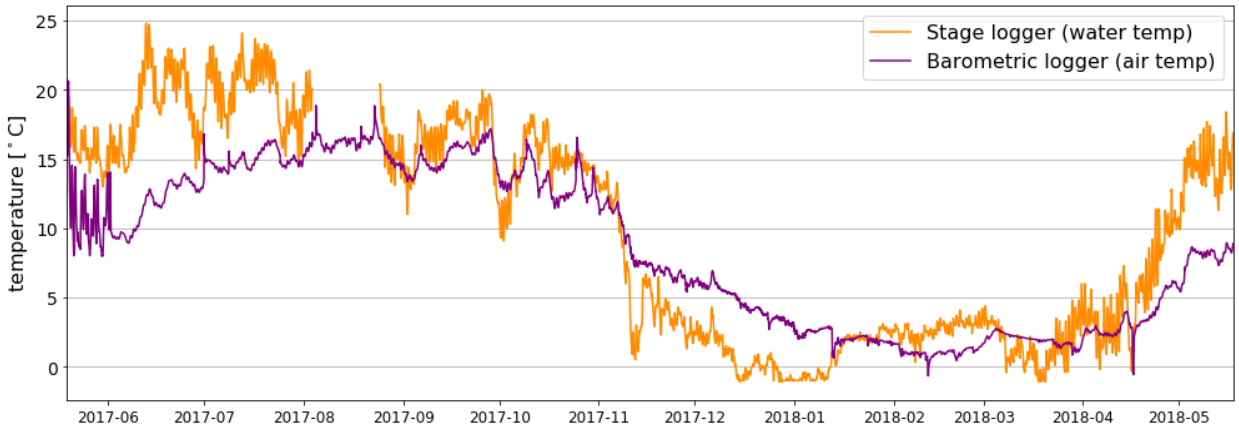

Figure A.25. Water temperature (recorded at 5-minute intervals) at Pawtuckaway River compared to air temperature from the barometric logger from 2017-05-19 to 2018-05-18. Data gap exists between 2017-08-03 13:40 to 2017-08-24 16:00 from failure to download correct logger data.

Table A.27. Dates and times when pressure transducer data was trimmed and filled with linear interpolation at Pawtuckaway River.

	Data trimmed		# of measurements interpolated
Date of data retrieval	Start time	Stop time	
2017-05-22	12:00	12:20	5
2017-06-01	14:00	14:20	5
2017-06-19	10:25	11:00	8
2017-06-22	11:25	12:45	17
2017-07-27	12:30	12:50	5
2017-10-13	14:00	14:20	5
2018-01-19	7:20	7:50	7
2018-04-08	6:30	6:50	5
2018-05-02	13:20	13:55	6

Table A.28. Dates and times when pressure transducer data was corrected for intentional and unintentional transducer relocations at Pawtuckaway River.

		Correction applied to record	
Intentionally moved	Correction [m]	Start date, time	End date, time
Yes	+0.185	2017-05-19, 00:00	2017-05-22, 12:10

Table A.29. Discharge measurements obtained at Pawtuckaway River using the velocity-area method and corrected stage used in the construction of the stage-discharge rating curve in Figure A.27.

Date Time	m	Measured at	Q [m^3/s]	Corrected stage [m]	Q uncertainty +/-%
5/19/17 13:45	20	0.6 depth	0.35393	0.266	7.88
6/15/17 13:05	22	0.6 depth	0.17988	0.130	7.67
7/8/17 10:00	22	0.6 depth	0.010114	0.022	10.47
7/26/17 10:45	21	0.6 depth	0.01694	0.084	10.65
8/8/17 16:20	21	0.6 depth	0.06038	0.132	7.77
10/13/17 14:15	19	0.6 depth	0.21241	0.236	8.00
12/8/17 15:15	20	0.6 depth	0.17459	0.226	7.88
1/19/17 7:30	20	0.6 depth	0.9545	0.428	7.88
4/8/17 6:30	23	0.6 depth	0.02507	0.106	10.29

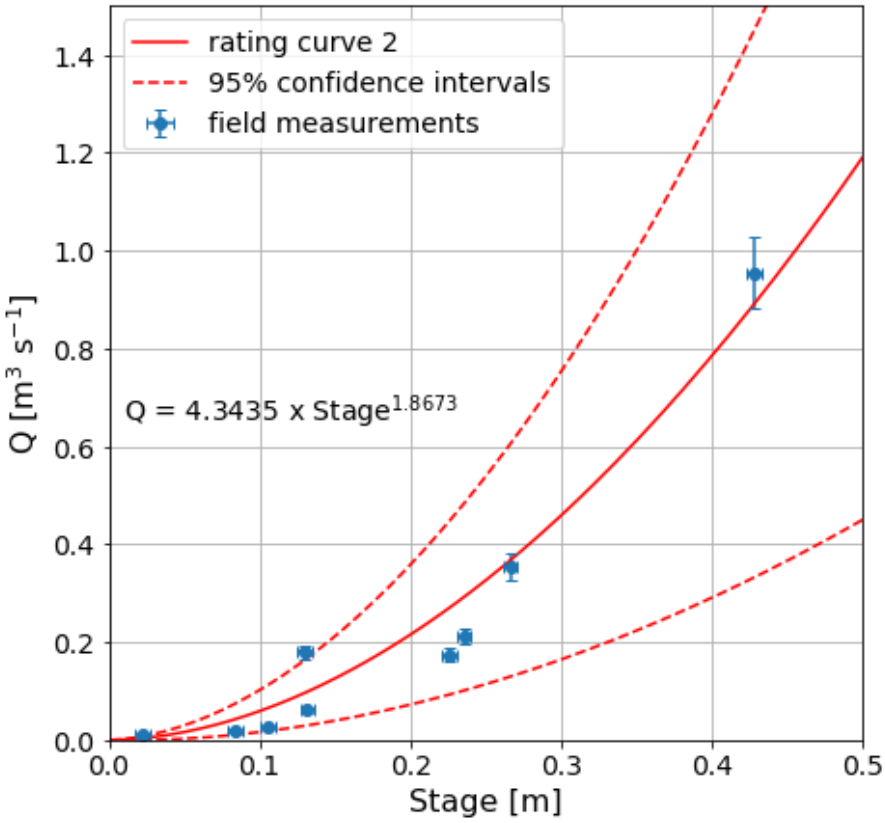

Figure A.26. Stage-discharge rating curves for Pawtuckaway River. Field measurements of discharge and stage are located in Table A.29.

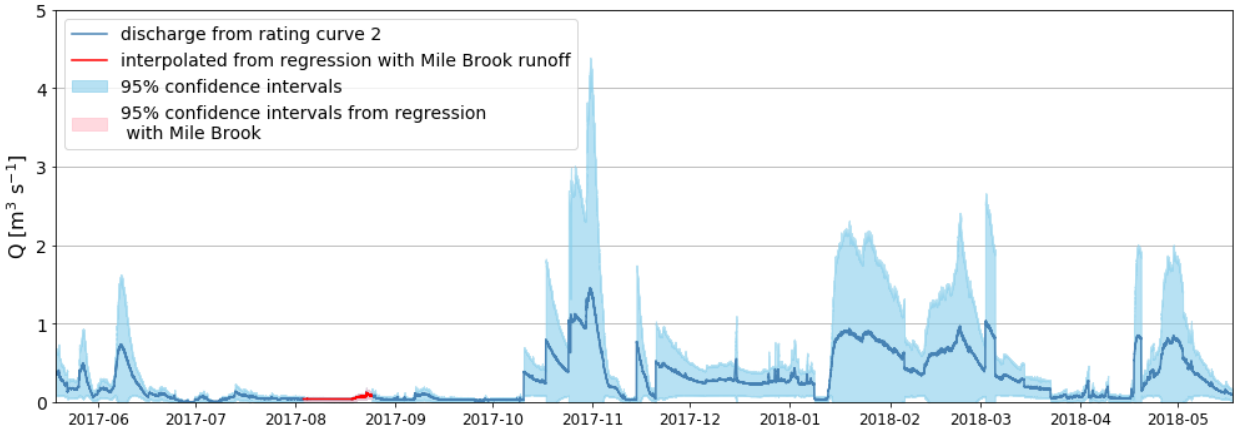

Figure A.27. Time series of discharge (Q) at 5-minute intervals at Pawtuckaway River from 2017-05-19 to 2018-05-18.

Table A.30. Nitrogen solute concentration measurements obtained at Pawtuckaway River.

Date	TDN [mg N/L]	DON [mg N/L]	NO3+NO2 [mg N/L]	NH4 [μg N/L]
2017-05-23	0.057	0.027	0.027	3.00
2017-07-26	0.187	0.098	0.088	1.00
2017-10-13	0.092	0.067	0.010	14.60
2017-12-08	0.218	0.186	0.027	4.59
2018-01-19	0.352	0.261	0.059	32.00
2018-04-08	0.419	0.214	0.197	8.00

A.8 Additional N concentration measurements

Table A.31. Nitrogen solute concentration measurements obtained in the reservoir.

Date	TDN [mg N/L]	DON [mg N/L]	NO3+NO2 [mg N/L]	NH4 [μg N/L]
2017-07-26	0.024	0.017	0.004	3.00
2017-10-13	0.097	0.077	0.010	10.40
2017-12-08	0.224	0.202	0.016	5.63
2018-01-19	0.321	0.247	0.060	14.00
2018-04-08	0.244	0.200	0.041	3.00

Table A.32. Nitrogen solute concentration measurements obtained at USGS gauge 01073500.

Date	TDN [mg N/L]	DON [mg N/L]	NO3+NO2 [mg N/L]	NH4 [μg N/L]
2017-05-23	0.353	0.228	0.103	22.00
2017-07-26	0.776	0.537	0.226	13.00
2017-10-13	0.717	0.354	0.360	3.00
2017-12-08	0.669	0.466	0.166	36.51
2018-01-19	0.619	0.421	0.172	26.00
2018-04-08	0.477	0.313	0.139	25.00

Table A.33. Nitrogen solute concentration measurements obtained at USGS gauge 01073319.

Date	TDN [mg N/L]	DON [mg N/L]	NO3+NO2 [mg N/L]	NH4 [μg N/L]
2017-05-23	0.057	-0.009	0.062	4.00
2017-07-26	0.187	0.063	0.112	12.00
2017-10-13	0.092	-0.001	0.090	2.90
2017-12-08	0.218	0.125	0.080	12.94
2018-01-19	0.352	0.157	0.150	45.00
2018-04-08	0.419	0.163	0.190	66.00

Appendix B: FrAMES Modeling Structure

B.1 Model Structure

The following sections describes the structure of the FrAMES modeling structure, where water and DIN flow paths within a modeled grid cell are visualized in Figure B.1.

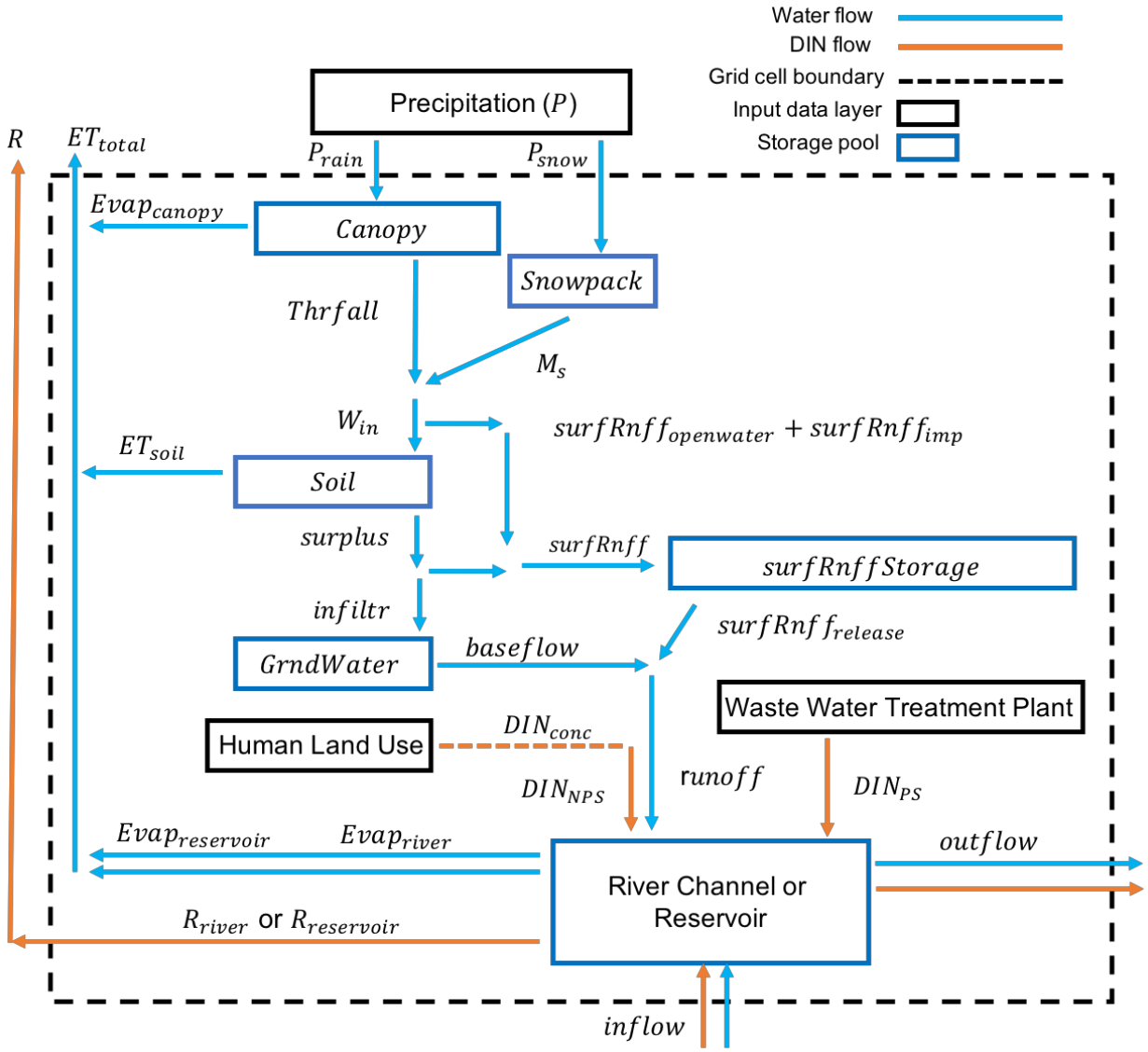

Figure B.1 Visualization of water and DIN flow paths within a single model grid cell.

B.2 Precipitation

Water enters a grid cell through precipitation (P) [mm] as either rainfall (P_{rain}) or snowfall (P_{snow}) depending on daily mean air temperature (T_{air}) [°C]. Precipitation is considered snowfall if T_{air} is below a snowfall threshold of -1.0 °C; otherwise, precipitation is considered rainfall.

$$P = P_{rain} \qquad if\ T_{air} \geq -1.0$$ Equation B.1

$$P = P_{snow} \qquad if\ T_{air} < -1.0$$ Equation B.2

B.3 Snow Melt

Snowfall is temporarily stored in snow pack ($Snowpack$) [mm] where it can then melt on days when T_{air} exceeds a snowmelt threshold of 1.0 °C. Snow melt (M_s) is calculated as,

$$M_s = 2.63 + 2.55 \cdot T_{air} + 0.0912 \cdot T_{air} \cdot P_{rain}$$ Equation B.3

B.4 Potential Evapotranspiration

Potential evapotranspiration (PET) is the amount of water lost to evaporation and transpiration when soil moisture is not limited. FrAMES calculates PET using the Hamon method (Hamon, 1963). Potential evaporation from the Hamon method (PET_H) [mm day^{-1}] is calculated as,

$$PET_H = 165.1 \cdot daylength \cdot \rho_{Sat}$$ Equation B.4

where $daylength$ is the fraction of daylight (calculated based on the Julian day of the year) and ρ_{Sat} is saturated vapor density [g m^{-3}] and is calculated as,

$$\rho_{Sat} = \frac{2.167 \cdot P_{sat}}{T_{air} + 273.15}$$ Equation B.5

where the vapor saturation pressure (P_{sat}) [kg m^{-1} s^{-2}] is dependent on T_{air} (Dingman 2008) and calculated as,

$$P_{sat} = \begin{cases} 0.61078 \cdot e^{\left(\frac{17.26939 \cdot T_{air}}{T_{air} + 237.3}\right)} & T_{air} \geq 0 \\ 0.61078 \cdot e^{\left(\frac{21.87456 \cdot T_{air}}{T_{air} + 265.5}\right)} & T_{air} < 0 \end{cases}$$ Equation B.6

B.5 Canopy Interception

If precipitation falls as rain, a portion is intercepted by vegetation where it is either lost to evaporation ($Evap_{canopy}$) or falls to the ground as throughfall ($Thrfall$). The interception capacity (I_{cap}) [mm] of the canopy is calculated as,

$$I_{cap} = s \cdot LAI$$ Equation B.7

where leaf area index (LAI) [-] is the total area of leaf surface over a given area, normalized by area and s [mm] is a storage capacity constant (default of 0.25; Dickinson 1984). Water lost to evaporation ($Evap_{canopy}$)[mm] in the canopy calculated as,

$$Evap_{canopy} = Canopy \cdot PET_H \cdot \left(\frac{Canopy}{I_{cap}}\right)^{(2/3)} \quad \text{Equation B.8}$$

where $Canopy$ [mm] is the amount of water stored in the canopy. Throughfall ($Thrfall$) [mm] is then calculated as,

$$Thrfall = P_{rain} + Canopy_{t-1} - Evap_{canopy} - I_{cap} \quad \text{Equation B.9}$$

The remaining rainfall that does not evaporate or fall to the ground is stored in the $Canopy$ storage pool.

B.6 Available Water and Impervious Surface/Open Water Runoff

Available water (W_{in}) [mm] is the amount of water that can enter the soil moisture pool ($Soil$) [mm] or enter the surface runoff retention pool ($surfRnffStorage$) [mm]. If a grid cell contains either impervious surfaces or open water such as wetlands, lakes, or reservoirs, then a portion of W_{in} is first diverted to surface runoff. How much water becomes open water runoff ($surfRnff_{openwater}$ [mm]) depends on the fraction of open water ($fracOpenwater$) within the grid cell and the area of the grid cell ($cellArea$).

$$surfRnff_{openwater} = W_{in} \cdot fracOpenwater \quad \text{Equation B.10}$$

How much water becomes impervious surface runoff ($surfRnff_{impervious}$ [mm]) depends on the area of impervious surfaces ($imprArea$) within the grid cell, and an impervious surface coefficient ($imprCoef$; Alley and Veenhius 1983).

$$surfRnff_{imp} = W_{in} \cdot imprArea \cdot imprCoef/cellArea \quad \text{Equation B.11}$$

$$imprCoef = imprArea^{0.4} \quad \text{Equation B.12}$$

The remaining available water is then calculated after deducting for surface runoff due to impervious surfaces or open water,

$$W_{in} = W_{in} - surfRnff_{openwater} - surfRnff_{impervious} \quad \text{Equation B.13}$$

B.7 Soil Moisture

Whether water enters or exits the soil moisture pool ($\Delta Soil$) at time step t depends on available water input (W_{in}), potential evapotranspiration (PET), the amount of water in the soil moisture pool from the previous time step ($Soil_{t-1}$), and the available water capacity of the soil (AW_{cap}) [-]. If W_{in} is less than PET, a drying function (dry) is used to determine the amount of water loss from the soil (Dingman 2008),

$$Soil_t = \Delta Soil_t + Soil_{t-1}$$ Equation B.14

where,

Equation B.15

$$\Delta Soil_t = \begin{cases} dry \cdot (W_{in} - PET) & if\, W_{in} < PET \\ W_{in} - PET & \text{if } PET \leq W_{in} \text{ and } (W_{in} - PET) < (AW_{cap} - Soil_{t-1}) \\ AW_{cap} - Soil_{t-1} & \text{if } PET \leq P_{in} \text{ and } \left(AW_{cap} - Soil_{t-1}\right) \leq (W_{in} - PET) \\ 0 & \text{if } AW_{cap} = 0 \end{cases}$$

where the drying function is given as:

$$dry = \frac{1 - e^{\left(-\alpha \cdot \frac{Soil_{t-1}}{AW_{cap}}\right)}}{1 - e^{-\alpha}}$$ Equation B.16

where α is a drying rate parameter (default of 5).

Water loss from the soil due to evapotranspiration (ET_{soil}) [mm] is then calculated by,

$$ET_{soil} = \begin{cases} W_{in} - \Delta Soil & \text{if } PET_H \geq (W_{in} - \Delta Soil) \\ PET_H & \text{if } PET_H < (W_{in} - \Delta Soil) \end{cases}$$ Equation B.17

B.8 Surplus and Groundwater

Any remaining available water (W_{in}) that does not enter the soil or become lost to evapotranspiration then becomes surface water surplus ($surplus$) [mm].

$$surplus = W_{in} - ET_{soil} - \Delta Soil$$ Equation B.18

A fraction of $surplus$ then infiltrates ($infiltr$) [mm] into the groundwater storage pool ($GrndWater$) [mm],

$$infiltr = surplus \cdot infiltrFrac$$ Equation B.19

where $infiltrFrac$ [-] is the fraction of surplus that infiltrates into groundwater (default of 0.5). Water leaves $GrndWater$ and enter sinto the river channel in the form of baseflow ($baseflow$) [mm] which is calculated as,

$$baseflow = GrndWater \cdot \beta$$ Equation B.20

where β is the fraction of the groundwater storage pool that exits via baseflow in each time step (default value of 0.0167). The water remaining in the groundwater storage pool at the end of time step t is calculated as,

$$GrndWater_t = GrndWater_{t-1} + infiltr - baseflow$$ Equation B.21

B.9 Runoff

The remaining fraction of surplus that does not infiltrate into groundwater combines with surface runoff from open water and impervious surfaces to become a single surface runoff term ($surfrunoff$) where,

$$surfRnff = surplus - infiltr + surfRnff_{openwater} + surfRnff_{imp}$$ Equation B.22

Surface runoff then enters the near channel surface runoff retention pool ($surfRffStorage$)[mm], which accounts for the lag for runoff entering the river network and also represents event flow from groundwater conceptually.

$$surfRnffStorage_t = surfRnffStorage_{t-1} + surfrunoff_t - surfRnff_{release}$$ Equation B.23

The surface runoff retention pool is represented as a storage tank where water drains ($surfRnff_{release}$) [mm] based on gravity and the height of water in the tank by,

$$surfRnff_{release} = \left(RhRt2 \cdot \sqrt{2 \cdot G \cdot surfRnffStorage}\right) + (surfRnffStorage - RRPMax)$$ B.24

where $RhRt2$ is a draining rate parameter (default value of 0.56), G is gravitational acceleration (9.8 m sec^{-2}), and $RPPMax$ [mm] is the maximum amount of water that can be stored in the surface runoff retention pool (arbitrary default value of 30 mm). Surface runoff released from the retention pool then combines with $baseflow$ to make up total runoff ($runoff$) [mm] and runoff volume ($runoff_{volume}$) [m^3 sec^{-1}] which then enters the river network,

$$runoff = baseflow + surfRnff_{release}$$ Equation B.25

$$runoff_{volume} = \frac{(runoff \cdot cellArea)}{86.4}$$ Equation B.26

B.10 Flow Routing

Water flow is routed between grid cells using a simulated topological network (STN), which provides a map of the direction of water flow downstream. For grid cells not containing reservoirs, the model uses the Linear Reservoir Routing (LRR) method to determine the amount of outflow ($ouflow$) [m^3 sec^{-1}] leaving a grid cell based on river channel storage ($Storage_{river}$) [m^3]. The relationship between $ouflow$ and $Storage_{river}$ is expressed as,

$$ouflow = \frac{C \cdot Storage_{river}}{\Delta t}$$ Equation B.27

$$C = \frac{1}{1+\frac{w \cdot L}{U \cdot \Delta t}}$$ Equation B.28

where C [-] is a routing coefficient, w [-] is the weight given to the river channel length, L [m] is the length of the river channel, and U [m sec^{-1}] is a constant flow velocity of 2.98 km hr^{-1} converted to m sec^{-1} (Fekete et al. 2001), and Δt is the time step conversion factor (converts from days to seconds). If a grid cell is a headwater location (does not have any upstream cells draining to it), then $w = 1$ otherwise w for time step t is calculated as,

$$w_t = \frac{inflow_{t-1}}{outflow_{t-1}} + \frac{runoff_{volume,t} \cdot \Delta t + Storage_{river}}{2 \cdot outflow_{t-1} \cdot \Delta t}$$ Equation B.29

where $inflow$ [m^3 sec^{-1}] is the total inflow entering the grid cell (that is the $Outflow$ from cells just upstream).

B.11 Reservoirs

If a grid cell contains a dam, the amount of outflow released from the impoundment depends on the dam type, dam purpose, a long-term average discharge at that location, and the reservoir water storage level (Grogan et al 2017). To incorporate reservoirs, a geospatial dam database providing location, maximum volume, surface area, upstream drainage area, dam type, and dam purpose is first read into the model. Dam reservoir types are represented in FrAMES as either managed (controlled outflow) or unmanaged (uncontrolled outflow). Managed dams are further categorized depending on their designated purpose and are assigned one of six operating types: generic, flood control, hydroelectric, irrigation, water supply, or recreation. For managed reservoirs, outflow released downstream from the impoundment is calculated using a bimodal log/exponential function based on reservoir storage (S),

$$outflow = \begin{cases} Q_{avg} \cdot [Q_{min} + a \cdot \ln(1 + c \cdot S)] & \text{if } S < S_{opt} \\ Q_{avg} \cdot [B + b \cdot (S - S_{opt})^p] & \text{if } S \geq S_{opt} \end{cases}$$ Equation B.30

where,

$$a = \frac{1 - Q_{min}}{\ln(1 + c \cdot S_{opt})}$$ Equation B.31

$$b = \frac{4}{(1 - S_{opt} + d)^p - d^p}$$ Equation B.32

$$B = S_{opt} - b \cdot d^p$$ Equation B.33

where Q_{avg} [m^3 s^{-1}] is the 5-year running average for annual discharge at the grid cell, Q_{min} is the minimum release allowed normalized by the long-term annual mean discharge for that location, S is the reservoir storage level [fraction of maximum reservoir capacity], and S_{opt} is the optimal reservoir storage level for the reservoir [fraction of maximum reservoir capacity]. Parameters c and p are set depending on dam purpose while a, b, B, and d are calculated. Figure B.2 shows managed reservoir outflow/storage curves for flood control and water supply dam purposes. Dams operating for recreation normally keep reservoir levels high during summer for boating, swimming, and fishing and low during winter and spring to allow for dock maintenance and accommodate extra runoff due to storms and snow melt. Therefore, dams with the operating type of recreation use parameters for water supply during May – October and flood control during November – April (Figure B.2)

Unmanaged dams are treated as small spillway dams where outflow over the spillway crest is calculated as,

$$outflow = \begin{cases} Q_{avg} \cdot \left(\frac{\sqrt{1+\beta \cdot S_e}-1}{\sqrt{\sqrt{1+\beta \cdot S_d}-1}} \right)^{1.6} & \text{if } fld \geq 0 \\ Q_{avg} \cdot \left(\frac{S_e}{S_d}\right)^{1.6} & \text{if } fld = 0 \end{cases} \quad \text{Equation B.34}$$

where,

$$\beta = \frac{4 \cdot fld}{res_{Area}} \quad \text{Equation B.35}$$

and,

$$S_e = H \cdot res_{Area} \cdot (1 + fld \cdot H) \quad \text{Equation B.36}$$

where Q_{avg} [m^3 s^{-1}] is the 5-year running average for annual outflow at the grid cell, S_d [m^3] is the reservoir storage when water level is at the spillway crest, S_e [m^3] is the effective reservoir storage when water level is above the spillway crest, H [m] is the 5-year running average of water level reservoir depth [m] in the grid cell, fld [m^{-1}] is the reservoir area flooding rate (default of 0.3), and res_{Area} [m^2] is the surface area of the reservoir at the spillway crest. Unmanaged reservoir outflow curves are shown for different reservoir area flooding rates in Figure B.3.

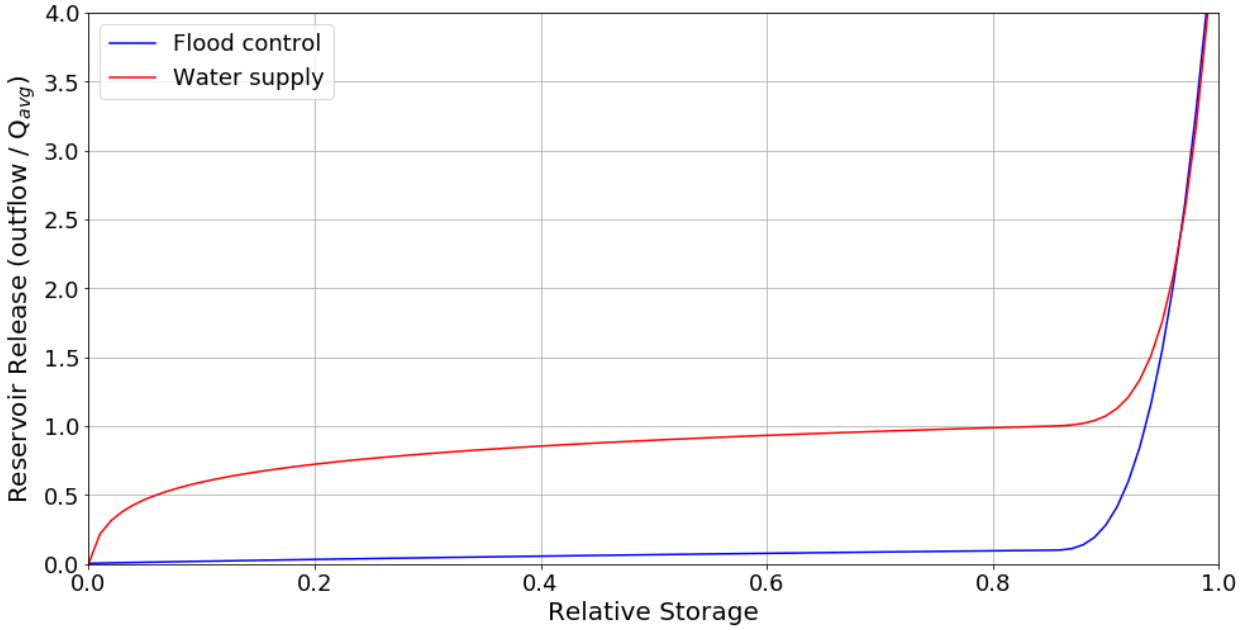

Figure B.2 Reservoir outflow/storage curves for managed dams with operating types of flood control and water supply. Reservoir outflow is normalized by the 5-year running average, Q_{avg}, for annual outflow at the grid cell and relative reservoir storage is given as a fraction of maximum reservoir capacity.

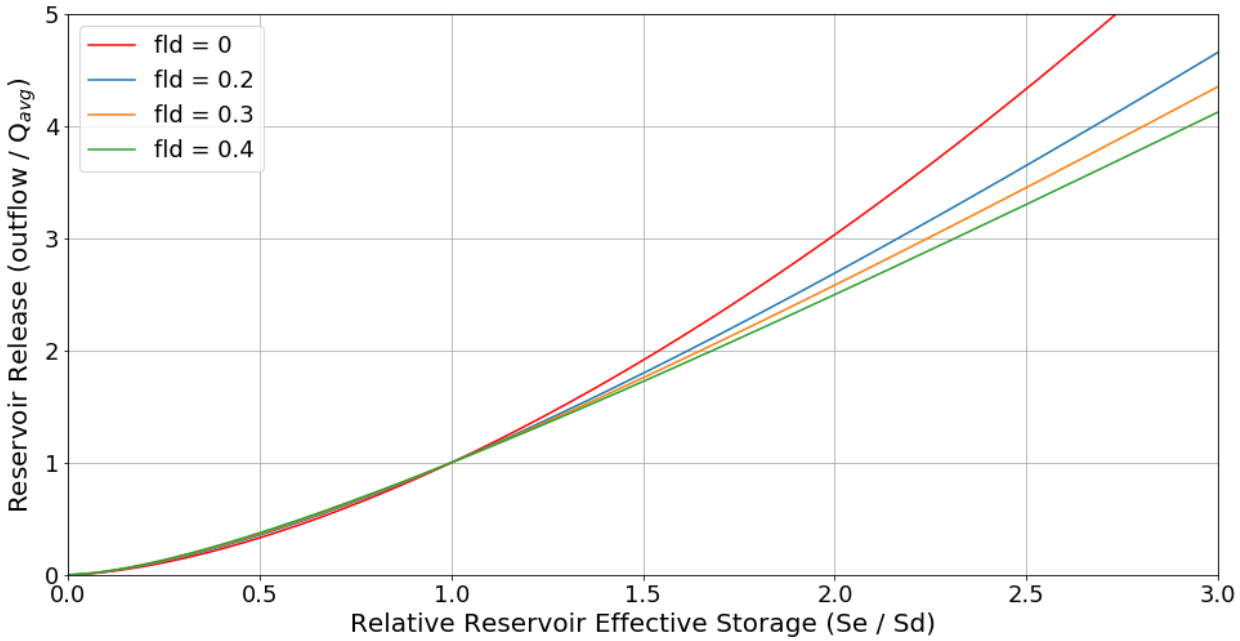

Figure B.3 Reservoir outflow/storage curves for unmanaged dams with different reservoir flooding area rates (fld). Reservoir outflow is normalized by the 5-year running average, Q_{avg}, for annual outflow at the grid cell, S_e [m^3] is the effective reservoir storage when water level is above the spillway crest, and S_d [m^3] is the reservoir storage when water level is at the spillway crest.

B.12 Water Surface Evaporation

Water can be lost in a grid cell due to free surface evaporation from either reservoirs $Evap_{reservoirs}$ [mm day^{-1}],

$$Evap_{reservoirs} = res_{Area} \cdot water_{Evap} \quad \text{Equation B.37}$$

where res_{Area} [mm^2] is the area of the reservoir and $water_{Evap}$ [mm^{-1} day^{-1}] is the evaporation rate, or from the river channel $Evap_{river}$ [mm day^{-1}],

$$Evap_{river} = river_{Area} \cdot water_{Evap} \quad \text{Equation B.38}$$

where $river_{Area}$ [mm^2] is the area of the river channel. Total water lost within a grid cell due to evapotranspiration ET_{total} [mm day^{-1}] is calculated as,

$$ET_{total} = Evap_{river} + Evap_{reservoirs} + ET_{soil} + Evap_{canopy} \quad \text{Equation B.39}$$

B.13 Water Temperature Routing

In-channel water temperature (T_w [°C]) is modeled during flow routing using the River Temperature Re-Equilibration Model (RTRM). Presented in Dingman (1972), this routing method assumes that there is a temperature equilibrium T_e [°C] at which no net energy is lost to

the atmosphere and has been used to simulate water temperature in the northeast United States (Stewart et al. 2013). T_e is calculated as,

$$T_e = T + \frac{solarRad - E_o}{E_c}$$ Equation B.40

where $solarRad$ [kJ m^{-2} d^{-1}] is the net solar radiation and is calculated based on the Julian day of the year and shading due to cloud and canopy cover ($CloudShd$) , E_o [kJ m^{-2} d^{-1}] is the heat loss rate, and E_c [] is the energy exchange coefficient. $CloudShd$ is calculated as,

$$CloudShd = cloudFr + (1 - cloudFr) \cdot canopySh \cdot \left(\frac{canopyHt}{width}\right)$$ Equation B.41

where $cloudFr$ [-] is the fraction of a grid cell covered by clouds, $canopySh$ is the fraction of the grid cell shaded by vegetation and is calculated based on Julian day and leaf area index LAI [-] which is fraction of leaf area to land area within a grid cell, $canopyHt$ [m] is the height of the canopy, and $width$ [m] is the stream width. E_o and E_c are calculated using an empirical relationship with wind speed W_v [m d^{-1}] that differs between clear or cloudy days,

$$E_o = \begin{cases} 105 + 23 \cdot W_v & \text{if clear } (cloudShd < 0.95) \\ -73 + 9.1 \cdot W_v & \text{if cloudy } (cloudShd \geq 0.95) \end{cases}$$ Equation B.42

$$E_c = \begin{cases} 35 + 4.2 \cdot W_v & \text{if clear } (cloudShd < 0.95) \\ 37 + 4.6 \cdot W_v & \text{if cloudy } (cloudShd \geq 0.95) \end{cases}$$ Equation B.43

A wet bulb correction (E_s) is then applied to T_e,

$$E_s = \log\left(rHumidity \cdot 10^{\left(\frac{7.5 \cdot T_e}{237.3 + T_e}\right)}\right)$$ Equation B.44

$$T_e = \frac{237.3 \cdot E_s}{17.27 - E_s}$$ Equation B.45

where $rHumidity$ [-] is relative humidity. RTRM also accounts for temperature mixing between baseflow and surface runoff with the river channel. The temperature of baseflow entering the river network $T_{baseflow}$ [°C] is calculated as,

$$T_{baseflow} = T_{groundwater} + bflowscale \cdot (T_{air15} - T_{groundwater})$$ Equation B.46

where $T_{groundwater}$ [°C] is the temperature of the ground water which is assumed to equal the average annual air temperature, $bflowscale$ [-] is a baseflow scale parameter (default value of 0.59), and T_{air15} [°C] is the 15-day running average for air temperature. The water temperature of all runoff T_{runoff} [°C] is then calculated as the weighted average of the temperatures in the various flow components,

$$T_{runoff} = \frac{(T_{surfrunoff} \cdot surfRnff_{release} + T_{baseflow} \cdot baseflow)}{runoff}$$ Equation B.47

where $T_{surfrunoff}$ [°C] is the water temperature of surface runoff and T_{air5} [°C] is the five-day running average for air temperature.

$$T_{surfrunoff} = T_{air5}$$ Equation B.48

RTRM then re-equilibrates in-channel water temperature T_w from mixing with T_{runoff},

$$T_w = \mathrm{T_e} + (T_o - T_e) \cdot \exp\left(-E_c \cdot \frac{\left(\frac{L}{U \cdot \Delta t}\right)}{depth}\right)$$ Equation B.49

where T_o [°C] is the in-channel water temperature prior to mixing, L [m] is the length of the river reach, U [m day^{-1}] is the water velocity, Δt is the time step conversion factor (converts from days to seconds), and $depth$ is the depth of the river channel [m].

B.14 DIN Modeling

DIN is loaded to the river network from both point source (DIN_{PS} [kg day^{-1}]) based on wastewater treatment plant effluent and non-point sources (DIN_{NPS} [kg day^{-1}]) based on human land use. For non-point source loading, WBM utilizes an empirical DIN loading function that was originally developed for the Ipswich River watershed located in northeast Massachusetts. This sigmoidal function relates the fraction of human land use upstream (both developed and agriculture) with the concentration of DIN in runoff (DIN_{NPS_Conc}) [g L^{-1}]. Specifically, DIN_{NPS_Conc} is calculated as,

$$DIN_{NPS\_Conc} = \frac{Asym}{1+e^{\frac{(Xmid-HLU)}{scale}}}$$ Equation B.50

where $Asym$ [g L^{-1}] is the maximum concentration found in runoff, HLU [-] if the fraction of both developed and agricultural land use, $scale$ [-] determines the range of HLU at which concentration rises, and $Xmid$ is the inflection point of that curve. $Xmid$ depends on runoff ($runoff$) and has an intercept ($Xmid_b$) and a slope ($Xmid_m$).

$$Xmid = Xmid_b + Xmid_m \cdot \log(runoff)$$ Equation B.51

DIN_{NPS} is calculated as,

$$DIN_{NPS} = \frac{DIN_{NPS\_Conc} \cdot runoff_{Volume} \cdot \Delta t}{(1000 \cdot cellArea)}$$ Equation B.52

Grid cells containing a waste water treatment plant receive DIN loading as,

$$DIN_{PS} = \frac{WWTP_{load}}{runoff_{Volume} \cdot \Delta t}$$ Equation B.53

where daily nitrogen effluent load ($WWTP_{load}$) [kg] for each treatment plant is read into the model. The total amount of DIN within the river channel of a grid cell $DIN_{outflow}$ [kg] is then calculated as,

$$DIN_{outflow} = \left[DIN_{inflow} + \left(\frac{DIN_{PS} + DIN_{NPS}}{Storage_{river}}\right)\right] \cdot (1 - R)$$ Equation B.54

where DIN_{inflow} [kg] is the amount of DIN entering the grid cell from upstream, $Storage_{river}$ [kg] is the amount of DIN stored in the river channel from the previous time step, and R [-] is the proportion of DIN removed within each grid cell by physical and biogeochemical processes. R is calculated for grid cells without reservoirs (R_{river})[-] and grid cells containing reservoirs ($R_{reservoir}$)[-] using both empirical and deterministic models. For grid cells without reservoirs, FrAMES uses the efficiency loss model (Mulholland et al. 2008) to calculate river channel DIN retention (R_{river}) with an uptake velocity (V_f) [m day^{-1}] that varies with both in-channel water temperature and DIN concentration. R_{river} is then calculated as,

$$R_{River} = 1 - \exp\left(-\frac{1}{V_f \cdot \frac{outflow}{river_{Area}}}\right) \quad \text{Equation B.55}$$

where,

$$V_f = 10^{(int + \log(DIN_{outflow} \cdot slope)} \cdot Q10 \quad \text{Equation B.56}$$

$$Q10 = 2^{\left(\frac{(T_W - Tref) \cdot Tscale}{Tref/2}\right)} \quad \text{Equation B.57}$$

where V_f is the uptake velocity of DIN [g km^{-2} d^{-1}], $river_{Area}$ [m] is the river channel area and is calculated from the channel width and height derived from empirical relationships relating discharge with reach-averaged width and depth, int [-] is the uptake velocity intercept (value of -2.975; Mulholland et al. 2008), $slope$ [-] is the slope of the uptake velocity (value of -0.493; Mulholland et al. 2008) $Q10$ is a water temperature correction factor, T_w is in channel water temperature [°C], Tn_{Ref} is the reference water temperature (default value of 20 °C), and $Tscale$ [-] is a temperature scaling factor.

Grid cells containing reservoirs retain DIN from the empirical relationship developed by Seitzinger et al. 2002, which relates the fraction of DIN removed within the waterbody to hydraulic load and utilizes the same water temperature correction factor as the efficiency loss model,

$$R_{reservoirs} = \left(0.88453 \cdot {H_L}^{-0.3677}\right) \cdot Q10 \cdot \Delta t \quad \text{Equation B.58}$$

$$H_L = \frac{outflow}{res_{Area}} \quad \text{Equation B.59}$$

where res_{Area} [m^2] is the surface area of the reservoir, H_L [m day^{-1}] is the hydraulic load, and Δt is the time step conversion factor (converts from years to days).